A Holocene flood record of the Lower Rhine

Overstromingen van de Beneden-Rijn gedurende het Holoceen
(met een samenvatting in het Nederlands)

PROEFSCHRIFT

ter verkrijging van de graad van doctor aan de Universiteit Utrecht
op gezag van de rector magnificus, prof.dr. G.J. van der Zwaan,
ingevolge het besluit van het college voor promoties in het openbaar te verdedigen
op vrijdag 4 oktober 2013 des middags te 4.15 uur

door

Willem Hendrikus Jacobus Toonen

geboren op 9 maart 1984 te Oss

Promotor:
Prof.dr. H. Middelkoop

Co-promotor:
Dr. K.M. Cohen

Dit proefschrift werd (mede) mogelijk gemaakt met financiële steun van Deltares.

A Holocene flood record of the Lower Rhine

Utrecht Studies in Earth Sciences

ISSN 2211-4335

Utrecht Studies in Earth Sciences 41

A Holocene flood record of the Lower Rhine

Willem H.J. Toonen

Utrecht 2013

Examination committee:
Prof. dr. M.G. Macklin, Aberystwyth University
Prof. dr. G. Benito, CSIC Madrid
Prof. dr. J. Herget, University Bonn
Prof. dr. J.C.J.H. Aerts, VU University Amsterdam
Dr. J.C.J. Kwadijk, Deltares

ISBN 978-90-6266-338-5

Cover: Meanders of the Old Channel (Saskatchewan River, Cumberland House, Saskatchewan, Canada). Courtesy of Dr. I.J. Bos.

Printed in the Netherlands by CPI-Wöhrmann Print Service, Zutphen.

De Rynstroom

Doorluchte Rijn, mijn soete droom,
Van waer sal ick u lof toesingen?
Mijn treckende geboortestroom,
Ghy koomt uit Zwitsersche Alpes springen,
Als hoofdaêr der begaefde Euroop.
De Donau, uw afkeerigh broeder,
Nam oostwaert op syn' snellen loop,
Ghy Noordwaert; doen een selve moeder,
Begort van regen ys en sneeuw,
U baerde voor soo menige eeuw.
Germanjen lagh noch wild begroeit
Van syn Hyrcynsche wilde wouden,
Tot dat het namaels werd besnoeit,
En door de tucht in toom gehouden.
Ten leste dorst ghy, strijdbre Rijn,
Den Tiber op syn feest bestoken;
Die voor u neegh, doen Constantijn
Van uwen oever opgebroken.
Ging strijcken met den ouden roof
Van Rome en 't Heidensch bygeloof.

Joost van den Vondel, (around AD 1630)

Contents

Preface

"No individual raindrop ever considers itself responsible for the flood."[1] If everybody who helped me academically, financially, or socially, considered themselves little raindrops, they are very much responsible for a flood. Here, I want to acknowledge the contribution of the biggest raindrops, and although not specifically mentioned here, all other persons that have been involved are thanked cordially.

When the first raindrops hit the ground and start to accumulate they gather into runoff, gradually increasing with more drops joining. Although they have not even entered a stream and do not yet contribute to a measurable discharge, the importance of their contribution in the final product cannot be neglected. Getting at the final stage of my dissertation, metaphorically much more streams adding up and resulting in a (catastrophic) flood, can be regarded in a similar way. For offering interesting research projects, being the early sprouts of my academic career, I want to thank Esther Stouthamer, Sanneke van Asselen, Nanne Weber, Kim Cohen, and Joshua Trampier. The experience gathered in pre-PhD projects not only encouraged me to pursue an academic career, but probably also helped to get where I currently am.

I am grateful for being offered the chance to write a dissertation, logistically made possible by a large group of people, most importantly my supervisors Kim Cohen and Hans Middelkoop. Kim, although we were occasional hazards to each other (– you with periods of over-frequent visits and totally irrelevant but funny stories and linguistic jokes, I with my streaks of high-pitched voice complaints and stubbornness), I enjoyed working under your supervision. Hans, although you had many people and projects to manage, I appreciate the time and effort you put in reading my manuscripts and your constructive comments. Your previous work proved to be a treasure trove for my research, and helped me to select some excellent research locations.

I also want to mention here Quirijn Lodder and Esther Stouthamer. Quirijn, because he and Kim are responsible for writing the research proposal that delivered the funding for this project. Esther, because she has been responsible for negotiating this proposal with TNO/Deltares. Ad van der Spek and Bob Hoogendoorn of Deltares BGS are thanked for financial and logistical support. Deltares BGS is in general acknowledged as the main funding organisation of this project together with Utrecht University. In the first years of this project, there has also been a considerable investment by TNO (Timme Donders) to support palynological analyses and coring campaigns.

Of all the private landowners and authorities (Staatsbosbeheer, Utrechts Landschap, Rijkswaterstaat, Waterschap Rivierenland, Naturschutz Kreis Kleve) that gave me permission to perforate their properties, I want to acknowledge Peter van den Broeke and Eckhart Heunks specifically for supporting an extensive coring campaign in the Waalsprong area near Nijmegen and providing excellent archaeological context for the research sites. The fieldwork gave me a head-start in this research and enabled us to construct a conceptual model for the sedimentary filling of abandoned channels. Henk Weerts is thanked for inviting me to an archaeological trench featuring an infilled channel at Houten, which increased confidence in our preliminary results.

---

1 Source quotation unknown.

Flood research has a very wide scope and many applications. Many different approaches exist to carry out research; e.g., hydraulic modelling, sedimentology, analysis of historical records, and statistics. It was a challenge to 'master' (at least understand) most disciplines and to be able to combine approaches. Fortunately, I could rely on experts, who were very patient with me (especially Hans van Aken for constructing a coring platform at a site where no coring was possible at all), and assisted when necessary. Two major factors in creating a flood chronology are the application of various dating techniques and the reconstruction of flood magnitudes from grain-size distributions of flood deposits. Hanneke Bos identified suitable plant remains for AMS dating; without that information all my clay-sieving hours would be useless. Frans Bunnik carried out important palynological quick-scans on the cores; this resulted in estimates on the age of the sediments, and spared me a lot of money and time spent on unsuitable research sites. Lennart de Groot is acknowledged for exploring the possibility of using palaeomagnetism as a dating tool on Holocene clay deposits; a collaboration that I hope to continue in the near future. Grain-size analyses of 3000+ samples were carried out in the Martin Konert sedimentary laboratory of the VU University Amsterdam. I admire (envy) the professionalism of the staff (Martin Konert, Martine Hagen, Roel van Elsas, Wieske Wentink, Jasmijn van 't Hoff, and Maarten Prins), the quality of the facilities, and the bright pink colour on the walls of the laboratory. I spent many days preparing and measuring my samples, which became more bearable by the coffee breaks. With Maarten Prins, I had amusing conversations in general and fruitful discussions. Maarten also performed End Member statistics on the data, which became a powerful tool in my research for the estimation of flood magnitudes and opened up opportunities for interesting side-projects (also based on the work of Gilles Erkens). For statistical expertise I could rely on Sofia Caires, who provided prefab statistical modules, which saved me loads of precious time and probably many errors, regarding my unorthodox modelling scripts. Maarten Kleinhans is acknowledged and thanked for discussing hydraulics and fluvial processes, and for provoking me (in general and) to think about research beyond basic academic skills.

Although most people in the Physical Geography department were not actively involved in my project, I thank them for creating a nice ambiance with the right combination between coffee breaks, drinks, and discussion. In my opinion, Juul Beltman and Chris Roosendaal form an essential part in the FG-biosphere. Juul keeps the show going by arranging everything and forcing people to bring cake on their birthdays. Chris has been vital for successful field campaigns with his technical insight and logical hands-on approach, something that is sometimes not very easy for scientists. Keeping up moral, in the field and in the coffee corner, is also an underestimated quality Chris possesses, but which can make a big difference in the joy of doing a PhD. Of course every frequent visitor of the coffee breaks (like I was) and the botanical gardens (only during sunny weather) is thanked for lending an ear to my occasional frustrations.

In these years, a bond has been forged with some of my closer colleagues, and for them I have some special words. First, my part-time roommate and paranimf Jan Peeters. I met Jan early September 2002 as my student tutor; I watched carefully, learned fast and became almost equally dedicated to student-life. You started your PhD-project half year later than me at the same department and got stationed in my room. We had great discussions and epic fun (e.g., greetings on German radio), but it was probably for the best that you were not here every day, as focus on research was sometimes difficult. Second, I have to mention my second paranimf Gilles Erkens. Gilles was already a very senior PhD-candidate when I started my project. I admire your attitude to research

(which resulted in collaboration on some side-projects) and life in general. Furthermore, I never met anybody before who prefers people calling him 'Daddy G'. Last, I want to mention Wietse van de Lageweg and Wout van Dijk. Although I frequently made fun of your experimental playing-in-the-sandbox-research, we had ongoing discussion about 'experiment – real world', which I found quite interesting. I liked the 'quid pro quo' deal of helping each other with hazardous jobs; I broke Wietse's back with a record-hand-core-drilling of 12.5 m through sticky clay, you broke mine during the filling and emptying of the Eurotank. Mondays mornings were always the perfect moment to reflect on football – me being often in a perfect mood. Together with Wietse I was involved in organizing workshops for PhD's of the Geosciences Faculty (UGG). Memorable were the numerous 'evaluatie-uitjes', sometimes multiple after a single event. I also want to acknowledge all other PhD's involved in the UGG; Marlous, Joyce, Lennart, Helen, Ralph, Joeri, and Jelle.

During my field campaigns, I was frequently accompanied by BSc and MSc students. Tiuri Konijnendijk, Ludo Nijsten, Tim Winkels, Michiel de Molenaar, Joost Aloserij, Jochem Ypma, Bas van der Meulen (as a KNAW-assistant), Merijn Bas and Mieke Huisman (Vrije Universiteit Amsterdam) are all thanked for their spirit in completing their theses, despite the hard work in the field and laboratory. I liked the refreshing scientific and social feedback that came out of these collaborations. Wim Hoek, Marcel van der Perk, Kim Cohen, Hans Middelkoop, and Maarten Prins are thanked for being co-supervisors in these projects.

Research and writing a dissertation is probably a way of living, but I treasure the important moments when I could put aside this immense project and could relax a little bit. For these moments I fortunately could rely on friends. Rob, Sjoerd, Jeroen, Eddie, Erwan, Barbara, Eric, Willem, Paul, Nico, and Renee, thanks for being part of my social life. A weekly joy was playing football with the Roze Rakkers. I am happy to see that the old guys have stayed (now nearly all PhD-candidate, and still giving everything) and talented and much fitter youngsters have joined. The main idea behind playing football was to stay in shape, but intensive extra times in the pub prevented any positive effect.

To conclude this preface, and I encourage people to read the rest of my dissertation, I thank my family. My parents are acknowledged for putting me in this world, listening to my oracle-style earth-science stories, and for being dragged to the flooded quay of Nijmegen during high stages of the river Waal in 2011. Of course the most important person to thank is Merian. Merian, thanks for being part of my life and for tolerating my mad-scientist behaviour. Although the last years were pretty slim on long joint holidays, I am glad you support my plans, wash my clothes ;), and make my life wonderful!

1 Introduction

1.1 Flood risk

Over the last decades, major floods caused extensive damage and life-loss throughout Europe (e.g., Benito et al., 2004). Large events occurred in AD 1993, 1995 (e.g., Meuse and Rhine), 2002, and in 2013 (e.g., Danube and Elbe). The magnitude of these '*floods of the century*', and the relative short interval in which they (re)occurred, raises questions about the current safety and protection standards against flooding.

Safety standards along most European rivers are protecting against floods with a recurrence time of few centuries to a millennium (in the Netherlands up to 1,250-yr recurrence time). Discharge measurements of the last century are commonly used in flood frequency analysis to estimate the discharge associated with set safety standards. A major problem in calculating the magnitude of design floods (for dike strength) is uncertainty, which mainly originates from (i) limited data availability back in time, (ii) choice of statistical distribution-fitting for extrapolating frequency-magnitude rating curves, (iii) measurements preciseness, and (iv) an unknown degree of non-stationarity of the flooding regime.

In most catchments measured discharge records span only 40-100 years. This is a limited length for predicting the recurrence time of extreme events (Klemeš, 2000), as short intervals probably poorly represent the distribution of extremes through time. Moreover, catastrophic historical floods (e.g., the AD 1374, and 1651 Rhine-floods, Herget & Euler, 2010; and flooding in AD 1784 across most of NW- and Central Europe; Demarée, 2006; Brázdil et al., 2010) are generally considered to have exceeded observed discharges of the last century, but are not formally included in frequency-magnitude curves (flood frequency analysis) to quantify the discharge of the design flood. In general, flood frequency analysis is often based on short observational records and leads to poor predictions of the recurrence time and discharges of rare events.

The unknown degree of stationarity of the flooding regime further complicates flood frequency analysis based on short data series. It is not expected that frequency and magnitudes of floods have a distribution that is fixed in time. During the Holocene, climate variability and growing human influence have exerted perturbations to the fluvial system, which translates to gradual changes in flood magnitude probabilities. Recent studies suggest that natural variability in the flooding regime echoes cycles of solar activity and intensity variations and shifts in continental-scale meteorological patterns (Jacobeit et al., 2003; Mudelsee et al., 2004; Bárdossy & Filiz, 2005; Brázdil et al., 2006; Macklin & Lewin, 2008; Czymzik et al., 2010). Furthermore, even small changes in climate can trigger significant change in flooding regimes of rivers (Knox, 1993). Timescales on which some of these variations act exceed the length of a single century. This is an extra reason why using exclusively the 20th century discharge record could result in biased flood frequency analysis outcomes – and may therefore not be representative for the system over longer periods. Moreover, by looking at non-stationarity in the past, useful insight may be gained about the possible effect of future climate change. Besides climate-induced non-stationarity, human alterations to the catchment, floodplains and river channel are a factor in changing flooding regimes, especially in

recent centuries (Lammersen et al., 2002; Bronstert et al., 2007; Vorogushyn & Merz, 2012). Increased run-off by gradual deforestation and urbanization (Hundecha & Bárdossy, 2004), and more effective flood pulse propagation by the large-scale construction of embankments and straightening of river channels (Silva et al., 2001; Lammersen, 2004) presumably has affected peak levels and recurrence intervals of floods.

The overall objective of this study was to reconstruct the size and occurrence of extreme river floods in the past centuries to millennia using historical and sedimentary archives, which should allow to improve current estimates of extreme (design) floods and to assess non-stationarity in flooding regimes. As sedimentary flood records were not yet readily available, a significant part of this study focused on the development of methodology to unlock sedimentary information for flood research. This includes; (i) identification of suitable fluvial environments for flood record registration, (ii) establishing how grain-size information from deposited flood beds relates to discharge measurements and historical records, (iii) determining to which degree general changes in floodplain morphology are contained in fluvio-lacustrine sequences, and may overprint pure flood signals, (iv) exploring how sedimentary information can be used to improve non-linear age-modelling and application of event-stratigraphy, and (v) strategies for compiling a composite flood record, based on multiple individual sites in the same region, but largely covering different periods.

This sedimentary approach to lengthen flood series was chosen as an alternative to complementary methods, which focus on generating information from existing datasets using coupled meteorological-hydrological models (e.g., Buishand & Brandsma, 2001; Te Linde et al., 2010), or exploring new statistical methods (Chbab et al., 2006). In this study, sedimentary records were cross-validated against observational measurement data and historical records, and among overlapping sedimentary records (Fig. 1). The Lower Rhine river (in Germany and The Netherlands) was used as a 'real-world' laboratory to develop this approach, because this is a flood-prone area, discharge measurement series and historical records are relatively long (respectively reaching back to AD 1901 and ~1350), and extensive previous geomorphological studies provide the ideal context for the setting of the research area for deploying a sedimentary approach (e.g., Berendsen & Stouthamer, 2001, Gouw & Erkens, 2007; Erkens et al., 2011).

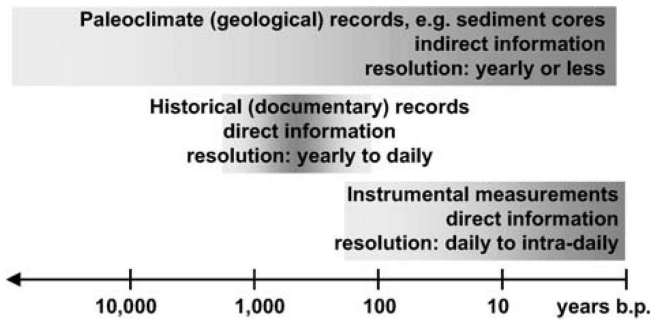

Figure 1: Available archives for flood records; shades indicate accuracy of data type (from Glaser & Stangl, 2004).

1.2 The river Rhine

Originating on the northern flanks of the Alps and flowing into the North Sea, the Rhine transverses approximately 1233 kilometers. After passage through the Rhenish Shield upland, where several large tributaries join (Moselle and Main; Fig. 2), the Rhine occupies a gradually widening alluvial valley, in which it has formed wide meander bends during the Holocene (e.g., Erkens et al., 2011). Where it crosses the border between Germany and the Netherlands the river splits in three distributaries of which the floodplains have been completely embanked since the 13th century (Fig. 2).

The principle gauging station along the Lower Rhine is located at Lobith, at the Dutch-German border (Fig. 2), just upstream of the delta apex bifurcations. Since AD 1901, daily discharge measurements are available. At Lobith, the mean annual discharge of the Rhine is ~2,200 m^3s^{-1}. In the modern situation, with silted-up embanked floodplains and a groynes-fixated and deepened navigable channel, most floodplains are inundated when the Rhine discharge at Lobith exceeds 7,000 m^3s^{-1}, although some parts of the floodplain start to inundate already at 4,000 m^3s^{-1} (Middelkoop, 1997). Largest measured floods occurred in AD 1926 and 1995, with respectively a discharge of 12,600 and 11,800 m^3s^{-1}.

Although flood pulses can be generated in several different ways in the Rhine catchment, the hydrological-meteorological situation that triggers largest floods is when thawing of large volumes of accumulated snow in the hinterland occurs simultaneously with high-intensity precipitation events brought by the passage of cyclonic depressions across central Europe and the northern Alps. Most such floods occur in January to March. The magnitude reached in the Lower Rhine during such situations is sensitive to the timing of flood pulses arriving from the main tributaries (Disse & Engel, 2001). Highest magnitudes in the Lower Rhine are experienced when flood pulses from the rivers Moselle, Main and Neckar enter the Rhine synchronously and add up to raised water levels in the Upper Rhine, as was the case during the major floods of the 1990s. Discharge peaks have not been the only flood-inducing mechanism in the Lower Rhine. In historical times, especially during the coldest part of the Little Ice Age (~16-18th century), ice jams have also caused catastrophic floods in the Lower Rhine, by locally raising water levels and weakening dikes by ice-loading towards the end of severe frost periods. In recent times, with channelised rivers, intensified shipping and industrially slightly warmed river water, ice jams no longer occur.

In 1993 and 1995, the Lower Rhine (Germany) and Rhine Delta (the Netherlands) suffered from discharges that were previously associated with recurrence times of respectively 80 and 100 years (Chbab, 1996). Inclusion of these events in flood frequency analysis for periodic re-evaluation of safety standards (Waterwet, 2009), turned out to lead to considerably shortened statistical recurrence intervals for large floods. It was reason to raise the discharge of the 1,250-yr design flood from 15,000 to 16,000 m^3s^{-1} (Chbab, 1999; Fig. 3). Under projected climate change with an increase in temperature and precipitation amount and intensity (Milly et al., 2002; Pinter et al., 2006; IPCC, 2007; Veerman, 2008), it is anticipated that the design standard for dikes in the Netherlands might be raised further.

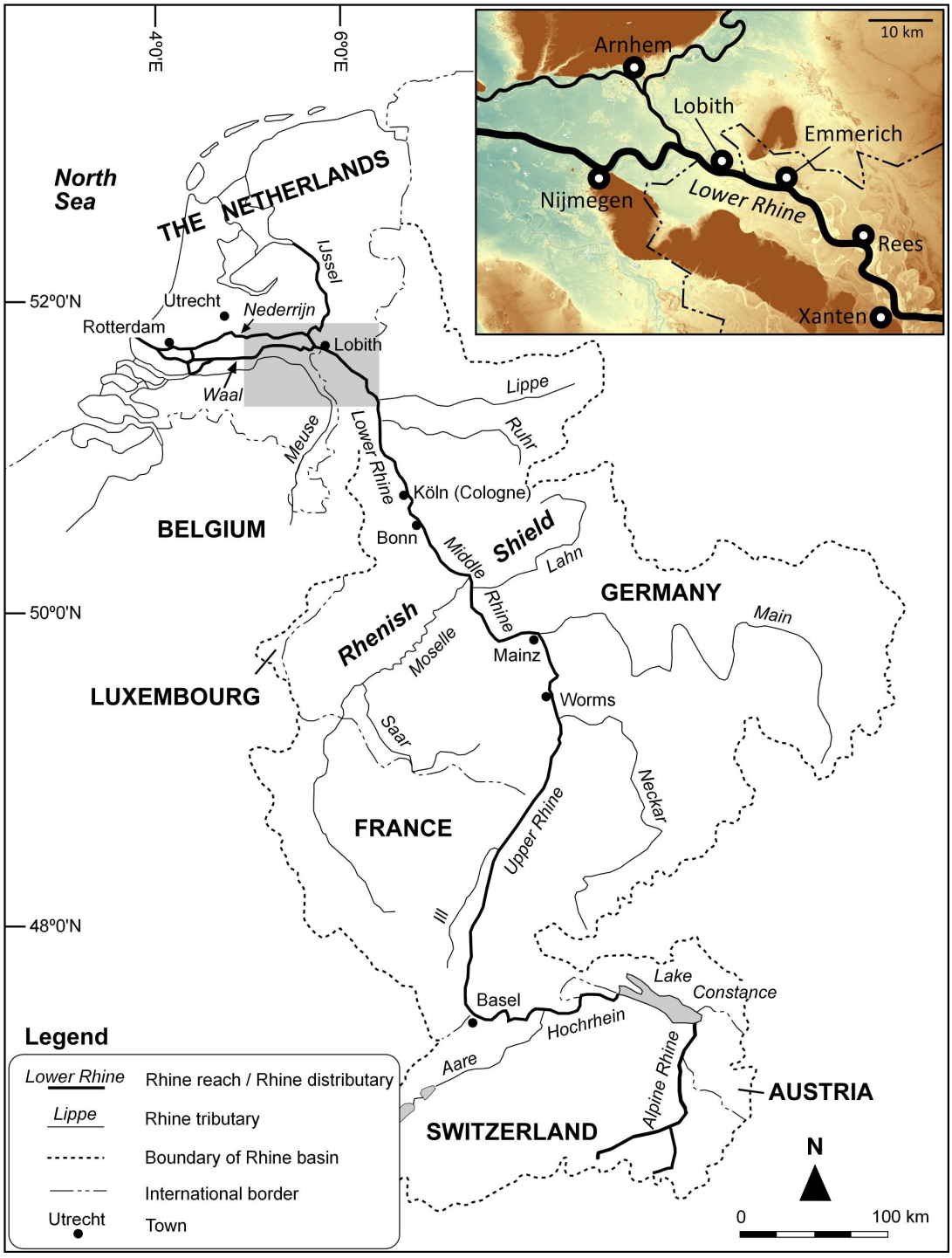

Figure 2: Drainage basin of the Rhine with main tributaries (after Frings, 2007; Erkens, 2009). The research area is magnified in the inset (brown colours = Saalian ice-pushed ridges, 20-80m +msl, and the Lower Rhine Valley, 10-20m +msl; green colours = Rhine delta plain, 0-10m +msl).

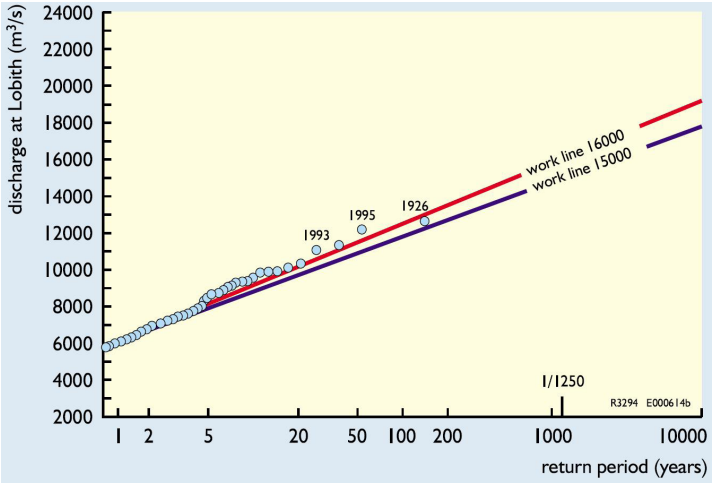

Figure 3: Established flood frequency-magnitude plot for the river Rhine at the Dutch-German border: The design flood (1/1,250-yr recurrence) follows from extrapolation. In blue: before the AD 1993 and 1995 floods were included, after in red (from Silva et al., 2001).

1.3 Palaeoflood hydrology

An important source of information that can be used for the protection against floods comes from palaeoflood hydrology. Palaeoflood hydrology is the study of floods that have occurred in the past without being monitored or have been documented accurately in historical records (Baker, 2008). The combined use of hydrology, geology, and statistics for reconstructing palaeofloods provides useful information on the magnitudes and recurrence times of extreme events, which are generally considered to be poorly assessable from short instrumental records alone (Klemeš, 2000).

Palaeoflood hydrology methods so far have mainly been developed at upper fluvial reaches (often deeply incised) in semi-arid environments, particularly using slackwater deposits as palaeostage indicators (SWD-PSI; Baker, 1987; Baker et al., 2002; Benito et al., 2004; Saint-Laurent, 2004). In these settings, SWD-PSIs can be combined with numeric hydraulic modelling to calculate fairly accurate palaeoflood discharges (Denlinger et al., 2002). Unfortunately, this approach is not transferable to lower fluvial reaches with broad alluvial valleys and in delta environments. In these lowlands with broad floodplains, SWD-PSIs are formed rarely at levels above the regularly inundated floodplain due to limited vertical separation of floods in the bankfull-exceeding domain. Also, flood event beds are difficult to trace in aggrading environments that receive sediment with every flood. Moreover, it is difficult to relate SWD-PSIs to absolute discharges in an alluvial valley, because of the dynamic geomorphology and vegetation, which requires extensive reconstructions of the palaeo-environment. In flood frequency analysis for downstream reaches, one cannot simply rely on upstream palaeoflood reconstructions – especially in large and complex catchments -, as flood pulses do not simply 'accumulate' in a downstream direction, but tributary flood waves tend to dissipate. Independent baseline studies and alternative approaches are required for studying flooding frequencies of lower fluvial reaches. Yet, palaeoflood hydrology studies in lower reaches of fluvial systems and river deltas are increasingly needed, as there is an increasing socio-politically

need for upgrading flood protection due to increasing population density and projected effects of climate change (IPCC, 2007).

The use of general palaeoflood hydrological methods in the apex area of the Rhine Delta and broad river valley of the Lower Rhine comes both with advantages and disadvantages for reconstructing palaeofloods, compared to upstream incised reaches in a (semi-)arid setting. Major advantages lie in the aggrading environment and lateral space for preservation of abandoned channels, which are blessed with a high preservation potential, theoretically for all-sized flood deposits larger than bankfull level. This creates an opportunity to study sedimentary characteristics and utilisation of this data to differentiate between flood magnitudes (e.g., Bøe et al., 2006; Wolfe et al., 2006; Moreno et al., 2008; Støren et al., 2010). The result is a more complete distribution of flood magnitudes and associated recurrence times. Other advantages are the availability of datable material in channel fill deposits and long historical records in densely populated delta environments (back to the Late Medieval period in Europe; Brázdil et al., 1999). Datable material, preserved in the clayey deposits ranges from local terrestrial seeds (AMS radiocarbon), pollen, organic content variations, and the possibility to use event-stratigraphic approaches in cross-correlating flood event layers in the network of investigated sites. Moreover, a significant part of the sedimentological flood record can be verified with detailed historical records (e.g., Buisman, 2000), which allows significant improvements in geochronology, palaeoflood magnitude and recurrence time reconstructions (Glaser & Stangl, 2003; Herget & Meurs, 2010; Macdonald & Black, 2010).

1.4 Research approach

As a starting point to lengthen flood records, available instrumental observational data on Rhine discharges and water levels from different stations in the apex area were gathered, combined and re-analysed in a flood frequency analysis assessment (Chapter 2). This resulted in discharge series back to AD 1772, which allowed analysis of the impact of increased data availability on estimated recurrence times associated to large floods. In further parts of this dissertation, this dataset is used as the calibration set for palaeoflood magnitude quantification based on grain-size records of flood beds contained in floodplain lakes (Chapter 5).

A second step was to find and select suitable locations for retrieving palaeoflood records from filled palaeochannels, which hold most-suitable sedimentary layering for palaeoflood history reconstruction. Working towards a network of cored sites from the apex of the Rhine Delta, preferably with overlap in time so that the records together produce a long sedimentary record out of multiple sites, required thorough understanding of the sedimentary architecture of channel fills and assessment of the suitability of avulsion-abandoned residual channels in the delta versus cut-off disconnected oxbow lakes (Chapter 3).

Third, high-resolution sedimentary data and high-resolution age-control were obtained from the sedimentary sequences. How channel fill sedimentology is used in refining age-depth models is developed in Chapter 4, for a selected Middle Holocene oxbow fill from near Rheinberg (Germany), based on a pilot study for this PhD-project. Sedimentary data analysis was expanded with laser diffraction grain-size measurements, continuous at a cm resolution. This enabled in-depth characterisation of the coarse-tails of grain-size distribution of encountered flood layers, amongst other by deployment of End-Member Modelling (Weltje & Prins, 2007). How well

this sedimentary information records flood magnitudes is described and tested on sites Bienener Altrhein (Germany) and Zwarte Gat (The Netherlands), making use of the overlap of the upper halves of the two sequences with the instrumental discharge series and historical record (Chapter 5).

Chapters 2, 3, 4 and 5 each serve as methodological development and cross-validation steps for palaeoflood reconstructions produced at individual sites, preparing the integrative step of a multi-millennia long record from multiple overlapping cores. To obtain an independent check on flood magnitudes and recurrence times inferred from sedimentary imprints in the realm of extreme floods, a more classical slackwater-palaeohydrological study was carried out (Chapter 6). Using Middle Holocene palaeostage indicators of rare extreme floods, the upper hydrological bounds were explored, including numeric estimation of the absolute discharge of a specific palaeoflood of millennial recurrence.

Chapter 7 presents the collated Holocene flood chronology for the Lower Rhine. A composite event history was established from the network of cored sites, distributed over the upstream part of the Rhine Delta and the Lower Rhine Valley to assure sufficient temporal and spatial resolution and cross-verification opportunity. This independent long record identifies the timing and relative size of major floods, back to 8,200 years ago. The record also enabled analysis of extreme flood magnitudes, their timing and clustering in time, and provided insight in long-term variability and non-stationarity of the flooding regime of the Rhine.

2 Flood frequency analysis and discussion of non-stationarity of the Lower Rhine flooding regime (AD 1350-2011)

Using multiple-site discharge data, water level measurements, and historical records

Toonen, W.H.J.* [1,2]

[1] Dept. of Physical Geography, Utrecht University, Utrecht, The Netherlands.
[2] Dept. of Applied Geology and Geophysics, Deltares BGS, Utrecht, The Netherlands.
* Corresponding author: E-mail: w.h.j.toonen@gmail.com

1 Introduction

Floodplains of the Lower Rhine river in the Netherlands are completely embanked since the 14th century to protect against floods (Hesselink, 2002). A national flood protection act (Waterwet, 2009) enforces protection against a flood with a statistical recurrence time of 1,250 years (the design flood, Q_{1250}). The value of Q_{1250} is periodically assessed from statistical extrapolation of observational data. Two broadly acknowledged problems in the accuracy and validity of such design flood estimations are (i) statistical uncertainties in estimated recurrence intervals of extreme events (Klemeš, 2000), and (ii) non-stationarity of the flooding regime (Knox, 1993; Redmond et al., 2002; Milly et al., 2008); the temporal variability of recurrence intervals associated with discharges.

Present estimates on the magnitude of Q_{1250} of the Lower Rhine yield relative large uncertainties (Chbab et al., 2006; te Linde et al., 2010). Estimates of Q_{1250} are based on extrapolated discharge measurements since AD 1901. This ~110 years of measurements is a limited interval for the prediction of extreme events as such a period has a high probability to lack sufficient registration of rare very large flooding events, troubling an accurate estimation of frequency-magnitude relations in the millennial recurrence domain (Klemeš, 2000). The sensitivity of design flood estimates to rarely occurring events was demonstrated in the Q_{1250} re-assessment that followed the large AD 1993 and 1995 Rhine floods (magnitude <Q_{100}; Chbab, 1996). Addition of these large floods as data-points to the extrapolation resulted in a ~7% increase in the estimate of Q_{1250} (from 15,000 to 16,050 m^3s^{-1}; Chbab, 1996).

Previous exercises to assess Q_{1250} and its uncertainty mainly depended on increasingly advanced numeric simulation techniques. This includes analysis of stochastically resampled 20th century datasets, the use of precipitation generators in combination with run-off models, and Bayesian weighting of different extrapolation methods (Chbab et al., 2006; de Wit & Buishand, 2007; te Linde et al., 2010). Although this maximises the use of 20th century datasets and creates useful

scenarios for engineering, these approaches still have difficulties to fundamentally improve the reliability of rare event magnitude and recurrence time predictions. Moreover, functions to describe extreme value distributions used routinely in flood frequency analysis are mainly chosen based on their goodness of fit on gauged data and lack specific hydrological justification (e.g., Kidson & Richards, 2005). This implies that statistically more-sophisticated approaches do not necessary lead to better characterisation of the hydrological system and may be poor predictors of extremes despite their goodness of fit on measured low-magnitude data.

Non-stationarity of the flooding regime further complicates frequency assessments of extreme floods. Non-stationarity includes changes in the relation between flood magnitude and frequency over time. In general it is assumed that small changes in meteorological patterns and flood distributions can have large effects on (the estimated discharges of) extremes (Knox, 1993). Human influence and climatic variability together are the main drivers of non-stationarity. Human-induced non-stationarity is the result of deforestation and other land use changes in the upstream basin, and ongoing river management. Deforestation of the Rhine hinterland, initiating in the Neolithic Period and reaching an optimum in the Medieval Period (Kalis et al., 2003; Lang et al., 2003), probably has influenced effective runoff, which increased the probability of large discharges downstream in the catchment (e.g., Hundecha & Bárdossy, 2004). River engineering works along the Rhine have intensified since the early 19th century (Lammersen et al., 2002). The embankment, fixation and deepening of the channel bed, shortening by artificial cut-offs, and recently the construction of retention basins, all have altered flood pulse propagation and flood regimes. Several studies (e.g., Engel, 1997; Pinter et al., 2006) suggest that extreme flooding of the Rhine has increased significantly in the 20th century, partly due to human influence on channel morphology, and valley and hinterland land use, besides climatic variation. Current measured discharge data do however not cover the pre-management era, making comparison and quantification of this effect difficult.

Climate-induced non-stationarity in flooding is widely recognised, especially for the Little Ice Age (LIA; e.g., Barriendos & Martin-Vide, 1998). Various studies have shown that decadal to millennial periodicities can be identified in Holocene flooding (e.g., Brázdil et al., 2006; Macklin & Lewin, 2008), which correlate with meteorological patterns or solar activity (e.g., Redmond et al., 2002; Czymzik et al., 2010; 2013). The existence of periodicity in flooding is problematic for flood frequency analysis, as estimates are biased when not the entire cycle is covered in the sample data set. Furthermore, in flood frequency analysis aiming to characterise the present situation, it is important to correct (i.e. normalise) or remove data from periods that differ from the current state of the flood regime. In this respect, only permanent changes or trends, or changes that are caused by climatic cycles that act on longer time scales than the discharge record spans, need to be assessed. Annual, decadal and even centennial cycles can be incorporated in flood frequency analysis if they are an intrinsic part of the fluvial system, and sufficiently covered in data series.

To achieve better estimates of the discharge of the design flood, and to be able to quantify the effect of non-stationarity, the most straightforward approach is to extend data series back in time. The current reference dataset for the Lower Rhine in the Netherlands is the discharge measurement series since AD 1901 at Lobith (Q_{Lob}; Fig. 1). Systematic discharge measurements at Cologne (Germany; Fig. 1) go back to AD 1817, continuous water level records go back as far as AD 1772 at several gauging stations in the direct vicinity of Lobith (Fig. 1), and historical records of Rhine

floods are sufficiently reliable starting from AD 1350 (Glaser et al., 2010). At present, the potential of these records has not systematically been explored for estimating Q_{1250} in the Netherlands. Inclusion of discharge data and water level measurements from alternative locations would roughly double the span of present data for calculation of the Q_{1250}, which provides, together with information from historical records, valuable information to assess non-stationarity over multi-decadal to centennial time-scales. Furthermore, comparison with palaeoflood chronologies (Benito et al., 2004; Baker, 2008) and reconstructed extreme events, based on historical information (e.g., Herget & Euler, 2010; Wetter et al., 2011), gives useful insight in the maximum possible discharge and timing of large events – which can serve as important input for current flood frequency analysis (Stedinger & Cohn, 1986).

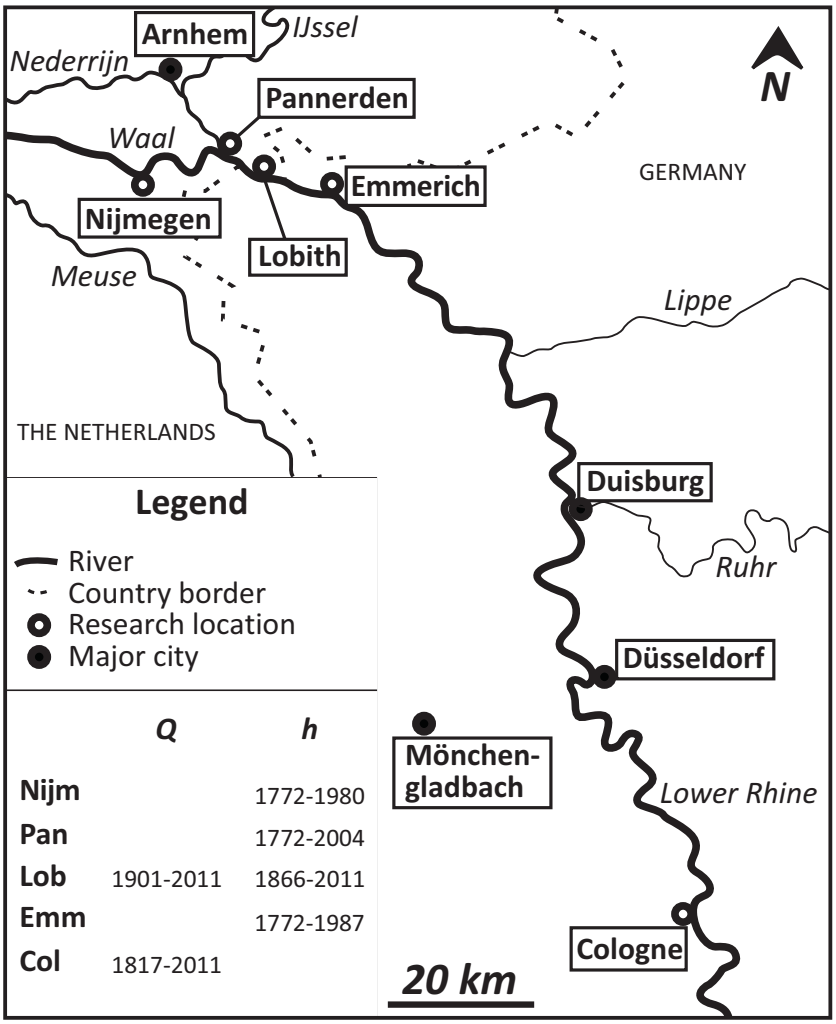

Figure 1: Map of the research area between Cologne (Germany) and the apex of the Rhine-Meuse delta (The Netherlands). The inset shows the length (years AD) of discharge (Q) and water level (h) data records used in this paper. Abbreviations in the inset relate to research locations on the map.

The goals of this paper are (i) to reduce uncertainty in the assesment of Q_{1250} of the Rhine at Lobith by extending data series using alternative data types, and (ii) to analyse the possible effects of non-stationarity of the flooding regime on the distribution of extreme events and the calculated magnitude of the design flood. Alternative data types are combined with existing discharge series in order to extend the reference period for estimating Q_{1250}. The generalised extreme value (GEV) distribution was applied in a frequency-magnitude analysis on the resulting reconstructed discharge series. Uncertainties in the original and converted data are carefully assessed and quantified, and included in the extrapolation. In an attempt to include information from historical flood records back to AD ~1350, the use of intensity classes is explored (Glaser & Stangl, 2003). With the newly gathered flooding data, the effect of non-stationary behaviour of the flooding regime on flood frequency analysis is discussed.

2 Discharge estimates from alternative sources

Data was gathered from several locations and source types, which asks for different pre-processing to merge them into a uniform discharge record. Depending on the source location, data type, and age of the measurements, discharge data comes with different uncertainties. This section elaborates on the methodology used to generate a uniform flood record and specifies involved uncertainty ranges.

2.1 Modern discharge data [AD 1901-2011]

Daily discharge measurements at Lobith go back to AD 1901 (Waterbase, 2012). Modern discharge data is often used in flood frequency analysis as a uniform series assuming similar uncertainties in measurements, or without consideration of uncertainties at all. It is however important to acknowledge that different methods have been used over time to record discharges, all with a different precision. As this paper aims at assessing all common sources of uncertainty and include these in the flood frequency analysis, it is important to quantify uncertainty in different periods – also in the modern era.

From 1901 until approximately AD 1950, discharge estimates for the Lower Rhine were based on the velocity of floating sticks on the water surface. Because this method only measures flow velocities at the surface, calculation of the total discharge depends on extrapolation (depth-velocity profiles), which results in a ~10% uncertainty (pers. comm. Rijkswaterstaat, Dienst Oost-Nederland, Meet- en Informatiedienst). From AD 1950 – 2000, current meters were used to produce velocity-depth profiles; the uncertainty of this method is estimated to be ~5% of the total discharge. Since AD 2000, Acoustic Doppler Current Profilers have been used. The uncertainty of this method is negligible, with exception of discharges of small floods exceeding bankfull discharge (for the Lower Rhine 4,000 – 8,000 m^3s^{-1}; Middelkoop, 1997), when large parts of the inundated floodplains have a too limited water depth to be accessible by boat and discharges are estimated by interpolation. In this range, an uncertainty of 5% applies to the data. Modern discharge data was not normalized for effects of river management in the last century, as this only results in a <1% increase for extreme floods (Parmet et al., 2001; Vorogushyn & Merz, 2012) – a value which is insignificant in comparison to measurement precision. In this paper, these specified measurement uncertainties were used for Monte Carlo resampling in flood frequency analysis (section 3.1).

2.2 Discharges Cologne [AD 1817-2011]

Annual peak discharges at the German city of Cologne were used to extend measured discharge series for the Lower Rhine in the Netherlands back to AD 1817. The distance along the river between Lobith and Cologne is roughly 160 kilometres. As both sites are located on the same fluvial trunk valley, share the same hinterland, and have only minor tributaries joining in between (Ruhr and Lippe; Fig. 1) discharge at Cologne correlates strongly with Q_{Lob}, based on a simple linear regression analysis (R^2 = 0.96; Fig. 2) for annual peak discharges in the period AD 1901-2011. Data was screened for multiple annual maxima that originate from the same flood wave – occurring within several weeks, but forming annual maxima in two successive years of measurement; the lower value was replaced by the second largest flood maximum of that year. For years in which several similar discharge peaks were recorded, the annual peak discharge of Cologne was not necessarily also the largest peak at Lobith. These 'mismatched floods' were replaced to fit the same discharge wave at both locations; Q_{Lob} at maximum 2 days after the peak discharge at Cologne. Mismatching floods were only excluded from the correlation between the two sites on which the conversion of data is based, and not in the extrapolation for the design flood (section 4 of this paper).

A linear regression (Fig. 2) was used to convert discharge at Cologne into discharge for Lobith. In the overlapping period of discharge measurements per location [AD 1901-2011], Cologne-predicted discharges for Lobith (Q_{Lob_QCol}) were compared with measured discharges. Despite the good correlation, the predicted Q_{Lob_QCol} ranges ~12.7% of the measured Q_{Lob} (in this paper two-sided 95% confidence intervals are given). This is probably caused by the various ways a flood wave can evolve over short distances – due to differing contributions of minor tributaries and discharge wave dispersion by floodplain inundation. During the first and second World Wars, there seems to be a particularly poor correlation, likely due to limited precision of measurements (the Cologne measuring station and several bridges were destroyed during World War II). Exclusion of war periods does, however, not significantly increase the correlation between sites and does not decrease the uncertainty interval. Based on the linear regression, annual peak discharges between AD 1817 and 1900 from Cologne were added to the Lobith record (Fig. 2).

2.3 Water level measurements [AD 1772 – 1987]

Daily water level measurements at Lobith (H_{Lob}) are available from AD 1866 onwards (Waterbase, 2012); fragmental data records are available for Lobith since AD 1824. For the period AD 1772-1866, water levels were reconstructed, based on information from the nearby gauging stations at Emmerich, Pannerden, and Nijmegen (Fig. 1). To convert water level information from alternative sites into discharge estimates, trends in water levels due to different local QH-relations were removed from all locations. Detrended water levels from alternative sites were correlated with measurements from Lobith in overlapping periods. Based on the linear regression between the sites, water level measurements from alternative locations before AD 1866 were converted into a water level for Lobith. The average of predictions from alternative sites was then used to estimate the water level for Lobith ($H_{Lob\text{-}region}$) and the associated uncertainty interval. The inter-location variability of predictions was used to detect outliers and to identify the deviating location and possible cause; in most cases ice-jamming during severe winters. This variability has also been used to verify water level measurements at Lobith after AD 1866. The estimated $H_{Lob\text{-}region}$ was converted into discharges ($Q_{Lob\_Hregion}$), using stage-discharge relations at Lobith.

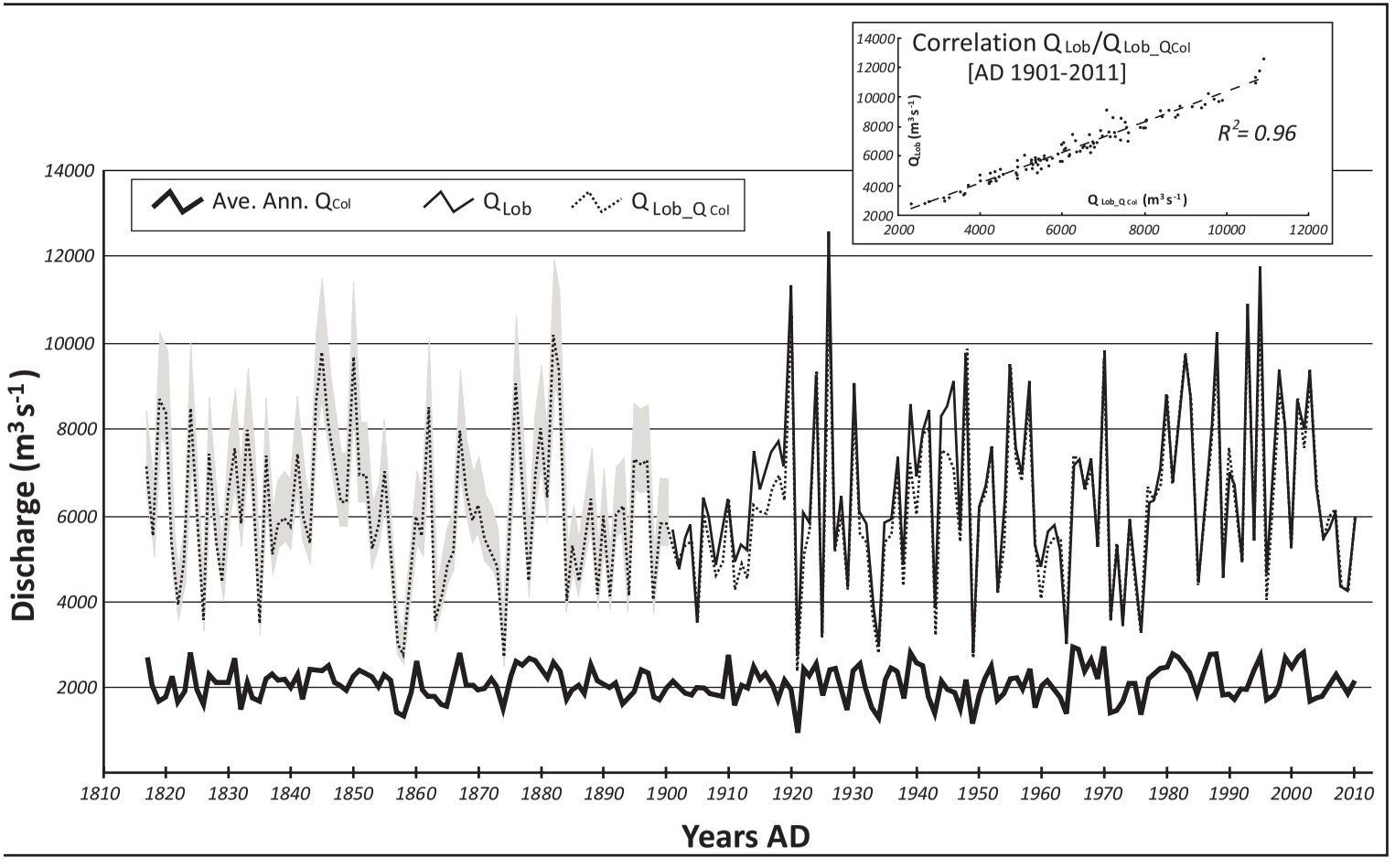

Figure 2: Annual average discharges at Cologne, predicted annual peak discharges for Lobith based on measurements from Cologne [AD 1817-2011], and annual peak discharges at Lobith [AD 1901-2011]. The linear regression (inset at top right) is used to relate discharge from Cologne to Lobith [AD 1817-1900]. The 95% confidence interval for QLob_QCol is indicated with a grey shade.

Trends in local water levels after AD 1817 (and to a lesser extent also before) are most likely related to changing bed morphology, as average discharges did not change significantly in the investigated period (Fig. 2). In an attempt to detect and remove the effects of changing bed levels, change point analysis (CPA; Taylor, 2000) was used to identify breaks in annual average water levels (Waterbase, 2012). The change points divide water level trends; intervals in between were detrended separately. Two important knick-points in water levels were observed (CPA >95% confidence level) for all investigated sites in 1856 and AD 1942 (Fig. 3). After AD 1850, major works commenced in the river Rhine, aimed at reducing flooding risk and improving nagivation. Along large sections of the river, groynes were constructed to reduce channel width (and increase depth), main channels were dredged, bars were removed, meanders were cut-off, and weirs were constructed (Silva et al., 2001; Vorogushyn & Merz, 2012). Before that period, the channel bed was degrading on average ~7 mm per year in Emmerich, while some aggradation occurred downstream. From 1856 to AD 1942, no significant changes in water levels are distinguished at Lobith (at the other stations some aggradation occurred; Fig. 3). The second knick-point in water levels (AD 1942) is presumably also due to long-term effects of river management (and dredging), although no specific project can be targeted. Since AD 1942, channel bed degradation occurred at Lobith with an average rate of ~11 mm per year. Pannerden also shows some bed degradation, although at a slower rate. Emmerich and Nijmegen show aggradation in the last measured decades, but this may be attributed to the limited length of those data series, which influences the validity of trendlines. Still, at these locations a transition to lower water levels and a similar trend to longer series at other locations is visible (Fig. 3).

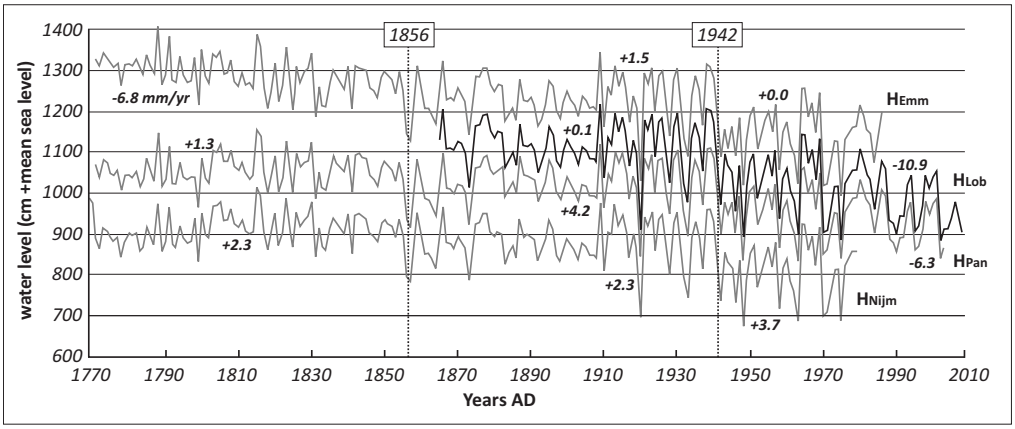

Figure 3: Annual average water levels from all research locations with identified change points (AD 1856 and 1942) and information on trends in channel bed aggradation or degradation (in mm/yr).

Following a similar approach as for the conversion of discharges from Cologne, with similar data series screening, annual maximum water levels from Emmerich (H_{Emm}), Pannerden (H_{Pan}), and Nijmegen (H_{Nijm}) were detrended using the identified change points (Fig. 3) and correlated to H_{Lob} with a regression-analysis in overlapping time periods (AD 1866-1942). Water level data after AD 1942 were excluded; the accelerated bed degradation in that period troubles accurate analysis (Fig. 3). Predicted water levels for Lobith from other sites yield only a 2-3% difference with truly observed water levels, demonstrating the quality and consistency of water level measurements after screening. The regressions allow extending water level data for Lobith from 1866 back to AD 1772

(Fig. 4), based on the longer time series of the alternative sites. Predictions for Lobith are based on the three alternative sites that were averaged. Based on cross-correlations of all sites, deviating predictions were traced. Where possible the source location of a deviating prediction was traced. If a measurement from only a single location resulted in an outlier, this location was excluded from the average (Tab. 1). Most such outliers match severe winters with recorded local ice jamming (IJnsen, 1981; Driessen, 1994), and major floods with dike breaching. Ice jamming occurred often in the past (e.g., Buisman, 2000; 2006), but it influenced annual-maximum water levels at our stations specifically in few years only. In 1781, 1799, 1809, 1820, and AD 1830 ice jamming had a regional impact, and for these years the highest observed water levels do not correlate among stations. For the 1799 and AD 1809 flood peaks, the ensemble average water level was used, because ice jams raised water levels, but at the same time dike breaches between gauging stations lowered local water levels considerably. Note that for dike breaches to happen on this regional scale, a large discharge must have occurred. In years when ice jams are reported but no large-scale dike breaches occurred, the lowest recorded water level was chosen (Tab. 1). The flood of AD 1820 was used to verify this procedure, as information from Cologne indicates a moderate flood only (Fig. 2), which suggests that ice jams were the main cause of deviating downstream water level rise.

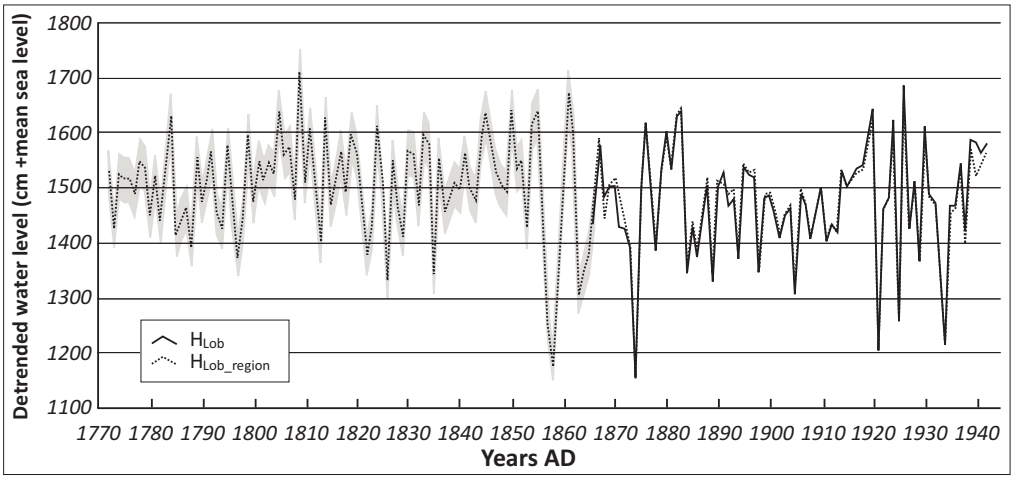

Figure 4: Detrended measured maximum water levels at Lobith [AD 1866-1942] and predicted water levels [1772-1942] with 95% uncertainty range.

Stage-discharge relations were used to convert predicted $H_{Lob\text{-}region}$ into discharges. The QH-relation for annual maxima in the period AD 1817-1942 was derived from the reconstructed discharges (Fig. 2) and water levels (Fig. 4): discharge predictions were adopted from Cologne (AD 1817-1900) and Lobith (AD 1901-1942), water level estimates were taken from the various alternative research locations (AD 1772-1865) and Lobith (AD 1866 – 1942). Data after AD 1942 was excluded for this reference, because bed degradation accelerated, which complicates the use of a single QH-relation for the entire period (van Vuuren, 2005). Years which fit poorly to the initial QH-relation were further investigated. Depending on the possible cause (Tab. 1), some years were excluded for establishing an iterated QH-relation (Fig. 5). Years with high discharges were not removed from the correlation as these are natural outliers. Differences between local water levels

and reconstructed discharges are mostly explained by local dike breaches, ice jams, and excessive contributions from the Ruhr and Lippe tributaries.

Table 1: Overview of poorly correlating water level data and years that are excluded for establishing the stage-discharge relation at Lobith.

Year AD	Type	Action	Cause (references)
1773	Error H_{Pan}	H_{Pan} excluded	Possibly the initiation of the construction of the Bijlands Canal by artificial meander cut-off.
1781	All sites H error	Minimum H_{Emm}	Ice jams (Driessen, 1994)
1795	Error H_{Pan}	H_{Pan} excluded	Ice jams (Driessen, 1994)
1799	All sites H error	-	12 dike breaches (STIBOKA, 1975), ice jams (Driessen, 1994)
1803	Error H_{Pan}	H_{Pan} excluded	Probably ice jams (IJnsen, 1981)
1809	All sites H error	-	Large Q, 9 dike breaches (STIBOKA, 1975), ice jams (Driessen, 1994)
1811	Error H_{Emm}	H_{emm} excluded	Ice jams (Driessen, 1994)
1820	All sites H error	Minimum H_{Emm}	Ice jams, 4 dike breaches (STIBOKA, 1975; Driessen, 1994)
1821	Error H_{Pan}	H_{Pan} excluded	-
1830	All sites H error QH-error	Minimum H_{Emm} Excluded for QH	Probably ice jams (IJnsen, 1981)
1834	QH-error	Excluded for QH	-
1841	Error H_{Pan}	H_{Pan} excluded	Probably ice jams (IJnsen, 1981)
1854	Error H_{Emm} QH-error	H_{Emm} excluded Excluded for QH	- -
1855	QH-error	Excluded for QH	Probably ice jams, 1 dike breach (STIBOKA, 1975; IJnsen, 1981)
1861	QH-error	Excluded for QH	3 dike breaches (STIBOKA, 1975)
1891	QH-error	Excluded for QH	Probably ice jams (IJnsen, 1981)
1940	QH-error	Excluded for QH	Ice jams (Rijkswaterstaat, 1942)

The 95% confidence interval in reconstructed water levels (Fig. 4) propagates in the application of the QH-relation back to AD 1772 (Fig. 5). This results in a ~12% uncertainty range for discharges, which is similar to discharge estimates based on discharge information from Cologne. Comparison of reconstructed discharges in the period [AD 1817-1900], either deduced from Q_{Lob_QCol} or $Q_{Lob\_Hregion}$, shows both results to correspond well. Only in AD 1855 and 1861 major differences exist (Fig. 5). Based on regional water level measurements, these are relatively large floods, while the predictions from Cologne suggest smaller discharges. At the delta apex, in these years reconstructed water levels only deviate several centimetres among sites, which excludes ice jamming as a major factor. From this it is concluded that for these two floods, measured discharge at Cologne is not representative for downstream discharges, most likely due to high discharges from the Lippe and Ruhr tributaries.

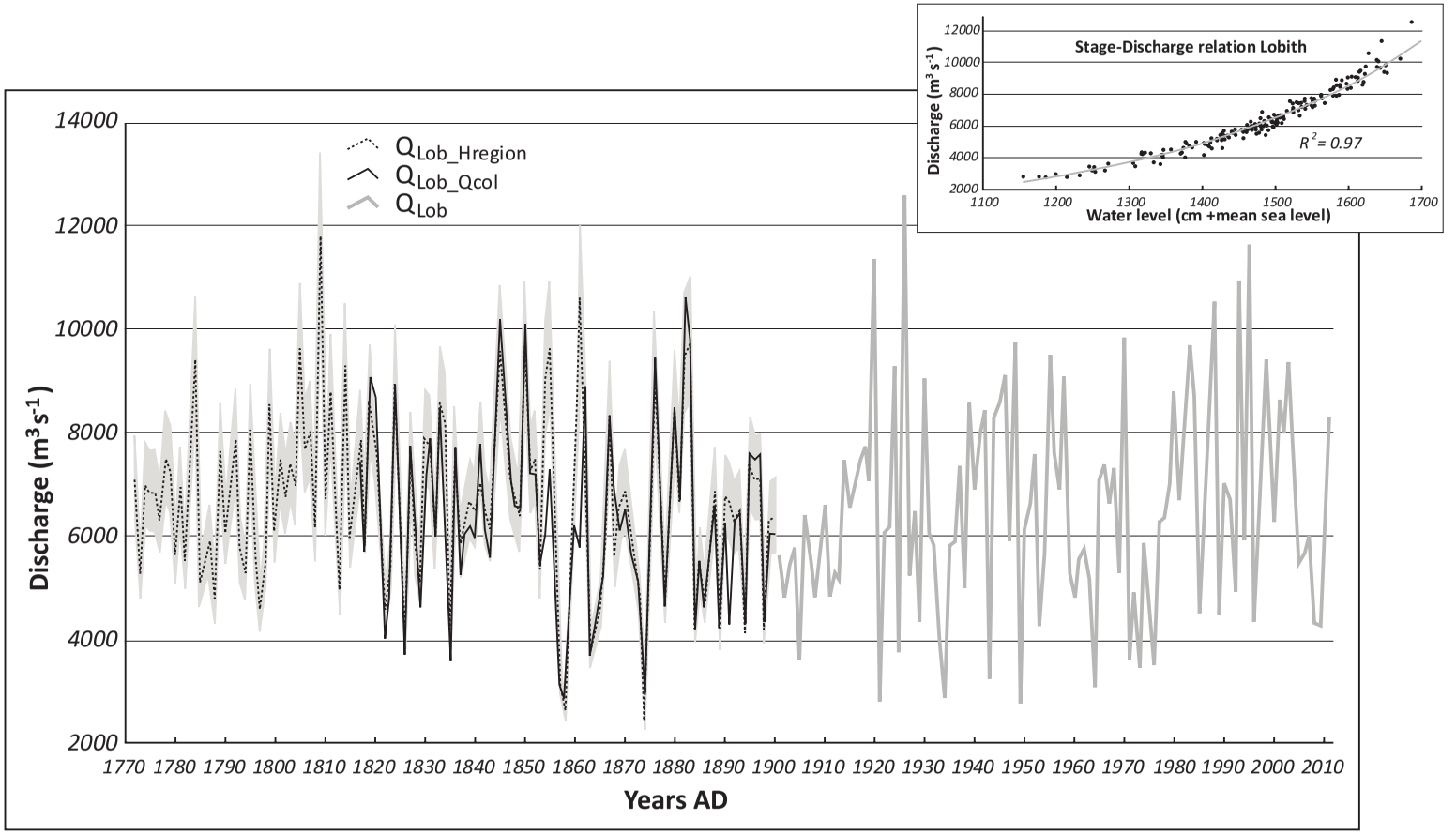

Figure 5: Predicted annual maximum discharges for Lobith [AD 1772-1900] with 95% uncertainty interval (grey shade), using reconstructed water levels (conversion by the AD 1817-1942 stage-discharge relation for Lobith; inset), and discharge estimates for Lobith, based on discharge data from Cologne.

2.4 Historical records [AD 1350 – 1772]

Historical records of flooding events and dike breaches were gathered from the entire Lower Rhine region (compilation from STIBOKA, 1975; Buisman, 1996; 1998; 2000; 2006 and references therein). Information on the period before AD 1350 is not used in this study, because the accuracy of records and source density becomes insufficient (Glaser & Stangl, 2003). Historical records reflect relative flood magnitudes as they are basically damage reports. A by-proxy magnitude of events was obtained following the classification approach of Sturm et al., (2001) and Glaser & Stangl (2003). The geographical spread of reports and extent of damage/life-loss determines class membership and scoring of a flood for the period AD 1350-1772 (Tab. 2). To describe trends in flooding, annual scores were averaged over a 101-year period, resulting in an indexed flood intensity (Fig. 6). This index interval is similar to the period over which estimates of the Q_{1250} are currently made in the Netherlands. For the period AD 1772-present, a similar flood intensity curve was constructed. Discharges were converted into scores, based on the statistical recurrence of the three classes (AD 1350-1772 period; Tab. 2) and associated discharge from flood recurrence-magnitudes relations (AD 1772-2011; this study).

Table 2: Class definitions to generate indexed flood intensity series (shown in Fig. 6) from historical flooding records and modern discharges.

Class/ Score	Description	Recurrence time (AD 1350-1772)	Discharge (AD 1772-2011)
1	+ Single dike breach + Minor damage	2,8 yrs (153 events)	>7160 m^3s^{-1}
2	+ Multiple dike breaches + Moderate damage + Local impact	5,0 yrs (84 events)	>8100 m^3s^{-1}
3	+ Multiple dike breaches + Major damage and life losses + Breaches in Lower Rhine Valley (Germany) and along all deltaic distributaries (the Netherlands)	11,4 yrs (37 events)	>9170 m^3s^{-1}

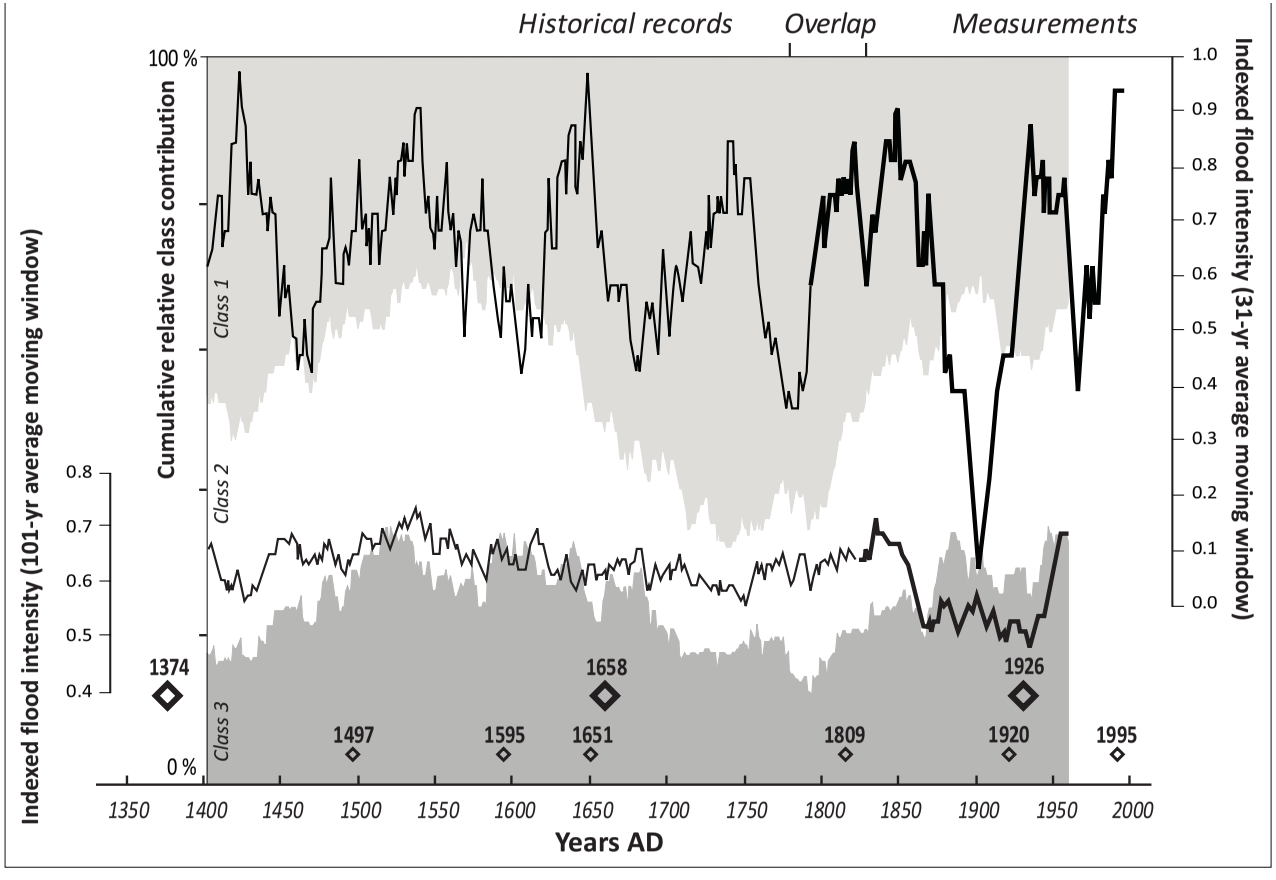

Figure 6: Flooding intensity of the Lower Rhine, based on historical records (lower black line before AD 1822) and recorded discharges at Lobith (lower black line after AD 1822). Mid-point values of the 101-year averaged window are plotted. The 31-year flood intensity is plotted with the upper line (alternative y-axis on the right). Relative contributions of each flood intensity class (Tab. 2) are plotted for the 101-yr window in grey shades in the background; class 1 at the top in light grey, class 3 at the bottom in dark grey. The timing of extreme events is illustrated by diamonds on the time axis. Small diamonds are floods that are assumed to have exceeded 11,000 m^3s^{-1}, large diamonds are floods that exceeded 12,000 m^3s^{-1}.

3 Flood frequency analysis and results

3.1 Generalised Extreme Value (GEV) approach

A flood frequency analysis was carried out to estimate magnitudes of low-probability events. To describe the extreme value distribution, and to estimate the recurrence intervals of extreme events and upper bounds to the system, the cumulative distribution function of the Generalised Extreme Value distribution (GEV; Eq. 1) was used (Fisher & Tippett, 1928; Hosking et al., 1985). In Eq. 1, μ is the location parameter (where the origin of the distribution is positioned), σ a scaling parameter (describing the spread of data), and ξ a shape parameter (controlling the skewness and kurtosis of the distribution). Fitting the shape parameter on the data is essential for describing extreme value distributions, because it importantly affects the upper tail. When $\xi = 0$, the distribution reflects the type I (Gumbel) distribution, $\xi < 0$ is a type II (Fréchet) distribution, and $\xi > 0$ corresponds with a type III (Weibull) distribution. Parameter values were established using probability weighted moments (pwm; Hosking et al., 1985). Ad-hoc tests indicated that the fit with the pwm method of the GEV on the data was slightly better than using maximum likelihood estimators (as used in Stedinger et al., 1988).

Equation 1a
$$F(x) = exp\left\{-\left[\xi\frac{x-\mu}{\sigma}\right]^{\frac{1}{\xi}}\right\} \qquad \xi \neq 0$$

Equation 1b
$$F(x) = -exp\left\{-exp\left[-\frac{x-\mu}{\sigma}\right]\right\} \qquad \xi = 0$$

Although many different approaches, distributions, and fitting methods to describe flood data exist, flood frequency analysis in this paper is restricted to the GEV-approach. This is because focus is not on the comparison of different statistical methods, but on extending data records and to assess non-stationarity with this data. The choice for the GEV distribution was based on previous studies (e.g., Chbab et al., 2006; te Linde et al., 2010) showing the good fit of this distribution on the flooding regime of the Rhine. Moreover, the three-parameter GEV distribution is capable of flattening off at extreme values (introducing an upper bound) by having a flexible tail, induced by the shape parameter. This could correspond with realistic hydrological bounds in a lowland setting, as the relative low valley shoulders near Lobith may have a limiting effect on downstream discharges.

To incorporate uncertainties and probability distributions of measured and reconstructed data, Monte Carlo simulations (1000 repetitions) were used. Values for each data point in the period AD 1772-2011 were resampled within the normally distributed 95% uncertainty interval of the screened measurement data. The width of this uncertainty interval differs according to data type.

3.2 Discharge distributions from historical records

To generate discharge data in the historical period, the modern relation between flood intensity index (average 101-yr score; Fig. 6) and the results of the GEV-discharge estimates for different flood magnitudes was used. If flood intensity is strongly related to the shape of the GEV-distribution, reconstructed historical flood intensities can be used to estimate the shape of the GEV-distribution, and use this information for generation of discharges in the historical period.

Flood frequency analysis was repeatedly carried out for a 101-yr moving window over discharges series in the period AD 1772 – 2011. GEV-results of these 101-year intervals were plotted versus the flood intensity index over the same period. The results show that (i) GEV-calculated discharges increase linearly with flood intensities for frequent low-magnitude floods, while predicted discharges for extreme floods show no clear correlation with increasing flood intensities (Fig. 7), that (ii) the occurrence of extreme floods (exceeding 11,000 m^3s^{-1} of discharge in AD 1809, 1920, 1926 and 1995) influences the outcome of GEV-extrapolations for moderate to extreme floods importantly – the entire linear relation between flood intensity and associated discharge shifts along the vertical axis (Fig. 7; introduction or removal of these data points within the window are marked with diamonds), and that (iii) GEV-predicted discharges for a given recurrence interval have increased in recent decades, with exception of low-magnitude floods.

Historical discharges were simulated, based on the above mentioned relations between flood intensity and GEV-results, derived from data over the same interval (Fig. 7). To mimic relations between flood intensity and the shape of the GEV-distribution (sudden vertical shifts and gradual linear changes), the timing of major historical floods and the general flood intensity index were used to estimate GEV parameters. Historical floods exceeding 11,000 m^3s^{-1} and 12,000 m^3s^{-1} were used independently to pre-set various base levels for GEV-parameter values. Extreme floods occurred in AD 1374, 1497, 1595, 1651, and 1658; estimates on the magnitudes of floods before the modern discharge record presented in this paper are mainly taken from reconstructions in Cologne (Herget & Euler, 2010). Within a 101-yr window around these events, GEV-parameters were set to a higher base-level, corresponding with the magnitudes of the vertical shifts visible in Figure 7. Next, for the period back to AD 1400 (the earliest mid-point value of the 101-yr window), discharge data was generated based on the reconstructed dynamic shape of the GEV-distribution – using the linear relation between flood intensity, and locality and added discharge effect of extremes floods. In this approach, it was assumed that the flooding regime (translating in the relations between flood intensities and GEV-results) in the period AD 1350-1772 was similar to the period AD 1772-2011.

4 GEV-extrapolation results

4.1 Modern discharge data [AD 1901-2011]

GEV-predictions using the various data series (including Monte Carlo simulations), produce design flood estimates that range between 12,970 and 14,380 m^3s^{-1} (Fig. 8: 1901, 1817, and 1772 curves; Tab. 3). These estimates are strikingly lower than results of previous studies (Chbab et al., 2006; Fig. 8; Tab. 3). The screened dataset results in a 7-22% lower value for Q_{1250} compared to various results of Chbab et al., (2006). A difference already occurs with a reanalysis using the modern dataset (from AD 1901 onwards). Differences originate from (i) a larger sample size by natural growth of the dataset, (ii) screening of our record (thereby lowering several annual maxima), (iii) homogenisation of discharge data for river management in previous research, and (iv) data-resampling methods used in Chbab et al., (2006). The combined effect of different pre-treatment and data series length since AD 1901 (from n=102 to n=110) is a ~7% decrease in Q_{1250} when compared to GEV-results in Chbab et al., (2006). A larger difference is seen with the data-resampling approach in Chbab et al., (2006); which draws upon 1000 hydrologically simulated discharge peaks generated from random combinations of 35 years of 20th century precipitation data

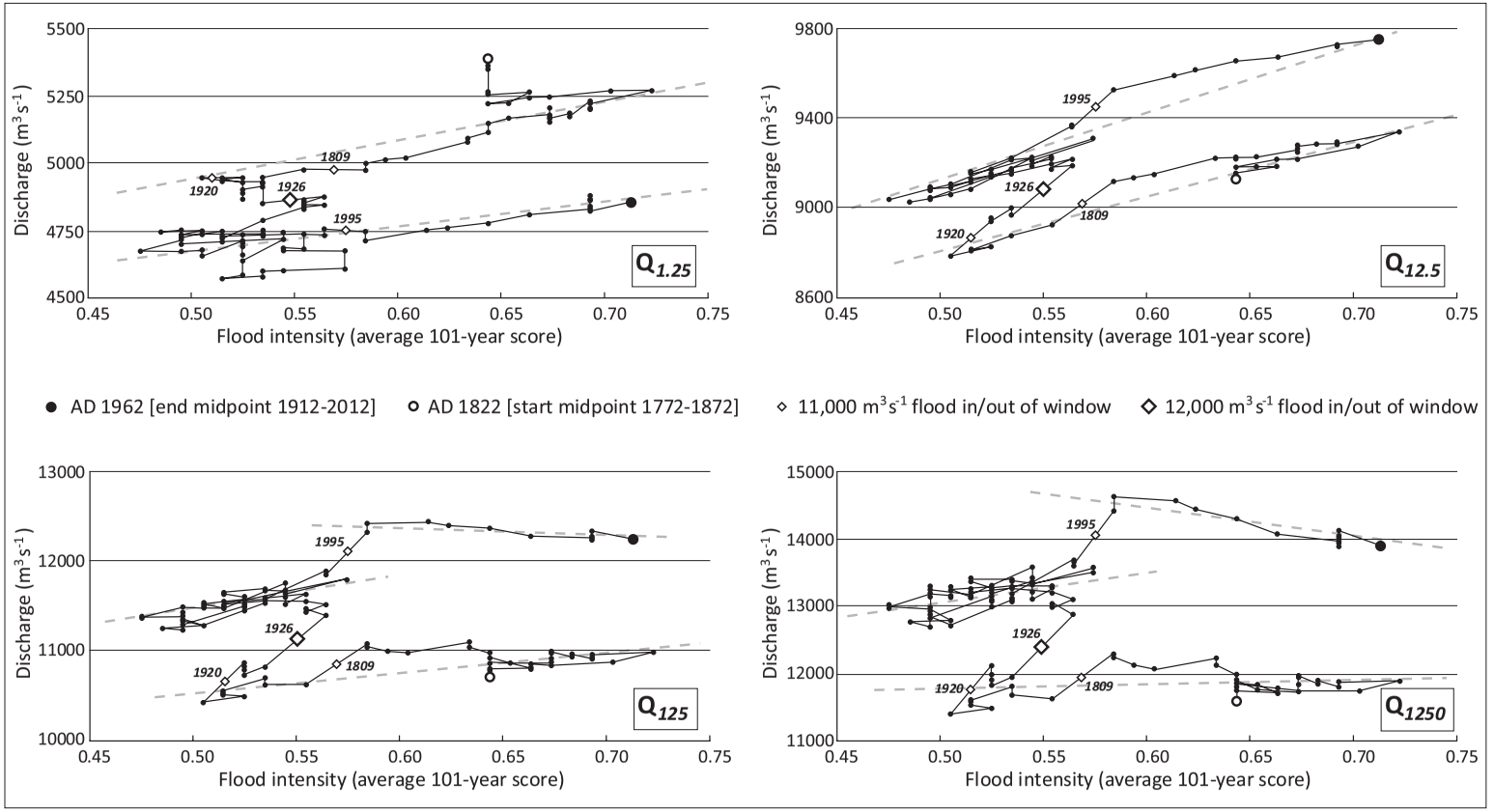

Figure 7: Correlation of GEV-estimated discharges for various recurrence classes (1.25, 12.5, 125, and 1250 years), calculated over a moving 101-year window from AD 1772-2011. Mid-point values are plotted for the moving window; diamonds indicate important changes in discharge calculations caused by inclusion or exclusion of large floods.

from multiple stations in the Rhine catchment. This procedure raises their GEV-estimate for Q_{1250} by ~13% in comparison to their standard series of measured annual maxima (Tab. 3).

Inclusion of measurement uncertainties through Monte Carlo simulations produces comparable results as the initial extrapolation (Tab. 3). The uncertainty range of the design flood is only ~1% larger. This is due to the relatively small measurement error of recent data. With the GEV-extrapolations, also the range in upper bounds of the system is determined. Although these bounds, ranging from 18,190 to 24,960 m^3s^{-1}, are comparable to cross-sectionally reconstructed discharge estimates for the Cologne flood of AD 1374 (Herget & Meurs, 2010), they are probably strictly numerical outcomes and improbable as realistic for the Holocene situation at the more downstream apex of the Rhine Delta. For example, considering the maximum amount of discharge that the catchment can generate (Lammersen et al., 2004) and cross-sectional calculations with slack-water flood marks as input (Chapter 6; Toonen et al., 2013).

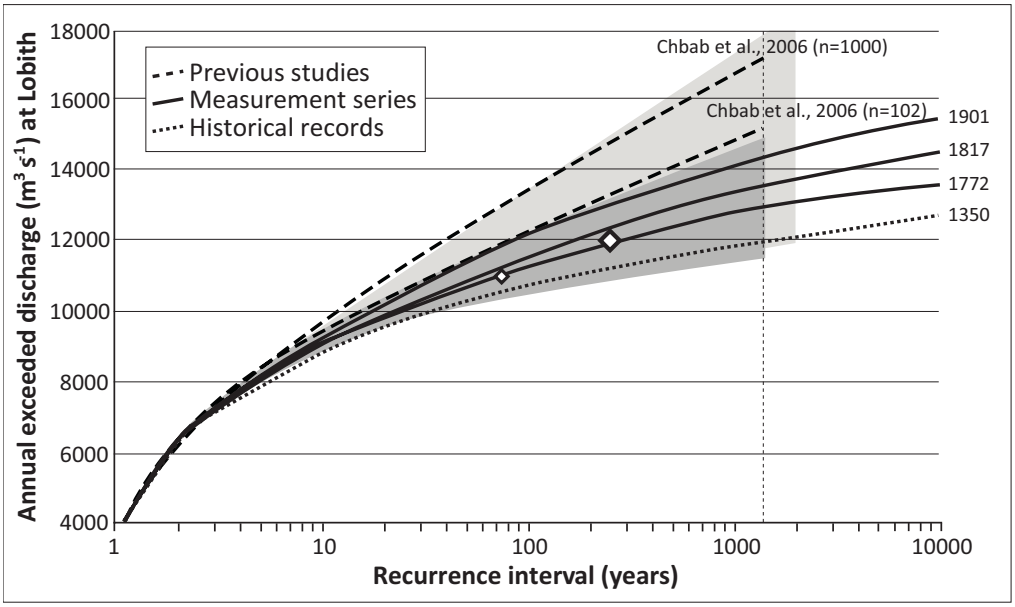

Figure 8: Extrapolation curves of various data series (Tab. 3). For the [AD 1901-2011] and [AD 1772-2011] extrapolations the 95% uncertainty range is shown respectively in light and dark grey. Diamonds indicate Peak-Over-Threshold recurrence of >11,000 m^3s^{-1} and >12,000 m^3s^{-1} floods in the AD 1350-2011 data series (same events as depicted in Fig. 6).

Table 3: Overview of the GEV-results with lengthened data series (n = sample volume, MC = number of Monte Carlo simulations). For the design flood and the upper bound, the lower and upper 95% uncertainty ranges and relative difference with the standard extrapolation (AD 1901-2011) are given.

Data	*n*	MC	Q_{10}	Q_{100}	Q_{1000}	*-2σ*	Q_{1250}	*+2σ*	*-2σ*	Q_{bound}	*+2σ*
1901-2011	111	-	9250	12060	14130	11990	14300	17710	-	20440	-
1901-2011	111	1000	9270 (+0%)	12110 (+0%)	14210 (+1%)	11990	14380 (+1%)	17920	18190	20720 (+1%)	24960
1817-2011	195	1000	9050 (-2%)	11600 (-4%)	13400 (-5%)	11870	13550 (-5%)	15700	16260	18060 (-12%)	20720
1772-2011	240	1000	9060 (-2%)	11330 (-6%)	12850 (-9%)	11500	12970 (-9%)	14960	14730	16010 (-22%)	17870
1350-2011	612	10	8880 (-4%)	10760 (-11%)	11850 (-16%)	11180	11920 (-17%)	12800	-	13480 (-34%)	-
Chbab et al., 2006	102	-	-	-	-	-	15260 (+7%)	-	-	-	-
Chbab et al., 2006	1000	-	-	-	-	-	17504 (+22%)	-	-	-	-

4.2 Extended discharge records [AD 1772-2011]

Extension of the data series back to AD 1817 and 1772 produces lower estimates for Q_{1250} (Tab. 3). The added period has a relative high flood intensity (Fig. 6), but lacks very large floods (with exception of AD 1809). This causes the GEV-extrapolation to decrease only slightly for medium floods, while the estimated size of the design flood decreases with ~5-9% (Fig. 8). If these estimates are representative for the current system, without major effects of non-stationarity, the AD 1926 flood of ~12,600 m^3s^{-1} can be considered as a rare event, of similar size as the design flood.

Upper bounds of the GEV-extrapolation are affected more severely; a 22% decrease based on data since AD 1772 places the upper bound on a similar level as the current design flood (~16,000 m^3s^{-1}). Obviously, the level of this bound corresponds poorly with the reconstructed discharges of the 1374 AD flood at Cologne (Herget & Meurs, 2010). Contrarily, it corresponds well with estimated hydrological bounds for the Lower Rhine in the Netherlands; model studies indicate that the maximum amount of precipitation-derived discharge in the catchment amounts ~18,700 m^3s^{-1}, while modelled floodplain inundation and upstream dike breaches presumably limit the maximum Rhine discharge at Lobith to ~15,500 m^3s^{-1} (Lammersen, 2004).

The uncertainty envelope of extreme flood discharges decreases in width despite the limited precision of the added measurements and reconstructions (Fig. 8). Especially the upper limit of the uncertainty interval decreases considerably (~10%). The resulting uncertainty interval is comparable to previous studies (e.g., Chbab, 1999), which indicates that long data series enable the use of fairly inaccurate data; the addition of 129 data points counteracts the low precision of alternative measurements.

An alternative method to compare the extrapolation results with historical information, and to have an independent check on the performance of extrapolation curves, is to estimate recurrence intervals of large floods by counting peaks over threshold (POT) over the investigated period. In the last ~660 years, reconstructions of historical floods indicate that at least 9 floods exceeded 11,000 m^3s^{-1}, of which 3 floods are thought to have been larger than 12,000 m^3s^{-1} (Fig. 6; Herget & Euler, 2010). The associated recurrence intervals of such events are respectively 73 and 220 years. Such recurrence intervals are compared with the results of the flood frequency distributions (Fig. 8). POT-comparison indicates that the initial data series (AD 1901-2011) is too short to accurately predict recurrence intervals of large events. The lengthened series (back to AD 1817 and AD 1772) correspond much better with these independent estimates from peak over threshold, and are suggested to be more realistic in the large flood recurrence-magnitude domain.

4.3 Historical by-proxy flood series

Addition of synthetically generated flood magnitudes for the period before AD 1772 (section 3.2), results in a further lowered estimate for the design flood (-17% compared to AD 1901-2011 initial estimate; Tab. 3). The design flood is even predicted lower than actually measured discharges in the 20th century. Although the upper bound is also much lower than previous estimates, it still exceeds any truly observed discharge in the past century. The addition of historical data also lowers discharge estimates with a decadal recurrence time, which shows that the relation between flood magnitudes and recurrence interval changes for all flood sizes. Obviously, the results of this explorative approach suffer from some important drawbacks, which make it difficult to establish the quality of this data for flood frequency analysis (discussed in section 5.3).

5 Discussion

Adding alternative data types to existing discharge series involves two important trade-offs; (i) introducing less precise measurements versus a gain in accuracy of extrapolated results for extreme events (precision of data vs length of series), and (ii) more precise estimates of the magnitude of the design flood by using a larger data set versus the representativeness of extended records for the current situation (length of series vs dynamic flooding regime).

5.1 Alternative measurements and extrapolation results

In this study, inclusion of discharge measurement uncertainty increased the uncertainty envelope of extrapolated design flood estimates only slightly, because modern measurements are fairly precise for the Rhine. In other catchments with less dense, less precise or shorter records of discharge measurements, the effect of reducing uncertainty will be larger. Inclusion of alternative data types (here: water level measurements) was straightforward for the Rhine, and a key benefit was that water level records could be verified among multiple sites. Changes to the fluvial system, such as channel bed changes that lead to variable stage-discharge relations, have been monitored and quantified for the youngest centuries to restrain the uncertainty of alternative data and conversion methods. Hence, addition of this information improved extrapolation estimates of shorter discharge records (Tab. 3). The addition of information based on historical records, describing the occurrence and extent of past floods, is probably less favourable for use in flood frequency analysis; this is mainly

due to inevitable use of a limited number of flood intensity classes for which absolute magnitudes are difficult to quantify.

The second trade-off is more complicated to assess. In our study, the addition of information further back in time resulted in a lower estimate for the design flood; Q_{1250} of the Rhine at Lobith. This lowering is mainly caused by the lack of extreme floods in the added period, which increases their estimated recurrence time. In case of a stationary flooding regime adding historical data better constrains the estimates of recurrence intervals of extreme events. Previous research, however, has proven that the assumption of stationarity in flooding regimes is not valid (e.g., Knox, 1993).

5.2 Non-stationarity

Variations in average annual discharge (Fig. 2) and indexed by-proxy flood intensity (Fig. 6) are small in our record. Although clear variations can be observed in the 31-year indexed flood intensity, almost no trends remain when a 101-year window is used, which implies that most variability occurs on a (multi-)decadal interval. It is common practice to normalise discharge records of the last century for river management, but according to Parmet et al., (2001), Bronstert et al., (2007), and Vorogushyn & Merz (2012), the effect of recent changes on discharges of extreme floods in the Lower Rhine is small. Gradually decreasing flood intensities can be observed in the record from AD 1400 to 1900 (101-yr window; Fig. 6), but part of this decline can be attributed to the historical nature of the data (discussed in next section), with a varying impact of historical floods over time that is not necessarily connected to discharges exclusively. Moreover, this trend is not reflected in the distribution of extreme events, so changing flood intensities and river normalisation seem to have little effect on the results of flood frequency analysis (Fig. 7).

Two important contrasting periods, which are both widely associated with anomalous climate conditions, are the LIA and recent decades. The LIA climate anomaly (AD 1550 – 1850; Glaser & Riemann, 2009) is in our record associated with 'normal' flood intensities, with a remarkably low frequency of large floods (class 3; Fig. 6). The occurrence of extreme floods and the amplitude of flood intensity do not differ much from that for the last ~150 years, which suggests that the LIA had rather similar flooding conditions as the last century. An important difference with the last century is the low frequency of large flood and occurrence of many minor events; this may importantly influence results of flood frequency analysis. It could be hypothesized that the 300-yr duration of the LIA biases the extrapolation result (Fig. 8) towards a situation with many small floods (producing similar flood intensities as later periods; Fig. 6). As this period encompasses nearly half of the dataset, this can explain the relative low design flood and upper bound predictions for the AD 1350 curve (Fig. 8). The suggestion that the LIA has been a period with 'normal' flood intensities and mainly minor events contradicts the generally accepted idea that the LIA was a period with extensive flood damage caused by many extreme floods in the Netherlands (e.g., Tol & Langen, 2000). During the LIA cold period, a considerable number of ice-related catastrophic flooding events were recorded in the Lower Rhine (in AD 1784 for example; Demarée, 2006; Brázdil et al., 2010), but the majority of those were presumably not associated with extreme discharges.

It remains unclear how the period of intense flooding of the recent decades fits in the discussion on non-stationarity. The rise of the flooding index in the youngest half century (Fig. 6) is probably a response of the flooding regime to an exceptionally warm and wet interval. However, based on the

reconstructed amplitude of flood intensities it could *hypothetically* also be part of a normal natural alternation in flood intensity, similar to the early 19th century (Fig. 6). Although several studies suggest intensified flooding in recent decades (e.g., Milly, 2002) and point to climate change as the main driver, other studies indicate that there are no major recent changes in the European flooding (Mudelsee et al., 2003; Brazdil et al., 2006; Glaser et al., 2010). Part of the rising trend may be attributed a limited observational period; if only discharges of the 20th century are assessed in flood frequency analysis (Fig. 6), it is easily assumed that changes are significant, and exceeding normal variability. Adding historical measurements and records, however, places recent changes in a context of ongoing longer-term variations in flood occurrences, and shows that periods with high flood intensities have occurred previously (such as the early 20th century).

No straightforward relation can be discovered between the variation in occurrence of extreme floods and periods of varying flood intensity (Glaser, 2001; and Fig. 6 in this paper). As especially extreme events have a profound effect on the results of flood frequency analysis and pose the largest threat to communities in lower reaches of large rivers, it is recommended to further investigate forcings on floods, the timing of extremes, and the relation between flood intensities and extreme events. Furthermore, detailed discharge reconstructions of historical events (e.g., Wetter et al., 2011), and flood series derived from sedimentological records (Chapter 3; Czymzik et al., 2013) can further increase available information on extreme events, and the possible effects, limits, and amplitudes of non-stationarity.

5.3 The use of historical records

Flood intensity indexing based on historical information and subsequently translation to discharge series by applying the relations in Fig. 7, allows to stretch flood frequency analysis over many centuries. There are, however, some drawbacks and limitations to this approach. In the current assessment, the relation between damage by flooding and associated flood magnitude is assumed to be stable over time. There are several natural and societal factors that can influence flood intensity over time. Natural variability in the relation between floods and dike breaches is caused by the dynamic discharge distribution of flood waters over different branches of the Rhine in historical periods and the occurrence, frequency, and severity of ice jamming. Until the construction of a fixed bifurcation (De Pannerdense Kop; Van de Ven, 1976) at the apex of the Rhine Delta in AD 1707 (Fig. 1), the right bifurcate channel (the Nederrijn; Fig. 1) became gradually abandoned since the end of the Medieval period (Kleinhans et al., 2011). Consequently, up to 90% of the discharge gathered in the Waal (left bifurcate channel), which resulted in increased flooding along this branch (Van de Ven, 1976; Glaser & Stangl, 2003). The effect of the changing discharge distribution on reconstructed flood intensities is however difficult to assess in the historical dataset. Intensified ice jamming in colder periods has probably also had a profound effect, as there are many reports about severe winters followed by catastrophic flooding. For much of the smaller, local floods it is very well possible that ice jams have raised water levels or created additional loading on dikes, and such contributed to raised flood intensities compared to warmer periods with less ice formation. For regional flooding, and particularly for catastrophic floods, ice jams have contributed to the extent of dike breaches, but regional floods are very unlikely to occur without increased discharges. Flood intensities in the LIA are similar or lower compared to warmer intervals and there is a limited number of extreme events (Fig. 6), which indicates that the resultant added effect of ice jamming in the LIA on flood intensity and the results of flood frequency analysis is small.

Especially in the historical timeframe also political and economical factors presumably were an important factor determining flood damage in historic times, and hence, our flood intensity estimates. Dike strength and failure were largely determined by maintenance. Periods of political instability led to fragmentation of governmental areas, leaving embanked areas under different rules with different standards (Van Heiningen, 1978). Occasionally, dikes were targeted by military actions to deliberately cause extensive flooding (e.g., Buisman, 2000). Although these events are extensively described in historical records, it is difficult to filter 'the human factor' in the occurrence and severity of dike breaches from the natural river discharge as a cause. Until Napoleonic-rule, local people were responsible for dike maintenance, resulting in different dikes strengths (Van Heiningen, 1978). This explains why even minor floods are well-documented, as there was always somewhere a weak spot where a breach could occur. As dike restoration after a breach was forced onto local people, it sometimes took more than a year to completely restore a dike, which may have resulted in repeated flooding in the following years as dikes were still not fully repaired (Van Heiningen, 1978). Severe flooding also resulted in raised awareness and extra investments in dike strength (similar to the response after the floods in the last century), until the necessity of maintaining dikes waned again.

If effects of ice jams and societal factors would be filtered from the flood intensity record, the indexed by-proxy flood intensity curve would presumably decrease to even lower values in the historical period. To quantify this decrease is however difficult. The effect on flood frequency analysis would be further increased recurrence times for large floods (Fig. 8), although these are already much lower based on generated discharges of the historical period in comparison with the estimates from counting peaks over threshold and extrapolation results over the period AD 1772-2011. As the occurrence of extreme floods has strong effects on the results of flood frequency analysis, it is questionable if further investigation of minor events described in historical records would produce essential information for assessing current flood risk.

6 Conclusions

Discharge series supplemented with discharge or water level measurements from nearby stations that can be converted into a single long discharge record are potentially very useful for improving estimates of the recurrence interval of large river flooding events, despite the lower precision of these alternative measurements, and uncertainty introduced by conversion methods. Extending the measured discharge series in this way (back to AD 1772, based on water level measurements) results in a reduction of the extrapolated design flood (Q_{1250}) by ~10% (compared to the AD 1901-2011 series; Fig. 8), and reduces the upper limit of the uncertainty envelope.

These results suggested that the current magnitude of the design flood for the Lower Rhine in the Netherlands that is based on discharge observations covering only the last century of discharge measurements is too short and biased to coincidently-recent larger floods, to represent the natural recurrence of extremes in the flooding regime of the Lower Rhine. The extrapolation results in this paper indicate that current protection levels along the Rhine are similar to the upper bounds of the system and are in agreement with current flood design standards. It should, however, be stressed that the extended data series provides no estimates for the largest discharges that can possibly occur in the future.

The direct use of historical records in flood frequency analysis is complicated, because flood magnitudes are derived from flood intensities, which are based on categorised flood magnitudes. Flood intensities are not exclusively reflecting discharges, but are also influenced by anthropogenic and environmental factors. This analysis demonstrates that the distribution and magnitudes of extreme floods are most important in flood frequency analysis, as illustrated by the responses of the GEV-extrapolation to extremes (Fig. 7). The occurrence of extreme floods correlates poorly with general flood intensities, making dependence on flood intensities for generating discharge data problematic. Instead, specifically targeted discharge reconstructions of large floods in the historical period at multiple locations, advanced hydrological modelling, and sedimentary flood magnitude reconstructions may provide important information on the magnitude and recurrence intervals of floods in historical times, and can be used to roughly verify extrapolation results based on discharge data from measurements.

The reconstructed flood intensities show imprints of non-stationarity, visible as variations in the flooding index curves (Fig. 6). Non-stationarity is often regarded as problematic in flood frequency analysis, as it may bias results when the past flooding regime was not similar to the present situation or possible future scenarios. Only the LIA cold period with relative many small events (but a rather normal flood intensity) can be considered as problematic for use in flood frequency analysis for the current situation. Except for this relative long interval of anomalous flooding, no clear *permanent* changes in the system are identified in the reconstructed flood intensities of the last centuries, as amplitudes of the observed alternations in flood intensities are within the limits of the last century variability.

Acknowledgments
The Dutch Ministry of Infrastructure and the Environment is acknowledged for sharing data and providing estimates on measurement uncertainties. Sofia Caires (Deltares, HYE) is thanked for guidance in statistical procedures. Kim Cohen and Hans Middelkoop (Utrecht University), Sofia Caires (Deltares, HYE), and Quirijn Lodder (Rijkswaterstaat) are thanked for comments on previous versions of this manuscript. This research is funded by Deltares BGS (Utrecht, The Netherlands) and Utrecht University (The Netherlands).

3 Sedimentary architecture of abandoned channel fills

Toonen, W.H.J. * [1,2], Kleinhans, M.G.[1], Cohen, K.M. [1,2]

[1] Dept. of Physical Geography, Utrecht University, Utrecht, The Netherlands.
[2] Dept. of Applied Geology and Geophysics, Deltares BGS, Utrecht, The Netherlands.
* Corresponding author: E-mail: w.h.j.toonen@gmail.com

Published in: Earth Surface Processes and Landforms 37:4, p 459-472. DOI: 10.1002/esp.3189

1 Introduction

Abandoned channels are a geomorphologic testimony of channel movement in river valleys. They are recognized as depressions in the landscape and located at the position of a formerly active channel, though typically of considerably reduced width and depth. The latter is due to infilling processes that operated during and after abandonment and implies a sedimentary record of abandonment is contained in the deposits.

Abandoned channels result from channel shifting processes, such as meander cutoff and channel-belt avulsion. Both sedimentary and palaeoecological data can be gathered from abandoned channel fills to examine fluvial dynamics such as fluvial style change, palaeodischarge variations, palaeoflooding intensity as part of autogenic river behaviour and response to climate change and human impact (e.g., Vandenberghe, 1995; Page and Nanson, 1996; Macklin and Lewin, 2003; Erkens, 2009).

Channel fills have also been used for environmental reconstruction, because the depressions functioned as a sediment trap during floods (resulting in layering of the sedimentary fill) and because they have a high preservation potential (Allen, 1965; Lewis and Lewin, 1983; Baker, 1987; Shields and Abt, 1989; Middelkoop and Asselman, 1998; Walling and Hu, 1998; Macklin and Lewin, 2003; Werritty et al., 2006). Common types of abandoned channels in lower fluvial reaches are (1) oxbow lakes, formed by single meander bend neck or chute cutoff (Fisk, 1947; Lewis and Lewin, 1983; Gagliano and Howard, 1984; Erskine et al., 1992; Hooke, 1995; Gay et al., 1998; Fuller et al., 2003; Micheli and Larsen, 2011) and (2) channels abandoned over multiple meander lengths, left inactive due to an upstream avulsion (Smith et al., 1989; Stouthamer and Berendsen, 2000). Basal parts of abandoned channel fills have proven to be useful positions for dating the terminus of channel activity (e.g., Törnqvist et al., 1996; Berendsen and Stouthamer, 2000; Morozova and Smith, 2000; Erkens et al., 2011). Organically infilled channels – found at a distance from contemporaneously active rivers – are suitable for reconstruction of floodplain vegetation (e.g., Kasse et al., 2005; Salvador et al., 2005; Bos et al., 2008; Parker et al., 2008; Lechner, 2009). Compared to the usage of channel fills for dating abandonment and

reconstructing palaeoenvironments, the sedimentological use of their contained clastics as a means for reconstructing fluvial dynamics is underdeveloped.

Text books on fluvial sedimentology (e.g., Reading, 1996; Leeder, 1999; Nichols, 1999; Bridge, 2003) and individual studies that mapped and dated the geomorphological elements of river valleys (e.g., Nanson and Croke, 1992; Cohen, 2003; Gouw and Erkens, 2007; Erkens et al., 2011) typically consider abandoned channel fills as single entities (one facies type, a single architectural element). These studies do not generally use the layering within fills as information on which to build detailed reconstructions. Obviously, the majority of palaeochannels in Holocene floodplains do not mark the termination of river systems, but mark the initiation of a new channel on a neighbouring part of the valley, thereby rerouting the river only locally over a sub-reach of the river system. For reasons of proximity, correlation may be suspected between clastic sedimentary records accumulating as part of a channel fill and the continued activity of the river at its new position, especially during floods. But how exactly this works, and how one should approach and utilise this in reconstruction studies are topics that are largely ignored in literature. To use sedimentary layering of channel fills as an archive, the geometry and internal architecture of abandoned channel fills, such as lateral and longitudinal variation, need to be documented and understood. Individual case studies document infillings in greater detail (e.g., Hooke, 1995; Salvador et al., 2005; Werritty et al., 2006; Hoek et al., 2011), but an explicit integrated theory or conceptual framework for channel filling has not been developed. This makes it difficult to give meaning to observed variations in styles of abandoned channel infillings, to relate these to site specific factors and regional forcings, and to improve knowledge on abandoned channel filling in general.

Multiple mechanisms of channel relocation and abandonment exist; meander neck and chute cutoff, and avulsion. Factors such as non-stationary discharge loss during abandonment (e.g., the rate at which abandonment proceeds may vary over time), variations in floodplain configuration (e.g., proximity to active branch), and other local factors (e.g., connectivity, re-occupation of the palaeochannel depression by crevasse systems) result in further variety of sedimentary outcomes. This is of particular importance when not just end-members, but a full assemblage of channel fill cases in a lowland river system is considered. Observed variation becomes more easily explained once a framework for channel-fill interpretation exists.

Our objective is to present field examples of various channel abandonment styles and associated sedimentary fill. Combined with information from previous studies, the different end-members of channel fills are presented in a framework of facies successions that make up the total fill and this is used for recognition of subsequent stages. Randomly collecting channel-fill sequences, i.e. without extensive mapping to identify optimal sampling locations, may not provide the best samples for the studies of particular purpose. Having knowledge of the three-dimensional build-up of the fill, the internal micro-scale variability of channel-fill deposits, and understanding how this varies between channel fills of different type and at different position in the floodplain enables more cautious site selection (e.g., for proxy record harvesting), besides allowing distinction between different types of channel fills initially. This is needed to (i) test and predict the positions in an abandoned channel fill that are most suitable for harvesting proxy records, (ii) compare records from different sections within a single fill, and (iii) to compare, unite and collate records from multiple fills.

2 Research approach

A framework for channel-fill interpretation should cover: (i) infilling processes starting at the initiation of an upstream bifurcation, proceeding during the abandonment process and culminating in a stage of residual filling; (ii) resulting types of sedimentary facies, their 3D geometry, and fine-scale sedimentary layering within the facies units including the thickness of alternating beds of individual floods; (iii) differences in infilling style resulting from the setting within the river plain (local factors). A literature review of oxbow channel-fill concepts provided an initial 'framework' for aspects of meander cutoff development (next section), which we applied as a test to the detailed lithologic interpretation of such an abandoned channel fill from the Rhine Delta apex (Case 1). Next, we tested the framework's suitability on a sub-recent residual channel (Case 2), for which extensive historical and geological contextual information exists, to expand application of the framework to the avulsive-abandoned channel type. To explain sedimentary dynamics during abandonment and differences between the two end-member cases, we utilise recent numerical modelling of sedimentary processes at bifurcation nodes (Kleinhans et al., 2008; Kleinhans et al., 2011). The results of the literature review and case studies are used to refine a facies model that is predictive for both meander bend cutoffs ('oxbows') and channels abandoned by avulsion ('residual channels').

3 Review of oxbow channel-fill concepts

Three stages of abandonment are generally distinguished during meander bend cutoff: (1) cutoff initiation – the triggering of the cutoff when the majority of the river discharge becomes diverted from the meander and starts to flow along the newly activated channel (Lewis and Lewin, 1983; Hooke, 1995); (2) plug bar formation – an in-channel sedimentary response to reduced discharge (and energetic conditions) that progressively causes blockage of the upper and lower entrances, leading to further discharge diversion and promoting trapping of bedload and suspended load (Fisk, 1947; Constantine et al., 2010); (3) disconnected stage – discharge is no longer carried regularly through the channel depression. The channel is 'disconnected' from the network of active river channels, and the former channel is transformed into a floodplain lake that only receives suspended load during floods (Fig. 1).

3.1 Bedform and barform preservation during cutoff

Channel abandonment initiates with the preservation of bedforms that have accumulated just prior to the cutoff event. Suddenly reduced energetic conditions make the channel incapable of altering the pre-existing bedform morphology. Along most of the former channel bottom, the contact between coarse bed- and finer suspended-load deposits is sharp; in both the deeper (e.g., pools in the apex of the bend) and shallower inner portions of the channel.

Pre-existing channel deposits can easily be recognised and separated from later fill deposits by its significantly larger grain size (relative coarse sands and gravels) and geometry similar to the active channel. When meander bend cutoff occurs, this effectively reduces the length of the flow path and increases the channel gradient in the new channel. The reduced transport capacity within the abandoned bend triggers mixed load accumulation and preservation of underlying channel bedforms (Fig. 1).

With the cutoff, the transfer of bedload appears to stop suddenly. Pointbar formation and outer bank cutting freeze instantaneously (Schumm, 1977; Piégay et al., 2008). Typically, the last major scroll of an abandoned pointbar is not noticeably different in sedimentological build up from penultimate scrolls. Numerous examples of frozen thalweg bedforms and barforms exist in outcrops of channel fills studied by fluvial sedimentologists and geomorphologists (e.g., Nanson and Croke, 1992; Constantine et al., 2010, also personal observations by the authors).

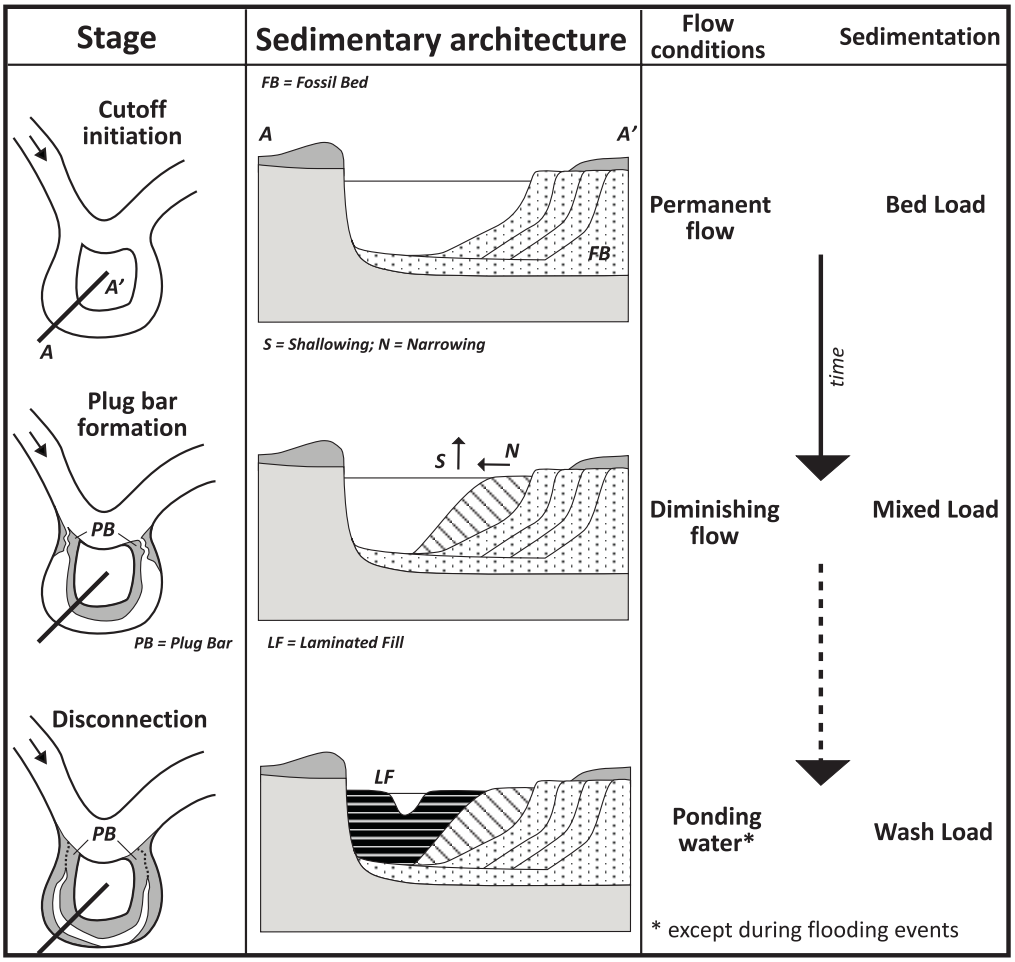

Figure 1: Stages of abandonment for a meander bend cutoff.

3.2 Stage of channel abandoning

Not each abandoning channel will automatically preserve as an abandoned channel, as it is well possible that discharge diversion halts and reverses. An abandoning channel may regain discharge over the course of next flooding events and develop in a new semi-stable channel bifurcation. This occurs often in low-angle splits with a limited difference in gradient advantages and relative long period of abandoning, usually found in avulsions and chute cutoffs of low-sinuous rivers. We focus

here, however, on the sedimentary record of those cases where cutoff did lead to full abandonment only.

After the initial cutoff event during a flood, sedimentary processes begin to seal off the channel, especially during the initial and subsequent floods. Ultimately, an abandoned meander can become a disconnected oxbow lake in the floodplain, which carries a very small percentage of the discharge during rare high-magnitude floods only (exceeding bankfull stage). The length of time that a cutoff channel remains in the intermediate stage is partly determined by the circumstances triggering the cutoff event (e.g., a neck cutoff or a chute cutoff). The speed at which disconnection develops is strongly determined by the first 'geomorphologically-active' larger floods following (and during) the initial cut off. In oxbow fills, repeated follow-up floods produce individually recognizable strata of relative large thickness. This creates an interbedded basal channel-fill sequence that is potentially useful to assess the rate of channel abandonment.

Completed disconnection, arbitrarily defined here as when through-flow falls below 10% of the total discharge (as in Kleinhans et al., 2011), is typically reached within several years after the initial cutoff event (Gagliano and Howard, 1984; Hooke, 1995; Micheli and Larsen, 2011). A main factor that determines sedimentation rates, and thus the length of time that full meander abandonment takes, is the angle between the channel entrance and the main flow direction (Constantine et al., 2010).

Two simultaneous effects of the angle of the channel entrance are in play coevally: those promoting plug bar formation at the channel entrances, and those causing shallowing and narrowing of the channel in the rest of the former meander. The combined processes decrease the through flow with each next passing flood. Plug bar formation occurs at the proximal part of the cutoff channel and is characterised by high sedimentation rates during the onset of abandonment. Thereafter sedimentation rates rapidly decrease (Hooke, 1995; Citterio and Piégay, 2009). Shallowing and narrowing act in the distal part of the cutoff channel and their rate of sedimentation tends to decrease more gradual (Piégay et al., 2008).

3.2.1 Plug bar formation

The plug bar (PB; Fig. 1) is defined as a bed sediment bar form at the entrance of a bifurcation channel, hindering flow into a channel (Fisk, 1947; Gagliano and Howard, 1984; Hooke, 1995). The main factors determining the presence and thickness (above the bed-level from pre-cutoff) of a plug are the configuration in the landscape and the angle of the channel entrance with the main flow. Bulle (1926) shows that channel entrances connected to inner bends are more susceptible to plug bar formation because of bedload supply. In contrast, outer bend channel entrances predominantly receive suspended load, which does not necessarily accumulate at the channel entrance. Building on the classic works of Fisk (1947) and Shields and Abt (1989); Constantine et al., (2010) point out that bedload aggrades most rapidly at channel entrances with high diversion angles (back-eddy effect), resulting in faster plug bar growth and channel disconnection. Hooke (1995) shows that vertical plug bar growth mainly takes place in the first years after initial flow diversion and that it decelerates sharply over time. Although Hooke (1995) draws conclusions from an upstream reach of a relative minor river, it is assumed that hydraulic processes and the principles of sediment division over closing and opening branches are not that sensitive to scale difference. This is supported by flume studies (e.g., Peakall et al., 2007), examples from abandoned channels

along tributaries (of variable size) along the Mississippi and the main Mississippi itself (Saucier, 1994), and similar examples of flow diversion in major rivers and in more downstream regions (e.g., Gagliano and Howard, 1984; Hoek et al., 2011; Micheli and Larsen, 2011).

Plug bars are similar to subaqueous levees in the sense that they flank an active channel, grow in size during successive floods and have an upward fining trend in grain size. Downstream plug bar growth into the abandoned channel depression can be compared with delta progradation, as some of the discharge remains directed into the abandoned channel and produces distinct fore sets in the plug bar body (Rowland et al., 2005; Citterio and Piégay, 2009). The maturity of the plug bar greatly influences the sedimentary processes in the distal part of the abandoned channel, as well as sedimentary processes and accumulation rates of channel fill during the next stages of disconnection. Rapid plug bar formation equates to a very brief period of relative coarse grained supply to the distal area. The presence or lack of connecting channels dissecting the plug bar may also influence flow retainment and sediment supply to the distal part of the abandoned channel (Rowland et al., 2005).

Increased rates of proximal bar build-up to seal-off the abandoned channel strongly reduce distal deposition (discussed later), because it raises the magnitude of each next flood needed to overtop the plug bar. This reduces the frequency of flooding through the palaeochannel and improves the functioning of a palaeochannel as a sediment trap for fines.

3.2.2 Shallowing and narrowing

In-channel deposition during channel abandonment results in shallowing (Fig. 1). In this paper we only consider palaeochannel shallowing due to sedimentation in the former channel bed as a result of redirected discharge during successive floods, not shallowing associated to a dropping water level (e.g., due to evaporation in arid climates). Silting-up of a channel results from the diversed river in-flow and decreased flow velocities, causing fall-out of coarser particles out of the suspended load. Deposition occurs as a sheet that drapes the pre-existing bed deposits and neighbouring abandoned pointbar swales. For abandoned meanders, Citterio and Piégay (2009) found that former channel geometry and channel connectivity are the main factors controlling shallowing; the thickness of the homogeneous sheet is positively correlated with water depth, and sedimentation rates are higher in channels that are connected to the active channel and channels that were not rapidly abandoned so they experienced a gradually reduced flow. They also conclude that a longitudinal trend in sheet thickness is absent, although this may be attributed to the limited length of individual oxbow lakes that they studied.

In-channel deposition not only causes shallowing, but importantly also narrowing of the abandoning channel (Fig. 1). This is caused by sedimentation at higher rates at the boundaries of the abandoned channel, which with help of establishing vegetation converts from a lacustrine environment into a terrestrial environment at accelerated pace (Steiger et al., 2001; Makaske et al., 2002). The centre of the palaeochannel transforms from channel to lake and remains a subaqueous environment. Narrowing is particularly effective on the inner bank of abandoned bends, where sedimentation occurs on the shallow side of the channel following up the pointbar-to-floodplain transition during the active channel phase [e.g., Allen's (1965) classic paper and many text books]. In this stage, reduced flow conditions restrict erosion on the outer bank. Inner bend deposition and restricted erosion at the outer bank explain the gradual narrowing of the abandoned meander

following cutoff (e.g., Piégay et al., 2008). Constantine et al., (2010) found a negative relation between the diversion angle and narrowing in meander bends, from which it can be concluded that the rate of narrowing is largely depending on the rate of plug bar formation. For example, stalled plug bar formation ensures sufficient through flow in the abandoned channel and relative coarse sediments are routed into the abandoned bend.

Both the rate of shallowing and narrowing are dependent on the duration of flow retainment: once the palaeochannel is entirely sealed off, it only receives sediment during infrequent larger floods and rates of shallowing and narrowing decrease considerably, allowing new processes to follow (next section). Given that oxbow lakes in the few studied cases became entirely sealed off within a decade after cut off (Hooke, 1995; Micheli and Larsen, 2011), the role of 'silting-up' may be relative limited for classic oxbow lakes. However, Holocene floodplains, and older fluvial sequences alike, contain many examples of palaeomeanders that are fully filled by silting-up. One could consider such abandoned meanders to have fully silted-up as a secondary channel, never making it to the fully disconnected stage of the classic oxbow lake, because shallowing and narrowing outpaced plug bar formation.

3.3 Full disconnection: trapping overbank deposition

Disconnection of the abandoned channel begins when the abandoned channel no longer continuously carries discharge. This implies that the channel may still be used as a secondary thread of flow during large floods, but that during mean flow conditions a lacustrine environment is present. Sedimentation is not entirely halted in this stage: the disconnected floodplain lake receives overbank deposition during floods. In between floods, autochthonous sedimentation in the form of plant detritus, organic lake muds (gyttja), calcareous precipitates (lake marl), and peat can accumulate, and become admixed with overbank sediment. This part of a channel-fill sequence is of interest for palaeoreconstruction studies, and many described examples of such usage and their lithology exist in the literature (e.g., Gaigalas and Dvareckas, 2002; Kasse et al., 2005; Lechner, 2009; Hoek et al., 2011).

Depending on the maturity of the plug bar and the proximity to the active channels, floods may temporarily cause a diversion of discharge through the former meander, delivering a pulse of suspended sediment. Because the palaeomeander is a subaqueous topographical depression, flow velocities are locally reduced and suspended load is deposited. When oxbow flooding is rare and autochthonous sedimentation thrives, distinct flood layers may register within the channel fill. Repeated flood pulses of differing magnitudes and sediment delivery, alternate with finer grained and organic rich levels, stacking into a laminated fill (LF; Fig. 1). A laminated fill is a good indicator that a palaeochannel reached the stage of disconnection. Oxbow lake fills typically produce these laminated fills, which are relatively easy to recognise in the field and in cores. This has been used to map palaeochannels and to select sites for palaeoflood and palaeoecological studies, and for dating purpose to put records in a chronosequence (Pons, 1957; Teunissen, 1986; Törnqvist, 1993; Lechner, 2009).

Oxbow lakes function for a limited time, although it may take several millennia before combined autochthonous and allochthonous infilling of the palaeochannel is complete (Hoek et al., 2011) and the former channel is transformed to a low area (meander scar) in the floodplain. Previous studies, however, have not provided guidance on the time that this process takes to complete, nor

on the expected length of sedimentary records contained in a certain type of channel fill. Hence suitable site selection for proxy records collected in previous studies was more depending on empiricism, trial-and-error, and mere luck.

4 Abandoned channel fills from the Rhine Delta apex

To test and improve oxbow channel-fill concepts in the setting of a delta plain instead of meandering river valleys, we examined a prehistoric oxbow fill of an abandoned meander and a sub-recently abandoned bifurcation channel of an avulsion from the apex region of the Rhine Delta.

4.1 Study area background

The Rhine Delta apex is located in the German-Netherlands border region, where the delta plain is bound by ice-pushed ridges from the penultimate glacial (Fig. 2). The climatic amelioration of the Late Glacial and Early Holocene caused a multithread braided river system to transform gradually to a single-thread meandering river (e.g., Pons, 1957; Berendsen and Stouthamer, 2000; Busschers et al., 2007; Erkens et al., 2011). By ~5000 yrs BP the delta apex had formed in the extreme west of the study area (Fig. 2), as inland response to the Holocene transgression. In the last 3000 years, the delta apex continued to shift upstream to its present position on the German-Netherlands border; no longer because of downstream sea level rise, but due to upstream controls (Gouw and Erkens, 2007). During this period, increased loads of suspended sediment were delivered to the Rhine from the prehistoric deforestation of the drainage basin, causing increased aggradation and renewed avulsive behaviour (Erkens and Cohen, 2009; Stouthamer et al., 2011). Floodplain sedimentation virtually ceased and channel migration was much reduced and confined to a controlled embanked zone, after the building of dikes was completed in the thirteenth century (Hesselink, 2002).

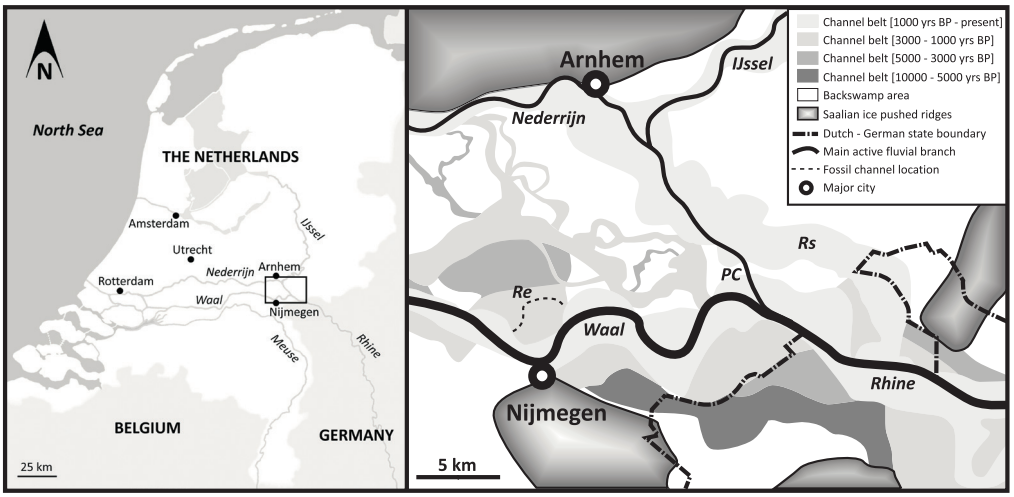

Figure 2: Location and geology of the research area, with the position of the meander bend cutoff of the Ressen (Re) channel-belt complex, and the Rijnstrangen (Rs) disconnected sub-reach of the Nederrijn bifurcation channel (after Berendsen and Stouthamer, 2000).

Many abandoned channels of complex geometry exist in the study area. Those with visible expression at the surface mostly date from the last 3000 years (Teunissen, 1986). We focus on those channel fills that by their vertical dimensions (> 5 m deep) are to be considered former main channels (comparable with the present Rhine), not underdeveloped secondary channels. Two such sites were selected as examples: (1) a pre-Roman meander fill in the Ressen channel-belt complex (Re; Fig. 2) and (2) the much longer multi-meander residual channel reach 'Rijnstrangen' (Rs; Fig. 2). The latter is an avulsion-abandoned channel belt (Kleinhans et al., 2011) that was anthropogenically disconnected in its final stage.

4.2 Fieldwork materials and methods

Research locations were selected using laser altimetry data (AHN: Rijkswaterstaat-AGI, 2005), borehole and core description databases (Utrecht University-LLG: Berendsen et al., 2007; Geological Survey of the Netherlands: TNO-DINO, 2009), palaeo-environmental reconstructions from previous research (Berendsen and Stouthamer, 2000, 2001; Van den Broeke, 2002) and historical maps (Van de Ven, 1976). To reconstruct channel geometry and to identify sedimentary phases, 40 boreholes were hand-cored along seven transects that run perpendicular to the former flow direction. Three transects traverse the abandoned meander in the Ressen channel belt (Fig. 3 and 4). The four transects along the Rijnstrangen channel were further apart than those in the Ressen channel belt to cover the longitudinal variation of deposits (Fig. 5). Borehole data was collected with the 'Edelman' Dutch auger, 3-cm diameter gouge, and Van der Staay suction corer (Van den Meene et al., 1979; Oele et al., 1983). Boreholes were logged in the field, noting macroscopic details per decimetre and describing sediment texture, organic matter content, colour, plant remains, and carbonate content (cf. Berendsen and Stouthamer, 2001). Particular attention was given to lamination-scale interbedding, noting the thickness and frequency of individual flood layers in laminated intervals. Results were added to the institutional borehole database. After collecting the cross-section data, the deepest channel-fill locations were revisited and sample cores retrieved. At the Ressen urbanized floodplain site, this was done using the Begemann mechanical drilling device (operated by Deltares GeoDelft). In the Rijnstrangen swamp sites, this was done using the hand-operated Bohncke-modified Livingstone piston corer (Department of Physical Geography, Utrecht University). Both methods deliver 1-m long segments of cored material from uncased boreholes, with near 100% core recovery to some decimetres beyond the base of channel fills and minimal sample disturbance during coring. Back in the laboratory, cores were split, photographed and logged in detail.

5 Case 1: 'Ressen' pre-Roman meander bend

The pre-Roman age of the selected Ressen abandoned meander is based on an established palaeogeographic reconstruction (Berendsen and Stouthamer, 2001) and palynological investigation of the channel fill (Bunnik, 2010). It is one of several former meanders in the channel-belt complex (Weerts, 1996), active around 3500 yrs BP. The channel had filled up to past floodplain levels by Roman times (~first century AD), based on archaeological evidence (Van den Broeke, 2002). It has been buried since the first millennium AD by the levee complex of the river Waal (Fig. 2); the left hand bifurcation channel of the Rhine Delta. Our identification of the channel is based on borehole data primarily, though the (poorly) visible surface depression supports the subsurface data.

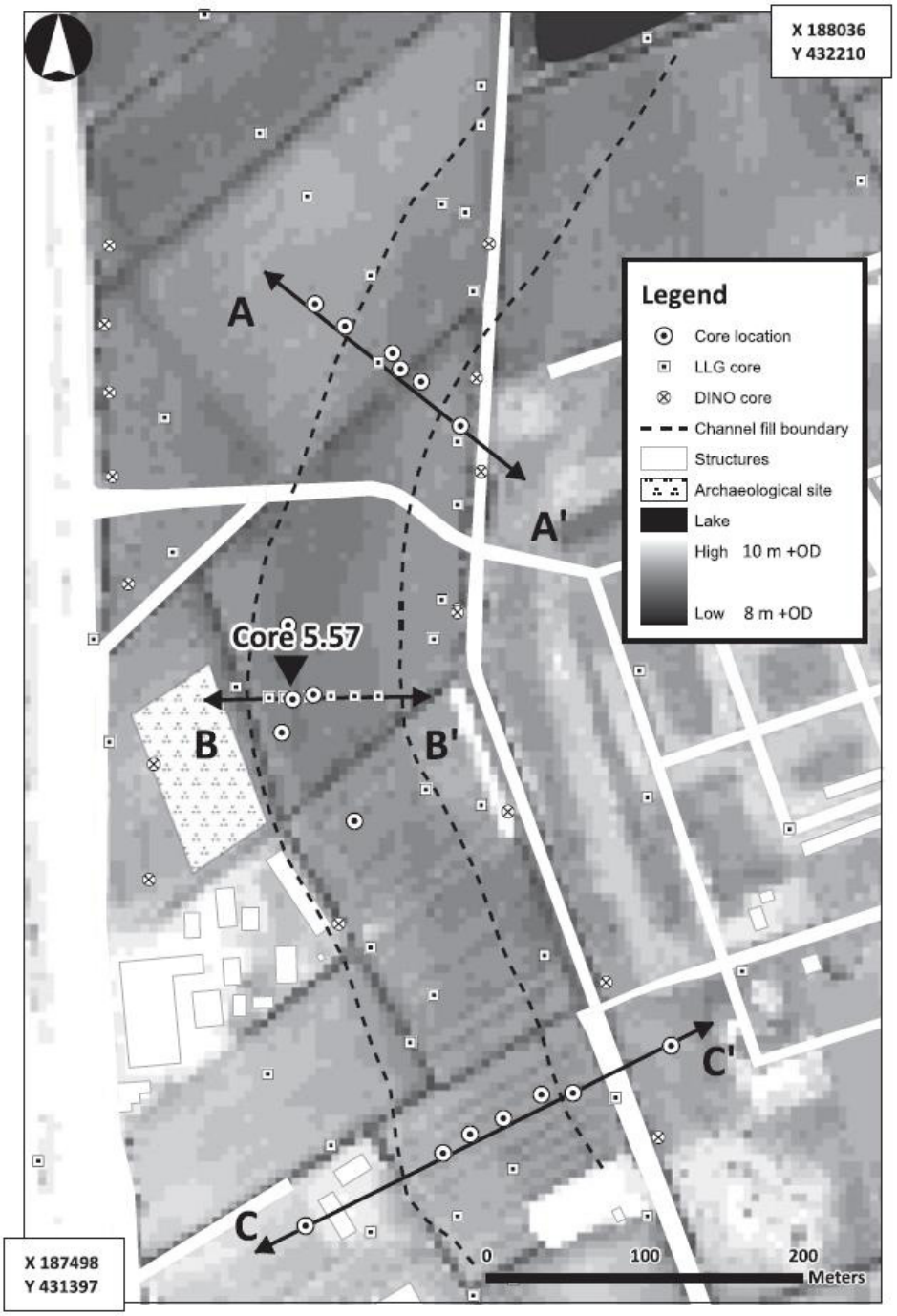

Figure 3: Site map of the Case 1 pre-Roman oxbow fill with coring and transect locations (with Dutch RD coordinates). Grayscale indicates centimetre-scale surface topographic differences, based on laser altimetry data (AHN: Rijkswaterstaat-AGI, 2005).

A 600-m long section of channel fill is studied (Fig. 3). The channel was probably abandoned as a result of a chute cutoff of a highly sinuous meander. Younger channel activity has eroded parts of both the northern and the southern ends of the palaeochannel, presumably removing large parts of the plug bar deposit. Channel-fill sediment accumulated until Roman times (~2000 yrs BP). Filling ceased when the younger 'supply' channel was abandoned in turn, and the modern river Waal came into existence (Pons, 1957; Van den Broeke, 2002). Both palaeochannels extend to the south, where they are dissected by the channel belt of the river Waal. At the approximate time of river Waal initiation, a crevasse channel re-occupied the pre-Roman palaeochannel, locally scouring into the pre-Roman channel fill (Fig. 4). Later overbank sediment delivery caused further burial of the channel fill and crevasse channel deposits. The present surface lies at ~9 m + OD (Dutch ordnance datum).

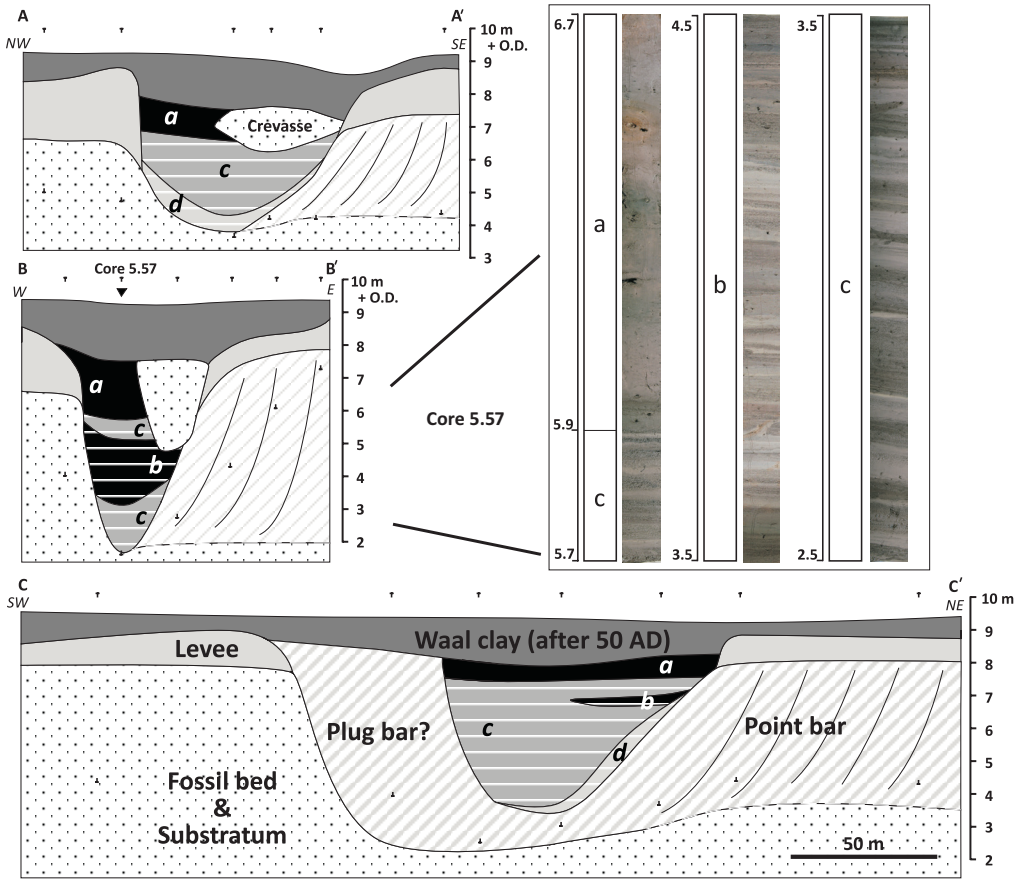

Figure 4: Stratigraphy of the Case 1 pre-Roman oxbow fill (location in Fig. 2), and subdivision of its laminated fill (classes a – d; Tab. 1), for three sections (Fig. 3).

5.1 General sedimentary architecture

Based on sedimentary facies characteristics, the channel fill depositional record is divided into five parts: (i) preserved coarse-grained pre-existing bed and pointbar deposits; (ii) transitional deposits between preserved bed and laminated channel fill; (iii) fine-grained laminated channel fill; (iv) a crevasse splay deposit; and (v) overbank deposits. The cross-sections also include 'older substrate' beneath and beside the channel, and 'younger superficial cover' that overlies the channel fill. The lithological characteristics of the channel fill (fine-grained silty clay deposit, thin centimetre-scale laminations) are distinct from underlying channel deposits (dominantly sandy, thick decimetre-scale beds). Lithological differences also exist between the meander belt (below and east of the channel depression) and 'older substrate' (to the west). The channel deposits are characterised as gravel-rich (toward the base of the channel there is a maximum of 70% gravel; > 2 mm), admixed to very coarse sands (M50 varying from 850 µm to 8 mm). A fining upward sequence is present between 4 and 7 m + OD, with sub-decimetre-scale fining upwards sequences. The upper metres of the palaeochannel outer bank consist of natural levee deposits of a pre-Roman age. These are buried by younger deposits of the pre-diked river Waal (Fig. 4). Levee deposits are fine-grained (M50 < 300 µm), have a maximum thickness of ~1·5 m, are moderately to well sorted and show a fining upward sequence with pedogenic features. The top of the levee contains archaeological evidence for human occupation in Roman times (van den Broeke, personal communication, 2011). These are buried by 70 cm of silty clay, which is a draping floodplain deposit of regional extent of post-Roman age. On the opposite side of the palaeochannel, a similar post-Roman floodplain drape overlies inner bend overbank deposits of the palaeomeander (~1.8 m thick, fine-grained, M50 150 – 420 µm). In turn these overlie a pointbar sequence to the east of the channel depression. Lower pointbar facies are found ~5 m below the present surface and grade into thalweg deposits (e.g., Gouw and Erkens, 2007: their transect A – A').

Table 1: Classes of channel-fill facies with mean lamination thickness (MLT), characterisation of flood pulse deposits (FPD; with mean thickness and coarseness), the matrix containing laminations, and miscellaneous remarks.

Class	MLT	FPD	Matrix	Remarks
A	Not laminated	No visible flood pulses	Clay	Bioburbated, oxidized, non-Ca
B	< 1 cm	1 mm; ø 105-150 µm	Clayey silt	Calcareous, humic
C	1 – 3 cm	< 1 cm; ø 105-150 µm	Silt	Calcareous, humic
D	> 3 cm	1 cm; ø 150 – 210 µm	Silty sand	Calcareous, plant debris

Deposits of the preserved pre-existing bed are found at variable depths reflecting the former thalweg topography during the active stage. The deepest point is found in the middle of cross-section B (~7.5 m below the surface (bs); Fig. 4). At the deepest portion of the core (below the channel fill), gravel content locally is up to 95% of the sediment, with a maximum diameter of 3 cm. In cross-section C, homogeneous sandy deposits (105 – 210 µm without gravel; 2 m thick) directly overlie the preserved bed at the western channel fringe. Elsewhere in the channel these sands do not occur between the thalweg and laminated channel-fill facies (Fig. 4). In this particular case, the homogeneous sandy deposits are probably deposited by backflow into the former meander bend, forming a plug bar. They are probably not the result of continuous shallowing, which would be evident by the deposition of homogeneous sand at all cross-sections in a single meander bend

(Citterio and Piégay, 2009). Although it may be difficult to differentiate between plug-bar sand and deposits from shallowing, the sharp transitions in sedimentary characteristics make clear that significantly different deposits have accumulated during the active, partially disconnected, and abandoned stages.

5.2 Channel-fill internal architecture

The channel-fill facies can be subdivided into four classes, based on internal lithological variability (Tab. 1). The principle division criterion is the style of visible interbedding, i.e. the presence and thickness of the laminations. This interbedding results from the alternation of flood pulses (from rare high-magnitude flood events) within a matrix of finer textured sediment (from more frequent low-magnitude floods) and material derived from autochthonous sedimentation. The boundaries between the classes are set arbitrarily, on practical grounds, with no a priori quantitative physical meaning in mind.

In a typical sequence, class A is encountered at the top and class D is encountered at the base of a channel fill. The fill shows a gradually fining upward trend with gradually thinner mean lamination thickness (Fig. 4). The lower part of the channel fill is generally dominated by stacked repetitions of ~3 cm thick beds of silty sand. These include ~1 cm thick fine sand laminations at the base that fine up internally (class D; Tab. 1). The middle part of the fill is dominated by classes c and b: which includes ~1 cm clayey silt laminations with 1 – 2 mm thick laminations of very fine sand. The upper meter of the channel-fill facies is finest-grained and visually lacks laminations (class A), because of post-depositional bioturbation and oxidation. Besides a fining upward trend, also a lateral fining trend appears to be present: at comparable depths below surface, sediments are finer-grained and more densely laminated towards the thalweg of the former channel depression (Fig. 4).

5.3 Oxbow channel-fill evaluation

Stages of abandonment and sedimentary style in Case 1 compare well to the literature conjectures (Fig. 7 – upper panel), despite the latter being mainly distilled from work in different fluvial settings and generalised textbook examples. We found well preserved channel bed sediment, clearly distinct from the final disconnected laminated channel fill (classes A – D), albeit of relative clastic infilling (organic-rich distal facies units are missing in the fill of Case 1).

Formation of transitional deposits by shallowing, narrowing and as plug bar formation is less evident (possibly less obvious to recognize). Here shallowing is not marked by the deposition of several meters of homogeneous sands throughout the entire abandoned channel. The sandy fill of transect C – C' may represent a stage of shallowing (or belong to the lower end of a plug bar). Narrowing is probably present in the last stage of pointbar build out, but difficult to record as no sharp transition in grain size has been found at the outer part of the pointbar deposits.

The channel-fill internal architecture (in terms of facies subclasses) shows a comparable sedimentary architecture along the entire abandoned channel. A general fining upward (in grain -size and lamination thickness) sharply changes to non-laminated clays at the top. Thicker and coarser laminations at the channel base record a stage when floods were redirected into the newly abandoned channel fairly frequently and that plug bars at the channel entrances had not aggraded sufficiently to prevent annual floods to re-occupy the former channel depression. The fining upward trend within the laminated fill shows that the oxbow was abandoned rapidly after initial cutoff and

received coarse flood sediments less frequently (common annual floods may not have been able to cause deposition) and in smaller volumes as time progressed (assuming that the recurrence of similar sized floods is stationary over time), as a result of further plug bar maturing.

Both lateral and longitudinal trends exist as the most distal and deepest sections are marked by finest grain-size and thinnest laminations (Fig. 4; transect B – B'). This is inherited from the former thalweg morphology, which was deepest in the outermost bend. The similarity in style of the laminated channel-fill facies indicates that the oxbow filled as a single entity after total disconnection. Hence, proxy records from the deeper parts of the laminated fill beyond the proximal plug bars can be considered as representative for the entire bend. This is of key importance for optimised site selection when aiming to collect proxy records from the channel fill.

6 Case 2: 'Rijnstrangen' sub-recently avulsed channel

The Rijnstrangen residual channel marks the historical right hand 'Nederrijn' bifurcation channel of the Rhine (Fig. 2). It is part of the broad bifurcation channel belt that marks the delta apex, which has functioned since ~2500 years ago (based on the regional initiation of overbank deposition; Paas and Teunissen, 1975). By 400 years ago, the 'Rijnstrangen' had lost all discharge to the other bifurcation channel ('Waal'), which can be seen as completing a ~2000 yr-long slow avulsion process. Since AD 1707, the Rijnstrangen channel no longer feeds the Nederrijn branch because of the construction of the Pannerdensch Canal (PC; Fig. 2). The Rijnstrangen bifurcation channel had naturally become disconnected during the sixteenth and seventeenth century AD (historical source compilation in Van de Ven, 1976; geomorphodynamic response analysis in Kleinhans et al., 2011). By AD 1700 the entrance was almost completely plugged. During larger floods, waters remained to be directed into the Rijnstrangen residual channel until AD 1959. Now, the Rijnstrangen channel only carries local drainage, and is upstream connected to the Rhine channel through groundwater exchange only.

Four transects were drilled over the channel-fill deposits of the 'Rijnstrangen' disconnected section of the Nederrijn branch (Fig. 5). To allow comparison of channel stratigraphy at contrasting settings within the same system, two transects were drilled along relative straight sections of the channel, and two across sharper bends. We presumed intermediate positions to contain more chaotic fillings, more difficult to intercorrelate, and to be less suitable to test and expand the schematised framework for channel fills. Older deposits of the Rijnstrangen channel belt are only treated here in relation to the final channel fill, focussing on the terminal 'abandoning' and 'fully disconnected' stages. The internal structure of the channel belt as produced during earlier stages of the slow avulsion process is described in Kleinhans et al., (2011).

6.1 General sedimentary architecture

The sedimentary facies of the Rijnstrangen area are grouped into: (i) preserved bed; (ii) transitional deposits (silting-up sequence); (iii) laminated channel fill; and (iv) overbank deposits overlying the channel fill (Fig. 6). The former thalweg position is identifiable from the sectioned deposits (Fig. 6) and matches positions on sixteenth and seventeenth century historical maps (e.g., Van de Ven, 1976; Kleinhans et al., 2011). Preserved bed facies are found at ~5 – 6m + OD. At greater depth below and greater distance adjacent to the channel fill, the bed deposits represent earlier stages of

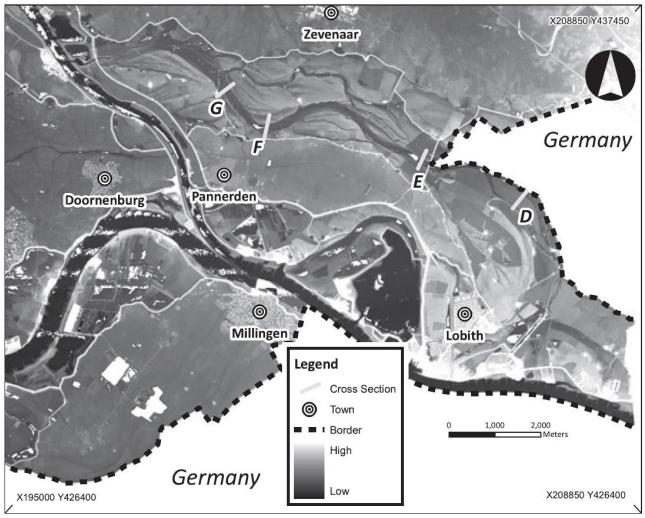

Figure 5: Site map of the Case 2 Rijnstrangen residual channel with the location of coring transects D – G.

channel-belt activity, when the branch was carrying a larger proportion of the Rhine discharge and was the main distributary. Occasional boreholes reach below 5 m + OD and have penetrated thalweg deposits. Below the channel fill, the top of the preserved bed is marked by gravel-rich coarse sands (~30% gravel; M50 600 – 1400 μm). These gravels are of modest grain size (< 1 cm). The sandy matrix is also of relative fine texture. Unlike in Case 1 and in the oxbows described in the literature, channel-fill deposits in this abandoned bifurcation channel do not show a marked boundary with bed sediment, but a gradual transition instead. These transitional deposits represent a phase of channel shallowing, when the channel was actively losing a proportion of its discharge. The sand (M50 300 – 850 μm) shows a fining upward trend with a decreasing gravel admixture and better sorting. In downstream direction, there is a reduction in the thickness of this sand (above the pre-existing bed; transect F and G, compared to D and E; Fig. 6). A downstream reduction in grain size is not recognized, however. Extensive discussion of this transitional shallowing and narrowing phenomenon is found in Kleinhans et al., (2011).

6.2 Channel-fill internal architecture

The residual channel fill consists of much finer-grained deposits. In longitudinal direction the thickness of the disconnected fill increases downstream, as the transitional sands below decrease in thickness. In the most upstream cross-section (D), proximal to the bifurcation (Fig. 5), the laminated fill is 30 to 110 cm thick. This laminated fill is ~2 m thick in the distal cross-section G. Toward the surface, the fill becomes more humic and sand content decreases – in upstream and in downstream sections alike. This signals decreasing energetic conditions in the abandoning channel that became more and more closed – similar as described for abandoning oxbows. The basal fill shows distinct laminations. In shallower and riparian-vegetation overgrown residual channels, the top of the channel fill is oxidised and heavily bioturbated, destroying laminations. In the laminated part, most channel fills do not show a sequence in style of lamination (Tab. 1; classes A – D), unlike in the meander bend cutoff of Case 1. One exception exists where the laminated residual channel fill is ~4 m deep in an outer bend (section F; Fig. 5). It appears that shallowing processes during

the transitional stage prohibited deep residual channels to develop for a considerable distance downstream of the bifurcation and thus thick laminated fill records are rare in this system.

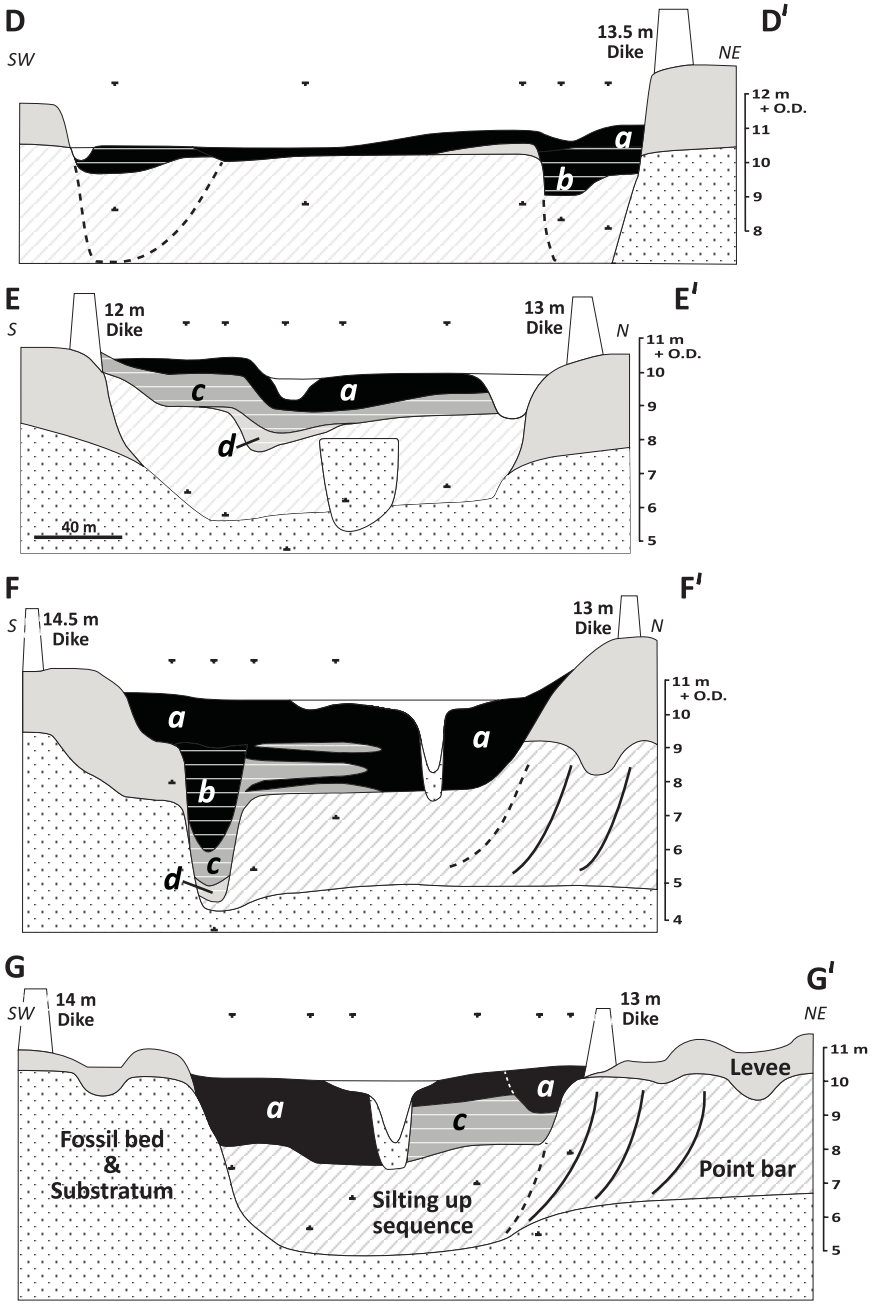

Figure 6: Channel-fill stratigraphy of the avulsion-abandoned bifurcate channel of the Case 2 Rijnstrangen (Fig. 5), with subdivision of the laminated fill (Tab. I), set in a secondary channel fill.

6.3 Framework extension: avulsion-abandoned channel filling

When the fill of Case 1 and Case 2 are compared, it is evident that in the avulsion-abandoned channel (Case 2), a large volume of channel-filling deposits is produced in the transitional stage (Fig. 7). Sedimentary products representing the process of shallowing occupy a significant larger volume of the entire channel fill in individual transects than observed in the abandoned meander infill. They extend over a large distance from the palaeochannel entrance. Both duration and mechanism of channel abandonment process (differing between individual bifurcation cases; Kleinhans et al., 2008) are important factors explaining the difference in channel-fill architecture of the abandoned bifurcation channel. Bifurcations at the delta apex function for a relative long time (centuries to millennia in the Rhine Delta), compared to meander cutoff (commonly within decades). This is because the outcome of the initial avulsion is not decided within few floods via gradient advantages, but impacted by temporising factors such as meander migration and channel width adaptation (Kleinhans et al., 2008; Kleinhans et al., 2011).

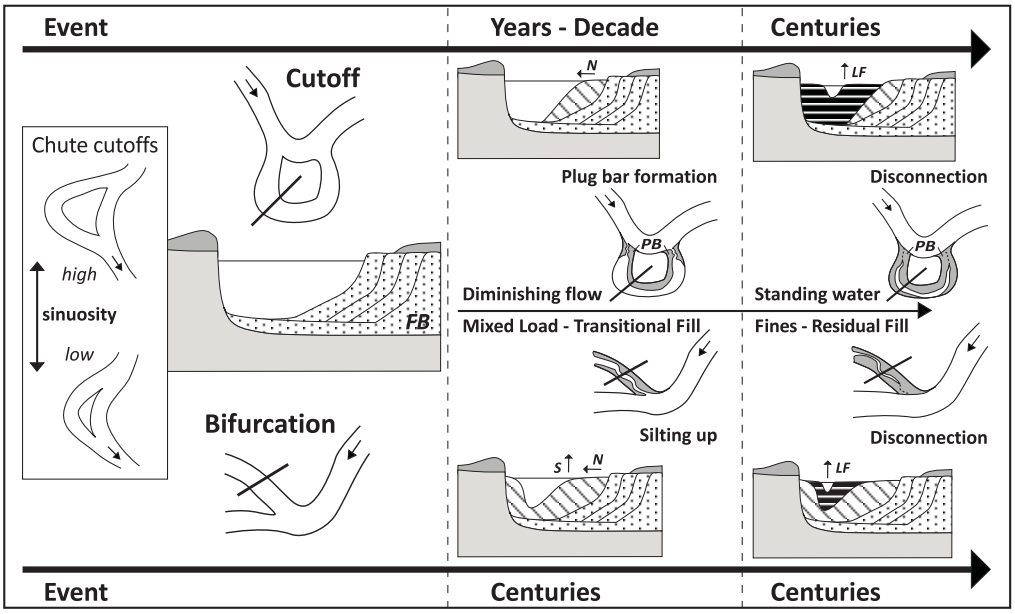

Figure 7: Integrated conceptual sedimentation model for channel fills, covering individually cutoff meanders (top panel) and avulsion-abandoned channels (bottom panel).

Abandoning bifurcation channels experience an extended transitional stage with shallowing and narrowing before they become fully disconnected and residual channel filling initiates. The longer duration of the transitional stage logically results in larger volumes of transitional channel fill and leaves less accommodation space for laminated channel fills than in oxbow lakes (those formed by neck cutoff and chute cutoff in highly sinuous rivers).

An important driver for this difference is the angle of connection with the active channel between both fluvial types. A smaller angle of the palaeochannel with the active branch favours prolonged flow in the avulsion-abandoned channel, as bedload is not necessarily deposited right at the channel entrance. Consequently, plug bars in avulsion-abandoned channels should not be seen as steep and

narrow underwater bars (in contrast to the typical oxbow case), but are initially much lower at the entrance and protruding further down the abandoned channel and can thus fill a larger part of the former channel depression (Fig. 7). This migration of sandy bars far inside the abandoning channel (up to several meander lengths) has been recognised on historical maps of the Rijnstrangen area (Kleinhans et al., 2011). As a result, the volume of laminated fill in avulsion-abandoned channels can only become dominant in a longitudinal downstream direction.

7 Discussion

7.1 Flow concentration and overprinting by secondary channels

Based on observations in the upper Columbia River (Canada), Makaske et al., (2002) point out a mechanism to be in play in abandoning channels during the transitional stage in avulsive systems (here termed as 'flow concentration'), which is hypothesised to lengthen the connectivity of bifurcating anastomosing channels. Flow concentration as a secondary channel process overprints and follows up on shallowing and narrowing as described earlier. It involves the formation of a smaller secondary residual channel within an originally wider palaeochannel. Such a residual channel may leave its own imprint on the final palaeochannel fill (e.g., local overbank deposits, formation of secondary channel bed), possibly causing disturbance of the pre-existing channel fill deposits and increasing the lateral and longitudinal heterogeneity of channel fill deposits. Our Case 2 example (Rijnstrangen) bears evidence for flow concentration of remaining local discharge through the palaeochannel. This maintained a small residual channel with a sandy bed, embedded in muddy primary channel-fill deposits. Furthermore, considerable lateral heterogeneity exists in the primary channel fill (Fig. 6). This suggests that deposits on either side of the secondary residual channel have not been deposited simultaneously under the same conditions, presumably due to flow concentration processes in secondary channels during the primary filling. Flow concentration would postpone complete filling of the abandoned channel and can explain the formation and preservation of secondary residual channels. Multiple examples of such residual channels are present in the central Rhine Delta; filled with organo-clastics and traceable over multiple meander wave lengths (e.g., Pons, 1957; Verbraeck, 1984; Teunissen, 1986; Törnqvist, 1993; Makaske, 1998; Berendsen and Volleberg, 2007). It has, however, not always been recognised to what degree these residual channels underfit the width of their parent primary channel fill and further surrounding channel belt. Understanding secondary overprints and masking of the primary abandoned channel fill is important to identify palaeochannel fills in the first place, to locate their sweet spot for collecting records for various reconstruction purposes, and to improve chronologies of channel abandonment (e.g., for avulsion frequency and avulsion duration; Stouthamer and Berendsen, 2000).

7.2 Channel fills and effects of fluvial migration

Channel fills can also play an important role in natural dynamics of channel migration. Channel fills can either facilitate or hinder migration of younger channels. Clay plugs (distal fills) may obstruct lateral channel migration by its erosion resistivity (Fisk, 1947). This seems to be a factor of importance in valley reaches without major aggradation, where floodplains are relatively narrow and where space to evade these subsurface obstructions is limited.

In contrast, in deltas with wide floodplains and avulsion-abandoned residual channels, abandoned bifurcates are common sites of channel re-occupation (e.g., Smith et al., 1998; Stouthamer, 2005) for a couple of reasons. Abandoned channels remain floodplain depressions for a considerable length of time, are likely to provide gradient advantages, and contain easily erodible sediments. Repetitive alternating re-occupation of abandoned channels can lead to the formation of long-lasting nodal avulsion site, provided that successive bifurcations develop relatively slowly (forcings in Kleinhans et al., 2008) with extensive deposition during the transitional stage.

7.3 Site specific factors

Whether a channel fill evolves according to our suggested stages (Fig. 7) and if deviations exist (in the duration of each stage, the volume of deposits, sedimentary characteristics formed during each stage, preservation potential and possibilities for future re-occupation), all largely depends on site specific factors. Rivers differ in size, in types of flood regime and composition of sediment carried as bed and suspended load (and in numerous other aspects). Moreover, chances of preservation may well differ for alluvial basins of different size and rates at which valley meanders reconfigure are variable between rivers and this possibly overprints sedimentary styles. This discussion further focuses on site specific factors that along a single section of river valley result in a variety of channel fills.

Examples of the differences in configuration of abandoned channels are shown in Figure 8, for an assemblage of channel fills along the modern Lower Rhine. It illustrates the variety in floodplain configuration, active channel proximity and entrance morphology within the assemblage, for abandoned channels of a range of ages (Holocene and Late Glacial; Erkens et al., 2011). Basic sedimentological and hydrodynamic insights regarding filling (e.g., distal versus proximal facies) and sediment transport (e.g., channel entrance angle and effectivity of plugging and shallowing) strongly determine the characteristics throughout the stages of development of the fill.

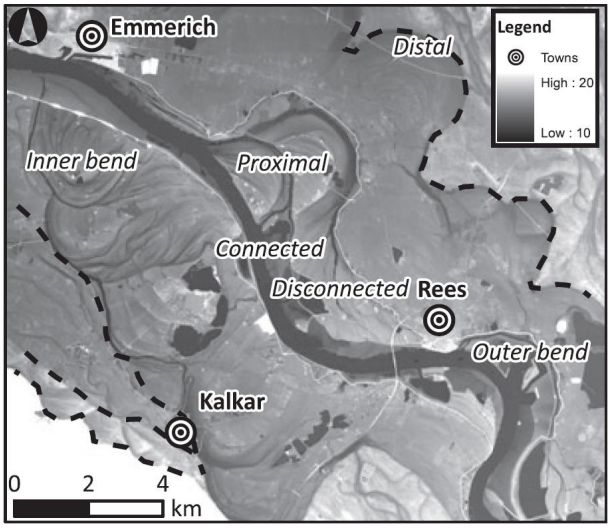

Figure 8: Site specific factors, exemplified for an assemblage of channel-fill localities (Lower Rhine Valley, Germany, directly upstream of the Rhine Delta apex). Dashed lines mark terrace scarps of Late Glacial and Early Holocene age.

Logically, the position in the floodplain largely determines actual sedimentation type and rates; with proximal abandoned channel being more susceptible to maintain an open connection with the active channel, as such increasing the imprint of the transitional stage (Fig. 8). The configuration of the active and abandoned channel influences plug bar formation. Abandoning channels located at inner bends are susceptible to a rapid sealing by plug bar growth, while abandoning channels attached to the outer bend of the active channel receive more discharge and suspended load, leading to relative slow plug bar formation as sediment is transported further into the abandoned channel. As a consequence, abandoned channels connected to the inner bend of the active channel are expected to seal off rapidly and therefore yield minor sandy sequences and are dominated by laminated fill facies. Distance to the active channel itself influences the typically received grain sizes and aggradation rates in the fully-disconnected stage (e.g., Gaigalas and Dvareckas, 2002).

Lastly, bend configuration is not static, as meander bends migrate downstream (Fig. 8). Kleinhans et al., (2008) explored this as a generic factor to explain bifurcation longevity (and pulsation), sustaining an extended transitional stage in channel filling. Neither is the configuration of the active channel necessarily static in the fully disconnected stage, when distal laminated channel fill accumulates. Shifts of the active channel away or towards a distant oxbow lake can change the frequency, volume and composition of clastics received during flood pulses (in selected cases visible as shifts in laminated subfacies of Tab. 1). Berendsen and Hoek (2005) provide a central delta residual channel example recording these kind of shifts from downstream of the study area. Erkens et al., (2011) report an oxbow example for this, from just upstream of the study area (Hoek et al., 2011).

7.4 Study limitations

The current work is developed on the Rhine upper delta and lower valley reaches in the Netherlands and Germany. As such, it is biased to Holocene mixed-load meandering rivers of moderate to large size and their bifurcating upper deltaic reaches, from mid-latitude temperate Europe (Rhine as a larger example), while many of the cited oxbow-filling field studies were on smaller rivers (and upstream reaches). Our framework for channel-fill interpretation builds on literature, field data and modelling work and primarily aimed to formalise description of channel fills for the various cases that occur next to each other in our study area. It has yet to be applied to sites outside our study area, and one may consider it to be limited to our study areas specific sedimentary environment; related to drainage basin size, regional climate, ruling draining regime, Pleistocene inherited valley morphology, and bed sediment. The two cases are selected examples and further collection of channel fills of different style is well possible just staying in the same study area. We believe, however, that the insight in timescales of oxbow cutoff versus avulsion-abandoned channels are generic and relevant to Holocene river systems elsewhere and for fluvio-deltaic sequences in reservoir geology.

8 Conclusions

The internal architecture of channel fills within meandering river channel belts is essentially determined in two stages: a transitional stage of active abandonment and a disconnected stage, commencing when abandonment is completed. An event of initial diversion of the main flow,

causing the meander cutoff or the avulsive bifurcation-abandonment, triggers the start of the transitional stage. It leads to plug bar formation at the entrance, and shallowing and narrowing in the channel downstream. These form architectural elements of which sedimentary contents record bifurcation and cutoff dynamics. The disconnected (or fully abandoned/residual) stage comprises sediments of finer texture, typically laminated, produced during flooding events. This architectural element is commonly used for palaeo-environmental proxy data and dating, and is of interest as a direct sedimentary archive of flooding too.

In oxbows, the transitional stage mainly results in plug bar formation at the channel entrances. Plug bar formation is efficient, because of instant gradient advantages and rapid flow diversion following the cutoff event. This triggers bedload accumulation to close off the oxbow. Less dramatic discharge loss is seen in avulsed-abandoned channels. Rapid plug bar formation is hydrodynamically prevented, allowing development of a bedload sheet into the closing channel, causing shallowing and narrowing over a larger downstream distance and much longer period than it takes to plug an oxbow.

Laminated channel fills are produced during the abandoned stage. They can be classified according to their lamination thickness and sedimentary characteristics. Due to rapid plug bar formation, oxbow fills typically yield thick sequences of laminated fill. Especially the proximal part of avulsed-abandoned channels rarely contain thick laminated fills, as most space has been occupied by deposits of the transitional stage. Downstream, thickness of the laminated fill increases, but there heterogeneity is larger than in oxbow fills as avulsed-abandoned channels are more susceptible for secondary overprinting.

This work can improve existing usage of palaeochannel fills as containers of datable material and environmental proxy data, and can serve new usage as direct records of past fluvial morphodynamics and archives of flooding, at least for the Lower Rhine area. We suggest the framework to be generically applicable as it is based on collected insights from literature on oxbow lakes and meander cutoff of various river systems. However, applicability to other river systems awaits demonstration.

Acknowledgements
The authors acknowledge Utrecht University MSc students J. IJmker, J. Hoekstra and T. Konijnendijk for participating in the fieldwork in the Rijnstrangen and Ressen areas. Gemeente Nijmegen ('Ressen' site) and Staatsbosbeheer ('Rijnstrangen' site) are thanked for site clearance and facility to carry out the research. The authors also thank W. Hoek (Utrecht University), F. Bunnik, T. Donders (TNO), E. Heunks (geo-archaeologist) and P. van den Broeke (Gemeente Nijmegen) for discussions, introducing specific sites, and establishing archaeological and palynological cross-links with channel geomorphology and channel fills. Two anonymous reviewers are acknowledged for useful comments. Editor Stuart Lane and assistant editor Fiona Kirkby are thanked for their guidance. Authors contributed to conception and design, data collection, analysis and conclusions, and manuscript preparation in these proportions: WHJT (50,70,50,60%), MGK (10,0,20,10%) and KMC (40,30,30,30%). This research was funded by Deltares, with additional funding from TNO Geological Survey of the Netherlands, and Utrecht University. Reprinted with permission of Earth Surface Processes and Landforms, John Wiley & Sons, Inc.

4 Oxbow channel fill sedimentology as a tool for age-depth modelling and reconstruction of palaeogeography and fluvial dynamics

Lower Rhine, Rheinberg, Germany

Minderhoud, P.S.J.[1], Cohen, K.M.[1,2,3,*], Toonen, W.H.J.[1,2], Erkens, G.[2,1], Hoek, W.Z.[1]

[1] Department of Physical Geography, Utrecht University, The Netherlands
[2] Deltares Research Institute, Utrecht, The Netherlands,
[3] TNO Geological Survey of the Netherlands, Utrecht, The Netherlands
[*] Corresponding author: POBOX 80.115, 3508 TC, Utrecht, K.M.Cohen@uu.nl

1 Introduction

In the Lower Rhine Valley (Nordrhein-Westfalen, Germany), a number of individual Early and Middle Holocene palaeomeander fragments have preserved on either side of the modern meander belt (Klostermann, 1992; Shala 2001; Erkens et al., 2011). One can quite confidently draw maps of meander configurations for any moment in time in the youngest millennia as a continuous series (ibid.). For older periods, however, such reconstructions (e.g., Cohen et al., 2012) become inherently sketchy. This is because in the central axis valleys record has been wiped out by younger river activity, rendering direct connection and correlation of floodplain-edge meander fragments problematic (e.g., Lewin and Macklin, 2003). Resulting incompleteness and discontinuity of the record also constrains its dating. The lateral preservation properties of meandering rivers hinder to stretch reconstructions of subrecent river activity from 'the last centuries' to 'the last millennia'. This is unfortunate, because unravelling total response to respective forcing factors on river system change such as gradually growing human impact and variable climate requires reconstructions reaching back several millennia.

Continuous reconstructions of river dynamics spanning the Holocene are inherently difficult to extract from geomorphological fluvial archives alone. From a preserved meander, one can collect dates of final activity and abandonment, amongst others using ^{14}C from the base of meander fills and OSL on sandy sediments preserved from last stages of lateral migration and channel filling (e.g., Erkens et al., 2011; Lauer et al., 2011). More difficult to get are independent age estimates for when such meanders began their activity, simply because reworking-lost geomorphological stages cannot be physically sampled. From the counts of preserved older meanders in typical geomorphological-geological mapping (e.g., in the Lower Rhine valley, Fig. 1), and comparison to such numbers for the meander record preserved from youngest millennia, it is clear that the Middle and Early Holocene valley floor features temporal preservation gaps. This limits the possibility to connect the results of fluvial geomorphological reconstruction studies to, for example, studies

documenting the river process dynamics, to reveal frequencies of meander migration and cut-off and associated processes of sediment transfer over time scales longer than the last centuries, and hence to discuss forcing(s) and variability of these processes.

In contrast to geomorphological archives, sedimentary sequences of oxbow lake fills may provide continuous records of fluvial dynamics. Starting with the meander abandonment event that initiated oxbow-conditions, these fills record for a relatively long period, especially when the subsequent active channels remain located at sufficient distance from the oxbow lake. Both river proximity and discharge regime may change while the filling continues. The former changes are due to natural and artificial channel migration, such as cut off and avulsion nearby in the valley (e.g., Erkens et al., 2011). The latter changes are due to climate variability (within the Holocene of subtle nature) and human impact (increasing towards the present), integrated over the larger drainage basin upstream (e.g., Erkens et al., 2006; Hoffmann et al., 2007).

In this study, we use a Lower Rhine valley oxbow fill of Middle Holocene age (Fig. 1) for a reconstruction of ~1750 years of fluvial dynamics, such as events of meander reconfiguration and periodical variations in recurrence of larger floods, in the particular valley segment. The oxbow fill accumulated over the period ~4.7 to 2.9 ka cal BP, the period during which prehistoric deforestation is believed to have commenced affecting the Rhine, and a period believed to have seen climatic variation (4.2 ka event; the Middle to Late Holocene transition; e.g., Walker et al., 2012). With oxbow-fill records, the resolution of reconstruction of fluvial dynamics can be improved. This in turn should aid the separation of autogenic-, human- and climate-induced record imprints.

Oxbow-lake records of palaeoenvironmental change are either based directly on the sediments (grain-size, organic versus clastic content, geochemistry) or on materials contained in sediment (e.g., pollen, charcoal, diatoms). Whatever the direct measurement or proxy obtained, using the record as an archive of palaeoenvironmental change requires to assigning ages to the irregularly accumulated sequence. In dominantly organic fills, an occasional encountered clastic layer can be dated by collecting bracketing spot ages, using AMS radiocarbon dating on terrestrial plant macrofossils from the organic beds bracketing the event layer. Within organic clayey beds (facies with organic content > 25%), one can determine sedimentation rates by collecting a densely spaced series of AMS ^{14}C samples throughout the interval: general availability of dateable material is not the problem. However, for the dominantly clayey organo-clastic intervals in cored sequences from oxbow fills in less distal situations (facies with organic content < 25%), organic material – such as mats of leaf-fragments – that is suitable for dating is present, but only at irregular depths and encountered by coincidence. This prevents dating a particular event bed from organic materials directly bracketing it. Dating sequences of event beds then relies on age-depth modelling, interpolating between what few spot ages could be acquired.

The aim of the paper is to develop a fluvial-dynamics reconstruction that makes maximum use of the sedimentary information contained in an oxbow fill, so that 1) recurrence times of distinctly recorded floods can be established; 2) distal-proximal shifts in channel position are revealed and timed; and 3) age-depth models for floodplain lake sedimentary archives in general are improved. Choice of site and data collection procedure were relatively straight forward, making use of earlier regional geological-geomorphological mapping. The methodological development is in the

analytical steps of age-modelling of the sequence and interpretations regarding its accumulation, which interrelate.

The geological setting of the selected case is provided in section 2. Because of the importance of the filling process for high resolution age-depth modelling, normal sedimentation processes and occasional flood event-bed registration, a rationale of current understanding of oxbow filling is provided early in the paper (section 3). Data gathering and methods of analysis build on that rationale (section 4). A site-specific interpretation of the oxbow fill and performance evaluations of newly-deployed techniques are the principal results (section 5), and these are discussed (section 6) in wider palaeohydrological and palaeogeographical context.

2 Geological setting of the Rheinberg palaeochannel

For this study we selected and cored the oxbow fill of a former meander of the river Rhine at Rheinberg, Nordrhein-Westfalen, Germany, which has a marked scarp at the margin of the Rhine floodplain, undercutting a higher elevated terrace (Meander A, Fig. 1). The palaeochannel was identified in a regional mapping and sectioning campaign in 2006, which also provided initial dates of the base of the channel fill sequence (Erkens, 2009; Erkens et al., 2011).

The abrupt basal contact of the channel fill, encountered at 'thalweg' depth, is indicative for the sudden abandonment of the oxbow channel. Many meters of laminated, fine-grained muddy oxbow fill abruptly overly coarse sand and gravels. The oxbow fill shows varying organic matter contents, both at the cm scale (interpreted as flood event beds) and at decimeter-to-meter scale (change in general sedimentation conditions, interpreted as channel reconfigurations). Towards the base of the fill, anoxic colour-banding was observed in what is interpreted as consecutive flood event layers. Radiocarbon dating of organics from near the oxbow-fill base (Erkens, 2009; sections below) indicate that infilling started around 4,750 cal yrs BP, so the preceding cut-off is believed to have occurred just earlier. In times between floods, the oxbow lake must have held a standing water column of 6 to 7 meters, based on the thickness of subaqueous facies, younger overburden, and surrounding borehole data (Erkens et al., 2011). The oxbow lake gradually filled with over 5 meter of Rhine flood-delivered organo-clastic muds. A facies transition to clayey peat results from when the oxbow had filled up close to water level (~1.5 m water depth).

The peat in turn became covered with silty floodplain clays, that regional mapping traced to Late Holocene meander and natural levee systems (Erkens et al., 2011). By this stage, the oxbow lake had transformed into regular floodplain environment. In Roman and Medieval times (1st millennium AD), humans intensified their cultivation on the elevated terrace to the west and south, and the Holocene pointbars and levees to the north and east (Klostermann, 1992; Shala, 2001). The peaty channel became used for local drainage towards the town moat of Rheinberg. In the main site core this is seen by an erosive contact into the floodplain clays, but the oxbow fill below is not affected. The paper focuses on the organo-clastic mud and topping peaty clay of the oxbow fill.

A second Middle Holocene palaeomeander has also been preserved (Fig. 1). This Meander B was also sectioned and dated (Erkens et al., 2011). LiDAR geomorphology and dating identify Meander B as Meander A's immediate successor palaeomeander. At its dating location, the fill is relative

shallow. The base is 4.2 meter above the channel base of the main site and overlies coarse sand of an in-channel bar facies whereas the coarse thalweg facies was not reached. The fill of this meander is overlain by a natural levee deposit of considerable thickness, regarded of the same broad age as the floodplain cover of the main site (~3000 cal yrs BP). These additional findings for Meander B help to constrain the dating and interpretation of the main site.

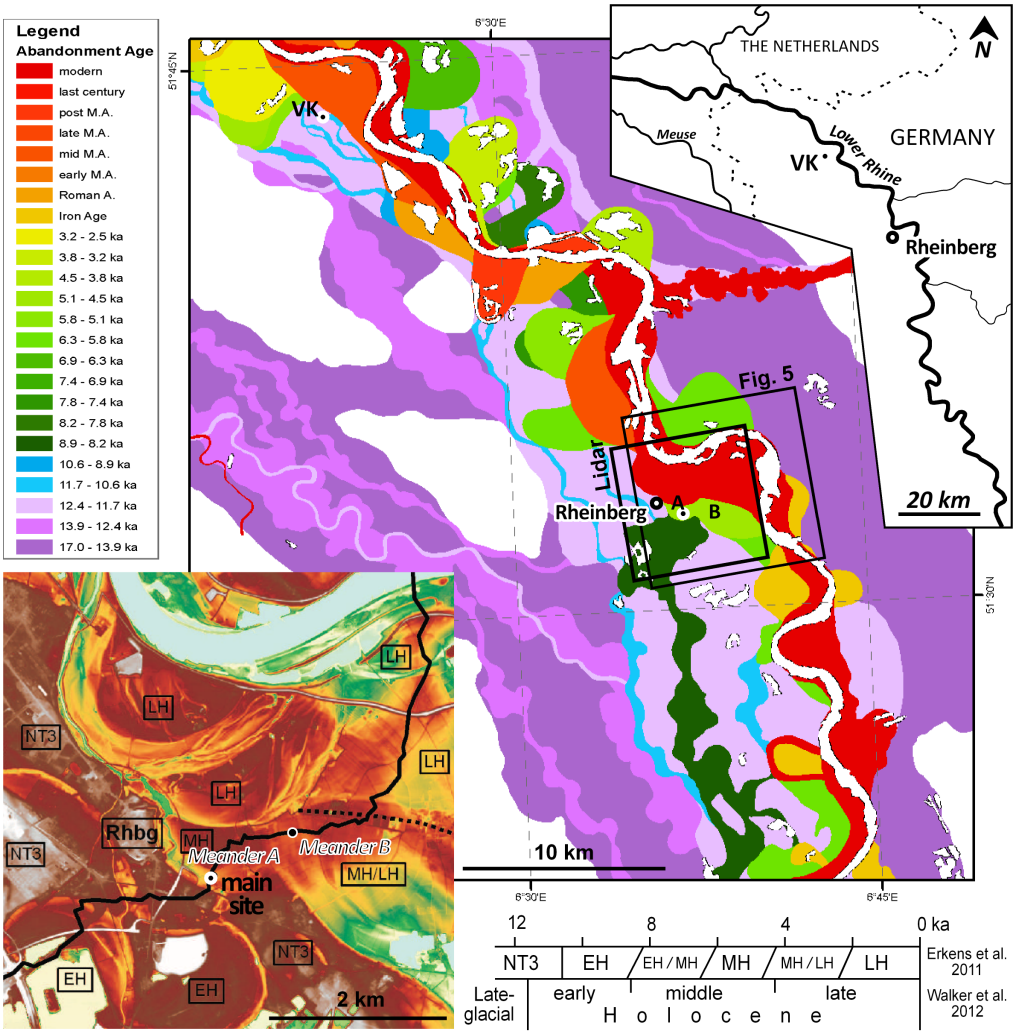

Figure 1. Rheinberg study area (Nordrhein-Westfalen, Germany). Geological map extracted from Cohen et al., 2012. Annotated LiDAR imagery after Erkens et al., (2011). VK = site of millennial flood marker from Toonen et al., (2013; Chapter 6).

3 Sedimentology of oxbow lake-fill records

In lowland rivers of meandering style and mixed sediment load, palaeochannels at moderate distance away from active channels accumulate organo-clastic deposits in subaqueous environments of oxbow lakes (Chapter 3). Once disconnected from the active channel, the deepest part of a newly formed oxbow lake matches the former channel's bend thalweg depth (6-10 meters in the case of the Lower Rhine). Close to the meander cut-off location, relatively coarse sediment accumulates as outcome of initial cut-off and plugging processes, which usually rapidly shallows the oxbow entrance within the decades following cut-off (Hooke, 1995). The more distal depositional environments that establish further within the oxbow show less dramatic shallowing (Citterio & Piégay, 2009; Dieras et al., 2013). Here, sedimentation rates are lower, and consist of locally produced organic material admixed to fine-grained floodwater-derived sediment layers (and intercalated with such sediment layers without organic admixture). If the oxbow lake is located at a distal position within the floodplain, its fill can record multiple millennia of semi-continuous sedimentation. Ultimately, a terrestrial floodplain environment replaces the subaqueous depositionary conditions.

Processes and variations in sedimentology and sedimentation rates that are highlighted here concern central parts of oxbow lakes. These have had a 'sufficiently distal' position relative to the active river which contain a subaqueous mud sequence that accumulated slowly enough to result in a record spanning a considerable length of time, but at the same time providing sufficiently sensitive sedimentary registration. Within oxbow lakes, the deeper parts of the oxbow lake are targeted, which contain the thickest fine-grained record and are regarded optimal for extracting palaeoenvironmental information (cf. Kasse et al., 2005; Wolfe et al., 2006, Lechner, 2009). The core from the Rheinberg meander is from the deepest part of a filled oxbow at sufficiently distal position within the floodplain, to have both the suitable sedimentology and the record length for our intended research.

3.1 Facies, sedimentation rates and frequency of flooding

Oxbow lakes fill relatively fast because they trap allochthonous pulses of sediment input at maximum and waning stages of river floods. Sediment-delivering floods vary in magnitude and duration, and recur irregularly. The amount of fine-clastic sediment received *per flood* depends on the flood magnitude, with larger influxes associated to greater discharge events, being more-sediment-laden and longer lasting (e.g., Asselman et al., 2003 – for the river Rhine). Irregular recurrence of floods in various ranges of magnitudes results in sediment variations at the scale of individual beds, in amount and composition. Received amounts further depend on the distance and connectivity to the active river. Both are properties that affect sedimentation during floods of all magnitudes and that may change during the 'lifespan' of oxbow filling. Individual flood pulses register as individual beds. These register as mm-to-cm thick, less-organic, silty-clay event layers from large floods that can be individually identified. Too thin event beds may not be recognised or be erased by processes at the lake bottom, thicker beds may preserve and develop internal grading (e.g., Czymzik et al., 2013). Their sediment mixes with autochthonous organics in the periods between floods. This results in the visually homogeneous facies.

Periods of less efficient delivery of sediment, but otherwise unchanged autochthonous production in the lake, register as fill intervals of relatively increased organic content. It darkens typical fine-grained matrix sediments (especially in fresh core cuttings, before oxidation) – as also seen in the infillings of subrecent floodplain lakes, such as dike breach scour hole fills (Middelkoop, 1997; Chapter 5). This fine-grained matrix is the result of what we call 'background' sedimentation in this paper. In suitable circumstances, flood sediment pulses register individually, as thin distinct lighter-coloured interbeds within darker 'background' sediment of the homogenous facies described above.

Processes at oxbow entrance locations affect sedimentation in the deeper part of the oxbow, and cross-reference can be made between facies changes at the base of the fill in deeper oxbow lake parts and the situation at the entrances. Near the base of an oxbow fill it is not uncommon to encounter cm-thick event beds, often showing up as lighter-darker alternated banding and visibly internally graded. In contrast to the thinner event layers mentioned above, such basal event beds can be regarded products of consecutive floods: they accumulate over a time period immediately following meander abandonment when plugging of the entrance has not yet completed. In this initial period of filling the beginning oxbow lake may even receive sediment at discharge stages lower than bankfull (Q_{bf}). From the time that the oxbow lake is fully disconnected sediment is only delivered during floods: when discharge exceeds $Q_{bf.}$

3.2 Length of contained record, position in floodplain, and preservation

Oxbow lakes may form and preserve at various positions within the floodplain and their infilling facies is dependent on this position. The best examples of semi-continuous laminated facies seem to occur in floodplain-edge oxbow lakes at intermediate distance of the active channel. Registration sensitivity decreases with distance to the active river, whereas contained record length increases: a trade-off situation that works out well for meanders at the edge of the active floodplain. From our mapping field experience in the Lower Rhine valley and delta apex (Berendsen et al., 1995; 2007; Gouw & Erkens, 2007; Cohen et al., 2009; 2012; Erkens et al., 2011; Stouthamer et al., 2011; Kleinhans et al., 2011; Toonen et al., 2012; Janssens et al., 2012), this is typically between 1 and 4 km from the active river. A more distal oxbow lake can cover a longer time period, but loses resolution for individual registration of flood pulse events of modestly large floods due to the reduced sedimentation rates at greater distance, and consequently greater effect of bioturbation. Furthermore, due to continued shifting of the active river, the oxbow distance to the active river changes during fill recording changes over time. This leads to variation in the event registration frequency *and* background organic content, which in turn can affect the sensitivity and resolution of the archive as a record.

Oxbow lakes that form at close distance to an active channel (< 1 km) typically fill in much faster than those in intermediate position. They hold relatively short records (e.g., just 10^2 years instead of about 10^3 years; Chapter 3), with very thick flood event beds with separating organic facies poorly developed, if developed at all. On top of their relative short record length, proximal oxbow fills do not preserve in large numbers for periods longer than a millennium (in natural situations; embankment and engineering in the modern channel have positively affected preservation of proximal fills from the last 500 years). Their proximity to the active river and their relatively coarse-clastic fill make them more easily erodible than more-distal mud-filled counterparts (Chapter 3).

4 Materials and Methods

4.1 Core collection and visual description

Using a hand-operated 6 cm-diameter Livingstone piston corer, from below 2.4 meters of younger floodplain sediment, we retrieved 0.7 m of clayey peat and 5.5 m of laminated, humic clay-gyttjaic mud in meter-long sections, at the Rheinberg site (section 2; main site in Fig. 1), where a reconnaissance probing borehole had indicated oxbow-fill down to 8.5 m below the surface. The cored segments were split and photographed (Fig. 2). Texture, facies and other properties were logged in the sediment laboratory at the Department of Physical Geography, Utrecht University. Core-recovery was near 100%. There is no indication for significant non-depositional or erosional hiatuses within the studied core interval from 8.44 to 2.42 m below surface. The channel fill base is at 8.44 m below surface, in sudden contact with thalweg gravels.

4.2 Loss-on-ignition data

The material was subsampled for loss-on-ignition (e.g., Dean, 1974; Heiri et al., 2001), as continuous rectangular blocks excavated from the split core. The typical subsample measured 1 cm^3: a length along core of 2 cm, a width along the split core of 1 cm and a depth into it of 0.5 cm. Where clearly distinct layers were encountered the sample size and position were adjusted to these layers' thicknesses. For cm-thin layers we calculated raw LOI measurement back to the 2-cm sample thickness of the continuous series in analysis of sedimentation rates and breaks therein. The full series comprises 326 measurements (Fig. 2).

First, LOI-samples were dried at 105 ˚C for at least 12 hours. Dried samples were weighted (DW_{105}) (0.002 g accuracy), then heated at 550 ˚C for 4 hours. The combusted sample was weighted (DW_{550}) and the percentage weight loss (LOI_{550}) was determined using Eq. 1:

$$LOI_{550} = ((DW_{105} - DW_{550})/DW_{105}) * 100\ \% \qquad (1)$$

The raw LOI results were screened for outlier results. Three positive LOI excursions at 3.35-3.37 m (botanical macrofossils, some used for ^{14}C date GrA-44788, see below) and 3.77 m (undetermined organics) and at 7.35 m (shelly layer) were corrected because inspection of the cores at these depth identified the spikes as due to detrital admixture. We replaced the erroneous sample values with the average value of adjoining samples, resulting in the 'cleaned' LOI series. In the main part of the fill, LOI values are between 5.4 and 18.8 % (humic clays; mean (1-σ): 12.9 (2.8) %). In the upper meter, LOI varies between 16.6 and 34.8 % (peaty clay/clayey peat; 24.7 (5.1) %). The LOI data confirmed visual lithological logging in earlier stages. For a typical LOI value of 15 to 20 %, obtained from samples with DW_{105} of about 2 gr, the measurement accuracy is ±0.20 %. Variations in LOI results between adjacent samples are significantly larger, even in visually very similar facies (Fig. 2), and thus considered of natural origin.

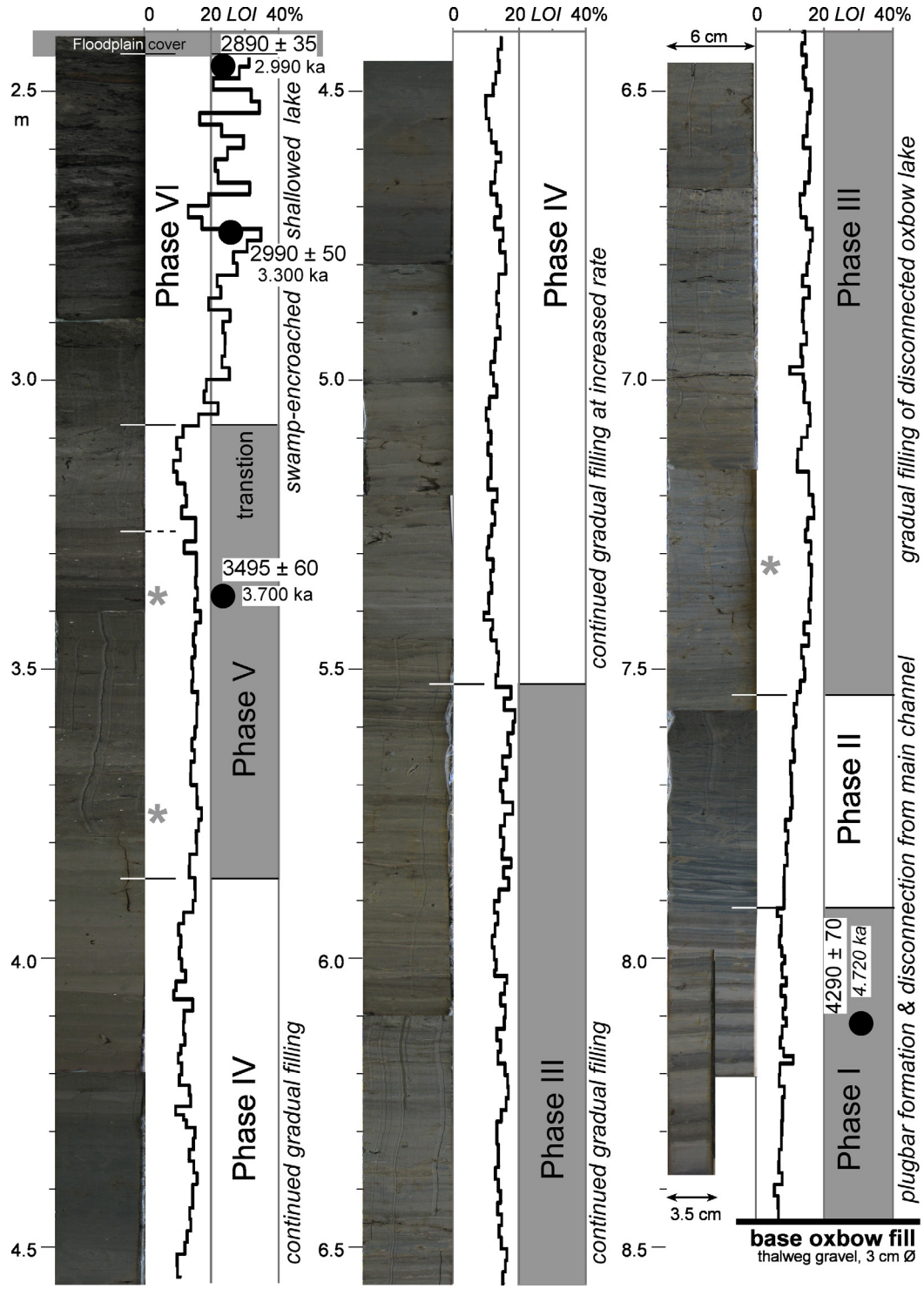

Figure 2. Collated core photos of the Rheinberg sequence, with sedimentological subdivision of oxbow infilling, LOI results, and positions of radiocarbon dates. Freshly cut core photographs are depicted. The photographed laminations are the combined textural (silt, clay), organic (diffuse admixture, concentrations of macrofossils), oxic-anoxic (ferro-sulfuric) overprint. In Phase III to IV, not all photographed thin layering is truly event-depositional.

4.3 Verifying visually observed trend breaks with LOI results

Change-point analysis (CPA v2.3; Taylor, 2000) was applied to the LOI data series, confirming visually observed breaks in sedimentation to occur just above 7.92 m, around 7.50, 5.52, 3.80 and 3.25 m (all within laminated oxbow-lacustrine facies), 3.08 m (base peaty interval, final oxbow filling), and at 2.42 m depth (base of floodplain clay, oxbow completely filled).

As a test, the CPA program was fed (i) raw LOI series, (ii) cleaned LOI series, (iii) window-averaged smoother versions, and (iv) truncated versions focusing only on the laminated part. The change point identification is sensitive to where the data series is truncated and to the cleaning of the raw data removing non-representative positive outliers, but in general the visually-interpreted breaks did independently reproduce in CPA on the LOI data (results summarised in Table 1, full output in Apendix A). Occasionally an unexpected extra change point was produced in an intermediate position, sensitive to the choice of series truncation, but not consistent through the complete series of tests. Such incidental hits were not used as boundaries in our further analysis. The CPA-reconfirmed trend breaks of Table 1 were used as the boundaries of the successive phases of oxbow filling, numbered I to VI (Fig. 2).

A further sensitivity test involved the choice of vertical resolution (2 cm). Synthetic LOI series were generated by resampling cleaned LOI series to increasingly coarser resolutions [4 to 10-cm]. At 4, 6 and 8 cm resampling, CPA still picks up the breaks at the base of the peat (~3.08 m) and the main breaks within the laminated part of the fill (~5.52 and ~7.55 m). Resampled to 10-cm intervals, CPA no longer resolved the breaks.

Table 1: CPA reproduction of trend breaks in LOI series

Depth (m) of trend breaks ('change points')	**Visual inspection based on core sedimentology + LOI data**	**CPA result:** *Full series*	**CPA result:** *No upper facies*	**CPA result:** *No upper facies No basal facies*	**Evaluation of the various CPA tests**
2.43-2.45	Base floodplain clay	R + S	xx	xx	Reproduced by CPA
3.05-3.09	Base peaty facies	R + C	xx	xx	Reproduced by CPA
3.25	accelerated shallowing	-	-	-	*not reproduced*
3.85-3.93	becomes a bit more distal	R + S	R + C + S	R + C + S	Repeated CPA hits
(4.23)	active chan. position varies (?)	-	-	C	*occasional hit*
(5.02)	active chan. position varies (?)	R	R	R	*R only*
5.44-5.52	becomes more proximal	R + C + S	R + C + S	R + C + S	Repeated CPA hits
(5.91)	-	-	-	R	*occasional hit*
(7.40)	Laminations above this level too thin/too bioturbated to be visually counted	-	-	-	Not reproduced. LOI signal changes 10-20 cm deeper than lamination signal
7.50-7.60	begin stable fill environment	R + S	R + C + S	xx	Repeated CPA hits
(7. 67)	-	C	-	xx	*occasional hit*
7.92 (7.87)	no more cm-scale pulses	R	R	xx	Repeated CPA hits
8.44	Base of channel fill				

R = reproduced by CPA on Raw LOI series, at 2cm
S = reproduced by CPA on Smoothed LOI series, at 2 cm, N=3 window
C = reproduced by CPA on Cleaned LOI series, at 2cm
xx = excluded in analysis in truncated runs
- = no change point detected

4.4 Radiocarbon dates and individual age calibration

Two radiocarbon dates were previously collected from prospective cores at the site: one from the base of the cored infill at the cored location, and one from the base of a coring in a nearby palaeochannel (Erkens et al., 2011; Fig. 1). Three radiocarbon dates were newly collected. Hereto cm-thick slices subsampled from the centre of the split core were wet-sieved over a 150 µm mesh. Macrofossils of riparian vegetation were picked from the sieved material (Tab. 2). A last date (SUERC-37131) comes from recent work ~25 kilometers downstream (site VK in Fig. 1), from a slackwater marker of a particularly large flood event, from a very distal channel fill at an elevated terrace position (Chapter 6; Toonen et al., 2013). Dating estimates overlap with the abandonment of our studied oxbow fill. Table 2 lists all radiocarbon dates and presents their calibrated ages and 1-σ uncertainties, using OxCal v4.1.7 and the Intcal09 calibration set (Reimer et al., 2009; Bronk-Ramsey, 2010).

The top of the sequence calibrates to 3028 ± 62 cal yrs BP (GrA-44329; Tab. 2). For the base of the core, the date collected from the Rheinberg oxbow fill itself (UtC-15064; at 8.5 m in the prospective borehole) calibrates to 4,870 ± 130 cal yrs BP, with relatively large uncertainty due to the small sample size. It is assumed that the sampled organic material was produced around the cut-off event. If the calibration of the oxbow's basal radiocarbon date is combined with that independently collected at site VK – thus adopting a scenario that considers the cut-off of Rheinberg Meander A being formed due to the very large flood event – this results in an age of 4720 ± 70 cal yrs BP. Alternative date-combining calibration scenarios involving the sequential abandonment of Meander A, Meander B and distinct flood event markers in the oxbow fill to the downstream rare-flood marker were evaluated as well. These scenarios place the VK very large flood decades to centuries after the cut-off of Meander A. Such scenarios, however, each turn out inconsistent with the new-collected sedimentary evidence (Appendix A). The calibration combining dates SUERC-37131 and UtC-15064 thus provides the most likely basal age.

4.5 Calibrated age-modelling assuming linear sedimentation

The starting point for age-depth modelling of the channel fill was to specify the sample depth of the radiocarbon dates and the position of the main lithological boundary at 3.09 m, and then calibrate using OxCal's U_Sequence function (see Appendix A). This implies assuming linear sedimentation in the lacustrine mud respectively the peaty clay interval with a knick-point at the specified lithological boundary (at 3.09 m core depth). Linear age modelling predicts the fill to cover 1730 ± 90 years, with the lacustrine fill spanning 1110 ± 70 yrs and the peaty top 620 ± 60 yrs (Fig. 3). The boundary at 3.09 m calibrates to 3640 ± 70 cal yrs BP.

In the age-modelling, the basal age is tied to 7.92 m core depth, because the age model concentrates on the laminated oxbow fill and the peat, and not the cm-to-dm scale event beds recorded at the very base of the sequence. Ad-hoc tests in OxCal linear age-depth modelling, tying the basal age to 8.44 instead does not significantly alter the age estimates in the upper meters: the age acquired for the mud-to-peat contact at 3.06 m meters is shifted 5-10 years older. The next sections further develop the age-depth model, replacing the linear model with one that incorporates the LOI data.

Table 2: Radiocarbon dates and calibrated ages

Lab nr	Lab age ± error [14C yrs BP]	Depth† [m below surface]	Materials	Meaning	Calibrated age mean ± 1σ [cal yrs BP]	Original reference
Rheinberg Meander A, deep oxbow lake fill, relative distal to active channels, central in oxbow lake. Location: 51.54068 N, 6.61546 E; Elevation +20.8 m N.N.						
GrA-44329	2890 ± 35	2.44-2.46	Alnus macrofossils[1]	Near top of peat, wetland oxbow fill	2995 ± 50 * (3030 ± 60)**	This paper
GrA-44756	2990 ± 50	2.74-2.76	Alnus & other terrestrial macrofossis[2]	Near base of peat, wetland oxbow fill	3300 ± 35 * (3180 ± 85)**	This paper
GrA-44788	3495 ± 60	3.36-3.40	various terrestrial macrofossis[3]	Near top of lacustrine oxbow fill	3715 ± 65 * (3770 ± 80)**	This paper
UtC-15064	4290 ± 70	8.5 (7.92-8.44)	Leaf fragments[4]	Base deep channel fill, suddenly abandoned	4720 ± 70 * (4865 ± 120)** 4720 ± 60 ***	Erkens et al., 2011
25-km downstream Rheinberg, rare-magnitude flood marker in residual channel of high floodplain terrace. Location: 51.72291 N, 6.36389 E; Elevation +15.6 m N.N.						
SUERC-37131	4135 ± 30	1.6 (7.92-8.44)	Single macrofossil [6]	Peaty clay top of residual channel fill, directly below millennial flood marker	4720 ± 70 * (4680 ± 80) **	Chapter 6, *Fig. 4*
Rheinberg Meander B, next-younger palaeochannel fill, more proximal and less deep, date not positioned central in the oxbow lake. Location: 51.54573 N, 6.62220 E; Elevation +23.3 m N.N.						
UtC-15065	4100 ± 50	6.22 (7.40)	Twigs and leaf fragments[5]	Base shallow channelfill,	4590 ± 60 *** (4640 ± 100) **	Erkens et al., 2011

Remarks

† Depth in original core. For samples not from Rheinberg core (Fig. 2): *correlated depth in that core given in italics between brackets*

1 Alnus: 10 fruits, 1 female, 1 male cone, 2 budscales;
2 Alnus: 4 fruits, 3 budscales, ½ female catkin; 5 *Mentha aquatica/arvesnis*, 3 Phragmites autralis, 6 *Lycopus europaeus*, 1 Oenanthe;
3 2 Polygonum/Rumex, 1 *Sagittaria sagittifolia* macrofossils, 1 Betula, ¼ Alnus fruits;
4 One *Lythrum salicaria* seed, leaf fragments;
5 Salix twigs, leaf fragments;
6 Alnus twig with attached buds.

Calibrated ages calculated with OxCal 4.1 (Bronk-Ramsey, 2010) and the IntCal09 reference dataset (Reimer et al., 2009).

* Linear model 2 result, U-Sequence calibration, pooling dates UtC-15064 and SUERC-37131
** Individually calibrated results
*** Result of a Sequence calibration pooling UtC-15064 and SUERC-37131, and enforcing a 80±7 years younger age for UtC-15065

4.6 Age-depth modelling with variable sedimentation rates

A non-linear age-depth model was developed for the interval 7.92 to 2.43 m (Phase II-VI). It uses the cleaned LOI data to enforce accelerations (low LOI, e.g., Phase III) and decelerations (higher LOI, e.g., Phase IV) in sedimentation rates in the modelled interval, in agreement with the sedimentology of oxbow fills (section 3). Compared to a linear model, this improves estimates of (mean) sedimentation rates per phase.

The LOI data was used in their original units with their representative original variance. Using a spread-sheet model we calculated a variable time increment (Δt; in years) for each sample by raising its LOI value (LOI_i) to a power x and multiplying by the sample thickness (D; in cm), with a specified duration of the entire interval to calibrate on.

The model uses the following equations:

$$\Delta t_i = LOI_i{}^x D_i \times \frac{T_N}{\sum_{j=1}^{N} LOI_j{}^x D_j} \quad (2)$$

$$Age_i = Age_{j=1} + \sum_{j=1}^{i} \Delta t_j \quad (3)$$

where i and j identify individual sampled layers, N is the total number of samples in the interval to which the model is tuned, T_N is the time duration covered by the interval (in years) and Age_i is the age of sample layer, with i=j=1 for the lower most layer. In Eq. 2, equals mean for the tuning interval. For more organic samples (relative increased LOI), decelerated sedimentation rates are expected and Δt_i should be larger than for less organic instances in the sample series. Exponent x was solved by regression, minimising the deviations between Eq. 3-modelled and independent-dating mid-point estimates for Age_i for the few layers where independent age estimation was available. After tuning x, the age-model was also employed below deepest and above youngest collected dates (j < 1 resp. j > N; extrapolation beyond the tuning).

In its most simple form (Fig. 3), the model was tuned for the interval 7.92-2.43 m (Phase II to VI). The age-model was ran two times, setting $T_{N=283}$ to 1558 years (short range) and to 1820 years (long range). The values for T are derived from the calibrated age range for top and base (Tab. 2). Exploring various age-model solutions served to evaluate age-model sensitivity. It also allowed to graphically inspect intermediate radiocarbon datings and their calibration ranges, relative to the sedimentary-information based age-depth model, helping to identify outliers, similar as U_ sequence modelling can do (Bronk-Ramsey, 2009). A third variant non-linear age model is the 'alternative top' model, which ties itself to date GrA-44756 at 2.75 m, rather than to the uppermost date. It was solved setting $T_{N=267}$ to 1500 years for the interval 7.92-2.75 m and regressing to $\text{GrA44788}_{j=236}$ (at 3.38 m) and $\text{GrA44329}_{j=283}$ (at 2.43 m; extrapolating). It resulted in a relatively long-range solution too (Fig. 3). The average of the short and long range solutions (1688 ± 88 years) served as the mean model.

The reported uncertainty age range around the non-linear solutions is that of the OxCal-obtained linear age model. In the future, the age-modelling prototyped in this paper could be tuned to the irregular distributions resulting from calibrating radiocarbon ages and produce uncertainty ranges in the same process at which x is optimised. Such improvement would require close integration with established radiocarbon calibration routines, which has not yet been attempted.

4.7 Experimental indexing of negative LOI excursions as palaeohydrological events

The cleaned LOI series was also explored as a flood intensity proxy record, focusing on marked negative excursions (flood event layers), produced by relatively rare floods of greater magnitude than the modest floods represented in the background sedimentation (section 3).

Negative spikes were identified, categorised and scored, and summed over a moving-window along a time axis to summarise and evaluate the results. It is noted beforehand that LOI is not a sediment property that necessarily distinguishes event layers by their magnitude. It is useful to identify flood event layers (e.g., Nesje et al., 2001), but spikes in the data – even at our high sample resolution – are not necessarily products of individual floods, especially in oxbow fills of intermediate proximity to the active channel that register relatively many events and have relatively low background

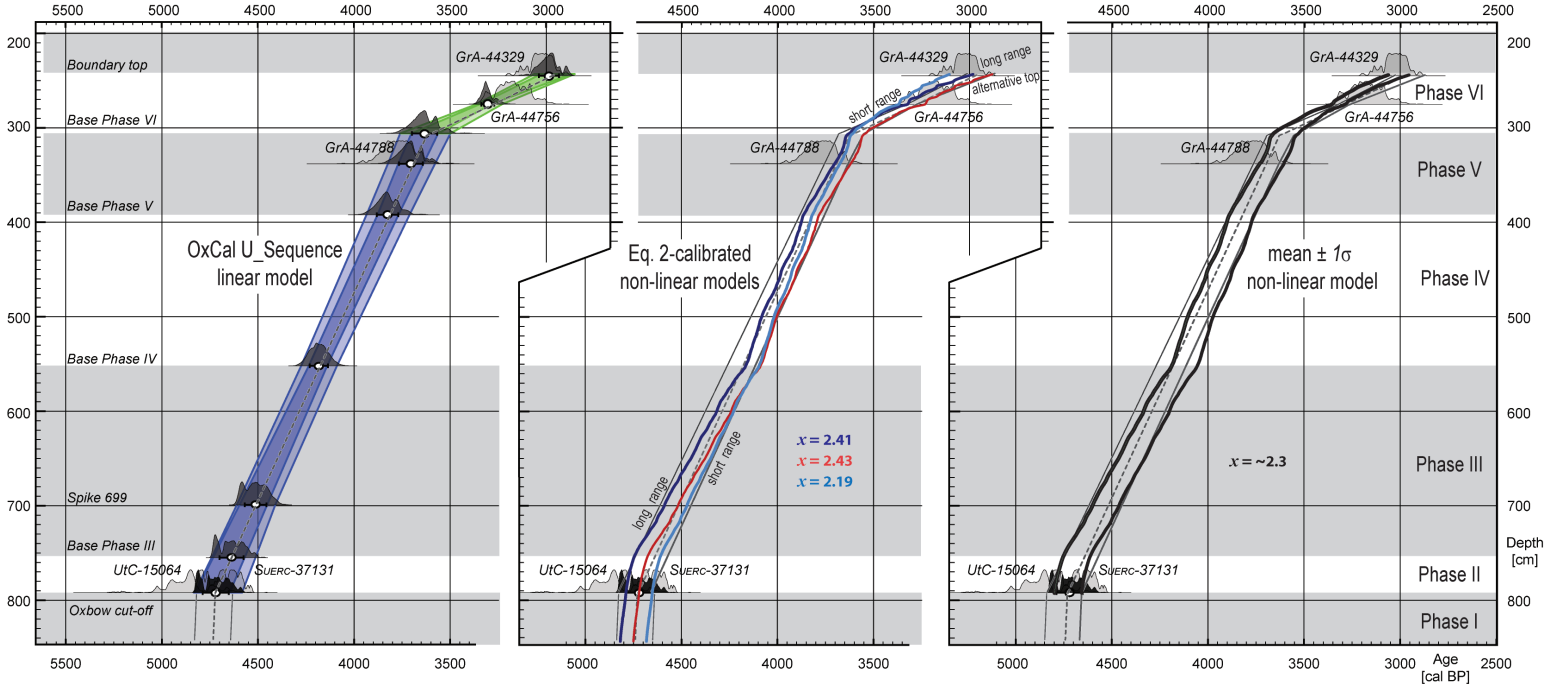

Figure 3. Age-depth models for the Rheinberg oxbow fill sequence.

LOI (our site; particularly in Phase IV and V). With this respect, analyses that determine grain-size distribution properties within flood-pulse layers may allow more confident magnitude-differentiation (Chapter 5). Moreover, not the absolute value of the negative excursion, but the relative deviation from the background typical value would indicate flood event strength. Lastly, regardless of what continuous data is used to read out the core fill, also at marked CPA boundaries in the sequence flood events may be invoked. Stepped changes in facies can be regarded additional events that are not resolved as a negative LOI excursion. The large flood linked to the very base of the oxbow fill also is such an extra event of facies-change registration.

To create an index of negative LOI excursions, a two-step *Z*-score (standard score) procedure was run over the 7.92 to 2.43 interval (Phase II to VI). As Step 1, linear regression trends were calculated in the depth domain for each CPA-bounded phase, and *Z*-scores were calculated for the residuals (Fig. 4A). All samples with $Z < -1.6\ \sigma$ were tagged as flood event layers (19 out of 283), all others were considered background (~94% of the samples). As Step 2, linear regression coefficients were recalculated over the background samples only and the Zscores were recalculated for all samples. The trend lines for each phase were assumed to express average conditions of 'background sedimentation' evenly for each phase (Fig. 4A). The lowered background variance makes that Z-scores for event layers are increased, relative to Step 1.

Arbitrary critical *Z*-values were used to categorise the Step-2 scored events. The category labels express (i) the level of confidence that these indeed are individual relatively large flood events, and (ii) rarity of the score from their recurrence in the series and constraints on their total covered timespan. All spikes scoring $Z < -1.1\ \sigma$ are regarded 'possible flood events' (n=32); those with $Z < -1.8\ \sigma$ (n=14) as 'possible large flood events' and $Z < -2.5\ \sigma$ as 'probable large flood events' (n=5). For subintervals within Phase IV and V, alternative linear regression lines and residual Z-scores were calculated (see Discussion). Three more 'flooding events' were invoked at the CPA-breaks (Fig. 4A, 7.57, 5.48 and 3.91 m). They were assigned to the middle category and attributed equivalent Z-scores. The cut-off event, equated to the base of the fill (8.44 m) is a fourth flooding event, of rarest-magnitude (section 4.4 and Chapter 6), and is assigned an equivalent Z-score.

The Z-scores were transformed to an experimental flood index (F.I.) by squaring them. Similar to flooding indices for the 14th to 18th century developed on damage reports for historical events (Glaser & Stangl, 2003; Chapter 2), the F.I. was summed over a moving-window of 31 years on the mean age-model (Fig. 4B). Blocky segments in the 31-yr F.I. are due to single marked large events in a period of relative quiescence. Where peaks in the 31-yr F.I. are irregular, they are the composite of multiple floods of variable strength alternating within relative short time.

For comparison and evaluation, cumulative probability density functions (CPDFs) from radiocarbon dates of fluvial activity and stability in valleys and hinterland by Hoffmann et al., (2008) were also plotted. Because they are based on ^{14}C dates, CPDFs can only resolve palaeohydrological variations at super-centennial scale. Radiocarbon dating and calibration uncertainty for individual dates (typically ±100 years; 1-σ) is inherited in CPDF construction, broadening 'stability' and 'activity' periods. This hinders intuitive graphic comparison with event-resolution moving-window indexes. A smoother alternative moving-window F.I. version is presented to better allow comparison. It is calculated with 34% contribution of a moving window that is 1-σ wide (~100-120 years), and 66% from the 2σ-wide sum window (~240 years). Also with

the age-modelling uncertainty factored in, the moving window F.I. remains of higher resolution than CPDFs.

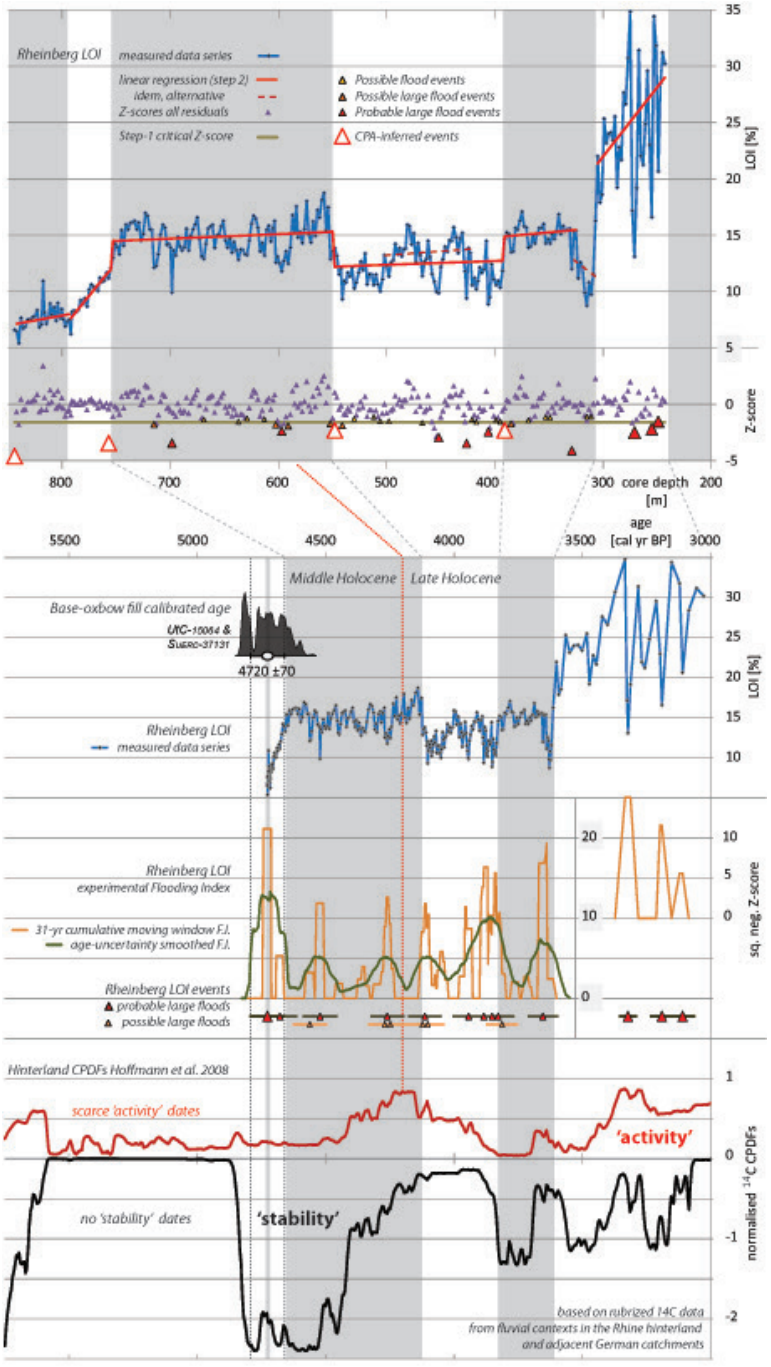

Figure 4. Panel A: LOI data series and CPA-detrended Z-scored residuals; plotted on a depth axis. Panel B: LOI data series, probable flood events identified and indexed from LOI excursions and CPA, and moving-window cumulative event flooding indexes; plotted on a time axis (mean non-linear age model). Also plotted: radiocarbon calibration results for dates UtC-15064 and SUERC-37131 at the base of the core. Also plotted: Cumulative probability frequency difference plots (CPDF) of radiocarbon-dated fluvial sedimentation from Rhine valley and hinterland (split for 'activity' and 'stability'), reproduced from Hoffmann et al., (2008).

The F.I. results are experimental and are intended to allow (i) evaluation of age-model non-linearity in records with event resolution, (ii) comparison of the resolution of oxbow flooding-event inventories to CPDFs, and (iii) qualitative and chronometric comparison of flooding indexes and CPDFs. The F.I. results are not intended for quantitative discharge reconstruction of large floods.

5 Results

5.1 Sedimentological interpretation per Phase

CPA-confirmed stepwise shifts in facies that occur in the lacustrine part of the fill are interpreted as sudden changes in active channel proximity due to sudden migration through renewed cut-offs in the main channel, whereas gradual change of facies is interpreted as gradual change in connectivity (e.g., due to plug-bar build-up) and gradual shifting river position (lateral channel migration: bank erosion and contemporaneous point-bar build-out), following general principles of oxbow filling and building on established concepts of meandering river morphodynamics. All superimposed smaller-scale variation reflect combinations in (i) delivery of clastics during smaller and larger floods, (ii) bioturbative mixing, and (iii) inter-flood organic production. A detailed interpretation per phase is presented below.

Phase I, the basal humic clay interval between 847 and 792 cm core depth, is lowest in LOI and the only interval to show cm-scale cyclic bedding. It marks the very initial oxbow filling stage, which was short lived. Ten consecutive individual deposition events are recognised. Their thickness drops from 6-7 cm to 1-2 cm with decreasing depth. This indicates progressive sealing off of the orphaned oxbow lake from its parent channel in about a decade, with initially high but rapidly decreasing sedimentation rates. This is similar to cases described by Piégay et al., (2008), Citterio & Piégay (2009), and Toonen et al., (2012; Chapter 3).

Phase II, between 792 and 755 cm, shows laminated humic clay. Thickness and clearness of laminations decreases upwards while organic matter content increases (Fig. 2). Especially towards the top, laminations no longer form a continuous series: some laminae become very thin and various subintervals show bioturbation disturbances that overprint lamination. Between 792 and 740 cm depth, an estimated 85 ± 10 event beds are present, based on visual counts on core-photographs (Fig. 2). Note that the visual signal disappears some 10-20 cm above the LOI trend-break that is used as the base of Phase III (Tab. 1). Loss of individual registration and thinning of flood pulse event layers indicates plugbar accumulation at the entrance of the oxbow to have proceeded. The plug bar is interpreted to have matured so much at this point, that at the entrance it fell dry during stages of normal discharge: the oxbow lake had become disconnected from the active channel water body. At higher stages discharge sedimentation would then continue and a natural levee could start to build over the matured plug bar. The formation of a 'plug levee' over the plug bar then further reduced the oxbow connectivity with every successive ≥ Q_{bf} flood. Alternatively, the increase in LOI values could indicate the active channel to have migrated away from the oxbow entrances, perhaps combined with connectivity change at the entrance and/or the establishment of so-called tie-channels (Rowland et al., 2005), but at Rheinberg, LiDAR imagery and age-considerations regarding Meander B (Fig. 2) rule out such caveats (see Appendix A). Some of the events registered in the lower half of Phase II may represent modest peak discharges of shorter return frequency (i.e. recurring every year), while at the transition to Phase III all registered events

represent true floods, exceeding $Q_{bf,}$ and not recurring every year but once in two to five years or so. Such considerations infer Phase I and Phase II together to represent the first 100-150 years after oxbow cut-off.

In Phase III, between 755 and 552 cm, LOI values no longer steadily increase. We consider the stabilised mean LOI value to indicate that the oxbow entrance sealing processes of Phase I-II had completed: the plug bar had matured and its natural levee top is at the same height as the natural levees on either side of the cut-off entrance, the site had become an isolated lake in the floodplain. Consecutive individual registration of flood events was lost and 'background' sedimentation alternated with incidental registration of a larger flood pulse seen instead. The organo-clastic fluvio-lacustrine background sedimentation is characterised as a clay-gyttja, contrasting the humic silty clay and clay loam of the intervals below. The negative LOI-excursion at 6.99 m (Fig. 2) coincides with a thin layer of fine sand, presumably registering a relatively large flood of rare recurrence. This excursion is particularly marked against the background, visually and in LOI measurements, suggesting it occurred in an otherwise relatively quiet period of flood pulses. Other negative excursions in the LOI record, higher up in Phase III and in Phase IV, might indicate similar flood events, but are less contrasted. Towards the end of Phase III, following a relative clayey interval around 599-589 cm, LOI background values increase a little, just before dropping dramatically at 552-cm.

In Phase IV, between 552 and 392 cm, mean LOI is relatively low (Fig. 2; Tab. 3), which translates to higher average input of clastics and increased accumulation rates compared to the previous phase. The abrupt change at 552-cm is here explained as a channel reconfiguration event (probably a chute cut-off) in the vicinity of the site, moving the active Rhine channel closer to the site. It increased the amount of clastics received during a typical flood (section 3) and decreased the background LOI signal (section 4). The receiving depositional environment and the autochthonous organic production rate are considered similar for Phases IV and III: the 552-cm break is a change in proximity only. Occasional CPA hits at 502 and 423 cm in the LOI data (Tab. 1) can be interpreted as further variation in the proximity of the active channel.

Phase V, between 392 and 308 cm, is the last lacustrine section of oxbow fill. The part between 392 and 325 cm has a slightly higher mean LOI than Phase IV. This change point could indicate further channel reconfiguration, moving the active channel away from the site, but probably not as far away as before in Phase III. The few last samples above 325 cm reflect a last phase of accelerating clastic deposition. This break is not picked up in CPA analysis (>95% confidence) at the present sampling resolution. The interval might mark a last reconfiguration event moving the active channel to nearby position, but given the position high in the fill sequence, more probably it marks a change in sediment trapping properties at the site itself. As the lake became filled, remaining open water became confined in a smaller area around the coring site. Besides the shallowing, vegetation began to encroach causing lateral narrowing of open water area. These processes of narrowing and shallowing are similar as for the cases described in Chapter 3. In the last stages of filling, reducing oxbow lake volume and unchanged sediment input would accelerate sedimentation. If so, the reduced sedimentation rates (lowered clastic input) represented by clayey peat of Phase VI are announced by accelerated sedimentation just below, amplifying the contrast at the facies break (Tab. 1; Fig. 2).

In Phase VI, between 308 and 243 cm, clayey peat with abundant wood marks replacement of open lacustrine conditions (Phases III to V) by very shallow waters in a swamp that encroached over the greatly shallow oxbow lake from its sides. The strong variation in LOI (Fig. 2; Tab. 3) is due to admixed woody materials. At 3.08 m, previous water depths are estimated ca. 1.5 m, also taking into account the thickness of the interval (65 cm) in its nowadays compacted state and the past position of groundwater tables in the areas flanking the oxbow low, for example indicated by pedological overprints (e.g., transect D-D' in Erkens et al., 2011). Groundwater seepage from the neighbouring terrace will have helped maintaining a high groundwater table year round, promoting swamp encroachment and sustaining peat formation for this floodplain-edge oxbow. The sharp boundary with Phase V marks rapid transition from subaqueous to wetland-terrestrial environment. Clay laminations in the peat reflect ongoing trapping of occasional flood sediments, albeit in considerably lowered frequency than in all phases before.

In Phase VII, above 243 cm, a homogenous floodplain deposit accumulated (silty clay, LOI 8%). The marked contrast with Phase VI suggests new reconfiguration of the active river, to a position much closer to the site. Geological, geomorphological and soil mapping studies for the wider Lower Rhine valley suggest regionally increased floodplain depositional activity in the last 3000 years (Klostermann, 1992; Erkens et al., 2011), which may also have influenced the transition from peat growth to floodplain deposition. The prehistoric forest clearings that explain the greatly increased fine sediment supply to the Lower Rhine valley and delta in the last 3000 years (Erkens et al., 2006; Hoffmann et al., 2007; Gouw & Erkens, 2007; Erkens, 2009; Stouthamer et al., 2011). This deforestation is archeologically known to have started well before 3000 years ago (e.g., Bos et al., 2008; Erkens et al., 2009). Sediment trapping elements in upstream parts of the Rhine drainage system, however, delayed transfer of the signal of increased erosion of fine-sediments to Lower Reaches for some time (Lang et al., 2003; Hoffmann et al., 2007; Erkens et al., 2011). The local dating of the top of the oxbow fill matches the Lower Rhine's regionally inferred onset-age for floodplain registration of human-induced increased overbank sedimentation. It is well possible that significant deforestation of the floodplains and terraces surrounding the Rheinberg oxbow occurred while its fill was accumulating. But the notice of delayed timing of increased fine sediment loads from deforestation in the wider hinterland implies that the ca. 1750 years of fluvial history up to Phase VII, represent local overbank trapping of suspended sediment yields at 'semi-natural' magnitudes. Yields may have begun to rise modestly, but were not yet at the doubled-to-tripled levels reconstructed for Roman and Medieval times (Erkens, 2009).

5.2 Evaluation of the age-modelling

The LOI-tuned age model (Eq. 2) broadly reproduces the OxCal derived linear age model (Fig. 3). All age-models result in an aggradation rate of 1.1 mm yr^{-1} for the peaty top interval. This is a typical rate for (clayey) peat accumulation in floodplain backswamp settings (e.g., Cohen et al., 2005), adding confidence to the age-modelling results. The non-linear model also reproduces the knick point at 3.09 m, without explicitly prescribing its vertical position (~3630 cal yrs BP in the linear model, ~3615 cal yrs BP in the non-linear model). Systematic differences between non-linear and linear model outcome do exist in the lacustrine part of the fill. The non-linear model places the Phase II/III transition ~40 years older, and Phase III/IV ~60 years younger. Phase III thus covers more time in the non-linear model (~555 versus ~460 years; Tab. 3), to the expense of Phase II and IV – as implied by the sedimentology and LOI measurements.

With the LOI-tuned division of the duration per phase, also the variation in sedimentation rates within the oxbow fill is quantified (accurate to ~10%, given the absolute age calibration uncertainty). Over the interval 7.92-7.55 m (Phase II), the LOI-tuned rate is 9.3±0.8 mm/yr (long range: 9.0; short range: 9.5), which is double the linear averaged rate for the lacustrine interval. Over the interval 7.92-7.40 cm, the rate is 6.4±0.5 m/kyr (long range: 6.2; short range: 6.7), i.e. 1.5 times the linear rate, and thereafter it drops (Phase II/III transition). For Phase III, IV and V, the mean sedimentation rates are 3.7, 5.4 and 3.7 mm/yr respectively, whereas the linear age-model rate was 4.4 m/kyr. Phase IV is thus 10-20% accelerated when compared to the linear model, and Phase III and V are stalled by 10-20% (Tab. 3).

The highest sedimentation rates occurred in the periods when the sedimentology indicates flood pulses to have registered consecutively, in Phase II and the very base of Phase III. The 85 ± 10 thin-but-visibly event layers of this interval are attributed 80 ± 7 years in the non-linear model, versus 120 ± 10 years in the linear model (Tab. 3). This suggests the events to have had an average return time of 0.94-1.00 years. Phase II has been reasoned to register consecutive semi-annual discharge peaks and the facies change to Phase III marks loss of consecutive registration (with a matured levee covering the plug bar; section 5.1). Indeed, about 60 thin sedimentation pulses registered between 7.92 and 7.55 in Phase II, which the age-modelling says to span 40 years, reconfirming these as semi-annual event layers. A further ~25 pulses are seen between 7.55 and 7.40 cm (the very base of Phase III), thought to span the next ~40 years and thus implying bi-annual registration, in the interval where we begin to loose registration of events smaller than $Q_{bf.}$ This insight can be further developed to claim that Q_{bf} was exceeded just over every 2 years, on average. The combination of sedimentary-tuned age-modelling and considerations regarding the oxbow-plug bar entrance thus offers a rare opportunity to assess Q_{bf} return times for a situation well back in the Holocene past. It suggests that at the end of the Middle Holocene, when the Rhine catchment and the Lower Rhine floodplain were still in mostly naturally vegetated conditions (Hoffmann et al., 2008; Chapter 6), the river exceeded bankfull discharge once every 2-3 year. This is a normal value for present-day mixed-load meandering rivers (e.g., Woodyer, 1968; Dury, 1973; Van den Berg, 1995; Bridge, 2003).

Oxbow fill phases					*OxCal U-Sequence age model*			*Sedimentation-tuned age-model*			*Differences*	
	Boundaries and intervals	Depth (cm)	Thickness (cm)	LOI Avg ± Std. (%)	Age ± Err (cal yrs BP)	Duration ± Err (yr)	Sed.Rate ± Err (m/kyr)	Age ± Err * (cal yrs BP)	Duration ±Err (yr)	Sed.Rate ± Err (m/kyr)	Age/Duration (yr/%)	Sed. Rate (%)
Floodplain cover												
VI	top	243			2988 ± 53			3028 ± 53			tied	
VI	*interval*		*63*	24.2 ± 5.5		620 ± 59	1.0 ± 0.1		575 ± 59	1.1 ± 0.1	93%	110%
VI	base	306			3612 ± 64			3601 ± 64			-11 yr	
V	*interval*		*86*	14.3 ± 2.0		210 ± 18	4.1 ± 0.3		230 ± 19	3.7 ± 0.3	110%	90%
V	base	392			3823 ± 63			3829 ± 63			+6 yr	
IV	*interval*		*158*	12.3 ± 1.7		360 ± 31	4.4 ± 0.4		290 ± 24	5.4 ± 0.5	81%	123%
IV	base	550			4178 ± 65			4119 ± 65			-59 yr	
III	*interval*		*205*	14.8 ± 1.5		460 ± 39	4.5 ± 0.4		555 ± 47	3.7 ± 0.3	121%	82%
III	LOI spike	699			4509 ± 68			4523 ± 68			+14 yr	
III	top visual lam.	740			4599 ± 68			4635 ± 68			+36 yr	
III	base	755			4635 ± 68			4676 ± 68			+41 yr	
II+III*	*'85 lam.'*		*52*	10.9 ± 2.4		120 ± 10	4.3 ± 0.4		80 ± 7	6.4 ± 0.5	67%	149%
II	*interval*		*37*	9.8 ± 1.5		80 ± 7	4.6 ± 0.4		40 ± 3	9.3 ± 0.8	50%	202%
II	base	792			4717 ± 69			4716 ± 69			tied	
I	*interval*		*55*	7.6 ± 1.0		10 ± 1 ***			10 ± 1	50.0 ± 5.0		
I	base	847			4730 ± 70			4730 ± 70				
Base of channel fill												

Notes: *Error of the sedimentation-tuned age model taken over from the U-sequence age model
**Interval 792-740 cm; 85±10 thin event layers visible
***Visual counts, 10±1 thick event layers

Table 3: Age-depth model comparison

Also the duration of Phase I (8.44-7.92 m) was calculated, extrapolating the age-model to below the interval on which it was tuned ($j < 1$ in Eq. 2 and 3). Such results should only be trusted when the sedimentary facies and LOI variance in the extrapolation interval match facies encountered in (part of) the tuning interval. The lower part of Phase II may come close in raw LOI values, but the event-bed thickness in Phase I exceeds that of event beds higher up in the oxbow fill. Extrapolation indicates Phase I to span ~30 years, which we regard an overestimate because the 10 ± 1 recognised sediment pulses would result from semi-annual floods (section 5.1). The overestimation of $\Delta t_{j<1}$ in the basal interval, i.e. underestimation of sedimentation rate, is due to the initially greater connectivity of the freshly cut-off oxbow and active channel. The mismatch between extrapolation and event-counting does not affect age-model realism higher up in the fill.

Lastly, we can evaluate age-model performance by looking at results for single layers of highest and lowest LOI. Individual values for Δt_i (Eq. 2) should translate to realistic values for $\Delta t_i/D_i$ (duration/cm). The slowest accumulating layers have a $\Delta t_i/D_i$ of 23 yr/cm, for the most peaty subsamples at the top (long range and alternative top solutions; Fig. 3). The fastest accumulation has a $\Delta t_i/D_i$ of 0.3-0.6 yr/cm, for the most pronounced event beds in the fill below the peat (Phase II to Phase V) and ~2 yr/cm for least peaty intervals in Phase VI. A typical background sedimentation organic mud is attributed 3 yr/cm in the lacustrine part and 10-15 yr/cm in the peaty part, about 90% of the phase-averaged mean sedimentation rates (Tab. 3). This illustrates the age-model solution 'within phases' to be only modestly non-linear at fine resolution, as is also seen graphically in Fig. 3. This adds confidence to the realism of the solution for x and supports to use the age-models when moving-window summarizing the F.I. results.

5.3 Evaluation of the LOI-based flooding event record

Before interpreting the LOI-based F.I. results as palaeohydrologically relevant, the validity of considering the LOI record to represent the ratio between incoming sedimentation and local organic production should be verified. Apart from the effects of occasional mats of plant material and shelly beds (cleaned from the raw record, Fig. 2; section 4.2), the possibility that fractions of the incoming sediment during floods may have been combusted during LOI analysis, and thus suppressed the negative LOI excursions in the record is to be excluded. This boils down to the component of carbonate that is known to be present in Lower Rhine sediment, particularly in the silt fraction (up to 30% by weight in the most-silty facies; own measurements). This happens to be mostly detrital calcite of upstream source (eroding hinterland regolith and loess cover). From series of paired tests, organo-clastic loss-on-ignition results ($5 < LOI < 35\%$) turned out to be insensitive for this silt-related calcite-type carbonate admixture (Konijnendijk, 2010). Strong negative excursions thus represent increased allochthonous sediment input, which is mostly siliciclastic (clay, silt, fine sand) and includes a part detrital calcitic carbonate of silt grain-size which is not greatly removed by LOI at 550°C. In rivers with different overbank sediment composition (hinterland) and autogenic production of organics and/or carbonates (climate), LOI at 550°C may be less suitable for contrasting event beds and background.

An important property for palaeohydrological applications is that oxbow fills offer continuous registration of every larger event that peaks over a certain threshold. Accepting negative LOI-excursions as a sedimentary proxy for above-threshold flooding, 9 'probably large flood events' and 7 more 'possibly large flood events' are present in the lacustrine part of the fill, which the age-modelling (section 4.6) associates roughly to recurrence times of 50 years and longer. Table 3

summarises the Zscoring results, and gives a breakdown of event recurrence per subinterval. Return times for the three categories of flood events are higher for Phase III and lower for Phase IV and V. The descriptive statistics behave as would be expected for a peak-over-threshold registering sedimentary record of larger river floods (sections 3 and 5.1), which adds confidence to the flooding index as an experimental way of palaeohydrological usage of LOI-data.

		Event count exceeding LOI Z-score (N)			**Age model**		**Event return estimate (yr)**		
	Total # samples	Possible flood events	Possible large flood events	Probable large flood events	Interval duration	Time in average backgr. sample	Possible flood events	Possible large flood events	Probable large flood events
	(N)	Z < -1.1	Z < -1.7	Z < -2.3	(yr) **	(yr) **	Z < -1.1	Z < -1.7	Z < -2.3
Interval		Fl. > 1.21	Fl. > 2.89	Fl. > 5.29			Fl. > 1.21	Fl. > 2.89	Fl. > 5.29
Peaty top	**33**	*not resolved*		**3**	**586**	**21**	*not resolved*		**195**
Organo-clastic fill	**242**	**33**	**15**	**9**	**1074**	**5**	**33**	**72**	**119**
of which:									
Transition (307-323)*	10	2	0	0	28	3	14	–	–
Phase V	43	8	3	2	214	6	27	71	107
Phase V* (323-391)	34	6	2	2	186	7	31	93	93
Phase IV+V*	117	20	8	6	472	5	24	59	79
Phase IV	84	14	5	4	285	4	20	57	71
Phase III+IV	189	24	11	6	843	5	35	77	140
Phase III	106	10	6	2	557	6	56	93	279
Phase II+III	126	11	7	3	602	6	55	86	201

* Transition interval = upper 14 cm of Phase V, immediately below the Peaty fill; Phase V* = Phase V excluding that interval

** Using the mean non-linear age model. Uncertainty: +/- 9% (long range resp. short range)

Table 4: Indexed flooding event counts and recurrence

In the 31-yr moving-window F.I. result, more blocky patterns are shown for Phase III, compared to Phase IV-V that is irregular from the stacking of multiple lower-category events. These latter phases have a greater LOI variance (Tab. 3) and mark increased proximity to the active channel. One may read their increased number of events to reflect the increased proximity: the critical level above which a flood produces a distinct event layer is lower in Phase IV-V than in Phase III. The Z-score calculation that underlies the F.I., by using the background LOI variance to standardise with, intends to subdue effects of changing LOI variance. Hence, it intends to subdue the effect of increased event-registration with increased proximity, but it may not fully counteract the proximity increase at Phase III/IV transition. Alternatively, Z-score standardisation can be regarded to fully counter the increase in proximity. In that case the moving window F.I. change from blocky to irregular may be the overprint of a change of flood regime, commencing around the time of the Phase III/IV transition. Indeed comparison with CPDF results (Fig. 4B; see below) suggests Phase IV-V to coincide with increased flooding 'activity', after a longer period of increased 'stability', around 4.2 kyr ago (Hoffmann et al., 2008). This age is associated to hydrological climatic change around the world widely in so many studies that it is a candidate boundary defining the beginning of the Late Holocene (Walker et al., 2012). The LOI record and derived proxies do not allow to infer changes in the magnitudes of largest experienced floods between the two periods, but do support more frequent occurrence of floods for some centuries around 4.2 ka BP.

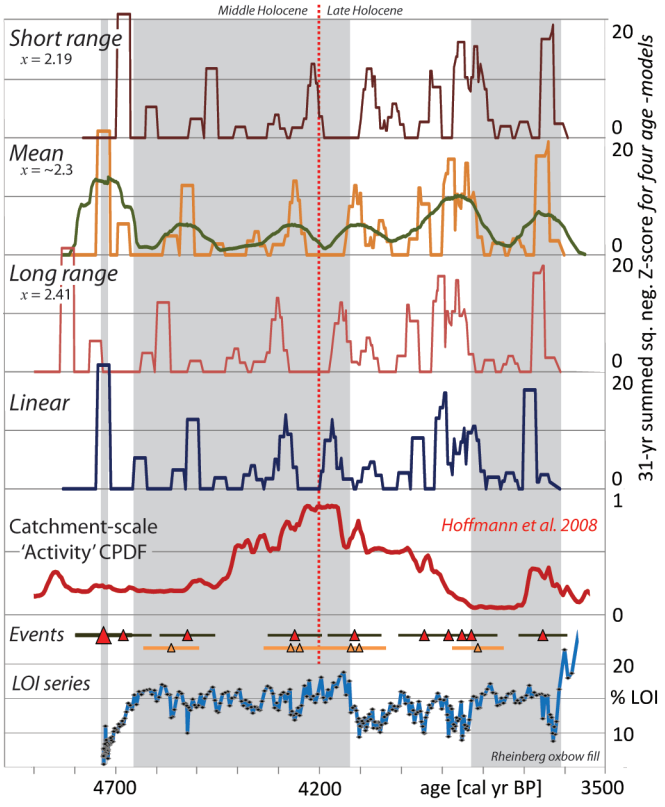

Figure 5. Dependence of event-based flooding index on age-model choice.

Regarding the integration of the age-modelling and the palaeohydrological application, it is clear that the calculation of event-return times (Tab. 4) and the comparison of moving-window F.I. results to CPDFs is sensitive to chosen age-model. Figure 5 illustrates this for the 31-year moving window F.I. Events from below 5.50 m core depth (in Phase III, after ~4100 ka BP) are relatively separated and events from above 5.50 m core depth (in Phase IV) are more condensed on the time axis in the non-linear models. Such differences affect the return time estimates associated to F.I.-scored events, but do not majorly affect our F.I. to CPDF comparison.

In the peaty top interval, the oxbow fill environment was much more distal, the threshold of registration much higher. The three LOI excursions registered in the ~575-650 years covered by the peaty interval are each to be regarded rare large floods. Smaller floods are not recorded and the temporal resolution in this interval is low. For these two reasons, the moving-window F.I. is not calculated for Phase VI.

6 Discussion

6.1 Comparing event-resolution F.I. to radiocarbon CPDFs

CPDFs are presumed to mimic the flooding intensity (e.g., periods of increased flooding frequency) of the catchment's outlet river (Macklin & Lewin, 2003; Lewin et al., 2005). In CPDFs, the uncertainty associated to each radiocarbon date is bound to smooth out detail and aggregate scattered flooding indications at the event scale (few weeks) to broader periods of intensified flooding (centennial resolution). Comparison with F.I. results offers a means to test this presumption and specify resolution limits of the CPDF method. In the CPDFs for the Rhine (and adjacent German catchments; Hoffmann et al., 2008), two increased flooding activity periods occur in the time frame overlapping the Rheinberg record, timed around 4200 and 3350 cal yrs BP (Fig. 4B). Note that 'residual channel dates' were excluded in the construction of the CDPFs because deciding whether such a date relates to an event that was local-valley triggered or upstream-catchment hydro-climatologically induced is not straight forward.

The CPDF 'activity' peak at ~3350 cal yrs BP coincides remarkably well with a first 'probable large flood' in the peaty top of the oxbow fill (Fig. 4B), and prolonged increased 'activity' is supported by two later similar events in the record. At this stage (Phase VI) the oxbow fill no longer has a superior resolution above the CPDF: the oxbow fill becomes an inventory of the very largest floods only, and provides no distinct coverage of other floods. The radiocarbon dates collected from this upper part of the channel fill can be used in CPDF calculations.

The centuries preceding the Rheinberg oxbow cut-off and the millennial flood, show a low in both the 'activity' and the 'stability' curves, meaning that valley sediments from this time period are scarce and relatively undersampled. The idea that indeed a catastrophic event swept through the catchment at about ~4720 ± 70 cal yrs BP, can provide explanation for the apparent CPDF undersampling of the centuries running up to the event. Erosional activity during the flood would have affected both types of sedimentary contacts providing 'stability' and 'activity' dates in the CPDF construction exercise, and leave 'shadow' of no data. While high-magnitude events may affect geomorphological preservation and thus *availability* of oxbow sites in similar 'overcasted' ways, oxbow fill *inventories* in principle do not suffer from such registration bias. In fact, they

record the largest flooding events more clearly than events that only modestly exceed the threshold to leave event-beds amidst background facies. A core from a distal oxbow lake that recorded the 4720 ± 70 cal yrs BP flood as an event-bed *within* subaqueous fill – rather than *at* its base as in Rheinberg Meander A, or in peats as in Site VK (Fig. 1; Chapter 6) – may further constrain the timing of the very large flood, reveal flood event history from before the event, and validate the suggested no-data shadows in CPDFs.

6.2 Palaeogeography 5000-3500 cal yrs BP

Sedimentary information contained in the Rheinberg oxbow fill adds resolution to the fluvial history in the vicinity of the site in the first centuries after cut-off. In Figure 5, the first and last panel summarise what could be reconstructed without incorporating the detail from the age-modelled oxbow fill (Erkens et al., 2011; taken as base map). Seven more panels sketch the in-between situations that are inferred with the new data.

From surface morphology (Fig. 1) and lithological sectioning and dating (Erkens et al., 2011), it is clear that adjacent Meander B abandoned only shortly after Meander A. Date UtC-15065 from Meander B post-dates abandonment of the main site by 100 to 300 years only. In isolation, it calibrates to 4640 ± 100 cal yrs BP (section 4.2; Tab. 2). While geomorphology suggests two generations of meanders, radiocarbon dating suggests one generation (cf. Erkens et al., 2011). So far, it was difficult to decide whether the small age-difference indicated poor dating results, or wrong geomorphological understanding. With the new findings from the oxbow fill sedimentology and the linkage to millennial flood marker downstream (Chapter 6; Toonen et al., 2013), it becomes possible to identify the point in Meander A's oxbow fill, where Meander B would be abandoned. This then allows to connect and evaluate the date obtained from Meander B, thereby further iterating and optimizing the geomorphological interpretation.

It turns out, that linking the millennial flood passage to the Meander A cut-off event (section 4.4), not only makes earlier mapping and dating consistent with newly added sedimentological findings, but also offers a way to explain the peculiar 'double' preservation of Meander A *and* Meander B within very short time after each other. The oxbow fill sedimentology from Phase I to II to III (Figs. 2 and 4) suggests Meander B to have moved away from the main site (i.e. eastward), if it migrated at all. The LiDAR-geomorphology (Fig. 1), however, suggests it to have last migrated westward. Only when Meander B is seen as the product of the same flood that caused Meander A to cut-off, LiDAR geomorphology and oxbow sedimentology are mutually in agreement. Systematic checking of all chronologically different correlation-scenarios fail on constraints from sedimentology and geomorphology (Appendix A). This implies that 'Meander B' is not a classic meander resulting from bank-erosion and bed-migration over longer time, but a faster formed major 'chute' channel.

Further support for the scenario that cuts-off Meander A during a very large flood, comes from geomorphological interpretation of subsequent stages of meander dynamics, as recorded in the oxbow fill. Meander B got its shape during the very large flood, but not too long after abandoned in turn, in favour of a new channel at greater distance of the main site. This is indicated by the relative high LOI values in Phase III (from 7.40 m upward), and occurred within a century; otherwise, Phase III's relatively distal facies is unexplained. The base of Phase III (ca. 80±10 years of sedimentation after 4720±70; Fig. 3) is thus equated with Meander B abandonment. Pooled calibration can then narrow abandonment dating for Meander B to 4590±60 cal yrs BP (Tab. 2).

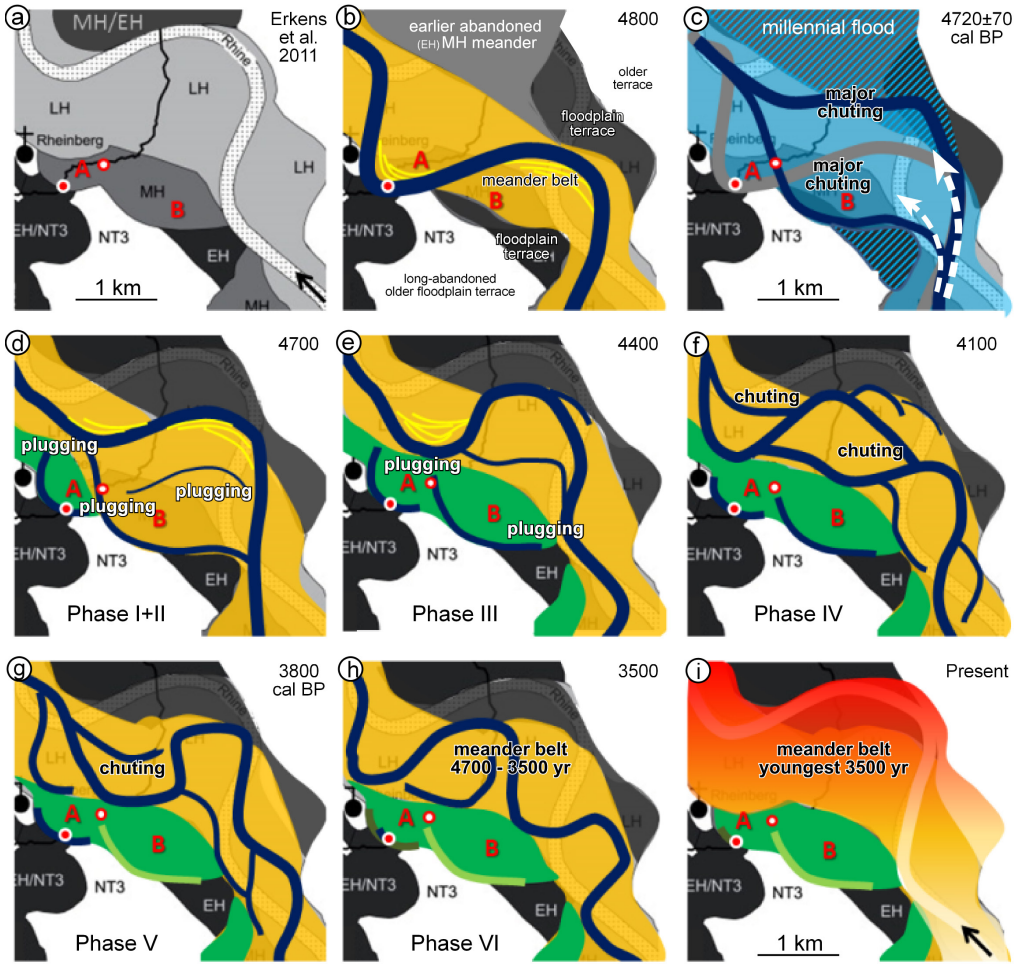

Figure 6. Palaeogeographical reconstruction of Lower Rhine meander dynamics in the study area in the third and second millennium BC.

Although Meander B kept functioning in the ~80±10 years after the very large flood, from the lithological data available it also appears to have shallowed (cf. Chapter 3). Meander B has considerable bed-load bars in its channel (e.g., at its dating site; section 2). This indicates the channel to have lost discharge directed into it at its bifurcation upstream (Kleinhans et al., 2013), i.e. a third channel must have existed that was becoming the main channel. The bed-load bars must have formed synchronously to the levee over the plug bar at the entrance of Meander A (section 5.1), by overbank sedimentation received from Meander B. There is no indication that Meander B abandonment was associated with a particularly large flood: around the transition of Phase II to Phase III no particularly thick bed is seen in this laminated fill. These findings together make it probable that the channel that took over the discharge of the Meanders A and B had co-functioned with Meander B since the 4720±70 very large flood, very likely being the product of the same very large flood, and given the shallowing of Meander B, functioning as the main channel (Fig. 6c).

While this successor channel can be seen as a successful local avulsion (cf. Heller & Paola, 1996), triggered at 4720±70 BP and completed some 80-130 years later (4590±60; Fig. 6d), Meander B can be seen as a chute-channel from during the triggering flood. Avulsive shifting of the channel axis can also explain the peculiar 'double' preservation of both the cut-off oxbow and the abandoned chute-channel (Meander A and B). The new-found channel axis has since been maintained, developing into the wide Late Holocene channel belt (Fig 6e-i), of which also the modern channel is part. Shortly following the avulsion, however, the meander belt was smaller and the registration of river dynamics in the Phase III to V of the oxbow fill (possibly also Phase VI) could provide record of the initial widening process. The apparent alternation between two active channel positions interpreted for Phase IV and V (section 5.1, 5.3) can be read as regular meandering behaviour, involving periodical chuting over its young pointbars (section 3.2). Recent flume experimental work on chute cut-off meander dynamics with application on systems such as the Rhine in mind also suggests such behaviour to establish in response to the carving of a new channel (Van Dijk et al., 2012; Van de Lageweg et al., 2013).

Linking geomorphological preservation of Rheinberg Meanders A and B to a rare very large flood control complements a previously established theory on the nature of the meander preservation. Schirmer (1995) mapped meanders in the Rhine catchment and tributaries and claims that preservation boils down to a fixed number of generations (two for the Middle Holocene) in all systems, which is believed to reflect a limited number of climatic events causing reorganisation of the system. A few high magnitude events control the preservation over millennial time scales in this theory. The alternative is to attribute more preservational overprint to regular magnitude events and autogenic processes in the meandering river (e.g., Erkens et al., 2009), which would lead to more random preservation, gradually reducing with time (e.g., Lewin & Macklin, 2003). The aforementioned potential problem of no-data shadows in CPDFs links into this discussion too. Of the three groups of Holocene meander generations that are classically distinguished (Early, Middle and Late Holocene), the Middle Holocene situation, with inherently terraced and densely forested floodplains and a single meandering channel at relative incised position, would be the most susceptible period to have major meander reconfigurations occurring during to very large events only (and similarly: could be the period where CPDF shadows are strongest developed). At least the single case of Rheinberg Meander A fits the Schirmer (1995) preservation model. It might be, however, that it applies to this particular case and stretch of Rhine only. Investigations of other meander cut-off cases throughout the Holocene – combining oxbow-fill sedimentary inventories with sequential dating and geomorphological mapping – is needed to decide what controls meander preservation in different periods and settings.

6.3 Wider applicability of oxbow-fill records of fluvial dynamics

The main reason to add oxbow-fill inventories to palaeoenvironmental reconstructions is that they contain continuous registration of events in the river system. This favours resolving the record in time (with age-modelling) and favours interpretation in terms of river reconfiguration, assessment of the rates and frequencies at which fluvial processes operated in the past, and palaeohydrological variations – all over times longer than the observational record – bridging a resolution gap and bringing river-process and landscape-reconstruction fields of geomorphology closer together.

Besides direct palaeohydrological relevance (section 6.1), and local palaeogeographical reconstruction relevance (section 6.2), identifying marker beds of rarest, largest events is important

for integrating reconstructions of catchment, valley and delta. The main way in which it enables this is because more accurate temporal correlations can be made within records of the same broad age, by deploying an event-stratigraphic approach on flood-marker beds. In this study, such is deployed by pooling the downstream flood-marker date with that from the base of the cut-off age. In turn, future event-stratigraphy constrained ^{14}C-calibration results can be used to construct CPDFs of potentially improved resolution, and be screened for data shadows of floodplain record removing events.

Lastly, combining sedimentary data and spot radiocarbon ages in the age-modelling, besides leading to more-realistic age-depth relations, is a way of forcing oneself to scrutinise one's data. All too often, subsampling for radiocarbon dating is opportunity driven, and once returned from the lab ages that do not suggest inversion are simply accepted, without any cross-check for what the sedimentology of record indicates. The spread-sheet age-modelling is a way of verifying (even quantifying) to what extent age-increment and mode of sedimentation are in mutual agreement. If the dating is free of outliers, and the sedimentology free of hiatuses, Eq. 2 and 3 result in realistic age-depth models that are trustworthy despite the low number of spot-ages. If the radiocarbon dating dataset contains outliers and/or hiatuses, then the model will produce results that are clearly unrealistic and counterintuitive, so such an exercise can be seen as a test for correspondence between sedimentology and chronology.

In principle, the age-modelling method could also be ran using other 'continuously sampled' sedimentary data – for example the silt/clay ratio obtained from grain-size analysis. For the fine-grained oxbow lake setting in this paper, LOI was favoured because it is an easier (low-cost) measurement, and also because already from visual inspection crude field-estimates of the organic content can be made. Ages derived for distinct event beds, in the future, may be event-stratigraphy cross-correlated between oxbow fills and datable types of overbank sequences with flood beds. In turn, the age-depth modelling and radiocarbon-date calibration can be further iterated and narrowed with such correlations. This type of usage of oxbow event-inventories is key to overcome the resolution methods of established mapping and dating methods.

7 Conclusion

Using the fluvial archive contained in the Rheinberg oxbow fill, and combining it with geomorphological mapping and dating of adjacent valley elements and event stratigraphy, a high-resolution reconstruction of meander belt development and flooding intensity was developed. The reconstruction covers the period from 4720 ±70 to 2950 ±50 cal yrs BP, centred around the Middle to Late Holocene transition and the period that the Lower Rhine discharge and sediment regime gradually began to be affected by progressing deforestation (Neolithic and Bronze Age clearings), but can still be regarded largely natural.

The key message is that the fills of oxbow lakes in lower reaches of larger rivers hold important information that can improve and validate palaeogeographical and palaeohydrological reconstructions. To make maximum use, it is essential to apply a form of age-depth modelling that considers sedimentary indications for periodically slower and faster sedimentation during collection of the fill. A regression age-depth modelling methodology is prototyped that uses continuous

collected LOI-measurements for this purpose. For individual phases, produced mean sedimentation rates differ from linear models by 10 to 20% in mid-sections of the fill, and by much greater in the bottom section.

The reconstruction outcome for the Lower Rhine near Rheinberg, is that meander abandonment and preservation are due to a major channel reconfiguration episode, triggered by a very large flood event, in a still mostly forested overbank situation (not yet majorly cleared). This cut-off Meander A (during the event), set-up Meander B to abandon too (in a century-long aftermath, recorded in the fill), and created a new channel away from the oxbow site. The avulsed channel developed the meander belt of which the modern river is still part. For ~1000 years, a background organoclastic sedimentation facies accumulates filling the oxbow up to ~1 meter below its water table. This facies is irregularly inter-bedded with mm-thick event beds, produced by floods exceeding a threshold discharge well above that of bankfull stage and result in distinct event beds. Continuous sampling at fine-resolution for LOI measurement resolves the larger of those event beds, and the age-modelling provides ages.

A flood-event index is developed to reveal periodical changes in this registration. The LOI-based flooding index is developed that is suitable for quantifying large flood recurrence, but provides only qualitatively indication for flood magnitude. Comparison with CPDF palaeohydrological reconstructions demonstrates resolution differences. Oxbow lake inventories can address sub-centennial-scale stability of discharge regimes, whereas CPDFs can only resolve such at (bi) centennial scale. Comparison further suggests no-data 'shadow' effects to exist in the datasets underlying CPDFs for ~500 year long periods leading up to very large events, affecting 'stability' and 'activity' subsets alike, particularly where these cover the Middle Holocene period. With this respect CPDFs suffer from similar inventory incompleteness as geomorphological meander mapping and availability of oxbow sites. Oxbow fills are principally insensitive to such no-data shadows and the way to overcome preservation incompleteness. They are the exception to the rule of sedimentary non-registration of incidental largest magnitude events.

Acknowledgements
This work started as a BSc thesis project by PSJM, designed and supervised by WZH and KMC. It served as a pilot project in PhD research on Rhine palaeofloods of WHJT, designed and supervised by KMC, and is part of long-running palaeographical reconstruction activities in the Lower Rhine valley (WZH, KMC, GE). Fieldwork was carried out by PSJM, KMC, GE and WZH. Lab analysis was carried out by PSJM, WHJT and WZH. We acknowledge Hanneke Bos for identifying macrofossils for radiocarbon dating. The age-model method was developed and sensitivity-tested by PSJM, KMC, WHJT and WZH. Change point analysis and comparison to visual description was performed by WHJT and KMC. Use of LOI data series for F.I. scoring event layers was explored by WHJT, PSJM and KMC. Tiuri Konijnendijk is acknowledged for LOI lab sensitivity tests, and Bas van der Meulen is acknowledged for assistance in age-modelling sensitivity tests, on materials from other Lower Rhine sites. Manuscript and supplementary data were prepared by KMC, PSJM and WHJT. Funding came from Utrecht University and Deltares Research Institute (Dept. of Applied Geology and Geophysics). Hans Middelkoop is thanked for comments on the manuscript. The prototyped LOI-tuned age-modelling finds inspiration in work by Jef Vandenberghe et al., (1997), where continuous grain-size data was input to age-depth modelling of a Central China loess sequence.

5 Lower Rhine historical flood magnitudes of the last 450 years

reproduced from grain-size measurements of flood deposits using End Member Modelling

Toonen, W.H.J.[1,2*], Winkels, T.G.[1], Cohen, K.M.[1,2], Prins, M.A.[3], Middelkoop, H.[1]

[*] Corresponding author: Heidelberglaan 2, 3584 CS Utrecht. w.h.j.toonen@gmail.com
[1] Department of Physical Geography, Utrecht University, Utrecht, The Netherlands.
[2] Department of Applied Geology and Geochemisty, Deltares BGS, Utrecht, The Netherlands.
[3] Department of Earth Sciences, VU University Amsterdam, Amsterdam, The Netherlands.

1 Introduction

Predictions of recurrence times and magnitudes of extreme floods are generally based on the extrapolation of measured discharge data. As these datasets often have a limited length (rarely longer than a century), estimated discharges for extreme floods come with a considerable uncertainty (Klemeš, 2000). To extend discharge data series, recent studies explored resampling of meteorological observations to simulate flood events using coupled rainfall-discharge models (Chbab et al., 2006; te Linde et al., 2010), or used alternative monitoring stations and water level measurements to reconstruct discharges back to the end of the 18th century (Chapter 2). For a limited number of large floods from before routine measurements started, discharge reconstructions are available that made use of historical or palaeoflood stage indicators (Herget & Meurs, 2010; Chapter 6). These studies provide useful specific information on single events, but in general palaeoflood inventories are discontinuous and fragmentary, which troubles accurate assessment of flooding regime variability, especially over longer periods and in the domain of rare large events.

As river discharges and flow velocities increase during a flood, increasing amounts of coarse grains are entrained in the suspended load transported in the channel, where it moves as bed-load during normal flow. Once part of the channel suspended load, it exchanges during peak discharge with overbank suspended transport and starts moving over the inundated floodplain. There, the sediment is deposited at various locations, importantly in local lakes and depressions that act as efficient sediment traps, where coarse grains can settle from their suspension relatively quickly. At such sites deposition occurs with every flood when discharge exceeds bankfull levels and floodplains are inundated.

This paper evaluates the suitability of several grain-size descriptors for reconstructing historical flood magnitudes, based on two separate research locations to demonstrate reproducibility. Multiple grain-size descriptive parameters were inferred from grain-size distributions of flood deposits; the median, mean, the mean of the sand fraction (MS), 95th percentile (P95), and various end member distributions (Prins et al., 2000). Although many studies only use the mean and median in flood

magnitude analysis (Beierle et al., 2002; Arnaud, 2005; Czymzik et al., 2013) or variations in organic content (Nesje et al., 2001; Chapter 4), which provides qualitative indication of flood magnitudes only, this paper aims to unlock the potential of P95 and the use of end member modelling (EMM; Weltje, 1997; Weltje & Prins, 2007) to describe the coarsest tail of grain-size distributions and to relate this information to peak discharges. Several studies have shown that variations in sedimentary characteristics, such as geochemical composition and the grain-size distribution of deposits have a relation with flood magnitudes (e.g., Parris et al., 2010; Berner et al., 2012), but these properties have not been used to reconstruct past flood event discharges from flood sediments over longer periods. Reconstructions of historical flood discharges may provide an additional source of data, which allows for a better representation of extremes, and can serve as input for studies aimed at assessing non-stationarity of flooding regimes induced by climate change and human impact (Knox, 1993; Chapter 2).

In the apex region of the Rhine Delta (Fig. 1), from two lakes in the floodplain acting as sinks of flood deposits, sedimentary sequences were retrieved. The lake fills contain a flood record that spans the last centuries. The top part of the deposits accumulated contemporaneous with modern discharge measurements in the same region, which made it possible to correlate sedimentary characteristics of flood deposits and discharge. The paper makes use of an extended observational discharge series for the Lobith gauging station back to AD 1772 (Chapter 2), and comparison with detailed historical records. Regression analysis between the various age-depth modelled grain-size parameters and measured discharges is used to demonstrate the improvement of flood magnitude prediction resulting from using standardized coarse-tail descriptive parameters. Found relations are applied for flood magnitude reconstructions beyond the period of overlapping records, i.e., before AD 1772. The resulting palaeoflood chronologies inferred for the individual sites are compared and used to present a Lower Rhine palaeoflood chronology back to AD ~1550. Furthermore, it is discussed how specific environmental settings affect the performance of the unlocked sedimentary records, and may complicate extraction of flood magnitude signals from sedimentary records.

2 Research Area

In the floodplains of the Rhine Delta apex area (Fig. 1), two types of sediment trapping lake features are common; abandoned channel fills and the fills of dike breach scour holes (in this paper referred to as 'scour holes'). Since AD 1350 all rivers are embanked in the Netherlands (Hesselink, 2002). This limited sediment delivery to distal parts of the former floodplain and oxbow lakes in those parts, but accelerated deposition close to the river. Starting in the 19th century, additional measures to regulate discharge to reduce flooding, and improve navigation were carried out, and many meanders were artificially cut off. Abandoned channels, either naturally or artificially cut off, have filled gradually with deposits during successive floods. The lower part of the fill has typically trapped bed load sediment during the gradual abandonment of the channel, the upper part of the fill consists of overbank-delivered sediment that accumulates with every flood that has exceeded bankfull discharge since the entrance of the channel has become completely plugged with sediment (Chapter 3).

Related to embankment, a second type of sink for sediments in the floodplain emerged, as deep scour holes are formed when a dike is breached during a flood (Fig. 1). Scour holes positioned

at the river-side of the repaired dike form deep lakes in the floodplain and fill gradually with flood deposits. Most scours have penetrated Holocene deposits and reached the underlying, easily-erodible Pleistocene sandy braided river deposits, resulting in occasional scour hole depths exceeding 10 meters (e.g., Hesselink et al., 2003; Cremer et al., 2010). Because of the abundant sediment supply in the active floodplain, most scour holes tend to fill completely in several centuries (Middelkoop, 1997). This ensures a high resolution of registered flood deposits.

Two research locations were selected in the vicinity of Lobith (Fig. 1), where discharge data and discharge reconstructions are available since AD 1772 (Chapter 2). A scour hole named Zwarte Gat (ZG), formed during the flood of AD 1644 (Buisman, 2000), is located ~25 km downstream of Lobith. From ~15 km upstream of Lobith, in the Lower Rhine Valley, the Bienener Altrhein (BAR) was selected; an infilled oxbow, which was abandoned around AD 1550 (Braun & Thiermann, 1981). Site choice was based on proximity to Lobith, and period of registration commencing as early as possible, albeit that part of the sedimentary sequence must be contemporaneous with discharge measurements. Both sites are located in parts of the floodplain that today inundate when discharge of the Rhine at Lobith exceeds ~6,500 m^3s^{-1}.

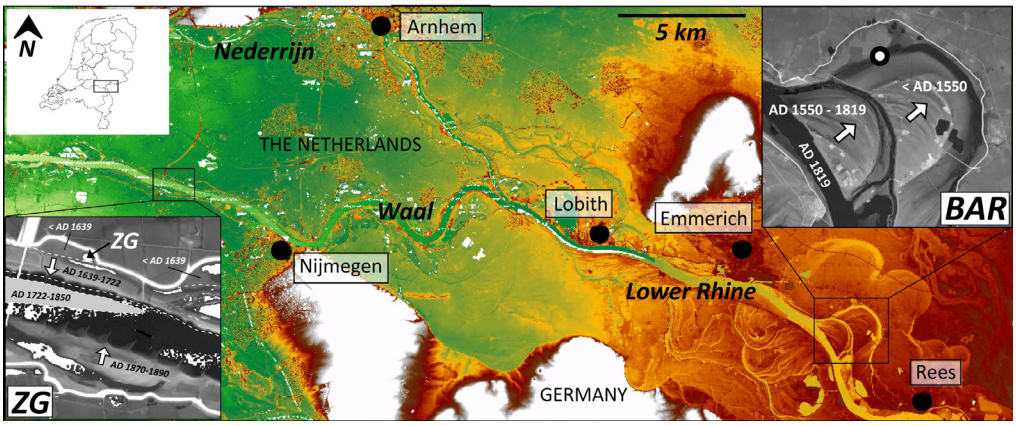

Figure 1: Overview floodplain elevation map of the apex region of the Rhine Delta (the Netherlands and Germany; Rijkswaterstaat-AGI, 2005; Cohen et al., 2009) – white and red colours respectively indicate high elevations of the Saalian ice-pushed ridges (20-80 m +msl) and the Lower Rhine Valley (10-20 m +msl), green colours mark the low-lying Rhine Delta (5-10 m +msl). Detail insets show core location surroundings (light = higher, dark = lower) with the historical development of local morphology (based on historical maps; references in the main text); white arrows and ages indicate the direction and period of fluvial migration.

3 Methods and Materials

Cores were retrieved with a modified Livingston piston corer. At site ZG, a first coring campaign in AD 1991 was ceased after ~9.8 m due to borehole collapse (Middelkoop, 1997). The very base of the fill thus remained unsampled, but is probably not much deeper as historical records mention a 30 feet (~10 m) deep lake directly after formation (Buisman, 2000). The further shallowed pond was revisited in AD 2011 to collect deposits of the last decades. Geochemical markers (pollutants)

in the upper meters allowed to tie both cores together. For site BAR, reconnaissance boreholes in AD 2010 located the thickest channel fill sequence. From this location, 8.5 m of laminated deposits was retrieved, reaching down to the gravelly channel base. Core segments were stored in sealed PVC-tubes in a refrigerator to prevent oxidation and decay. After opening, cores were photographed and sedimentary characteristics described down to the level of individual laminations, and samples were taken for sedimentary analysis and various dating techniques. The investigated flood deposits have formed fairly recently and are located below the present water level, so limited compaction has occurred. Force exercised by the piston corer has compressed sediments slightly. Coring depths were carefully recorded and have been used to stretch the recovered material to original depths. The bottom of each core segment equals its true depth, so stretching was applied linearly (no intra-core changes in bulk densities were detected), and extending to the bottom of the core segment above.

3.1 Grain-size measurements

Continuous samples for grain-size analysis were taken with semi-regular sample thickness of 1-2 cm. Based on visual laminations, sample intervals were slightly adjusted to correspond with visual flood layering. Laminations smaller than 1 cm were not sampled individually, due to the minimum required sample volume. Because some flood event-layers span more than 2 cm, adjacent samples may reflect stages within single events. In those cases, which are not coincidentally the largest floods, the coarsest sample was adopted for comparison with measured peak discharges. Samples were successively pre-treated with 10 ml 30 % H_20_2 to remove organic matter, with 5 ml 10 % HCl to remove calcium carbonates, and with 300 mg of $Na_4P_2O_7.10H_2O$ to further disperse grains (Konert & Vandenberghe, 1997). Grain-size distributions ranging from 0.1 to 2000 µm in 56 bins were measured with a Sympatec HELOS KR laser-diffraction particle sizer available at the VU University, Amsterdam.

3.2 Descriptive statistics and End Member Modelling

The median, mean, MS, P95, and the EMM-derived proportional contributions of coarser end members describing the grain-size distributions were calculated. The former (median and mean) describe the entire grain-size distribution, whereas the latter describe the coarse tail of the grain-size distribution (MS, P95, and EMM). For EMM, the DRS-Unmixer model (Heslop et al., 2007) was used to unmix different populations. For each site, a model with five EMs was established to describe measured distributions (Fig. 2). The use of EMM on fluvial deposits is explorative, as it allows statistically decomposed (or unmixed) grain-size populations, to which a physical meaning is assigned on sedimentological and hydrodynamic grounds. Mixing models with more EMs explain a larger proportion of measured distributions, but adding more than five EMs did not lead to significant unmixing improvement in which case they are not considered geologically meaningful (following practices established in Weltje, 1997; Prins et al., 2000).

Because the distance between the two research locations is limited (~40 km) and sediment is distributed from the same source during flooding events, end members are similar (Fig. 2). Small differences in the grains-size characteristics of end members (especially the coarsest end member, EM1) is explained by site-specific factors, such as the distance and connectivity of a sediment trap to the active river (Prins et al., 2000), and the type of research location (Erkens et al., 2012). For characterising flood magnitudes with the end member approach, only the two coarsest end members (EM1 and EM2) were used. Finer end members represent suspended and wash load populations, for which it is assumed that limited differentiation occurs between different flood

magnitudes (Fig. 2), as these fine particles are also in suspension during normal flow and minor floods. This assumption is supported by nearly identical wash load end members at the different research locations, and the apparent admixture of different grain-size populations in deposits belonging to floods of different magnitudes (Fig. 2). For such bimodal grain-size distributions EMM is an adequate tool to assess data, as mixed populations and the distribution of these EM are site-specific, and are statistically established from the full array of grain-size distributions present in the entire sequence.

Changes in the distance and connectivity of the sediment trap to the active channel (gradually or abruptly) and infilling processes related to water depth (e.g., encroachment of vegetation and turbulence in shallow water) cause phasing in sedimentary fills (commonly observed; e.g., Chapter 3 and 4). To prepare records for flood magnitude analysis, one needs to normalise data; e.g., a phase of nearby river activity is not necessarily a period with larger floods, although deposited material is generally coarser. The position of breaks in sections followed from change point analysis (CPA; Taylor, 2000) on particular grain-size descriptors. Trend-breaks exceeding a 95% confidence level were used to separate different sections. Data in the separated sections were linearly detrended, and grain-size data was normalised into Z-scores per section (Chapter 4). Using Z-scores allows unification in a single continuous record of data from different sections as flood magnitudes are recalculated as a function of the background values, which are fines deposited during minor floods and forming the bulk of the studied sedimentary fills (EM3-5; Fig. 2).

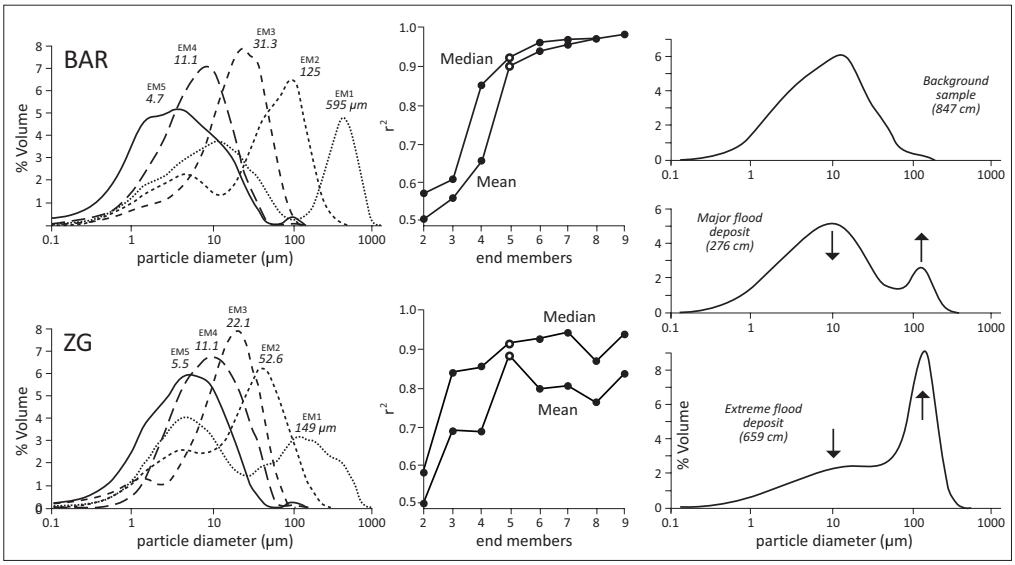

Figure 2: Grain-size distributions in a 5-end member model, and coefficients of determination (mean and median R^2-values of the fit of EMMs on all grain-size bins) for models using a different number of end members. The right panel depict 'typical' grain-size distributions of the BAR (depth of plotted samples indicated in cm) associated with deposits belonging to various flood magnitudes – showing the successive admixture of a coarse grained population with increasing discharge.

3.3 Age-Depth modelling

Meaningful comparison of laminated sedimentary core data with time series of discharge data and historical flood events demands highly accurate age-depth models. Several dating techniques were combined to provide tie-points for the initial age-depth model; (i) XRF and traditionally acquired pollutant-geochemistry were used to pinpoint the onset of heavy-metal pollution contemporaneous with the Industrial Revolution (~AD 1860 in the Lower Rhine), and a temporary decrease in pollutants during World War II (Middelkoop, 1997), (ii) palynological information marks the presence or absence of specific time-indicator species (e.g., maize, pine, buckwheat, an rye), (iii) ^{210}Pb-dating provides absolute ages in the last century, and (iv) historical documents describe the year of channel disconnection or dike breach, which correspond with the base of the sequence, and major adjustments to the floodplain and river that are reflected as changes in sedimentary style and facies. These various constraints were used to create initial stepped-linear age-depth models.

The initial age-depth model was then further optimized by using the event chronology of historical flooding events. Known large floods of the last five centuries (Buisman; 2000; Herget & Meurs, 2010; Chapter 2) should correspond with the coarsest flood beds in the cores. Following this assumption, extra tie-points were specified in the age-depth model. First, largest flooding events were selected from historical records, identified by numerous dike breaches and a regional impact of flooding (notably AD 1658, 1809, and 1861; Chapter 2). Starting with the coarsest imprint in the sedimentary record, spikes were correlated with historical events, using the initial age-depth model as a reference for approximate or minimum age. The initial age model was updated with each added tie-point, after which a next coarsest flood layer was assessed. This process was repeated until all major historical floods and most moderate events of the last centuries were assigned to a flood layer. Apparent uncorrelated events, not found in either historical records or in the sedimentary record, were further investigated. Possible explanations are discussed later (section 4.4).

3.4 Linking flood-bed coarseness to observational discharge series

The age-modelled flood events from after AD 1772 were lined-up with the observational discharge series from Lobith (Fig. 1). For each research location, a linear regression was calculated between normalised grain-size descriptors and measured discharges. The coefficient of determination (R^2) was used to quantify performance. Resulting regression functions were applied to the deeper sections of the core (before AD 1772), to reconstruct discharges back to the mid-16th century. Comparing results from temporally overlapping sites allowed investigating method accuracy, and the heterogeneity in flood registration. An independent check on the relation between grain-size distributions of deposited material and discharge comes from Middelkoop & Asselman (1998), who collected overbank sediment deposited during the AD 1993 flood (10,940 m^3s^{-1} at Lobith) in the direct vicinity of ZG, using artificial turf sediment traps of 50 x 50 cm in a cross-floodplain transect. The material was reanalysed in this study, subject to the same procedures and methods as used on all other samples (including EMM and Z-score calculation; incorporated in the upper normalised section of the ZG scour fill).

4 Results

4.1 Fill sedimentology

The sedimentary fill at both locations matches common channel fill sequences (Chapter 3) with (i) a coarse-grained basal lag from when the site formed, (ii) relative coarse and thick flood beds

at the base of the fill, which gradually decrease in thickness upward into (iii) the main part of the sedimentary sequence with strongly laminated fines and varying coarseness, covered by (iv) near-surface deposits that have been influenced and altered by local factors interacting at the transformation of fluvio-lacustrine into terrestrial floodplain environment (Fig. 3).

Site BAR features a relative thin interval (~25 cm), probably spanning several years only, of channel disconnection-related coarse deposits at the base of the fill. This indicates that plugging and disconnection from the main channel occurred rapidly after the initial chute cut-off (Chapter 3). Thereafter, deposition into the disconnected channel occurred during flooding events only, which resulted in relatively uniform facies of laminated deposits (Fig. 3); no CPA sections are recognized, other than at the very top (see below). Distinct layers of relatively coarse deposits, presumably marking large flooding events, are distributed throughout the core. The coarsest flood bed is found at ~6.5 m core depth (Fig. 3). From at a depth of ~1.5 m, the general coarseness of laminated deposits starts to increase towards the surface. Such gradual facies changes at the top of the fill was also observed in previous studies (Chapter 3 and 4), and mark the transformation from sub-aqueous to terrestrial conditions and sedimentary processes (including the encroachment of vegetation). The upper meter of the fill consists of non-laminated coarse sand. The bright yellowish colour, high angularity, large grain-size, and poor sorting of this top layer deviates strongly from fluvial deposits encountered in the channel fill or nearby floodplain. Likely these sands were introduced during the construction of a sluice in the nearby downstream connection with the Griethorther Altrhein in the 1920's (Fig. 1). Hence, samples from these deposits were excluded from the end member model.

Three sedimentary sections are CPA-recognized in the ZG sequence (Fig. 3). Scour holes are generally created during a single event, and are not gradually disconnected from the active channel, and normally no facies corresponding to a disconnecting-phase exists. The general coarseness and abundance of sandy event layers change importantly around 7 and 4 m core depth. In the lower section (7.0-9.8 m), sandy layers occur frequently while the general background matrix is relatively coarse (fine silts rather than clays). Around 7 m, there is a sudden shift towards finer background sediments (Fig. 3). Event interbedding remains frequent, although their coarseness decrease along with the background sediments. This shift can be explained by altered floodplain configuration, affecting flood-stage connectivity of the pond with the active river (via the small ditch running adjacent to the scour hole; Fig. 1), or by change in the distance to main channel thalweg due to southward meander bend migration and the accretion of large gravel bars at the northern bank (Fig. 1). The upper section shows decreasing coarseness, and decreasing occurrence of event layers – although several very coarse flood layers are found near the surface. Besides changes in floodplain connectivity and geometry (e.g., distance to river thalweg, vertical channel bed movement, and ongoing floodplain deposition), this change may also be due to the limited remaining water depth in the scour hole. Especially during major events, turbulence exerted by flow in the inundated floodplain may repeatedly have eroded previously deposited material at the top of the scour hole-fill in this shallowing stage. Another explanation can be sought in the ongoing river management (e.g., construction of groynes and removal of sand bars), which has resulted in channel incision (Ten Brinke, 2005), thereby possibly influencing the coarseness of grains that can be transported onto the floodplain during stages of high discharge.

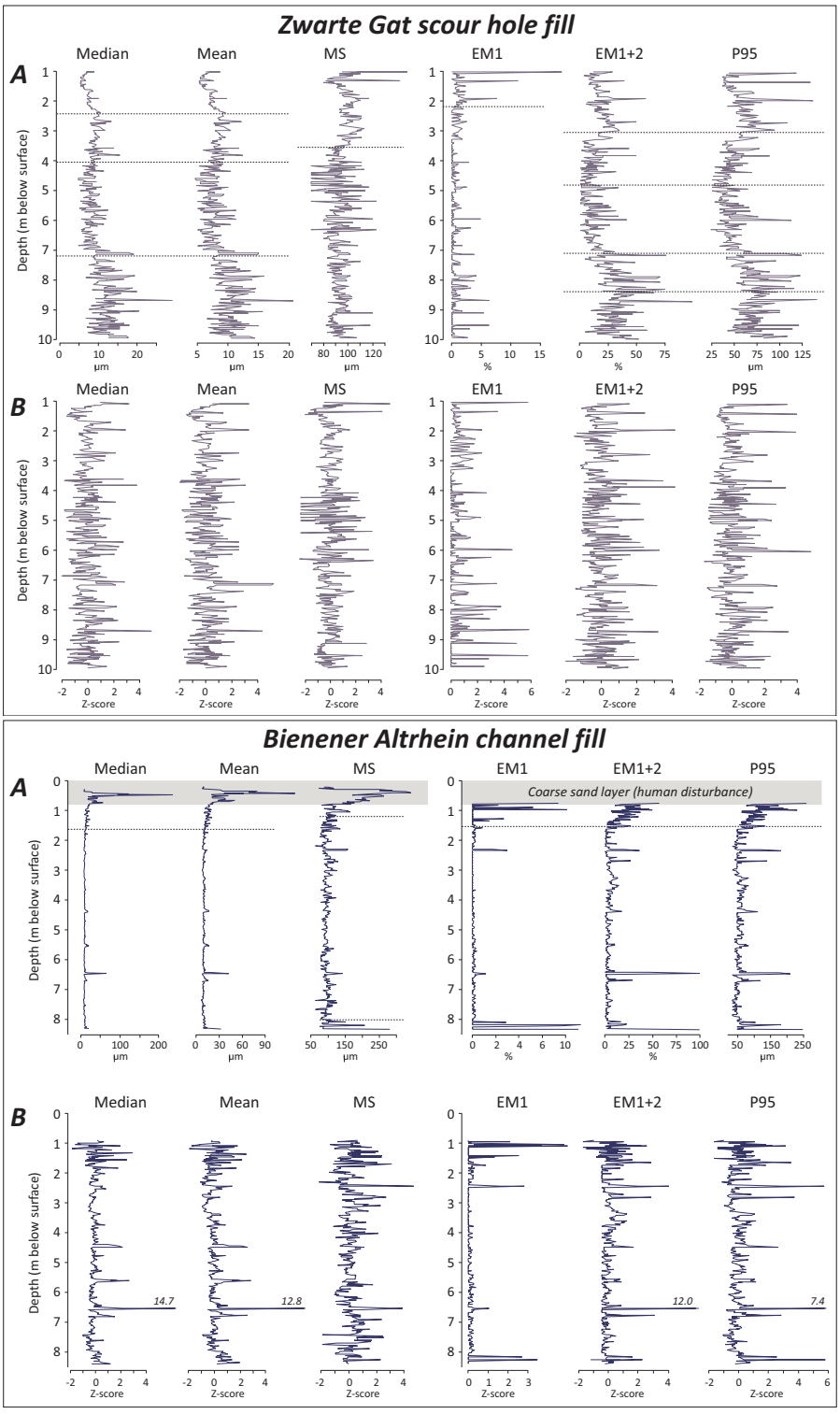

Figure 3: Raw grain-size data (A) and normalised Z-score data (B). Sections in the sedimentary sequences are illustrated by dashed lines in the raw data at the location of identified change points.

4.2 Raw grain-size data analysis

Although the various grain-size descriptors show similar trends and produce the largest peaks associated with event layers at the same depth, especially the resolution and sensitivity of recording moderately-sized peaks differs importantly (Fig. 3). The median and mean grain-size of the entire distribution resolve few coarse-grained event layers. This is mainly because of the poor sensitivity of bulk characteristics of flood layers to changes in the coarse tail of grain-size distributions, which are dominated by clays and fine silts. Especially at site BAR, differentiation in coarseness is poorly resolved using median and mean grain-size descriptors. An increase in observed detail occurs when MS, P95, or end member contributions are used to identify flood layers. These all focus on the coarse part of the entire grain-size distribution, which demonstrates that especially the transport and deposition of sandy particles is sensitive to floods of variable magnitudes. This also demonstrates that during increasing discharge, coarse grains are admixed to the suspended load, while fines are still deposited. Such simultaneous deposition of coarse sands and fines is also indicated by the distribution of EM1 and EM2 (Fig. 2); the bimodal distribution shows that coarse-grain deposition is always associated with considerable admixture of fines.

The use of solely the coarse part of the grain-size distribution to characterize flood deposits can be erroneous, as some results may be based on a very small sample volume; for example if only very few grain-measurements fall in the considered bins. This may influence accuracy and reproducibility, especially for MS and EM1. For the MS, it can be observed that results occasionally approach the lower limit of the sand fraction (63 μm). These could be valid measurements, although closer investigation of the total grain-size distribution of these samples indicates a complete absence of sands. Moreover, the error-proneness of such samples is relatively high as flocculates and organic fibres, which might occasionally have survived sample pre-treatment in small quantities, can influence outcomes heavily. For EM1, the lack of registration in most samples also complicates the use of Z-scores, which results in a different distribution and is therefore not comparable with other grain-size descriptors (i.e. the same Z-score will mean a different magnitude; Fig. 4). Addition of EM2 largely resolves this issue, although it also reduces the Z-score of several coarsest event layers. At more proximal locations in the floodplain, the use of EM1 only may be sufficient for registration for floods of all magnitudes. For research locations in intermediate positions in the floodplain and lacking an open connection with the main channel, the use of more EMs increases the completeness in registration of moderately large events.

4.3 Z-scored grain-size data

In general, Z-scored measurements show details in the record more-sensitively compared to raw data plots. This is most obvious for median and mean grain-size (Fig. 3), but also affects the coarse-tail descriptors. From counting event layers, defined as all maxima (peaks) in the dataset, with the grain-sizes expressed as a cumulative distribution of Z-scores (Fig. 4), it becomes clear that flood registration is similar for all data types, with exception of EM1. However, it has to be noted that especially large events are associated with a wide range in Z-scores among different descriptors (Fig. 3). The number of identifiable events matches floodplain inundation recurrence times of the Lower Rhine. Smallest recognized individual flood events in the ZG and BAR records respectively have an average recurrence time of 3.1 and 4.1 years (number of events divided by the time interval), at present roughly corresponding with floods exceeding 7,500 m^3s^{-1} at Lobith (Fig. 1; Chapter 2). From this it can be concluded that background sedimentation – i.e. core matrix samples not recognized as event layers – indeed mainly represents stages of flood sedimentation by minor

discharge peaks that just inundated the local floodplain, and the waning stages of larger floods (post peak discharge).

Z-score normalisation in combination with CPA-analysis has some disadvantages. In sections, where data conversion builds on limited sample data (mainly occurring in ZG; Fig. 3), results may be biased (as calculations are depending on average values and the standard deviation of individual sections). Especially in the upper parts of BAR and ZG, Z-score normalisation is not able to completely remove anomalous trends; still the frequency and scores of event layers are different from lower sections of the cores, although this theoretically may be a valid representation of changes in fluvial dynamics and the natural distribution of floods.

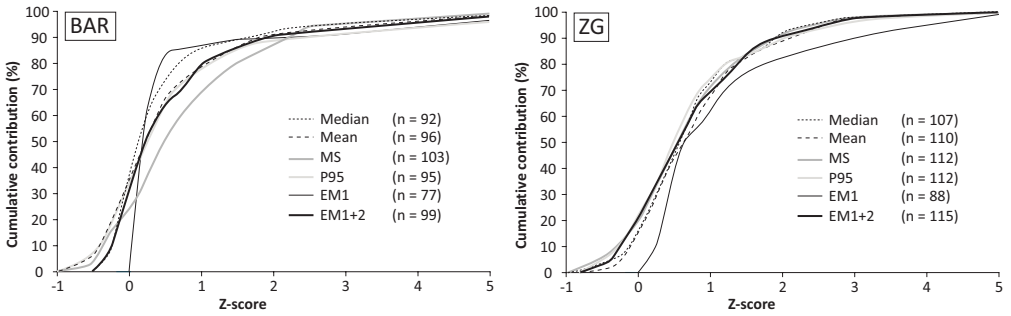

Figure 4: Cumulative distribution of flood bed Z-scores and number of identified events per grain-size predictor.

4.4 Age-Depth models

4.4.1 Bienener Altrhein

Information from various sources (Tab. 1) provided initial age-depth models for each site (Fig. 5). For the BAR oxbow many age tie-points are available in the upper meter of the sequence; recent deposits at the surface (AD 2010), palynological information, sands introduced during the construction of the sluice (AD 1920), and pollution data all suggest deposition of the upper meter in the last century. Further down, tie-points in the initial age-depth model refer to minimum ages, as palynological information and historical records of the abandonment of the channel are not sufficiently accurate for defining an age range. The BAR initial age-depth model indicates a considerably lowered accumulation rate in the upper meters. This contradicts trends observed in grain-size data (Fig. 3); the upper meters are coarser, normally suggesting higher accumulation rates.

For further age-model iteration, ages were assigned to coarse flood layers, starting with easiest targets (black dots in Fig. 5), being events located near tie-points in the initial age-depth model (e.g., AD 1784, 1809, 1861), clusters of large events (e.g., AD 1651-1658, 1709-1711, 1726-1729, 1882-1883), extreme events marked by exceptional flood deposition (e.g., AD 1658, 1784, 1809), and large floods placed in decades of limited occurrence of other candidate-major floods (e.g., AD 1784, 1882-1883). Also for moderately large floods (white dots in Fig. 5), that were mainly dated by interpolation of ages between large events, local dike breaches are historically documented in the wider region (Buisman, 2000). The event-chronology-updated age-depth model differs several decades at most from the initial model in linearly poorly age-constrained sections and coarse

flood layers line up well with historical information. Thus, historical-sedimentological flood event chronologies are useful for establishing age-depth models in such fluvio-lacustrine sequences, when traditional dating techniques cannot be deployed or provide limited accuracy.

In the iterated age-depth model, three phases of differing sedimentation rates can be distinguished (Fig. 5; these are other phases than those in Fig. 3). A lower phase (BAR-I) with moderate sedimentation rates, and recording of many moderate-scoring events, a middle phase (BAR-II) with increased sedimentation rates, and also with many moderate-scoring events – which are though poorly correlating with historical records, and the upper phase (BAR-III) in which sedimentation rates decreased, but with registration of many large events.

The gradual increase in sedimentation rates at BAR during the 17-18th century (Phase I and II), can be related to migration of the active channel. The steadily approaching active channel (inset Fig. 1; AD 1550-1819 bend migration) resulted in increasingly efficient sediment delivery and overall thicker flood deposits. Changed proximity of the research location also may explain why sedimentation rates suddenly decrease at ~1.5 m, as an artificial channel cut-off in AD 1819 displaced the active channel farther away (Fig. 1). The upper meter of decreased sedimentation rates yields however relatively coarse deposits, which are likely attributed to a more frequent occurrence of large floods in the 19th century; at the few moments when sediment was introduced during large floods, deposits are relatively coarse, while flood layer thickness is limited and background sedimentation rates by minor floods are low. Moreover, progressive plug-bar and levee formation at the entrance of the BAR oxbow, and the presence of an additional palaeochannel sediment trap in front of it, further reduced the amount of background sedimentation over time.

Table 1: Dating information used as tie-points for the initial age-depth models.

Site	Depth (m)	Age AD	Type	Source
BAR	0.00	2011	Current waterfront	Personal observation
	0.30	1900 – 1975	Channel fill	Palynology; *no hemp/maize, much rye/pine*
	0.81	1920 – 1930	Sand layer	Construction Dornicker sluice
	1.10	1860 – 1870	Channel fill	Onset heavy metal pollution (XRF-scans; unpublished)
	1.84	< 1880	Channel fill	Palynology; *much hemp and buckwheat*
	8.49	~ 1550	Channel base	Historical records (Braun & Thiermann, 1981)
ZG	1.00	> 1995	Top deposits	Personal observation
	1.21	1991	Top previous core	Middelkoop (1997)
	1.55	1965	Scour hole fill	^{210}Pb-dating (Middelkoop, 1997)
	1.59	1939-1945	Scour hole fill	Temporary dip in heavy metal pollution (Middelkoop, 1997)
	1.89	1940	Scour hole fill	^{210}Pb-dating (Middelkoop, 1997)
	2.24	1915	Scour hole fill	^{210}Pb-dating (Middelkoop, 1997)
	2.70	1860 – 1870	Scour hole fill	Onset heavy metal pollution (Middelkoop, 1997)
	7.00	< 1722	Sediment phasing	Historical maps (van Geelkercken, 1639; Couwater, 1722)
	~10.00	1644	Base scour hole	Historical records (Buisman, 2000)

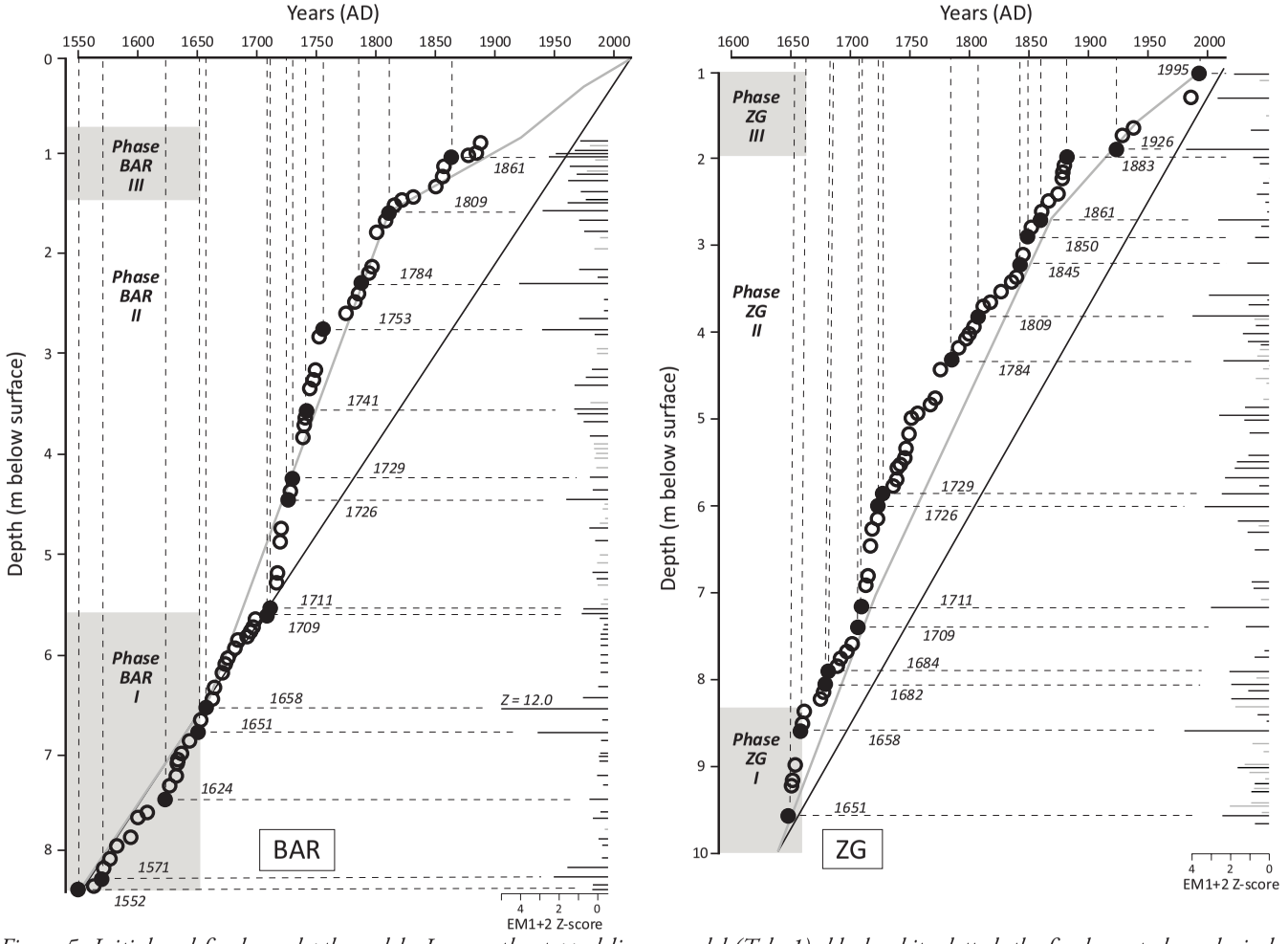

Figure 5: Initial and final age-depth models. In grey, the stepped-linear model (Tab. 1); black-white dotted, the final event-chronological age-depth model. Black dots are tie-points for the updated model (major events), white dots represent moderate events that are successfully correlated between the sedimentary and historical records. Grey background shades indicate various phases in flood registration and general sedimentation rates. Bars along the vertical axis illustrate flood magnitudes (Z-scores of EM1+2); grey bars indicate flood layers that are not correlative with historical records.

The relatively high number of event beds that could not be correlated to known floods that characterize phase BAR-II (Fig. 5) is likely due to channel migration of the active river. This induced erosion of the sandy plug-bar, which in turn introduced extra sand *and* lowered the discharge threshold for this sediment to be delivered to the floodplain. Erosion of the plug-bar, and possibly crevassing into the palaeochannel, may explain the 'extra' event beds. In the decades before the AD 1819 diversion, the channel fill temporarily also registered events that did not necessarily exceed bankfull levels, and which historical sources do also not document. To prevent over-interpretation of such flood layers in flood magnitude reconstructions, non-correlated events of minor magnitude are not used to estimate discharges (section 4.6).

Vice-versa, there are also several flooding events in 19th century annual discharge series and historical records, that are not clear event beds in the BAR sedimentary record. Without exception this concerns relatively minor events (post-1772: less than 9,000 m^3s^{-1}; pre-1772: a single mention of a dike breach). The coarseness of flood beds may not have exceeded background values, which would make them unrecognised as events. Alternatively, thin flood layers could be under-sampled by the 2-cm sampling resolution, which resulted in bulked-sampling if they are not visually distinguished. Moreover, due to a limited thickness they are more easily eroded than thick layers belonging to major events. Last, fine-grained layers may have been misinterpreted as having formed during the waning stage of larger events (fining top of graded flood layers). Three short periods exist during which many smaller floods are missing: AD 1650-1660, AD 1750-1760, and the mid-19th century (Fig. 5). Poor flood registration of smaller events in the 19th century corresponds with the more distal location of the site relative to the river, when the matured plug-bar at the entrance was overtopped during relatively large discharges only. The AD 1750-1760 period is marked in the sedimentary record by thick fine-grained deposits, suggesting that these events led to deposition but are not derived from the background signal using current methods. For the AD 1650-1660 period, the poor registration has presumably been caused by several major events in that decade, which may obscure or having eroded smaller event layers.

4.4.2 Zwarte Gat

The ZG age-depth model shows a similar discharge registration and gradual site infilling signals as site BAR, with gradually decreasing sedimentation rates to the surface (Fig. 3). Again, most dating information is available in the last century, which makes this part of the initial age-depth model best resolved. The exact year of scour hole-formation is documented (AD 1644; Buisman, 2000), which strengthens the quality of the initial age-model considerably in the historical period.

Assigned ages to coarse event layers mark the same events as in the BAR. Site ZG has filled more gradually until recent times. This allows for higher vertical resolution and more large events recognised and used for tie-points in the age-depth model in the 19th and 20th century (e.g., AD 1995/1926; Fig. 5). The further iterated age-depth model also fits nicely with the initial model, albeit age-depth relations have shifted to generally higher ages. Also, the age model in the lower part of the sequences is somewhat altered, with higher sedimentation rates in the lower part (phase ZG-I), and gradually decreasing sedimentation rates further upward (phase ZG-II). The transition between the two lower phases is dated to the late 17th century, so shortly after formation of the scour hole. Three plausible explanations for gradually lowering sedimentation rates in the ZG can be found in a geomorphological context (Fig. 1). Geomorphological reconstructions of the location of the main river, based on series of historical maps (van Geelkercken, 1639; Couwater,

1722; von Wiebeking, 1800; Beijerink, 1809; Goudriaan, 1830; Bonneblad 532, 1890), reveal a rapid southward migration of the main channel and the formation of extensive gravel bars in river on the northern bank soon after the ZG was formed. Latest by AD 1722 (Couwater, 1722), the thalweg of the active river became located near the southern main dike, which may have decreased sedimentation rates in the ZG. An alternative explanation can be sought in the connectivity of the ZG with the main river by a small ditch (Fig. 1). On some historical maps (e.g., Beijerink, 1809), an open connection exists between this ditch and the scour hole. Closure of the open connection and gradual infilling of the ditch probably influenced the transport of sediment from the active river into the scour hole, and may have caused a decrease in sedimentation rates. A third reason for decreasing sedimentation rates may be the construction of the Pannerdens Canal in AD 1707, which redirected discharge to the northern Nederrijn distributary (Fig. 1), leading to reduced discharge in the Waal channel at ZG (van de Ven, 1976).

The upper phase (ZG-III) becomes finer-grained, but this is unlikely to resemble simple proximity to the active channel, as the engineered river was forced northward, at the end of the 19th century (inset Fig. 1; formation of southern bank). Contrastingly, sedimentation rates decrease, which suggests that other mechanisms are involved. In recent times, bed degradation has accelerated in response to the fixation and narrowing of rivers by groynes, and ongoing floodplain deposition may have increased the difference in elevation between river water levels and the scour hole. Despite increased proximity, this would have raised threshold discharge at which admixed coarser-fractions start to get delivered to the floodplain. However, significant lowering of river bed levels starts in the mid-20th century only (Ten Brinke, 2005; Chapter 2). Imprints of moderately-sized floods are lacking in Phase ZG-III, while they are present in the discharge series (Chapter 2). The top interval of the fill thus contains an incomplete flood record. Where the more-clayey matrix composition is ascribed to increased elevation difference between channel and floodplain, the non-registration of moderate events is ascribed to shallowing of the progressively filling scour hole. This can explain the occurrence of coarse peaks correlating in size and position to discharge records, and relative thick fine-grained deposits, which are formed as (re)settling material during the waning stages of these large floods.

4.5 Relating normalised grain-size data to discharge series

The grain-size data for the two sites have different overlap with the observational discharge series. Site BAR allows comparison from AD 1772-1920. Site ZG allows comparison from AD 1772 to present; recent decades have been recorded fragmentally. The AD 1784 flood was excluded from establishing the BAR regression; this year is marked by a severe winter (IJnsen, 1981), and major ice-jamming in the Lower Rhine (Buisman, 2000), which locally raised water levels, caused many violent dike breaches, and probably disturbed discharge-sedimentation dynamics as the inferred Z-score for this event is much higher than any other flood in the last centuries (Fig. 6), while the reconstructed discharge was not significantly higher (Chapter 2).

The correlation between grain-size data and discharges (Tab. 2) demonstrates that median, mean, and MS (for BAR only) are fairly poor predictors of flood magnitudes. P95 and EM1+2 are however fitting much better, and show a clear linear relation between flood discharges and the coarseness of deposited material. The use of EM1 only results in a very poor correlation, which is likely caused by the limited registration of moderately-sized events. Regression results show that addition of EM2 to EM1 greatly increases the correlation, which demonstrates that using just

the few coarsest grains (EM1) for estimating flood magnitudes is error prone – instead, slightly conservative (P95 and EM1+2) approaches using a larger volume of the total grain size distribution is more robust for assessing a larger range of flood magnitudes.

Deposits collected in a transect across the inundated floodplain at ZG at the time of the AD 1993 flood (Middelkoop, 1997), provide an independent check on the established regression between sedimentary and discharge data. EM1+2 Z-scores of deposits in the distal parts of the floodplain reach values up to 0.72 (0.39 on average; sediment coarseness mainly depends on local floodplain topography). Z-scores of these surface samples correspond poorly with the trend line of scour fill samples and measured discharge (10,940 m^3s^{-1} at Lobith), as deposition of coarser material is expected during such a major flood. As no ice jamming has occurred in recent decades and because similar sized floods (e.g., AD 1861, 1926, and 1988) fit well to the established regression between EM1+2 Z-scores and discharges (most variance occurs with moderate floods), other factors must be responsible for this misfit (further discussed in section 5.1).

Table 2: Coefficients of determination for the linear regression between various grain-size descriptors and measured discharges.

Parameter	ZG R^2	BAR R^2
Median	0.49	0.50
Mean	0.51	0.61
MS	0.28	0.60
EM1	0.23	0.15
EM1+2	0.80	0.79
P95	0.75	0.72

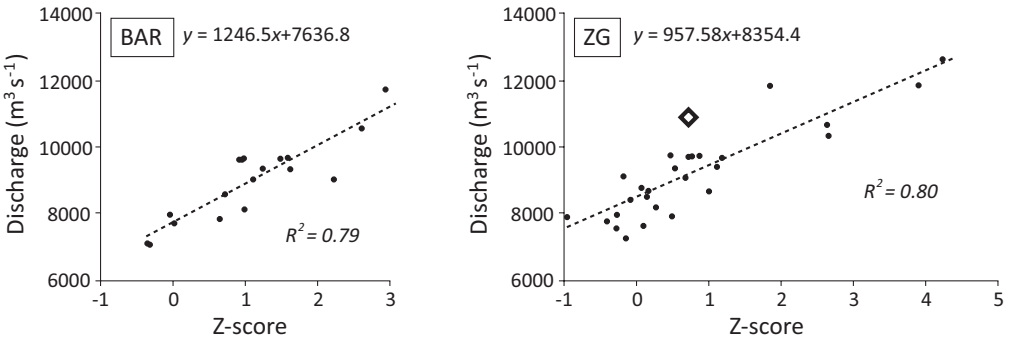

Figure 6: Regression plots of Z-scored EM1+2 data and observed discharges for the same events. The diamond in the ZG-diagram plots the coarsest floodplain deposits of the AD 1993 flood (10,940 m^3s^{-1} at Lobith; Middelkoop, 1997), sampled in the direct vicinity of the ZG scour hole.

4.6 Historical flood magnitudes

For flood beds in the lower parts of the fill (older than AD 1772), the discharge was predicted by applying the EM1+2 regression relations (Fig. 6). Only EM1+2 was used for this calculation, because other parameters yield lower coefficients of determination and have a similar distribution of Z-scores (Fig. 4). As can be expected from the good correlation (Fig. 6), using EM1+2 to predict flood magnitudes performs well in the 19th century (Fig. 7). The only poor prediction in the calibration period is found in AD 1784, when ice jamming probably influenced local flooding (Fig. 7), and resulted in transportation and deposition of relative coarse deposits. The over-prediction by both sites indicates that in this year, ice jamming had a regional extent, which is consistent with historical records (Driessen, 1994). Discharge estimates from both research locations correspond well for the 19th century, but start to deviate progressively from the late 18th century to earlier periods (Fig. 7), as ZG systematically produces higher discharge estimates. Comparison with measured discharge in this period suggests the BAR results to be the more realistic, although relative few events for verification exist. Although ZG and BAR produce discharge estimates in similar years before AD 1772, systematic higher estimates by ZG continue, which can be a propagation of a calibration misfit in the used regression (section 5.2).

Based on the BAR inventory, two periods in flooding are identified: (i) the 18th century marked by a many large floods, lacking extreme events though and with very limited flooding in AD 1750-1780, and (ii) the earlier part of the record before AD 1700 with many <8,000 m^3s^{-1} floods, several very large floods (AD 1571, 1651, 1658), and a period of limited flooding from AD 1570-1620. The periods of limited flooding correspond with slightly reduced flooding intensities, inferred from analysis of historical documentary records (Chapter 2).

Largest events, AD 1571, 1651, and 1658, are estimated to have exceeded 10,000 m^3s^{-1}. The BAR estimate for the AD 1658 flood even exceeds 22,000 m^3s^{-1} (based on an EM1+2 Z-score of 12.0). That value seems out of range of meteorological bounds and hydraulic limitations (embankment heights and valley morphology), which limit discharges at the Rhine Delta apex respectively to ~18.700 m^3s^{-1} and ~15,500 m^3s^{-1} (Lammersen, 2004). As AD 1658 is marked by a severe winter, and frequent ice jamming of rivers is reported (Buisman, 2000) it is likely that the BAR flood deposits in this year are anomalously coarse; similar to the coarse imprint of the AD 1784 ice-jam flood (Fig. 6). As a test, the EM1+2 Z-score was replaced by the smaller P95 Z-score of 7.4 (Fig. 3; P95 has a nearly identical Z-score distribution; Fig. 4). This results in a still extreme but physically more realistic discharge for the AD 1658 event of ~16.800 m^3s^{-1}. The ZG EM1+2 estimate for this flood is much lower, albeit still representing a major event, suggesting a discharge of ~12.600 m^3s^{-1}. This equals the size of the AD 1926 flood, which has been the largest discharge recorded in modern data series.

Other years may also have been influenced by ice jams, although no extreme discharges are reflected in the sedimentary records. AD 1571 is also associated with a severe winter (Fig. 7), but the regional extent of damage reports in historical record indicates that also large discharges must have been present, which renders the estimated discharge of ~10.500 m^3s^{-1} plausible. For AD 1651, when certainly no ice jamming occurred, a discharge is calculated of 11.500 m^3s^{-1}. An independent estimate for this flood from Cologne (Herget & Euler, 2010) suggests a discharge of at least ~12.000 m^3s^{-1}. Considering the uncertainties in reconstructed discharges (in both studies), our BAR conservative estimate and common downstream discharge loss by flood wave propagation, these estimates could be corresponding to a similar discharge.

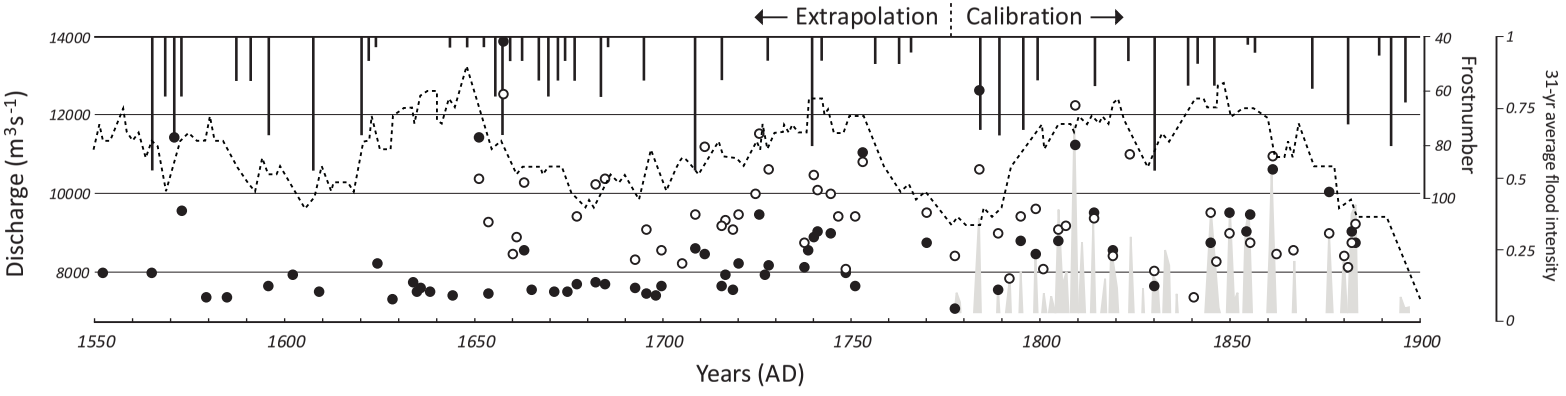

Figure 7: Discharge reconstructions based on the EM1+2-discharge regression for the period after AD 1772. Dark dots represent BAR event layers, white dots ZG event layers, grey peaks (AD 1772-1900) indicate reconstructed discharge for Lobith (Chapter 2). The dashed line indicates an indexed 31-year flooding intensity (Chapter 2), and bars at the top indicate winter severity (number of days of frost; frost number; IJnsen, 1981).

5 Discussion

The results of this study indicate that Lower Rhine (palaeo-)discharges can be quantified from sedimentary flood records, when data is collected at high resolution, a coarse-tailed grain-size descriptor is selected, and after normalisation treatments. Even then, straightforward interpretation of grain-size to flood magnitude is hindered by several factors, each causing variation in the way floods are registered at and amongst research locations. These include dynamics in local geomorphology, formation of river ice, river management, uncertainties in age-depth modelling, uncertainties in correlation between grain-size data and discharges, and the use of regressions to estimate discharges of historical floods all propagate in the final difference between discharge reconstructions from BAR and ZG (and the partly overlapping discharge record).

5.1 Geomorphological overprinting

The BAR and ZG case studies show trends in sediment composition and accumulation rates in response to local changes in floodplain geomorphology. Linear detrending and converting direct proxy data into Z-scores largely eliminates the variation induced by geomorphology, and results in a more uniform record (Fig. 3). Nevertheless, over intervals with limited numbers of samples, gradual changes in Z-scores can still be recognized – i.e. the upper meters of BAR shows many more large floods, which can be caused by natural variability of the flooding regime, but can also relate to insufficiently normalised trends. Over the past 450-yr period, it is possible to compare flood dynamics with discharge series and historical documentation, which gives insight in the most likely explanation for the origin for gradual changes in Z-scores, and can help to improve the regression plots and discharge estimates by identification of outliers that are to be attributed to other processes than peak discharge (Fig. 6).

Especially the connectivity with the main channel, which for sites ZG and BAR changed over time, can create independent phasing in deposition, but is difficult to assess from individual flood records. The two contemporaneous sites produced similar flood chronologies, but contain occasional variability which is not traceable over relative short distances along the same fluvial trunk valley. Building flood chronologies out of sedimentary records of abandoned channels and scour holes becomes more reliable when multiple sites are investigated and compared. Although this can be time consuming and costly, geomorphological overprinting of the flood record can be too difficult to assess at a single site – especially when no overlap exists with modern discharge records or historical information. Records of palaeo-environmental change, such as probability density functions of widespread geomorphological changes in fluvial settings (e.g., Hoffmann et al., 2009; Macklin et al., 2012) or avulsion intensity records (Stouthamer & Berendsen, 2001) and other proxy records indicating climatic variability may be used for comparison and may confirm the existence of periods of intensified flooding as indicated by sedimentary records in prehistoric times, such possibly eliminating local factors. In this respect, ice jamming has probably been a more a temporary problem only, as embankment of the Lower Rhine floodplains has worsened their effect on catastrophic flooding – ice can pile-up against high dikes and can raise water levels significantly – and they occurred mainly during anomalous cold periods, such as the Little Ice Age (Tol & Langen, 2000). Both the period of embankment and the Little Ice Age are sufficiently covered by historical records to assess overprinting of the sedimentary record by ice jamming; although insufficient information may be available to correct overestimated discharges, historical records on

severe winters and ice jamming may certainly provide caution for calculated discharges in specific years.

A last, so far unmentioned, hydro-geomorphological factor in sedimentary flood registration (part of the ~20% unexplained regression variance; Fig. 6) is induced by the shape of the flood wave. The rate of floodplain inundation and the timing of maximum discharge during a discharge wave determine dynamics, which are of importance for the transported material; e.g., flow velocities and hysteresis-effects (Asselman & Middelkoop, 1998; Berner et al., 2012). In-channel measurements of sediment fluxes and mobile grain-sizes (Frings & Kleinhans, 2008), and analysis of deposited material after the AD 1993 flood (Middelkoop, 1997) indicate a relatively wide range of transported material during a single flood, and among various floods of similar magnitudes. Most variability in deposited material is present in moderate-size floods (Fig. 6), which suggests that the coarseness of transported material during these events is influenced more severely by the shape of the discharge wave than for floods of higher magnitudes. Also, spatial variability in grain-sizes and the volume of deposition is likely more influenced by local topography during minor floods with lower inundation levels (Asselman & Middelkoop, 1998).

5.2 Calibration and extrapolation

Both research locations yield good correlations (R^2=~0.8) between coarse-tail grain-size descriptors and measured discharges, which demonstrates the potential of particular types of sedimentary records for reconstructing palaeoflood magnitudes. Although current regressions solve palaeoflood magnitudes well, reconstructions from individual sites are prone to a relative large uncertainty (Fig. 7). For the extrapolation period before AD 1772, discharge estimates from ZG are consistently higher than BAR-estimates. This persisting offset cannot be explained by natural variability – one would expect uncertainty to be distributed more randomly. Presumably the difference in reconstructed palaeoflood discharges originates from the calibration data, which has for both sites a limited length. The calibration period in BAR yields relatively high Z-scores and variability (Fig. 3) compared to lower/earlier sections, which can lead to underestimation of discharges and a limited ability to distinguish variability of moderately-sized floods. The opposite occurs at ZG, where the calibration period is marked by limited variability and registration of moderate flood. From this, it can be assumed that BAR-estimates can be regarded as minimum discharges and ZG-estimates as maximum discharges.

Recurrence times associated with reconstructed floods are compared with results of flood frequency analysis (discharge data only; Chapter 2). This provides a crude, but independent check of the quality of generated discharge data. Based on counting peaks that pass certain discharge thresholds, recurrence times for floods of different magnitudes correspond for both sites with recurrence times established from measured discharge data; the range in recurrence times in flood frequency estimates comes from the use of datasets with alternative lengths (Tab. 3; Chapter 2). From this comparison it is concluded that discharge series from both locations are in line with estimated recurrence times from the last ~240 years. Results from site ZG approach the upper limit (shortest recurrence times) calculated in flood frequency analysis, while at site BAR large events yield slightly longer recurrence times and are placed in the mid-range of flood frequency estimates. BAR recurrence times for moderately large floods (10,000 m^3s^{-1}) almost double estimates from ZG and flood frequency analysis. Besides being interpreted as a conservative estimate, the recurrence times derived from the BAR series may also represent truly decreased flooding from AD

1550-1650, as non-stationarity of the flooding regime may cause fluctuations in recurrence times associated with discharge. It is however questionable if the effect of non-stationarity can cause a such an impact (doubling the recurrence time of moderate floods) in this specific period, especially because historical records do not indicate anomalously low flood intensities in that period (Fig. 7) and recurrence times of larger events are in line with estimates from more recent times.

Table 3: Peak-over-threshold estimates of the recurrence time associated with flood magnitudes. Counts after AD 1900 come from discharge series; the number of added modern counts, incorporated in the total, is bracketed. Results are compared with flood frequency analysis on discharge series (Chapter 2).

Threshold ***(m^3s^{-1})***	***Count BAR*** ***(AD 1552-2012)***	***Recurrence***	***Count ZG*** ***(AD 1644-2012)***	***Recurrence***	***FFA*** ***(Chapter 2)***
10,000	12 (4)	38 yrs	19 (4)	19 yrs	~20 yrs
11,000	9 (3)	51 yrs	9 (3)	41 yrs	40-70 yrs
12,000	3 (1)	153 yrs	3 (1)	123 yrs	90-300 yrs

5.3 Application to flood research

The suitability of floodplain lake sedimentary records for the construction of continuous flood records (timing *and* magnitude of peak discharges) and as recorder of local geomorphological dynamics is demonstrated by the results. These records, combined with accurate age-depth models based on existing flood event chronologies, historical information, or other contemporaneous research sites, allow detailed reconstruction of past fluvial environments. Data availability for studying fluvial dynamics and changes in the flooding regime can increase considerably as the approach presented in this paper is possible for the entire Holocene period in the Lower Rhine region. Millennial flood records can give important insight in past responses of fluvial systems and flooding regimes to climatic and anthropogenic changes. Knowledge of such relations is not only important for assessing current safety levels with flood frequency analysis, but also for assessment of the impact of future climate change. Moreover, excellent natural flood records probably exist in many other low-land regions, also for poorly monitored fluvial systems, which can increase data availability spatially (to a global scale) and allows regional comparison of changing flood dynamics in response to climate and human impact.

6 Conclusions

This study demonstrates that sedimentary records of abandoned channel fills and dike breach scour holes are suitable as flood records. Although changes in the local geomorphology are reflected in general sedimentary rates and the coarseness of flood deposits, standardization and detrending techniques, and comparison with historical records are effective in identifying and filtering overprints caused by migration of the main river channel and unlocking the fills for flood magnitude reconstruction. Overprinting of the main flood record by changes in connectivity, by local ditches in the floodplains or tie-channel dissecting plug-bars, are more difficult to assess. Because periods of increased connectivity are marked by frequent layering, historical records or additional sites are needed to verify the nature of such intervals.

When inferring flood magnitudes from grain-size characteristics, using the 95th percentile and/or the coarsest two (out of five) end members is most accurate (Tab. 2). Bulk measurements, such as

median and mean grain-size, can be used to detect sedimentary trends and are limitedly usable as indicator for flood layers, but are not very suitable to provide quantitative estimates of discharges. Although Z-scoring measurements allows to distinguish more flood signals (Fig. 3), focusing on the coarsest tail of grain-size distributions yields much better information – specifically for floods of higher magnitudes.

Age-depth modelling at the studied locations in the last centuries is challenging, as most traditional dating technique do not yield highly precise results (on clayey deposits, largely lacking datable organics) or do not reach beyond the last century (^{210}Pb-dating). It is demonstrated that flood event-chronologies from historical records can be used to improve age-depth relations (Fig. 5). For the Rhine, the timing, cause, and magnitudes of historical floods are well recorded. As the largest events in the sedimentary records are corresponding well with the historical records, it is possible to assign ages to specific flood layers. These event-based chronologies constrain the range in age-depth models, which in turn makes it possible to assign ages to floods of lesser magnitudes – a progressive approach that allows matching most historical floods to flood deposits with sufficient confidence.

For both research locations it was possible to correlate flood deposits to contemporaneous discharge measurements from the same region. Application of the regression between grains-size and discharge resulted in discharge estimates for historical floods. Year of flooding and relative magnitudes corresponds well among sites and to historical records. However, reconstructed discharges from the ZG-scour hole are systematically higher than estimates for the BAR abandoned channel. Presumably, this difference originates from local geomorphological imprints affecting data in the calibration periods; relative fine-grained deposits of the ZG cause flood magnitude overestimation of generally coarser flood layers in deeper parts of the sequence. The opposite applies for BAR (coarse at the top, finer at larger depths), which suggests that at these sites detrending and normalisation techniques cannot fully remove local trends in the sedimentary record. The results are though promising, and in correspondence with historical damage reports the ZG-estimates are interpreted as an upper-end estimate and the BAR-results as a conservative estimate of historical discharges.

Acknowledgements
The authors thank J. Aloserij, J. Ypma, J. Peeters, H. van Aken (Utrecht University), and F. Smit (now at Aarhus University), for assistance in the field. T. Bäumen (Kreis Kleve) and W. Cornelisse (Waterschap Rivierenland) are acknowledged for giving clearance to respectively the BAR and ZG sites. F. Bunnik carried out palynological analyses (TNO), S. Foulds, S. Rassner, and M. Macklin (Aberystwyth University) are thanked for providing XRF core scans data. M. Hagen, M. Konert, R. van Elsas, W. Wentink, and J. van 't Hoff (Vrije Universiteit Amsterdam) are thanked for assistance in the sedimentary laboratory. This research was funded by Deltares BGS, TNO, and Utrecht University.

6 Middle-Holocene palaeoflood extremes of the Lower Rhine

Toonen, W.H.J. * [1,2], de Molenaar, M.M.[1], Bunnik, F.P.M.[3], Middelkoop, H.[1]

[1] Dept. of Physical Geography, Utrecht University, Utrecht, The Netherlands.
[2] Dept. of Applied Geology and Geophysics, Deltares BGS, Utrecht, The Netherlands.
[3] TNO, Geological Survey of the Netherlands, Utrecht, The Netherlands.
* Corresponding author: E-mail: w.h.j.toonen@gmail.com

Published in: Hydrology Research 44:2, p 248-263. DOI: 10.2166/nh.2012.162

1 Introduction

Flood safety assessment for the Lower Rhine in the Netherlands and Germany demands insight into the recurrence interval and magnitude of extreme events. Flood safety legislation in the Netherlands is based on the discharge of the 1/1,250-yr flood. The actual size of this statistical magnitude needs to be specified, as it is used in the design and maintenance of dikes in the Rhine Delta (The Netherlands). Current practice is to calculate the design flood (Q_{1250}) by statistical extrapolation from an observational flood series that covers the 20th century, which is too short for an accurate estimation of extreme events. The inclusion of the relatively large 1993 and 1995 floods in this series in a recalculation more than a decade ago raised the projected size of Q_{1250} from ~15,000 to ~16,000 m^3s^{-1} (Chbab, 1996). This demanded extra financial investment and altered land use planning for embanked floodplains to maintain the present-day safety standards. Furthermore, in the anticipated future climate the Q_{1250} is expected to rise by 10 – 15% (Kwadijk & Middelkoop, 1994; Shabalova et al., 2003), which increases the need to reduce uncertainty in the prediction of Q_{1250}. The 95% confidence interval for the current estimate of Q_{1250} stretches from 13,220 to 18,630 m^3s^{-1} (Chbab et al., 2006). To narrow this interval and to quantify Q_{1250} as precisely as possible, methods other than statistical extrapolation of gauged observations of the last ~110 years should be investigated.

It is likely that Q_{1250} exceeds the largest flood of the Rhine observed in the last century (Lobith, Fig. 1; ~12,600 m^3s^{-1} in AD 1926). Herget & Euler (2010) clearly illustrate that since AD 1300 at least five Rhine floods were larger than the 1993 and 1995 floods at Cologne (Germany), of which two (AD 1374 and 1651) probably had discharges comparable with or higher than the current design flood. Constraining the magnitudes of extreme palaeofloods (here defined as floods with a recurrence time larger than 1,000 years) may significantly improve the outcomes of flood frequency analysis. Their magnitude can be estimated using a combination of geological evidence and palaeohydrological calculations (Benito et al., 2004; Herget et al., 2013). In this paper, we assess palaeoflood magnitudes associated with sedimentary palaeostage indicators of Middle Holocene age in the Lower Rhine Valley, downstream of the last main tributary, with the goal of constraining the lower limits of the Q_{1250} flood.

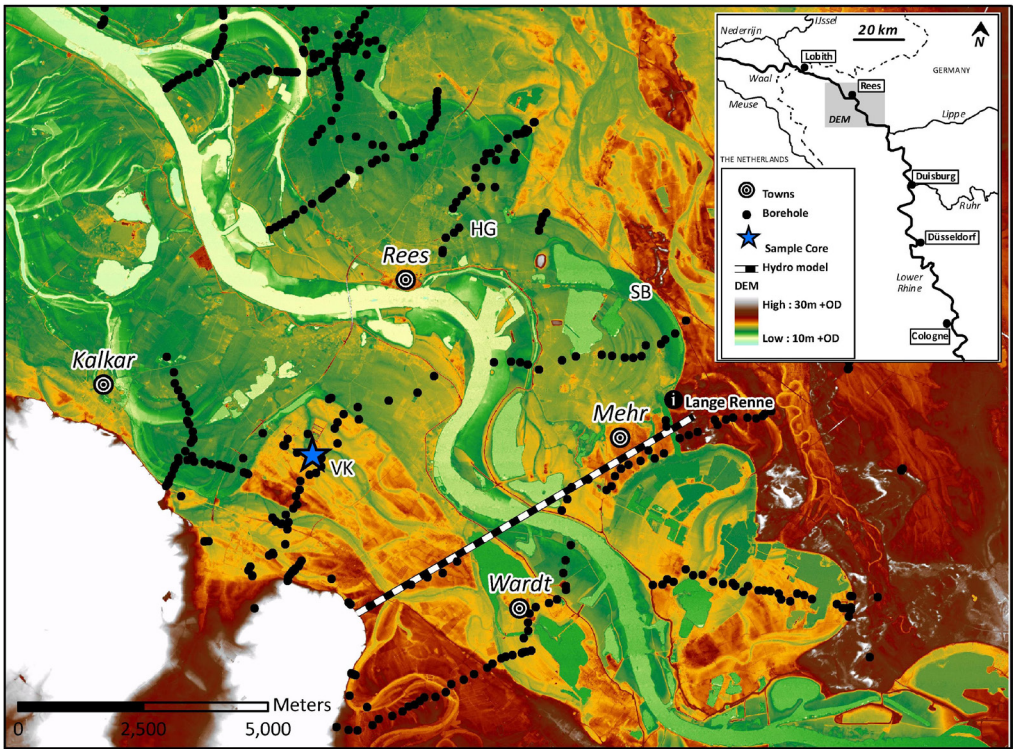

Figure 1: DEM of the Lower Rhine research area with location of the model transect, boreholes, the Vossekuhl (VK) sample core, and the Middle Holocene palaeochannels 'Schloss Bellinghoven' (SB) and 'Haus Groin' (HG).

Palaeohydrological estimates of extreme discharges (e.g., Baker, 1987; Baker et al., 2002) have larger uncertainties in reconstructed magnitude and recurrence interval than gauged records of more moderate flows. Nevertheless, results are often suitable to 'bracket what is physically possible' (Redmond et al., 2002). They can be used to create flood envelopes between lower estimates of palaeoflood discharges and upper non-exceedance limits (Levish, 2002; O'Connell et al., 2002). This constrains statistical flood frequency-magnitude extrapolations between limits in the reach that lie beyond the recurrence times of moderately sized gauged floods.

In this study, a palaeohydrological lower limit for Q_{1250} is reported, based on highest Middle Holocene palaeoflood markers. Observations were derived from a time when the Lower Rhine Valley and its hinterland were still largely naturally forested, but with a similar fluvial style as in the human-influenced Late Holocene. In the Middle Holocene, the Lower Rhine reached its maximum incision before Late Holocene aggradation initiated (Erkens et al., 2011), so only extreme floods with a large amplitude could leave deposits on the elevated terraces flanking the valley. These rare depositional events are more easily traced and have been better preserved in the local depressions on the elevated terraces (such as organically infilled palaeochannels, abandoned in the Early Holocene) than Late Holocene deposits of individual floods, which are difficult to distinguish among common overbank deposits of that period. Moreover, Late Holocene deposits on elevated terraces are near or

at the surface, making them highly vulnerable to post-depositional disturbance by bioturbation and ploughing.

For a selected transect across the Lower Rhine Valley (Germany; Fig. 1), a Chézy-based hydraulic cross-section model was set up using carefully selected geological data: Middle Holocene channel dimensions, surrounding floodplain landscape, surface roughness (channel bed and vegetation) and palaeostage indicators (water level proxies). In multiple scenarios, set-up parameters were varied within realistic limits to explore the range of discharges and as a means of sensitivity analysis. First, the hydraulic model is described, with an explanation of the input data and their value range used in different model scenarios. Second, the range in discharge outcomes is discussed, with the focus on the origin of uncertainties and the contribution of different input variables. Last, the utilisation of these data is discussed: i.e., how should one use these model results in modern flood frequency analysis?

2 Palaeoflood reconstruction methodology

Hydraulic radius (wetted cross-section), slope and surface roughness are the main inputs for the calculation of the palaeoflood discharge in a valley-wide transect. These all depend on the characteristics of the palaeolandscape. The palaeotopography was reconstructed starting with a Digital Elevation Model (DEM; LiDAR-based 10 × 10 m grid, sub-decimetre vertical resolution, filtered vegetation and urban areas; Landvermessungsamt Nordrhein-Westfalen, Germany; as used in Cohen et al., (2009)). Elevation of the present surface was sampled every 10 metres along the 13.3-km long transect (Fig. 1). An extensive handcoring programme (34 in the transect, 232 in region) provided geological information to correct modern surface elevation to the palaeosurface for the Middle Holocene situation. Later deposits were removed based on extensive lithological mapping, cross-cutting relationships of deposits and the existing chronology of deposits, which has been established in previous studies with radiocarbon, OSL and archaeological dating (Klostermann, 1992; Erkens et al., 2011). Coring and mapping methods for the floodplain deposits and palaeochannel geometries are described in Erkens et al., (2011) and Toonen et al., (2012; Chapter 3), respectively.

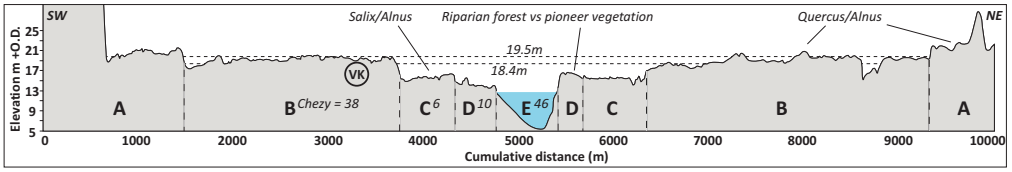

Figure 2: Modelled valley cross-section with classification per floodplain compartment with general vegetation composition, the projected location of the Vossekuhl (VK) sample core, upper and lower estimated water levels, and zone-averaged Chézy roughness values for the best guess estimate (BGE). Parameter values for bed slope and vegetation are shown in Table 2.

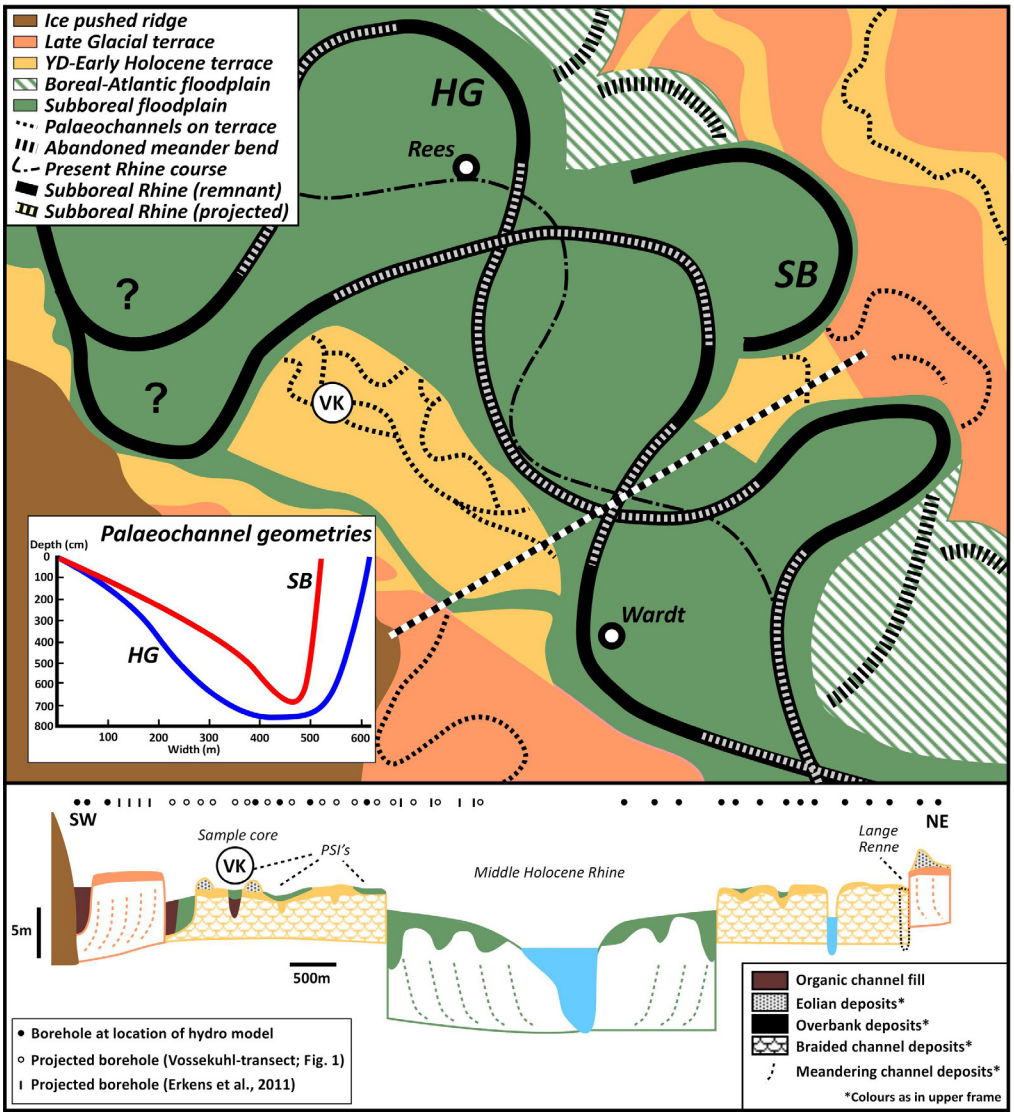

Figure 3: Reconstruction of the Middle Holocene Lower Rhine Valley with Subboreal Rhine courses and older morphology (after Klostermann, 1992; Erkens et al., 2011; Geurts, 2011; Van Munster, 2011). YD = Younger Dryas. The inset shows palaeochannel dimensions of the Schloss Bellinghoven (SB) and Haus Groin (HG) palaeochannels, which have been used as variables in model scenario 4. A schematised geological cross-section is shown in the lower frame (modified after Erkens et al., 2011; Geurts 2011). VK = projected Vossekuhl sample core location.

To minimise uncertainty in palaeohydrological calculations, a section along the Lower Rhine was chosen where the position of the main channel has changed relatively little since the Middle Holocene (Fig. 1-3). A relatively large part of this section is characterised by higher terrace levels, which have rarely experienced Middle Holocene flooding (Klostermann, 1992). This choice

minimises uncertainty in several calculation inputs; it secures the availability of sites that record palaeostage indicators (PSIs) for the highest floods only and it reduces the number of options for palaeochannel bedmorphology (discussed below). The multiple terrace steps in the terrain combined with the presence of PSIs in residual channels provide excellent constraints on the water levels during floods (Fig. 1 – 3). The residual channels on the high levels provide (1) registration of the minimum water level during extreme flooding events (occasional clay intercalations in dominantly organic channel fills), (2) constraints on the timing and recurrence interval of such an event (encased in easily datable, non-reworked material) and (3) indicative means to reconstruct past floodplain vegetation out of the preserved fossil pollen assemblages. Palynological analyses indicate a widely forested floodplain at the beginning of the Subboreal period, which is in agreement with existing archaeological insights in timing and propagation of agricultural revolutions (i.e., Neolithic to Bronze Age transition; e.g., Lechner, 2009) and palaeogeographical insights in the impact thereof on the Lower Rhine (e.g., Erkens et al., 2011). The recurrence intervals of the PSI-producing floods are inferred from acceleration mass spectrometry (AMS) dating and palynological analysis of the channel-fill deposits.

2.1 Discharge calculations

Palaeoflood discharges were calculated with Chézy-based formulas, following a slope – area approach on a single transect (cf. Dalrymple & Benson, 1968). The transect was divided into five floodplain compartments (Fig. 2), because conditions may vary significantly over a submerged floodplain during floods. Input values for hydraulic radius, slope and roughness were gathered from the field and literature to estimate values for five floodplain compartments separately. Compartments were based on terrace topography, elevation above the reconstructed Middle Holocene floodplain and associated vegetation type.

The standard Chézy-formula (Equation (1)) was used to calculate mean flow velocities that occurred during the flood stage reconstructed from the PSIs. Open channel roughness values (Zone E; Fig. 2) were calculated using Equation (2) (Keulegan, 1938; Van Rijn, 1984). Equation (3) was used for densely vegetated floodplain compartments where surface roughness is determined by (partially) submerged vegetation, and where the effect of bed friction can be neglected (Baptist et al., 2007). In the case of partially submerged vegetation, only the first part of Equation (3) is used, and vegetation height (k) is replaced by water depth (h). This formulation for the Chézy-roughness over flooded vegetated floodplain compartments is derived from parameterised semi-natural vegetation plots (Keijzer et al., 2005; Baptist et al., 2007) (and is the main reason for applying Chézy instead of other methods to estimate roughness). In Equation (3), $m*D*k$ can be substituted with Ar (representative stem surface; $m^2m^{-2}m^{-1}$), to calculate roughness in forested areas. Cross-sectional area and flow velocity were calculated per 10-m interval in the cross-section and their products are summed to obtain the total discharge.

$$\overline{u} = C\sqrt{Ri} \qquad (\textit{Equation 1})$$

$$C = 18\log\frac{12h}{k_s} \qquad (\textit{Equation 2})$$

$$C = \sqrt{\frac{2g}{C_D m D k}} + 2\sqrt{g}\ln\left(\frac{h}{k}\right) \qquad (\textit{Equation 3})$$

where u= depth-averaged velocity (m s^{-1}), C = Chézy coefficient ($m^{1/2}s^{-1}$), R = hydraulic radius (m), i = water level slope, k_s = sand roughness of Nikuradse (m; Keulegan, 1938), g = gravitational acceleration (9.81 m s^{-2}), C_D = bulk drag coefficient, m = number of vegetation stems per m^2 horizontal surface area, D = vegetation stem diameter (m), h = water depth (m), k = vegetation height (m).

2.2 Model parameters and scenarios

For ten input parameters we selected a range based on literature, local geological data and personal observations (Tab. 1). This results in a spread of outcomes in palaeodischarge calculated for these parameters. In 18 different model runs, the range (minimum and maximum estimate) and best guess estimate (BGE) of each parameter were used to evaluate the discharge response to individually changing parameters. These minimum and maximum values for the input parameters were aimed at: (1) estimating a realistic minimum flood discharge; and (2) assessing the uncertainty in discharge outcomes that results from the range in geologically derived input parameters. Our BGE aims to provide a specific lower limit for flood magnitudes as can be used in flood frequency analysis.

2.2.1 Water depth

The water depth is here defined as the difference between palaeotopographical level in each subsection and the water level during floods reconstructed from PSIs. To reconstruct the palaeotopography, elevation artefacts were removed first. Artificially raised areas such as dikes, elevated roads and urbanised areas were removed. Gravel pits were restored to the surrounding levels of the undisturbed floodplain. These changes were fixed in the model and do not vary between scenarios. Correction of modern elevations for natural changes due to channel migration and overbank sedimentation is less straightforward, and was therefore varied between scenarios. This also goes for removing or reconstructing artificial channels in the floodplain, in particular the 'Lange Renne' (Fig. 1). As no documentation exists regarding the origin of this channel – it may be an entirely dug channel or a modified residual channel – the transect may either be corrected to surrounding terrace topography or be replaced by a previously existing palaeochannel. Because a palaeochannel may carry an important amount of discharge during highwater events, scenario 1 was used (Tab. 1) to evaluate differences in discharge outcomes during standard terrace topography (no channel), and by introducing a copy of the nearby palaeochannel on the same terrace level (Fig. 1).

In the following step, Late Holocene clay cover was stripped from lower parts of elevated terrace levels (Younger Dryas – Early Holocene; Fig. 3), palaeochannel fills and the Middle Holocene floodplain. On pre-Holocene terrace levels, the topsoil consists of fine overbank deposits of Early Holocene age (Erkens et al., 2011), which have not been removed as they were already deposited prior to the investigated period. However, palaeochannel fills (which are depressions in the same terrace levels) hold Rhine deposits of Late Holocene age. This indicates that in our modelled cross-section, renewed floodplain aggradation may also have occurred outside the palaeochannels on top of Early Holocene terraces since the Iron Age (Fig. 4). Due to extensive ploughing, the contribution of younger aggradation is difficult to distinguish from earlier deposits, as palaeosols have been destroyed and the coarser Late Holocene overbanks have become admixed with the typically denser and finer Early Holocene deposits (Erkens et al., 2011). The thickness of the Late Holocene overbanks is estimated to be 0.3 m at maximum, as this is the depth of plough horizon (scenario 2; Tab. 1). Late Holocene aggradation on the lower floodplain (scenario 3) was stripped using data

from boreholes (this research and Erkens et al., 2011); the thickness varies between 1.0 and 1.8 m (generally around 1.3 m).

The shape of the present day Rhine channel is different from the Middle Holocene channel. The Rhine channel has shown natural morphological responses to changes in discharge and sediment load owing to deforestation of the floodplain and hinterland (Lang et al., 2003; Hoffmann et al., 2007; Erkens et al., 2011), and human modifications of the channel for navigation purposes and flood mitigation (Lammersen et al., 2002). In the transect, the modern Rhine channel is replaced by channel bed morphologies reconstructed from palaeochannel deposits (following Toonen et al., 2012; Chapter 3) a few kilometres downstream of our section (Fig. 3). These palaeochannels are of varying size and geometry, but typically wider, shallower and more sinuous than the present Rhine. The wider 'Haus Groin' (HG) palaeochannel serves as our BGE for the palaeochannel shape. It is considered most representative for a channel traversing the 'bottleneck' between older terraces where our transect is located (Fig. 3). The narrower and more sinuous 'Schloss Bellinghoven' (SB) channel would be an alternative (that results in a lower discharge estimate; scenario 4), but the palaeogeographical situation limits the fit of such a sinuous channel with a very wide point bar through the modelled cross-section (Fig. 1 and 3).

Table 1: Overview of model input parameters with associated scenario, parameter range and data sources.

Model parameter	Factor	Scenario description	Range MIN	BGE	MAX	Source
Hydraulic radius	Palaeotopography	1. Removal of Lange Renne bypass channel.	Complete	Complete	Replacement	Borehole data; DEM; Erkens *et al.* (2011)
		2. Stripping of overbank deposition on Early Holocene terraces.	None	None	0.3 m	
		3. Stripping of Late Holocene sedimentation of Middle Holocene floodplain (Zones C+D; Figure 2).	1 m	1.3 m	1.8 m	
		4. Palaeochannel dimensions SB/HG (Figure 3).	SB	HG	HG	
	Palaeostage indicator	5. PSI in palaeochannel fill, Early Holocene terraces, and non-exceedence boundaries (Figure 1).	18.4 m +OD	18.4 m +OD	19.5 m +OD	
Slopes	Bed slope	6. Local and regional slopes of floodplain levels.	Table 2; data displayed per floodplain compartment.			Erkens *et al.* (2011); Van Munster (2011)
		7. Sinuosity of palaeochannels.	$\Phi = 1.5$	$\Phi = 1.3$	$\Phi = 1.2$	Palaeo-reconstruction (Figure 3)
Roughness	Bed	8. Grain size in thalweg deposits of palaeochannel fill, estimated dune heights and channel bed roughness during floods.	$ks = 0.5$	$ks = 0.3$	$ks = 0.15$	Borehole data; Hesselink & Kleinhans (2002); Wilbers & ten Brinke (2003); Frings & Kleinhans (2008)
	Vegetation	9. Vegetation composition ratios (climax vs pioneer; on lower floodplain compartment only; Table 2).	$C = 5:1$	$C = 4:1$	$C = 2:1$	Wolf *et al.* (2001); Van Velzen *et al.* (2002a, 2002b); Field observations; palynological analyses
		10. Density and maturity of vegetation type.	Table 2; data displayed per floodplain compartment.			

Table 2: Scenario parameters for slope and specific vegetation for the different floodplain compartments (shown in Fig. 2).

		Slope (*10^{-5} = cm/km)			Vegetation (C_D*Ar) or ($C_D^*$$m$*$D$*$k$)		
Compartment (Figure 2)	**Description**	**MIN**	**BGE**	**MAX**	**MIN**	**BGE**	**MAX**
A	LG terrace	21	22.5	27	1.5*0.13	1.5*0.05	1.5*0.023
B	YD-EH terrace	21	22.5	27	1.5*0.13	1.5*0.05	1.5*0.023
C	MH floodplain	17	18	22.5	1.5*0.13	1.5*0.05	1.5*0.023
D	Levee zone; mixed vegetation	17	18	22.5	1.5*0.13 1.8*140*0.003*0.2	1.5*0.05 1.8*100*0.003*0.2	1.5*0.023 1.8*50*0.003*0.2
E	Channel	17	18	22.5	–	–	–

LG = Late Glacial; YD = Younger Dryas; EH, MH = Early, Middle Holocene.

Constraints on the water level during palaeofloods were obtained from PSIs in channel fills and on different terrace levels (Fig. 1 – 3). Collected PSIs (both clay deposition and non-exceedance boundaries) from the highest flooded terrace levels in the transect and immediately downstream of it, were corrected for the regional valley slope to create lower and upper limits of possible water levels. Deposition of clays on the lower parts of the Early Holocene terrace levels and in palaeochannel fills indicates a minimum flood water level of 18.4 m +OD (Amsterdam Ordnance Datum (NAP) = approximately mean sea level; Fig. 2). Non-exceedance boundaries on higher elevated terraces and in more elevated palaeochannel fills constrain the maximum water level above these deposits to 19.5 m +OD (scenario 5). Because the main aim was to obtain a minimum for the peak discharge value, the lower PSI level of 18.4 m +OD was adopted as the BGE.

2.2.2 Slope

Channel and floodplain surface slopes of the various compartments were derived from locally collected geological borehole data and geomorphological analysis (Van Munster, 2011). These were compared with more regional estimates by Erkens et al., (2011). In scenario 6, a range for the slope of each compartment was set up from these two information sources (Tab. 1). Differences in slope mainly originate from the distance over the research area that was used to calculate individual slopes. The slope of the channel compartment (Zone E; Fig. 2) was corrected for thalweg sinuosity of palaeochannels. Based on the palaeogeographic reconstruction of the fluvial history of this region (Fig. 3), the BGE for the sinuosity was 1.3 (present is ~1.2) with a maximum of 1.5 (scenario 7; Tab. 1). These estimates relate to the choice and likeliness of HG or SB for channel shape.

Examples from other palaeohydrological studies (the majority of which are from confined valleys using slackwater PSIs, or from tributaries rather than our floodplain PSIs) highlight that water slope deviations due to non-uniform flow contribute significantly to the uncertainty in discharge calculations (e.g., Webb & Jarrett, 2002). A strongly schematic DEM of the Middle Holocene Lower Rhine Valley was used to assess the effect of water slope variations during non-uniform flow conditions. Non-uniform flow is mainly caused by the downstream variations in valley/floodplain width, and fluvial style. Test runs with the SOBEK 2D hydraulic model (Delft Hydraulics and Dutch Ministry of Transport, Public Works and Water Management, 1997) revealed local water level differences due to water slope effects to be 2 dm at maximum in our research area. Given the location of our PSIs on terraces flanking the channel, these water level deviations are minor compared to other effects influencing the calculated discharges. In our relatively wide and low

gradient lower valley setting (with a rather uniform valley shape), 50 km upstream of the Middle Holocene delta apex, and ~180 km upstream of the coastline, the passage of extreme flood waves seems to be less affected by spatial effects and non-uniform flow effects than in the steep, confined settings of other studies. Further non-uniform flow effects were not evaluated in our modelled scenarios.

2.2.3 Roughness

Two types of surface roughness were distinguished: in channel bed roughness and vegetation roughness in floodplain areas. Bed roughness in channels can be predicted based on grain size ($k_s = 3*D_{90}$), dune heights ($k_s = 0.5*h_{dune}$), or can be calibrated from velocity profile measurements of an observed discharge wave (Van Rijn, 1984). In scenario 8, a range is set up for k_s (Tab. 1). To estimate k_s, data were used from bed form roughness studies in the Lower Rhine at the Dutch – German border (Kleinhans et al., 2011), located ~30 km downstream of our modelled cross-section. There, bed material and substrate geology are very similar to these at our transect location. The minimum discharge scenario uses a relatively high value for k_s that is based on dune heights (h_{dune}) in the thalweg of the Rhine at maximum discharges in 1995 and 1998 (Wilbers & ten Brinke, 2003; Frings & Kleinhans, 2008). The maximum discharge scenario uses a relatively low value based on an estimated D_{90} for Rhine thalweg sediment (Frings & Kleinhans, 2008). The BGE is an intermediate value that is consistent with values based on velocity profiles of the 1995 flood and historical floods (Hesselink & Kleinhans, 2002). The values are applied over the full width of the open channel segment, which locally causes an overestimate of k_s at the channel fringes. However, k_s values have been estimated from moderate floods; extreme floods likely form larger dunes with higher k_s values in the middle of the channel, thereby compensating for the underestimate at the channel fringes.

For each floodplain compartment (Zones A – D; Fig. 2), vegetation roughness was taken as a single value. The vegetation generally consisted of riparian forest, which was dominated on the lower parts of the floodplain by dense *Salix* and *Alnus* stands of up to 6 m high; on the upper parts by *Quercus* and *Alnus*. It is unlikely that large strips of bare soil (or open grassland) existed on the floodplain prior to forest clearance and the beginning of agriculture (Fig. 4). Vegetation roughness coefficients were calculated for every floodplain compartment (Tab. 2), based on bulk drag coefficients, vegetation density and the average size of tree stems (variable in scenario 10). A range in parameters was set up from information from vegetation guides (Wolf et al., 2001; Van Velzen et al., 2002a; 2002b) and is in agreement with observations in plots of currently unmanaged riparian vegetation, and information on the general vegetation composition from the pollen assemblages in the investigated abandoned channel fill (Fig. 4). Scenario 9 was created to estimate the effect of vegetation composition ratios (different proportions of pioneer vegetation in stands of forest). This was only done for the floodplain compartment adjacent to the open channel, because this area is most influenced by fluvial erosion and deposition, which creates suitable locations for pioneer vegetation to establish. Moreover, this low-lying zone is submerged in deeper waters during floods than other floodplain compartments, so especially here, differences in vegetation composition may induce large variations in discharge.

At present, uncertainties in floodplain vegetation roughness estimates are up to ~30%, despite the use of modern techniques (Straatsma & Huthoff, 2011). This leads to water level deviations of several decimetres for a given discharge. As no detailed reference for specific natural floodplain

vegetation exists, there is little merit in attempting an extremely data-demanding method for accurately reconstructing past vegetation. Instead, a wide range of vegetation densities and stem sizes was used to determine their effect on the total discharge (Tab. 1). Because vegetation parameters were assumed to be the same for various vegetation types on the different terraces (Van Velzen et al., 2002a), the palaeofloodplain vegetation was treated as a single forest type per zone in Figure 2. The range of different vegetation densities was represented by varying mean density values per floodplain compartment (Tab. 2).

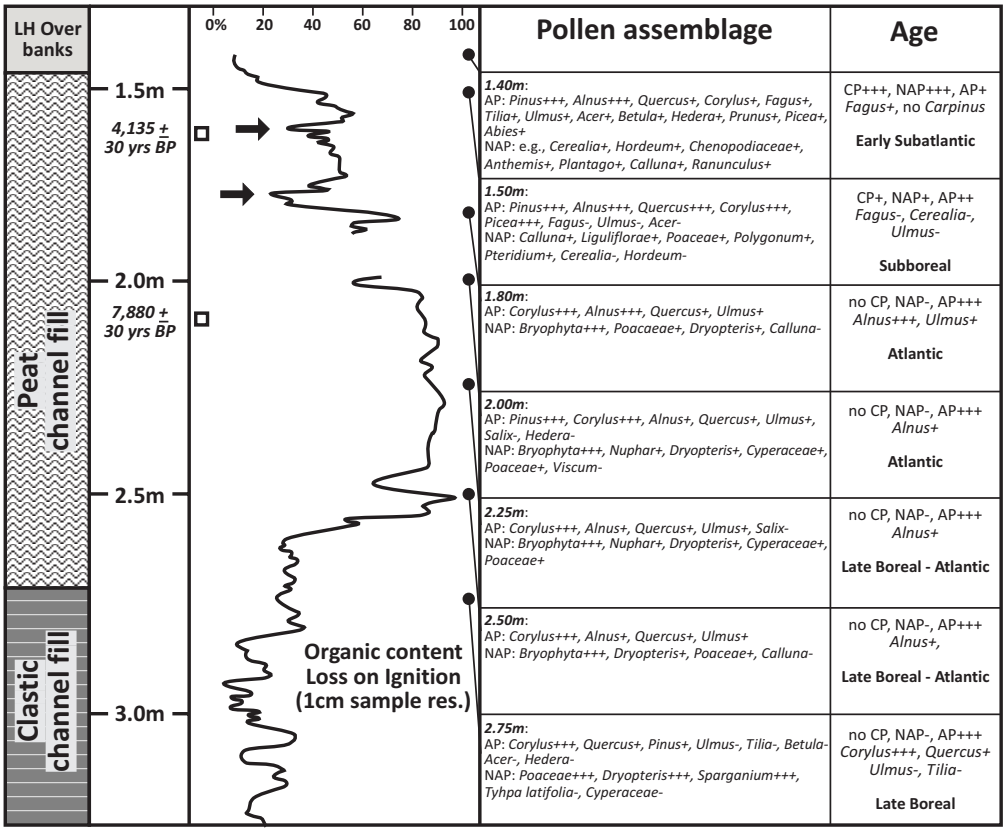

Figure 4: The Vossekuhl sample core with general lithology, organic content, pollen assemblages and estimated ages (CP = culture crops pollen, NAP = non-arboreal pollen, AP = arboreal pollen). Arrows indicate the location of extreme floods (clay laminations in peaty matrix), squares represent AMS dates in radiocarbon ages (upper sample: SUERC-37131, Alnus twig and bud; lower sample: SUERC-37130, Alnus twig), and black circles mark the location of samples for the palynological analyses.

2.3 Validation test with observed discharges

A validity check of the method and parameters used was performed on the DEM of the embanked floodplain for the gauged discharges of the 1993 and 1995 floods (at Rees; Fig. 1). For this test, surface roughness of the grasslands in the present floodplain and modern channel depth profiles were adopted respectively from Van Velzen et al., (2002a) and Baur & Jagers (2002). With the BGE estimates (Tab. 1), modelled discharges were ~3% lower than the observed discharges (11,100 m^3s^{-1} in 1993; 11,800 m^3s^{-1} in 1995).

3 Palaeoflood discharges

3.1 Palaeoflood magnitudes

The BGE discharge outcome is 13,250 m^3s^{-1} (Tab. 3). The outcomes of the various scenarios vary over a wide range (7,300 – 25,600 m^3s^{-1}) as a result of the broad range of possible values (Tab. 1). Plausibly, some input parameters may deviate from our BGE and could be near the values of the minimum and maximum for scenarios. It is, however, highly unlikely that all factors deviate in the same direction (towards lower or upper limits) and that such a combination results in a realistic estimate for the minimum magnitude of extreme palaeofloods in the Middle Holocene. The value of our BGE slightly exceeds the largest measured flood of AD 1926 (12,600 m^3s^{-1}), but is lower than the reconstructed magnitude of the AD 1374 flood. Herget & Meurs (2010) calculated the AD 1374 flood at Cologne to have peaked at 18,800 m^3s^{-1} (adopting their minimal scenario). A difficulty is that palaeochannel shape and urban surface roughness for medieval Cologne and surroundings are essentially unknown and harder to reconstruct than for the Middle Holocene situation of our study area. Modelling studies that link generated stochastic rainfall to catchment-scale discharge routing and valley-scale flood wave propagation models generate Q_{1250} floods of 16,700 – 18,500 m^3s^{-1} (Te Linde et al., 2010). Our BGE extreme palaeoflood is below these values, reflecting our conservative aim to provide a realistic geological minimal limit for extreme palaeofloods. With the effects explored using the maximum parameter values in scenarios (Tab. 3), the Middle Holocene PSIs could match a similar flood magnitude as the ones reconstructed and simulated in previous studies. However, a flood event with a similar recurrence interval as the Middle Holocene flood would probably generate a larger discharge in the current situation, because deforestation has increased effective runoff in the catchment area and canalisation and embankment have caused a steepening of the peak discharge wave (discussed below).

The lower limit of 7,300 m^3s^{-1} is strikingly low given that it is based on a PSI that is considered to be the result of a 'rare' and 'extreme' flood. Floods of this magnitude are estimated to recur every ~5 years in the Lower Rhine at present (Chbab et al., 2006). Accepting this lowest value as an extreme flood would imply that the Middle Holocene discharge regime was very different from the last century and historic times. The outcome is mainly this low because of the assumed channel dimensions (paleochannel SB in scenario 4; -30% effect). The lower limit for scenarios adopting HG for channel shape is ~10,500 m^3s^{-1}, and these are the morphological scenarios that fit the palaeogeographical setting more logically. The maximum modelled outcome is 25,600 m^3s^{-1}. This represents an unlikely theoretical maximum for the value of the lower limit of extreme palaeofloods in the Middle Holocene, as it was obtained for the parameter combination that pushes all factors to the maximum discharge producing values that are thought to be possible. It includes a maximum water surface elevation of 1.1 m above PSIs valleywide. Current flood frequency extrapolation estimates (Chbab et al., 2006) suggest such palaeoflows to occur more rarely than once in 10,000 years. In the context of flood safety measures at regional scale, design focuses on rare events (such as Q_{1250}) but not on freak events; floods that are generated by other mechanisms than normal meteorologically induced floods and occur far beyond that range. Figures on freak events may be important for local protection (e.g., nuclear power plants), but would be prohibitively costly to apply regionally.

Table 3: Modelled discharges for palaeofloods in the Middle Holocene Lower Rhine (BGE, MIN, MAX), and deviations compared to BGE per varying model parameter.

		Discharge m³/s			
Best guess estimate		13,244			
Overall minimum		7,328			
Overall maximum		25,594			
Individual scenarios					
Input	**Scenario**	**MIN**	**%**	**MAX**	**%**
Hydraulic total		*8,721*	*– 34%*	*18,070*	*+ 36%*
1	Lange Renne bypass	BGE	–	13,373	+1%
2	EH overbank	BGE	–	13,360	+1%
3	LH sedimentation	12,573	–5%	14,393	+9%
4	Palaeochannels	9,264	–30%	BGE	–
5	PSIs	BGE	–	16,497	+25%
Slope total		*12,054*	*–9%*	*15,401*	*+16%*
6	Floodplain slopes	12,869	–2%	14,801	+12%
7	Channel sinuosity	12,428	–6%	13,727	+4%
Roughness total		*12,224*	*–8%*	*15,996*	*+21%*
8	Bed roughness	12,249	–8%	14,594	+10%
9	Vegetation ratio	13,192	–0%	13,453	+2%
10	Vegetation density	BGE	–	14,403	+9%

3.2 Recurrence interval

In the period covered by the PSI-containing channel fill, only two extreme flood events were registered in the period 7.8 – 4.1 ka BP (AMS dates and pollen data in Fig. 4). The position high above the channel system of the same age is reason to consider them deposits from rare magnitude events. Only the upper event layer is modelled, as it probably represents a larger event with higher water levels than the lower PSI of the earlier event – although the limited difference of ~0.2 m would probably not produce significantly different results. The position of the event layers within the dated interval suggests a recurrence interval between 1,250 and 2,500 years; there are only two events in the dated interval of ~5,000 (calendar) years, but because both layers are located in the later half of this period, a minimum recurrence interval of 1,250 years was adopted.

This range for recurrence intervals only applies to the flooding regime in the dated interval (Fig. 4). It is possible that non-stationarity in the flooding regime complicates utilisation of these observations in the assessment of recurrence intervals of extreme floods at present (Redmond et al., 2002; Milly et al., 2008). Even though no major differences in climate exist between the Middle Holocene and the last centuries for the research area (Davies et al., 2003), minor climatic changes may have influenced recurrence intervals of floods (Knox, 1993), and caused the occurrence of intensified flooding episodes (Macklin et al., 2006). However, the effect of non-stationarity on extreme events, which approach the physical limit of meteorologically induced flood magnitudes, is largely unexplored scientific terrain. Therefore, it may well be that the effect of climatic-induced non-stationarity is not sufficient to significantly affect recurrence intervals in the range of extreme floods.

3.3 Effect of parameter uncertainty

In the case of this study, palaeotopography, slope and roughness turn out to contribute significantly to total uncertainty (Tab. 3). The combined effects of these parameter groups are at least an 8%

deviation from the total BGE discharge. A further breakdown of introduced uncertainty shows that channel geometry, flood levels (PSIs), slopes and bed roughness are the main contributors, with each a >10% effect on the total discharge. Although channel geometry and the PSIs are precisely reconstructed in the field, still the estimated parameter ranges are relatively wide (Tab. 1). Slopes have also been reconstructed accurately and the range is rather limited, but still the induced uncertainty is large. This indicates that small variations in slope have a major influence on modelled discharges.

Smaller individual contributions (<5% effect) to the uncertainty in modelled discharge result from the stripping of Late Holocene overbanks on higher terrace levels, adjusting anthropogenic by-pass channels, and varying vegetation composition on the lower part of the Middle Holocene floodplain. In the case of the Late Holocene overbanks, it is clear that this is caused by the tight range of the input data. The minor effect of the anthropogenic by-pass channel can be ascribed to its limited size and location on a relatively high terrace level. No large water depths are reached even during an extreme flood. The effect of vegetation ratios and vegetation in general is more difficult to assess. It was thought that the vegetation would have a profound effect on modelled discharges and uncertainty – even more when the low accuracy and wide range of set-up model parameters are considered (Tab. 2). A possible explanation is that flow velocities are, compared to slope-induced variations, relatively insensitive to vegetation roughness. Perhaps a larger effect can be forced with a wider range of vegetation types and densities, especially when a dominance of grass- and shrublands are considered to be possible in the Middle Holocene floodplains of the Lower Rhine. So far, palynological information gives, however, no reason to adopt such scenarios in the investigated period, as the pollen spectra are dominated by arboreal species (Fig. 4).

4 Implications for future flood predictions

To use the minimal magnitude of Middle Holocene palaeoflood extremes in flood frequency analysis for the present situation, issues regarding the translation of the past to the modern catchment run-off situation and flood-wave dynamics need to be addressed. Non-stationarity in palaeohydrology is often thought to be primarily produced by natural climatic variations, but in the setting of the Middle and Late Holocene Rhine (pre)historic human actions may have had stronger progressive effects on the river and its flooding regime (Erkens et al., 2006; Hoffmann et al., 2007). To allow projection of our results to the present, human-induced changes need to be assessed on a catchment scale. Deforestation became significant at catchment scale in the Bronze Age (i.e., since ~3.5 ka BP). The increasing sediment supply and effective run-off by a decrease in the buffering effect of vegetation may have resulted in more discharge to be released from catchments under similar meteorological conditions. Hundecha & Bárdossy (2004) indicated that a given amount of precipitation results in 10 – 19% higher peak discharges nowadays than in a fully forested catchment for magnitudes of the 1993/1995 floods in major tributaries of the Rhine. Ward et al., (2011) report corresponding results for similar floods in the Meuse catchment. Importantly, the effect of deforestation on Q_{1250} appears to be non-significant in their model, in contrast to the effect on moderate events.

In addition, major engineering works have been carried out on the Rhine: the river has been embanked and straightened in recent centuries. This effectively reduced river length and eased

the downstream transport of large discharge volumes (Disse & Engel, 2001). It enabled the same volume of water to pass in less time, which causes higher peak discharges and higher peak water levels by a steepening of discharge waves (Lammersen et al., 2002). The impact of this effect on Q_{1250} is estimated as 6% since the beginning of the Industrial Revolution (Parmet et al., 2001; Lammersen et al., 2002). Recent river and floodplain adjustments, focusing on the construction of retention basins, are expected to flatten the discharge wave again (Lammersen et al., 2002).

Although more specific research is needed on the actual effect of the above discussed factors, especially for extreme floods, the combined effect on discharge of these major changes for the Lower Rhine is conservatively estimated to range between 6 and 16% since human impact began. In this combined estimate, the effect of river training is considered minor (Lammersen et al., 2002) compared to the possible effect of deforestation (Hundecha & Bárdossy, 2004). As indicated by Ward et al., (2011), the effect of deforestation on extreme floods may be smaller than the effect on large floods (similar to the 1993/1995 floods), so the lower estimate of 10% change by deforestation by Hundecha & Bárdossy (2004) was adopted. Accordingly, our BGE for Middle Holocene extreme floods would correspond to a discharge that ranges between 14,050 and 15,370 m^3s^{-1} under modern conditions; discharges that have not been observed in the last century, but are very close to the present design standard.

In frequency-magnitude plots, the range of modelled palaeodischarge outcomes presents a lower limit of possible palaeoflood magnitudes. Figure 5 plots our BGE plus 6 – 16% 'deforestation and engineering' with a recurrence interval of 1,250 to 2,500 years. This lower limit for flood magnitude and the range in recurrence interval provide a geological check for the current Q_{1250} in the Lower Rhine. The current frequency-magnitude relation (Chbab et al., 2006) corresponds well to our lower limit for extreme events. Because this study is not suitable for producing an accurate estimate for the upper limit of palaeoflood discharges, no conclusions can be drawn regarding the maximum discharge values and the upper range of uncertainties in current estimates of flood frequency analysis.

To further exploit Middle Holocene paleoflood results and to make it an effective way to reduce uncertainty in flood frequency analysis, uncertainty in the magnitude estimates should be narrowed further. This can be done by: (1) carrying out a similar exercise at alternative suitable transect locations in the Lower Rhine Valley – for example at the present day delta apex; (2) improving accuracy of input parameters; and (3) assessing the effect of major changes in the catchment on Q_{1250} using numerical modelling for palaeosituations. In the case of non-stationarity it is important to accurately quantify the differences in discharges for similar extreme floods in terms of generated runoff and recurrence intervals between different periods during the last 5,000 years.

In spite of the uncertainty in the reconstructed peak discharges of palaeofloods, millennial-scale geological evidence is extremely useful for estimating modern flood safety limits. Modern gauged records are too short for predicting extreme events, while historical records are mostly inaccurate and need additional reconstruction techniques to estimate flood magnitudes. Geological records provide a unique resource for the reconstruction of extreme events and are particularly useful in obtaining physical limits for flood magnitudes despite the associated uncertainty. For the Late Holocene, there is even more geological evidence available from palaeochannel fills and floodplains, which can be used for palaeohydrological modelling, also for less rare events. Further research

should aim at predicting the frequency and magnitude of large flooding events from these records to verify and further constrain the results from this study. Further integration of historical and palaeofloods with modern floods is also essential, so that the design standard for dikes is established more accurately.

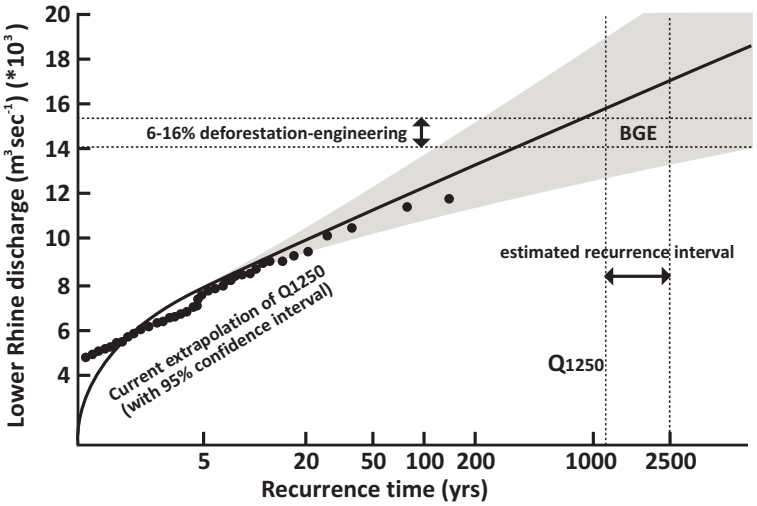

Figure 5: Current flood magnitude-frequency extrapolation (redrawn after Chbab et al., 2006) with our calculated range in recurrence interval and the BGE for the lower limit of Middle Holocene palaeoflood extremes. The BGE is corrected with 6-16% for 'deforestation and engineering' – see main text.

5 Conclusions

A Chézy-based hydraulic model, using a slope – area approach, was run to estimate the magnitude of extreme floods of the Middle Holocene age in the Lower Rhine Valley. For such extreme events, dating to between 4.1 and 7.9 ka BP, palaeostage indicators have registered in a filling palaeochannel located on a relatively high floodplain terrace. Ten explorative scenarios regarding the sensitivity to various input parameters, based on geological, geomorphological and vegetation information, give a best guess range estimate for the size of the minimal exceeded discharge during the PSI-producing events. The resulting best guess estimate modelled discharge is 13,250 m^3s^{-1}, which exceeds gauged floods of the last century. The recurrence interval of floods exceeding this value is estimated to be between 1,250 and 2,500 years.

The sensitivity analysis shows that besides the exact flood level, the palaeochannel geometry, slope reconstructions and bed roughness estimates are the main contributors to uncertainty in discharge estimates. For most input parameters this is a direct effect of a relative wide range of possible values, despite the accurate reconstruction of associated physical limits in the palaeolandscape. Modelled discharges are particularly sensitive to bed slope estimates, which are defined in a narrow range, but still introduce a significant amount of uncertainty in model outcomes.

For application in modern flood frequency analysis, palaeodischarge results must be converted to equivalent discharges for the modern situation with altered hinterland land cover, and embanked floodplains and straightened rivers. Applying literature-based conversions suggests a 6 – 16% increase in absolute discharge. This suggests that our BGE coincides with the currently used design flood in the Lower Rhine Valley.

Acknowledgements
We acknowledge Utrecht University MSc students A. Geurts and B. van Munster for participating in the fieldwork. We thank W. Z. Hoek, G. Erkens and K. M. Cohen (Utrecht University) for field assistance. K. M. Cohen, W. I. van de Lageweg and M. G. Kleinhans (Utrecht University), and two anonymous reviewers are thanked for comments on earlier versions of the manuscript and model. This research was funded by Deltares, with additional funding from TNO Geological Survey of The Netherlands, and Utrecht University. Reprinted with permission of Hydrology Research, IWA Publishing.

7 A composite Holocene palaeoflood chronology of the Lower Rhine

Toonen, W.H.J.*[1,2], Donders, T.H.[1], van der Meulen, B.[1], Cohen, K.M.[1,2], Prins, M.A.[3]

[1] Dept. of Physical Geography, Utrecht University, Utrecht, The Netherlands.
[2] Dept. of Applied Geology and Geophysics, Deltares BGS, Utrecht, The Netherlands.
[3] Department of Earth Sciences, VU University Amsterdam, Amsterdam, The Netherlands.
* Corresponding author: E-mail: w.h.j.toonen@gmail.com

1 Introduction

Most palaeoflood records are retrieved from upstream regions and are either continuous records from pro-alpine lakes (e.g., Bøe et al., 2006, Wilhelm et al., 2013) or reconstructions of major events using slackwater deposits in fixed bedrock canyons (Benito et al., 2003). Upstream records in complex larger catchments do not necessarily directly relate to flooding in vulnerable downstream regions, as individual tributaries may play an important role in flood pulse accumulation and propagation, and upstream flood waves dissipate easily (Disse & Engel, 2001). In lower reaches of fluvial systems, which are typically densely populated, palaeoflood records can be harvested from sedimentary fills of oxbow lakes. After disconnection from the active channel, oxbow lakes act as fluvio-lacustrine sediment traps during floods (Chapter 2). Accumulation rates and grain-size characteristics of the fill mainly depend on proximity to and connectivity with the active river, and the magnitudes of successive flooding events.

This chapter presents a composite record of seven oxbow-fill palaeoflood datasets from the Lower Rhine region (Fig. 1), covering the last ~8,200 years. The last ~240 years overlaps with the discharge record based on observational data for Lobith at the apex of the Rhine Delta (Fig. 1). The apex region was selected for this study, because firstly it is the location where the trunk river is undivided, and all major tributaries have joined. Second, it avoids complexity in flood record registration that is introduced by varying discharge division over deltaic branches (especially for pre-historical gradual avulsions; Stouthamer & Berendsen, 2000), and marine storm-surge and tide-influenced river signals. And third, multiple infilled oxbow lakes with a-priori information on age and proximity to past active river channel were available locally (e.g., Berendsen & Stouthamer, 2000; Gouw & Erkens, 2007; Erkens et al., 2011). Moreover, valley confinement results in higher vertical amplitudes of flooding than in the wide delta environment. Together with the relative wide range in grain-sizes carried by the Lower Rhine, this facilitates differentiation in grain-size characteristics of individual flood deposits, resembling flood magnitudes.

Information on palaeoflood magnitudes was derived from normalised cm-resolution grain-size data obtained from flood bed-layered oxbow lake fills (Chapter 3). Individual sites – each recording centuries to millennia (Chapter 3) – were combined by using the partial overlap in recorded period. The seven individual oxbow fills differ in their proximity to the active river, and consequently they

differ in the frequency-magnitude threshold above which sedimentary flood registration occurs. Proximal lake fills resolve flood beds of each flood exceeding bankfull-discharge, while more distal fills registered larger floods only.

Comparison, analysis, and integration of flood records from different periods may provide valuable insights in (i) the magnitudes and occurrence of largest Holocene floods, including their suspected regional geomorphological imprint, (ii) possible periodic behavior in flood deposition and associated climatic forcing, and (iii) transient changes in flood intensities, including changing relations between flood magnitudes and recurrence times (non-stationarity; Knox, 1993), such as induced by deforestation and river engineering, and climatic variability. This information is important for flood risk assessment along major rivers, as potentially largest floods might not be present in modern discharge records (Klemeš, 2000), and for assessing possible changes in 'future' flooding regimes caused by climate change (IPCC, 2007).

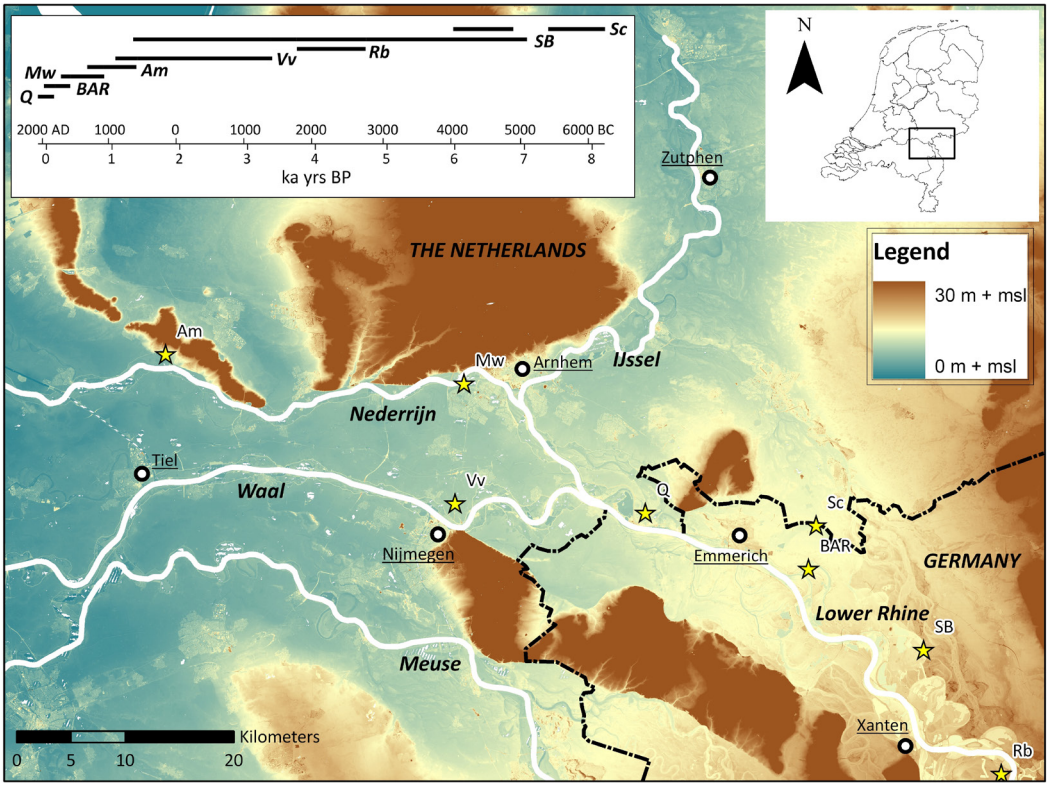

Figure 1: Topography of the Rhine-Meuse delta with research locations indicated by stars on the map, and site chronologies (inset). Q = discharge series at Lobith; BAR = Bienener Altrhein; Mw = Meinerswijk; Am = Amerongen; Vv = Visveld; Rb = Rheinberg (located ~10 km farther to the south); SB = Schloss Bellinghoven; Sc = Schriek. For detailed research location information, see Appendix B.

2 Methods

The quality of a collated sedimentary flood record depends on its input records: their dating control, record length and sample resolution, and the accuracy of flood magnitude estimates from individual flood layer grain-sizes. In the previous chapters, concepts and methods are presented to extract high-quality records at individual sites (Chapter 3, 4, and 5). Age-models for such sites were improved by incorporating sedimentary information besides 'spot'-datings (Chapter 4). Relative magnitudes of floods were characterised by Z-score normalised values of parameters that describe the coarse tail of grain-size distributions of specific flood beds (Chapter 5). In this section it is further described how recurrence times for larger events were established from the age-depth information of continuous relative flood-magnitude records, and how these were compiled into a composite flood record.

2.1 Flood magnitudes & age-depth models

Previous detailed mapping and dating of channel belt locations and ages was used to select oxbow fills for sampling with a desirable age range and proximity to the then active channel (Berendsen & Stouthamer, 2000; Erkens et al., 2011). The thickest channel fill sequence is typically located in the most distal part of the oxbow at the position of deepest active river thalwegs (Chapter 3). Deposits were recovered in meter-segments using a modified Livingston piston corer. Samples for grain-size analysis were taken continuously at a 2 cm resolution. Occasionally the thickness and position of samples was shifted to accommodate visual layering in flood deposits. Standard pretreatment procedures were used to remove organic and calcium-carbonate components, and to maximise the dispersion of individual grains (Konert & Vandenberghe, 1997). Grain-size distributions were measured at the VU University Amsterdam Sediment Laboratory using a Sympatec HELOS KR laser-diffraction particle sizer.

From occasional organic intervals, leaves and seeds were collected for AMS dating (Appendix B), whereby the use of terrestrial plant material avoids hard-water effects (Törnqvist et al., 1992). The fragile nature of selected organics ensures local origin and precludes dating of older material that could have been eroded upstream and transported by the river. Age calibration and age-depth modeling was carried out using the IntCal09 calibration curve and Oxcal U_Sequence modeling (Bronk Ramsey, 2009; Reimer et al., 2009). Sedimentological information, organic content variations (Chapter 4) and/or grain-size of the background matrix (Chapter 5), were considered as boundaries in the age-depth model (Appendix B).

After performance tests (on site BAR) on the interval that overlaps with the observational record (Q at Lobith; Fig. 1), the 95th percentile of grain-size distributions (P95) was adopted to infer flood magnitudes (Chapter 5). For all sites, P95 was normalised by linear detrending and conversion into Z-scores (Appendix B). This largely corrects for variations in grain-size due to differences in overall proximity of sites to the active channel, and for shifts in active channel position during accumulation of the fills due to meander migration and cut-off (Chapter 4 and 5), and prevents over-interpretation of flood occurrence and magnitudes in phases of increased active channel proximity.

Resulting records are not directly intercomparable, because Z-scores still represent site-specific grain-size populations and lower threshold for flood registration. The same Z-score for flood bed P95 grain-size of different sites does not imply that the flood magnitudes were similar. Hence, the Z-scored P95 values provide relative flood magnitude indications only (Chapter 5). To enable comparison and unification of flood records from different research locations, Z-scores were converted to recurrence times. Recurrence times per Z-score were estimated by dividing the dated interval by the frequency of exceeded Z-scores. Regression lines were fitted to relate Z-scores to recurrence time (Appendix B). This simple approach works well for frequent minor events, which are abundantly present and generally well distributed throughout the record, but is more uncertain for rare large events. Recurrence times of most extreme events, represented a single time in a long record, are presumably underestimated as recurrence time estimates are constrained by the time span of the local record. Estimates on the recurrence time of largest events were therefore derived from cross-correlation of flood beds contained in temporally overlapping sites, occurrence of the events in the longer composite record (extending the observation period, albeit based on other research locations), and extrapolation of the site-dependent relation between Z-scores and recurrence times.

2.2 Composite flood record

Flood series from individual locations were combined in a composite record using the results of age-depth modeling and estimated recurrence times of large floods; the same major events in various records were wiggle-matched. Temporally overlapping records were assessed to prevent double registration of a single event. Flood beds identified to belong to the same event, falling in the same age range (±2σ of the Oxcal age-depth model) and sharing comparable flood magnitudes, were merged to produce only a single data point. Flood events overlapping with historical records (which are for the Lower Rhine region reliable back to the 14th century; Glaser et al., 2010) were directly correlated and assigned to years of extreme flooding, provided that a historic flood of similar size (impact) was placed in the ±2σ age range of the age-depth model.

Event records of high-resolution intervals were considered most reliable for reconstructing magnitudes of minor floods, as these have often not been registered at more distal locations. Relative high numbers of radiocarbon dates and minor fluctuations in accumulation rates provide the proximal high-resolution sites with the best constrained age-depth models. Hence, age information of large events is adopted from these sites. The recurrence times of events exceeding a centennial recurrence time were based on records of lower temporal resolution. These typically span several millennia and produce more precise estimates for flood recurrence time of rare events. The final composite flood record covers the last 8,200 years; the inset in Figure 2 shows the sections of each individual site that has been adopted for the main flood chronology.

2.3 Variability in the flooding regime

In an effort to gain better understanding of the distribution of large flooding events, the number of events exceeding a 25, 50, 100, and 250-year recurrence time were summed and plotted per century. This was done to indicate which periods in history experienced anomalous flooding, to determine if different flood magnitudes have divergent variability over time, and to assess whether the occurrence of extreme floods corresponds with periods of anomalous flood intensities.

Next, periodicities in the data series were assessed using spectral analysis (Red-fit; Schulz & Mudelsee, 2002), which allows testing of the significance in periodicity by comparison with a first-order red-noise model (Welch-type window, bootstrapped significance testing). Periodicities were assessed on the P95 grain-size data per site. Besides demonstrating fluctuations in the occurrence and magnitudes of floods, periodicities may indicate possible forcing, when these correspond to known climate cycles and are consistent through time and transferable among different coring sites. The most prominent cycles across different sites were band-pass filtered to assess the temporal evolution of the signal amplitude (provided in Appendix B). Amplitude variations that agree between different sites are considered regionally significant.

Last, derivative functions of the site-specific relation between Z-scores and recurrence intervals were determined to demonstrate the effect of non-stationarity and to identify periods with anomalous flooding regimes. If climate and catchment have changed significantly over the last millennia, and resulted in major non-stationarity of the flooding regime (Knox, 1993), this should be visible in deviating shapes of flood recurrence time-Z-score distributions.

3 Results

3.1 Description of the flood record

The combined record stretches back for more than eight millennia. Apart from the period 7,0-7,3 ka BP, floods are documented continuously, with site-dependent lower thresholds of registration. Phases with annual floods are repeatedly recorded in proximal channel fills, while centennial events are recorded in more distal oxbow fills or phases of low deposition rates following the transition of channel fill into general floodplain at proximal sites. Highest resolution and replication of the flood record is acquired in the last ~5000 years. Especially in the last ~1500 years registration is very sensitive; recording annual floods in two clusters in the last centuries (Q-series, and during part of the 1st millennium AD) and registration of decadal floods in between (Fig. 2).

Apart from major floods in recent times (e.g., AD 1809, 1926, 1995; Q exceeding 11,000 m^3s^{-1}; Chapter 2), largest events are dated to AD 1658, 1571, 1374, 1342, and approximately AD 784, 596, and 237. Between 1.4 and 3.2 ka BP, only floods with a recurrence time larger than ~25 years are represented. This part of the flood record is recovered from slowly accumulating distal fill intervals at sites Vv and SB. Importantly, both sites indicate that during this phase no extreme floods have occurred: the fills hold evidence for centennial floods, but no millennial floods were recorded. From 3.2-4.7 ka BP, the sites allow recording smaller floods again (Fig. 2); besides the distal fill of SB, this interval is also covered by the more proximal Rb site, which contains deposits of most floods exceeding bankfull level (Chapter 4). At the beginning of this period two major events of millennial recurrence time are indicated, timed at 4.5 and 4.7 ka BP.

The record from 4.7 to 8.2 ka BP is based on single sites SB and Sc. These records do not overlap in time, prohibiting cross-verification of events, and leave a ~300-year hiatus centered around 7.1 ka BP (Fig. 2). Moreover, both are distal sites, so for the period 4.7-7.0 ka BP only events of centennial or rarer recurrence are registered. Centennial events are distributed fairly evenly throughout this period, and at 6.2 ka BP (~4,200 BC in Fig. 2) one extreme event (exceeding millennial recurrence) stands out.

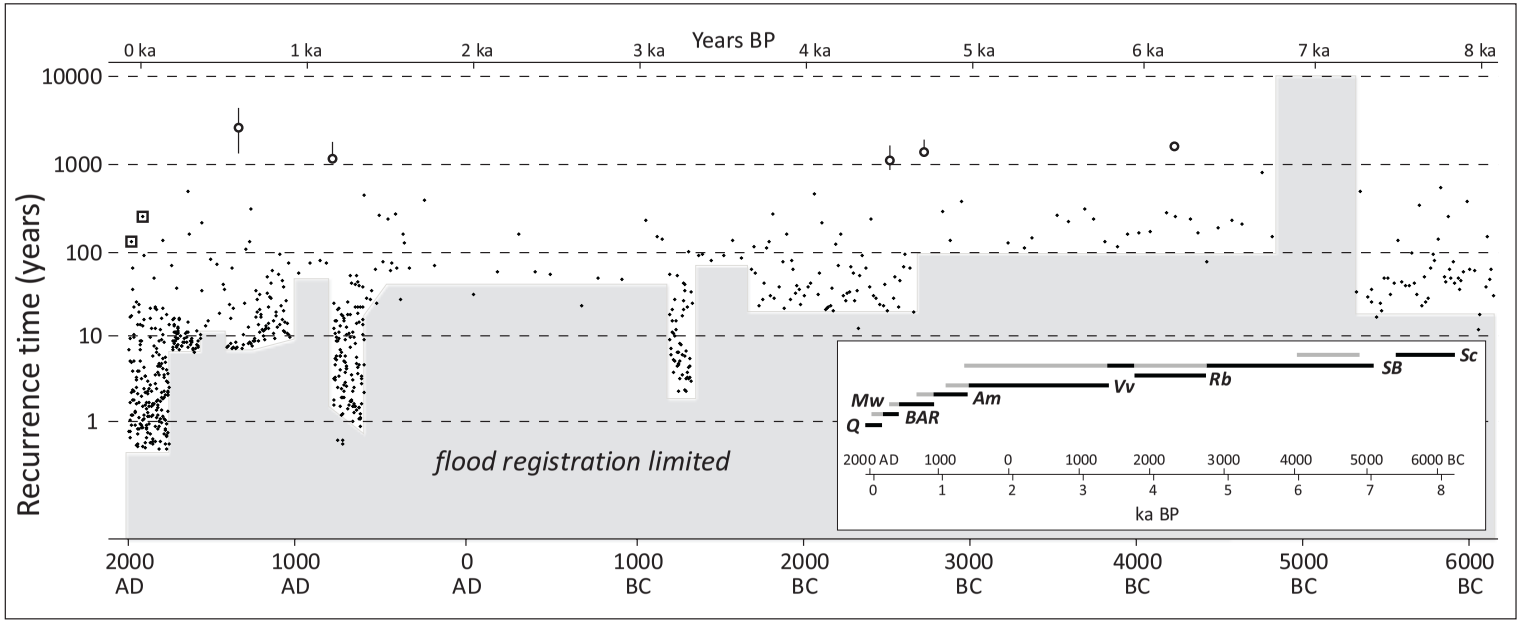

Figure 2: Holocene composite flood record of the Lower Rhine. Recurrence times are indicated, which is indicative for flood magnitude. The lower threshold to flood registration varies along the compiled record (shading). Millennial flood events are marked by larger dots; error bars indicate the range in estimated recurrence time, adopted from different estimation approaches (section 2.1). Squares indicate largest measured discharges of the last century (AD 1926 and 1995; respectively 12,600 and 11,900 m^3s^{-1}). The inset shows which parts of the individual sites are incorporated in the composite record (black bars), and which part is used as overlap for verification of flood magnitudes (grey intervals).

3.2 Variations in flood intensities

Frequencies for various flood magnitudes, summed over century bins, illustrate the variability of event occurrence over the analysed period (Fig. 3). Very large floods (>250-year recurrence time) are spaced rather evenly trough time, with exception of the absence of large events from the Middle Bronze Age to the Roman Period (1.8-3.8 ka BP) – which is not an artifact of sampling or age-depth modeling, as sites Vv and SB duplicate the temporary reduction in the occurrence of large events. The frequency of centennial events shows a similar pattern – although some events now plot in the Iron Age, the 1st millennium BC is still underrepresented of truly major floods, especially in comparison to the previous and next millennia (Fig. 3). For the 1st and 2nd millennia AD, the 9-12th century stands out as a period lacking major flooding, coinciding with the Medieval Climate Optimum (Mann et al., 2009). It appears that for this period the Lower Rhine record corresponds with dendrochronological records from Germany (indicating dry conditions; Büntgen et al., 2010) and reduced flooding in the northern Alps as compiled by Swierczynski et al., (2012).

When flood intensities are inferred from events exceeding a 50-year recurrence interval (Fig. 3), more temporal variability becomes apparent. The period of intense flooding in the last two millennia are the early Middle Ages, the end of the Middle Ages, and the last century. Besides the Medieval Climate Optimum (for which 50-year floods may be poorly resolved; Fig. 2) also the Little Ice Age is a period of low flooding intensity, despite the possible effect of ice jamming overprinting on reconstructed peak discharges (Chapter 5). Few floods also occurred in the first millennium BC (Fig. 3), although this may be attributed to the lower limit of registration in that period, which probably also affects floods with a 50-year recurrence interval. Moderately large floods in the Holocene prior to 3.5 ka BP seem to be of rather similar occurrence as in the last century – with maxima in flooding occurring around 3.8-3.9, 4.1-4.5, and 7.9-8.1 ka BP, matching flood records from Britain (Macklin & Lewin, 2003). Patterns in flood frequency are very similar for moderate floods (25-year recurrence; Fig. 3); differences between periods increase, but can be attributed to limited registration. From comparison with the distribution of millennial floods, it becomes clear that the timing of extremes is not necessarily related to periods of increased flooding frequency, which has previously also been suggested from analysis of historical documents (AD 1350-1772) and discharge series (AD 1772 – present; Chapter 2).

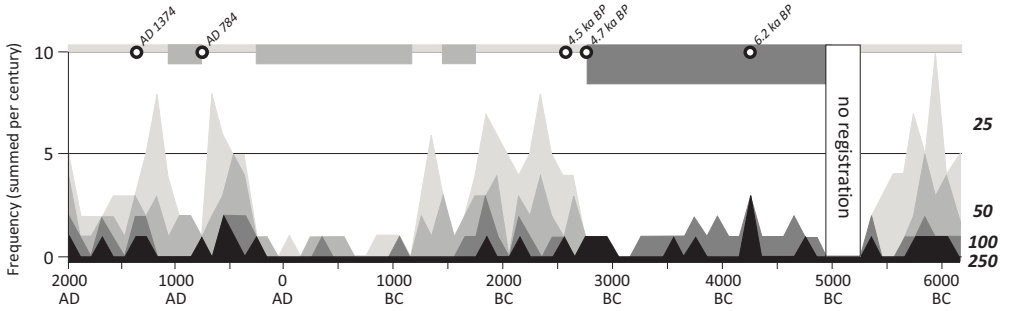

Figure 3: Flood frequency per century illustrated by the frequency of various flood magnitudes, exceeding recurrence times of 250, 100, 50, and 25 years and respectively corresponding with black, dark grey, grey, and light grey. The timing of millennial floods is indicated by dots at the top of the figure. Lower limits of registration are also shown at the top; shades correspond with the minimum class recorded.

3.3 Flooding periodicities

Periodicities in sedimentary sequences of individual sites can be of many origins, including repetitive centennial patterns in channel migration and floodplain building, internal grading of flood deposits exceeding typical sampling thickness, and general sample resolution. If such periodicities are present in flood series, these should be identified and assessed prior to linking cyclicity in flood deposition directly to external climatic forcing. The results of the spectral analysis provide an inventory of all periodicities in individual records. Significant periodicities are present throughout the compiled series, and could indicate that cyclic climatic forcing is reflected directly in the occurrence of flooding (Tab. 1).

In the measured discharge series (AD 1772-2011), periodicities are significant in the range of 3-7 years and ~35 years (Tab. 1). Because this data series is derived from annual maxima, site-specific elements, inaccuracy in age-depth modeling, and sample resolution can be excluded as cause. Similar periodicities are recognised at all proximal research locations that are able to temporally distinguish such small events. This strongly suggests that the flooding regime is subject to sub-decadal periodic variations in flood occurrence, at least continuously since ~AD 600 (Tab. 1). The 35-year periodicity, recognised in the discharge series, is also encountered in the sedimentary archives (Tab. 1). A slightly smaller periodicity of ~30 years from 3.7-4.7 ka BP may be linked with a similar forcing, but producing different results due to inaccuracies in age-depth relations. In the older part of the flood record, such a periodicity is absent, partially due to insufficient sample resolution.

Decadal periodicities are non-significant in discharge records (Tab. 1). Many sedimentary records, however, yield 11-18 yr periodicities, and doubles of that period (22, 45, and 85 years), often with very high significance levels (Tab. 1). While differing site-dependent age-depth accuracies may result in the relative large variety of decadal cycles observed in our records, the decadal variations may also not be stationary in time (Appendix B). Incorporation of additional dating techniques (e.g., by progressing work on palaeosecular magnetic variation), or acquiring additional tie-points with traditional dating means and event-stratigraphic correlation, and further calibrating sediment-tuned non-linear age-depth modeling (Chapter 4) may reduce effects and disturbance by age-depth models in analysis of periodicities. Nonetheless, current reproduction of similar decadal periodicities among proximal sites suggests that present linear age-depth models are performing adequately.

Centennial periodicities are difficult to assess based on discharge records, as the typical discharge record length is limited to a century. Sedimentary records indicate significance of various centennial periodicities only between 3.7-7.0 ka BP (Tab. 1). Longer periodicities are found for individual research sites, but do not duplicate between records. Hence, it is more probable that such periodicities relate to pseudo-cyclic regional geomorphological processes (e.g., meander cut-off; Chapter 4) or a limited temporal sample resolution in intervals of very low accumulation rates, rather than climate signals.

Table 1: Periodicities in flooding; single asterisks indicate significance levels of 95%, double asterisks indicate a 99% significance level. Limits to registration at individual sites are grey-shaded.

Site	*Q*	*BAR*	*Mw*	*Am*	*Vv*	*Rb*	*SB*	*Sc*
Record length (yrs)	240	377	633	708	2264	990	6081	2205
Mean resolution (yrs/sample)	1.0	1.1	1.9	1.3	7.0	4.5	26.9	11.9
Periodicity (yrs)								
1527							*	
757					**			
261								*
153						*	*	
104-106						**	*	
84-86			*				*	
60-64							*	
45-46					**			
33-37	**		*	*	**			
29-30					**	*		
20-22						*		*
16-18				**	*			**
13-14.5			**		**			**
11.5						**		
7	*	*		**				
5-6	*	**		*				
3.5-4	*	**	*	*				
2.5-3	*	*		*				

3.4 Non-stationarity

Non-stationarity is identified by comparing the shapes (derivative functions) of the flood Z-score probability-recurrence time functions of individual research locations, spanning various periods. A comparable shape of the distribution of floods indicates similar ratios between floods of differing magnitudes; if the ratio between magnitudes of a centennial and decadal flood is similar throughout time, derivative functions will have a similar slope. This only applies for relative flood magnitudes, absolute floods magnitudes may differ while having similarly shaped derivative functions; offsets in absolute discharges by non-stationarity is discussed in section 4.3.

Derivative functions gather in three clusters; (i) the steepest flood frequency-magnitude curves occur in modern times, illustrated by the discharge series (AD 1772-present; Q in Fig. 1), and in the relative long records of the Middle Holocene (SB and Sc), (ii) rather similar but less steep curves belong to flood series from 0.9-4.7 ka BP (Am, Vv, Rb), and (iii) two distinct outliers are associated with the relative short records from the Little Ice Age and Late Medieval Period (BAR and Mw). From a temporal perspective, this suggests that the flood frequency-magnitude distribution has leveled off since the Middle Holocene, with a minimum in the last millennium, but a steep recovery in the youngest centuries towards a frequency distribution similar to the Middle Holocene period. The flattening of the distribution is thought to mainly affect the magnitudes of moderate to major flooding (up to centennial recurrence; Chapter 2). Indeed, relatively high Z-scores are attributed to

sub-centennial recurrence between 0.2-0.9 ka BP at sites Mw and BAR, in comparison to similarly proximal sites from other periods, such as Rb and Am (Fig. 4). In addition to generally decreased flood intensities, this demonstrates that the entire flood frequency distribution was different during the Little Ice Age.

The temporal cover of derivative curves differs, as individual sites span several centuries to millennia (Fig. 1). Hence, the longer time series are expected to subdue the effects of decadal to centennial variations associated with non-stationarity. This may explain why the BAR and MW produce such large offsets compared to other series (Fig. 4), as they record a relative short but strong anomaly in the flooding regime. Similar short anomalous periods can be present in longer records, but will affect the overall distribution only to a small degree. Nonetheless, the resemblance between the flooding regime of the last ~240 years and Middle Holocene records is striking – both regarding the shape of flood frequency plots and flood intensity estimates (Fig. 3).

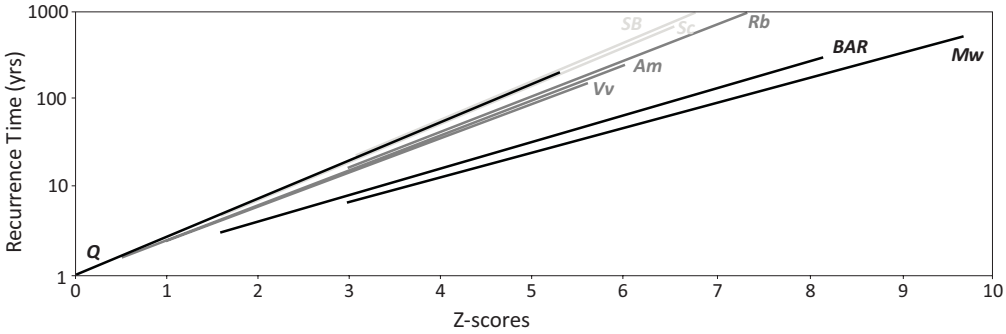

Figure 4: Derivative functions of flood frequency distributions; shade of the lines indicate relative age (last millennium in black to Middle Holocene in light grey).

4 Discussion

4.1 Extreme floods in geomorphological records

The current Lower Rhine flood record can be compared with other records on flooding from the same catchment area to investigate upstream-downstream relations. This is opportunistically illustrated by examples of regional correspondence and likely relations between extreme floods observed in our record and geomorphological imprints elsewhere.

The occurrence of very coarse flood beds in sedimentary records often coincide with floods reported in historical records and geomorphological imprints in the research area. In the historical period, flood magnitudes correspond well with damage reports; especially the AD 1374 flood has been suggested as the largest event of the last millennium (Herget & Meurs, 2010), which is consistent with our findings. An event of similar magnitude probably occurred in the late 8th century (at least a millennial flood; Fig. 2). No historical records exist for this period in the Lower Rhine region, although this period is associated with major fluvial reconfigurations; i.e. the formation of the northward IJssel-distributary (Fig. 1; Makaske et al., 2008). Such analogy between extreme flooding and geomorphological changes confirms the effectiveness of major floods as geomorphological

agent, as indicated by Kale (2007). Moreover, this study can provide independent evidence for hypothesised large flood events that have been used in the past to explain geomorphological changes of rivers and floodplains.

For other major palaeofloods presented in this paper similar geomorphological imprints are suggested. The 4.5 and 4.7 ka BP events are, respectively, linked with a local avulsion in the vicinity of the site Rb and the abandonment of the Rb meander itself (Chapter 4). Dated slackwater deposits on an elevated fluvial terrace indicate a major event contemporaneous with the 4.7 ka BP event. In Chapter 6, we estimated the associated discharge to be ~13,250 m^3s^{-1}. Similar to the 4.7 ka BP flood, the 6.2 ka BP flood is probably represented as a slackwater deposit on high Lower Rhine floodplain terraces (Chapter 6; Toonen et al., 2013), thus resembling similar discharges (exceeding 13,250 m^3s^{-1} in the Middle Holocene setting).

As major floods propagate through the entire trunk valley, it is likely that reflections of the largest events are present in both upstream and downstream regions. Implicit examples are some of the avulsions in the Rhine Delta (Stouthamer & Berendsen, 2001) or periods of rapid geomorphologic change in fluvial settings (inferred from metadata analysis of radiocarbon databases; e.g., Hoffmann et al., 2008). Detailed study and disentanglement (e.g., Slingerland & Smith, 2004) of autogenic forcing (levee build-up and crevassing) and allogenic triggering (large floods), and fine-tuned dating of avulsion events, has now become possible with the creation of the current flood record. This also goes for analysis of meander cut-off (and preservation), and validation of explanations that suggest floodplain geomorphological communality between valleys by the large flood-triggered processes (Schirmer, 1995).

4.2 Periodicities in flood deposition

Periodicities observed in the discharge and sedimentary records point to climate forcing of floods. Especially sub-decadal periodicities and a ~35-year periodicity are commonly observed. Although the consistent climatic periodicities of 3 to 5 year are not typical of the North Atlantic region, such periodicities characterise the El Niño – Southern Oscillation (ENSO) (e.g., Moy et al., 2002), although direct ENSO forcing of NW Europe is unlikely. Modulation of North Atlantic climate by ENSO has been shown in climate reanalysis and model data (Toniazzo & Scaife, 2006), and is likely highly non-linear. The unpresedented length, resolution and catchment-wide character of our composite flood record potentially reveals ENSO forcing for the first time. The persistent ~35-year periodicity may be driven by comparable cycles in the Atlantic meridional overturning circulation (Timmermann et al., 1998; Wanner et al., 2008). Global climate systems are known to cause widespread changes in fluvial geomorphology (Macklin et al., 2012). This could possibly explain the observed periodicities, but the specific responsible mechanism is not constrained enough to conclude causal connections.

Some of the longer periodicities coincide with centennial cycles in solar activity (Wanner et al., 2008) or resemble the ~1,500-yr Bond cycles (Bond et al., 1997). However, based on the limited consistency of these longer periodicities among various individual flood records presented in this study (Tab. 1), it is more likely that these periodicities are linked to autogenic fluvial dynamics.

4.3 Anthropogenic non-stationarity and absolute flood magnitudes

The record expressed as relative flood magnitudes is usable for identification of non-stationarity, flood intense periods, and for identifying the most extreme events that occurred during the Holocene. Ideally, the absolute discharges associated with the estimated recurrence times are also derived. For the period of observational discharge records, this can be done using the results of flood frequency analysis (Chapter 2). Such analysis includes only data from the last centuries which troubles transposition onto older records, as both climate and catchment have probably changed significantly over the last millennia, resulting in non-stationarity of the flooding regime (Knox, 1993).

From the Bronze Age onward, the Rhine catchment has seen large-scale deforestation, reaching an optimum from the Iron age until the Medieval period (Lang et al., 2003). This likely increased river peak flows due to increased hillslope surface-runoff from catchments (Ward et al., 2008). In the pre-deforestation state of the catchment, a millennial recurrence time corresponds with minimum discharge estimates of 13,250 m^3s^{-1} for the 4.7 ka BP flood (Chapter 6). Based on modeled effects of deforestation in the catchment on discharge generation (Hundecha & Bárdossy, 2004), a similar event would translate to 14,000-15,000 m^3s^{-1} for the current situation. This provides is a palaeodischarge estimate for one single millennial event only. For other similar events in the Holocene, such estimates are not available. Existing reconstructions of upland erosion by agricultural activities, however, indicate gradual deforestation since the Neolithic period (Kalis et al., 2003; Lang et al., 2003). The minor changes in flood frequency distributions (Fig. 4) give little reason to suspect major anthropogenically-induced non-stationarity further back in time.

Prior to AD ~1200, when embankment of the Lower Rhine started, the natural floodplains were much wider and probably more densely vegetated (inducing more roughness), so flood wave dispersion by inundation in the Lower Rhine valley (with a length of ~200 km), would probably also result in lower discharges than today. Additional adjustment to flood pulse propagation by large scale embankment of the Lower Rhine at the end of the Medieval period may present another phase of rapidly changing relations between absolute discharges and recurrence times. From the historical period, three important events for which discharge estimates are available are the AD 1342, 1374, and 1658 floods. These are respectively associated with recurrence times of 300, ~2000, and 500 years (this study). Their respective estimated discharges are ~12,500 m^3s^{-1} (at Cologne; Herget & Meurs, 2010), ~15,500 m^3s^{-1} (at Lobith; the minimum Cologne discharge of ~18,800 m^3s^{-1} from Herget & Meurs, 2010, is assumed to be limited by downstream dike breaching and overflow of the low valley shoulders; Lammersen, 2004), and 12,600 – 15,500 m^3s^{-1} (at Lobith; from floodplain lake flood beds; Chapter 5). Although it is speculative to draw straightforward conclusion from this limited set of paired recurrence times and discharge estimates, it is suggested that this data is in general agreement with the flood frequency curves fitted to discharge dataseries of the last centuries (Chapter 2). From this it can be assumed that highest-observed discharges do not indicate a rise of extreme flood levels due to anthropogenic adjustments in the last millennium.

At this point, further assessment of non-stationarity is challenging, especially for floods of lower magnitudes, due to a lack of suitable data. Analysis of modern discharge data (Chapter 2), catchment modeling (e.g., Ward et al., 2011), and varying flood intensities (this study) suggest that moderate floods are more strongly affected by non-stationarity than extremes. This stresses the importance of further research aimed at identifying the various causes and (linear or cyclic)

effects of non-stationarity in the flooding regime. Additional studies aimed at absolute discharge reconstructions can (i) further constrain uncertainty in existing palaeodischarge estimates, (ii) provide more independent estimates for translating relative flood magnitudes in discharges, and (iii) result in increased temporal coverage to assess non-stationarity, including floods of lesser magnitudes. If absolute discharge estimates can be transposed onto contemporaneous palaeochannel sequences, discharge estimates can be derived for complete chronologies, including floods as minor as bankfull discharge. Combination of geomorphology and reconstructions of catchment and floodplain vegetation density with hydrological modeling, and geomorphological studies focusing on deriving discharge characterisation from the palaeo-competence (e.g., reflected in meander wavelengths, channel size, levee size; Baker et al., 2002) may further produce data which can be used to quantify non-stationarity of the flooding regime.

5 Conclusions

The Holocene flood record of the Lower Rhine, presented in this paper, suggests that increased flooding activity of the last decades is not anomalous in terms of the magnitudes of floods or the frequency of large events. Events exceeding magnitudes of recent floods are numerous; most notable events of millennial recurrence times occurred in AD 784 and 1374, and 4.5, 4.7, and 6.2 ka BP (Fig. 2). These extreme floods presumably had a wider geomorphological impact, as these periods are associated with regional changes in fluvial environments recorded both upstream and downstream in the catchment.

Non-stationarity of the flooding regime is evident from temporal variations in flood intensities for different flood magnitudes, encountered periodicities in flood deposition, and changing flood recurrence-magnitude curves. The frequency of major floods varies strongly over the past millennia, with several phases of relative intense flooding (e.g., AD 300-700 and 1700-2700 BC) and periods of reduced occurrence of major events (e.g., Little Ice Age, AD 800-1000, and AD 300 to 1200 BC; Fig. 3). The timing of extremes seems to lack a straightforward correlation with phases in flood intensity, which is in line with conclusions from previous research.

Periodicity in flood deposition is encountered in all sedimentary records. Comparable cycles in flooding are distinguished at multiple sites, ranging from conspicuous variability around multi-annual and a ~35-year band, to more scattered (multi-) centennial cycles (Tab. 1). At this point, similarity of these periodicities to known cycles in North-Atlantic climatic systems suggests causal links, but are not conclusive, since many site-specific factors (e.g., sample resolution, accuracy of age-depth modeling, and pseudo-cyclic geomorphological processes) may produce comparable results. The presence of periodicities in flooding regimes does nonetheless suggest that flood deposition is also not stationary across short intervals.

Strongest anomalies in the shape of flood magnitude-recurrence curves are encountered in the last millennium (Fig. 4). The last century is, however, fairly comparable to the flooding regime of the Middle Holocene. Comparison of flood magnitudes during the Holocene is restricted to relative flood magnitudes based on recurrence times. A conversion of flood magnitudes into absolute discharges is restricted to several individual events, for which hydraulic conditions could

be reconstructed. Insufficient data is currently available to perform relative-absolute data conversion for the entire dataset – especially for floods of smaller magnitude.

Acknowledgements
Local municipalities and landowners are acknowledged for granting access to the various research locations. J.F. Berger (Obresoc-project, University Lyon2, France) is cordially thanked for sharing age and grain-size data collected for the Schriek research location. H. Bos (ADC) selected and determined macrofossils for radiocarbon dating. F. Bunnik (TNO) provided palynological scans for first age indications of sampled material. Utrecht University students T. Konijnendijk, A. Geurts, B. van Munster, M. de Molenaar, T. Winkels, J. Aloserij, J. Ypma, VU University Amsterdam students M. Huisman, M. Bas, Utrecht University staff W. Hoek, C. Roosendaal, P. Minderhoud and G. Erkens, and VU Laboratory personnel M. Konert, M. Hagen, R. van Elsas, W. Wentink and J. van 't Hoff are thanked for support in the field and laboratory. H. Middelkoop is acknowledged for comments on an earlier version of this manuscript. K. Cohen and Q. Lodder are acknowledged for writing the research proposal for this PhD-project. This research was funded by Deltares BGS, TNO Geological Survey of the Netherlands, and Utrecht University.

8 Synthesis

The main aim of this research was to gain understanding of river flooding regimes over longer periods – as this is key in assessing flood risk levels – by developing new approaches for unlocking sedimentary archives for the construction of flood records. Extending flood record length back in time from ~110 years to multiple millennia generates information about temporal changes in flood intensities, extremes (size and occurrence), and relations between (climate) forcings and major events. The flooding history and sedimentary archive of the river Rhine in the Dutch-German delta apex region was used in this study to develop the general methodology, to evaluate its performance, and to demonstrate gained insights in flooding extremes and temporal variability.

8.1 Main conclusions

8.1.1 The use of alternative documentary information

By compiling, cross-correlating, and screening water level and discharge data from gauging stations in the Dutch-German border region, it was possible to extend annual peak discharge information for the Lower Rhine back to AD 1772 (Chapter 2). This made the data series used for flood frequency analysis ~2.5 times longer than previously used series. It puts frequency-magnitude relations for the current situation in a slightly different perspective, as over a ~240 year window, large floods (>11,000 m^3s^{-1}) appear more rare than considered over 20th century data alone. This confirmed generally assumed limitations of the suitability of relative short discharge records for estimating the magnitude of very rare events, and demonstrated the added value of alternative data types in flood frequency analysis. An important conclusion is that incorporation of less precise data types can help to decrease the uncertainty range associated with the estimated discharge of design floods. It also demonstrated that the precision of historical observational data, at least in the Rhine case, is less important than the choice of extreme value distribution and the data series length.

The extended dataset reveals variability of flood intensity over multi-decadal periods, which confirmed the existence of a temporally highly variable flooding regime. No clear linear change of the flooding regime in the last ~240 years is observed. Decades of high flood intensity, such as experienced in the last decades, have historical counterparts, for example in the early 19th century. From this it was concluded that no major further detrending of the compiled observational discharge series was necessary to use it in flood frequency analysis. The observed variability in the occurrence and magnitudes of floods is to be considered an intrinsic part of the system and should therefore be incorporated in flood risk assessments, especially for measures designed to protect for centuries in the future.

Extension of the flood record back to AD 1350, using historical descriptions of dike breaches, further demonstrates the presence of multi-decadal variations in flood intensity. Although extension into this period makes the record include two events that *exceed* the largest floods of the 18-20th century, experimental inclusion of this period in flood frequency analysis resulted in a significant *decrease* of estimated discharges of rare events. Contrasting with the record extension towards AD 1772, the use of older historical data is not improving flood risk assessment for the present

situation, as it includes the Little Ice Age, which featured a completely different flooding regime (as confirmed from sedimentary records; Chapter 5 and 7). This probably biased flood frequency estimates importantly.

8.1.2 Preparing sedimentary archives for flood records

To investigate general trends in flooding and the timing of largest floods during the Holocene (millennial floods), records longer than the historically documented period are required. These can be obtained from sedimentary archives of Lower Rhine. The first step in unlocking depositional flood records was to identify suitable research locations. Subaqueous environments in the floodplain collect fill with consecutive floods, are unaffected by pedogenic homogenisation and agricultural overprints, and contain deposits that are suitable for dating purposes. Residual fills of abandoned channels are natural examples of such sites, and many of them exist in alluvial valleys and delta plains, albeit of different types. An inventory of abandoned channel fills of the Lower Rhine ruled out avulsion-abandoned channels and oxbow lakes in distal parts of the floodplain as suitable for detailed flood registration (Chapter 3), and attention was focused on oxbow lakes and dike breach scour holes with relative proximal position to the active channel. The proximity for sites was determined from sedimentary facies of the fill and (previous) regional geomorphological mapping and dating campaigns.

Oxbow lake fills with reasonable proximity to the active channel (1-3 km typically) record relatively long periods (several centuries to millennia), yield sufficiently thick flood beds for individual sampling and analysis, and contain registration of events ranging from just exceeding bankfull discharge to most extreme events with accordingly differentiation in grain-size of deposits. Trends in general channel fill sedimentology reflect phases of changing river channel proximity (by natural bend migration and/or chute cut-offs; Chapter 4) and more local geomorphological factors influencing connectivity with the main channel (Chapter 5). Using change point trend breaks and Z-score standardisation methods, sedimentary intervals were separated, detrended, and normalised, allowing comparison of flood magnitudes in different sections (Chapter 4 and 5).

From two research locations, both covering the same period and part of the sedimentary sequence overlapping with discharge series of the last ~240 years (Chapter 2), it was tested how well specific grain-size descriptors perform as proxy information for discharge quantification. Although median and mean grain-sizes are commonly used to characterise flood beds, it was concluded that especially descriptors of the coarse tail of grain-size distributions, such as the 95th percentile and modeled proportions of coarser End-Members, allow for accurate discharge estimation (Chapter 5). These descriptors were used to formulate a relation between grain-size and discharge on the period after AD 1772, which could be applied to estimate historical flood discharges in the lower parts of cores. This way, quantitative estimates for peak discharges of historical floods in the period AD 1550-1772 were provided, of which magnitudes correspond well with qualitative magnitude indications from historical records. The two investigated sites in the same region produce similar flood chronologies, albeit that persistent offsets in discharge estimates occur. This was mainly attributed to local geomorphological factors that influenced the calibration period.

Based on the good correlation of flood beds with contemporaneous historical records, an event-stratigraphic approach was successfully tested; the position of coarse flood beds in the age-depth modeled core corresponded well with the historical dates of catastrophic floods. The event-marker

functionality of distinct relatively-coarsest flood beds is neither restricted to cored sequences at individual sites, nor to historically known largest events from the last centuries. Their event-marking applies regionally across the wider floodplain and can be made used of in prehistoric time too. The timing of extreme floods matches that of major changes in floodplain configuration (Chapter 4) and independent records of change in fluvial geomorphology in both upstream and downstream regions (Chapter 7).

Moreover, general channel fill sedimentology has proven to be suitable as a proxy for sediment accumulation rates and can be used for improvements to traditional (stepped) age-depth models (Chapter 4). Although this approach has currently not yet been applied to its maximum potential for all investigated locations, Chapter 4 demonstrates the potential use of sedimentological information for age-modelling purposes.

8.1.3 Extreme floods

Building on the developed methodological concepts, a composite sedimentary flood record was created in a network of sites, with temporal overlap and covering a large part of the Holocene period (Chapter 7). The composite record shows that largest floods of the Lower Rhine, exceeding a millennial recurrence time, occurred at AD 1374, 784, and 4.5, 4.7 and 6.2 ka BP. None of these floods occurred in the last centuries, nor are they included in current flood frequency analyses for design flood assessment. Statistical estimates of magnitudes for rare events (century to millennial recurrence times) are however highly sensitive to the inclusion of extremes (Chapter 2). With the increased knowledge on the pre-historical timing of millennial floods, these extreme events should now also be incorporated in flood risk assessments. Sedimentary records clearly shows that in the Holocene past, a considerable number of events has also exceeded flood magnitudes recorded in the last centuries. The discharge attributed to floods of millennial recurrence, however, has likely changed through time, mainly due to anthropogenic changes to the catchment (deforestation and river training). Discharge of the AD 1374 flood has previously been numerically estimated to may have exceeded 18,800 m^3s^{-1} at Cologne (Germany; Herget & Meurs, 2010), which is considerably larger than the current design discharge for flood protection in the Netherlands (16,000 m^3s^{-1}). It is suspected that such a discharge peak would not reach the downstream Rhine Delta without dispersing, when floodplains get inundated and dikes are overtopped (if not breached) along the Lower Rhine valley between Cologne and Lobith (e.g., Lammersen, 2004).

In the Middle Holocene, millennial floods are considered to have had lower peak discharges. Hydraulic modeling of slackwater deposits on elevated fluvial terrace levels indicates that the 4.7 ka BP flood event exceeded at least ~13,250 m^3s^{-1} (Chapter 6; Toonen et al., 2013). Further studies – cross-validating the above quoted results at other points in the valley, for example – may produce better estimates on the physical limits to the size of extreme floods of the Lower Rhine posed by upstream geomorphology and the maximum amount of precipitation in the catchment area. Major changes in the floodplain and catchment since the 4.7 ka flood (and 4.5 and 6.2 ka counterparts) can only partly explain the difference in discharge. Tentative correction of the 4.7 ka BP flood allows to translate its palaeodischarge into 14,000-15,000 m^3s^{-1} in the modern situation. Precise information about the discharges of all major floods, however, is still largely lacking. Based on the results of this dissertation, and considering limits to downstream flood pulse propagation, it is suggested that the upper limit to discharges that can reach the apex area of the Rhine Delta is roughly the same as current safety standards. Thus, it can be concluded that current dike heights

(designed to protect against ~16,000 m^3s^{-1}) are meeting a safety level which corresponds at least with a 1,250-year recurrence time.

8.1.4 Non-stationarity of the flooding regime

Non-stationarity of the Rhine flooding regime is discussed in its various forms in several chapters. In Chapter 2, it was demonstrated that the flooding regime has been highly variable over the last centuries, with clear fluctuations on a (multi-)decadal scale. It remains unclear from this study specifically if intensified flooding of the last decades (e.g., the AD 1993 and 1995 floods) fits the natural variability of the past centuries or is to some extent the product of anthropogenic changes to river system and climate system combined. Reconstructed flood intensities are very high for this period, but in view of the longer data series made available not classified as anomalous. Moreover, in this relative short interval (~240 years), no major systematic changes are identified that can directly be related to permanent changes in the river system, such as the construction of upstream weirs or channel normalisation. Observed non-stationarity of the last centuries is periodic (Chapter 7) in cycles of 3-7 years and a cycle of ~35 years, which suggests that this type of non-stationarity is induced by climate. Millennial flooding, however, shows no clear relation to periods of high flood intensities (Chapter 2 and 7), suggesting that these are anomalous in every regard and *not* simply a result of periodic changes in intensified or increased precipitation.

Implications for long-term non-stationarity come from the composite flood record (Chapter 7), which shows various periods of anomalous occurrence of moderate and large floods (sub-millennial recurrence time). Periods of frequent flooding are for example 1,700-2,700 BC, AD 300-700, and the last two centuries. Periods of reduced flooding occurred around 1,200 BC – AD 300, AD 800-1000, and during the Little Ice Age, which for the latter matches with results of historical records analysis (Chapter 2). Within these anomalous periods, the recurrence time-flood magnitude distribution of floods is different, most evidently illustrated in sedimentary records and from historical records for the Little Ice Age (Chapters 2, 6, and 7).

A different type of non-stationarity, related to 'permanent' changes in the catchment, mostly due to anthropogenic influence, is also observed in flood deposition. In combination with the numerical discharge results (Chapter 6), recurrence times of the 4.7 ka BP millennial flood could be translated in absolute discharges – resulting in ~8-17% lower discharges than floods of the same recurrence time estimated from statistical extrapolation of discharge records (Chbab et al., 2006; Chapter 2). Still the conversion of Middle Holocene discharges to present day discharges comes with large uncertainties, as no accuracy estimates exist on the absolute effect and pace of human-induced changes on catchment and floodplain vegetation, and the effective translation of precipitation into discharges.

8.2 Further research

8.2.1 Improvements to the current methodology

The main approach to improve the quality and representativeness of flood records (either from individual sites or the composite record) involves refining dating methods and increasing data density by adding more sites. Increased understanding of the translation of sedimentological data

in flood discharges, and the relation of statistical extrapolation curves with hydrological concepts deserve equal attention, as there is much progress to be gained also in these parts of flood research. As the basic single-core flood records are based on dating information and sedimentary characteristics of flood deposits, advancements can be achieved by improving the dating techniques and the analysis of sedimentary data for flood magnitude reconstructions. In general, in clastic channel fills suitable organics for AMS dating are not easily available. Thus, dating cannot simply be improved by densification of spot sampling for radiocarbon dates. Most traditional dating methods are unsuitable in clayey deposits, but a promising approach, currently under development in affiliation with this research, is to use palaeosecular magnetic variation signals. These are recorded in the clayey channel fills and relate to historical positions of the magnetic pole (Ojala et al., 2002). If such information is combined with traditionally collected radiocarbon dates and non-linear age-depth modeling incorporating continuous sedimentological information (Chapter 4), chronological cross-correlation of sites in the investigated network can improve greatly.

Another dating improvement, which becomes increasingly important at secondary levels of data integration (combining multiple records), is to make use of so-called 'event stratigraphy'. Chapters 4 and 7, clearly demonstrate that especially the largest events are traceable between individual records spanning the same period in the main trunk valley of the Rhine. Major events are also associated with major regional changes in geomorphology (e.g., river migration events). Coupled calibration of datings of such synchronous events decreases uncertainty in age-depth models of individual sites (Chapter 4). Furthermore, they can be used as stratigraphic markers in chronologically poorly resolved sequences – or at newly cored sites of broadly known age. Such stratigraphic markers are not restricted to the specific research area and fills of abandoned channels; major flood events will probably have their imprint in geomorphology, sedimentology, floodplain vegetation and human occupation along the entire trunk valley of the Rhine and in the downstream delta. This may tie important regional changes reflected in different proxy records together, and makes it possible to differentiate between possible causes of regional changes in the palaeo-environment in a fluvial setting.

The dissertation demonstrates that flood magnitudes can be inferred from grain-size measurements. Discharge estimations are restricted to sites where part of the record can be calibrated to an observational data series with partial temporal overlap. Further work should try to make such inference more generic, so that it can also be applied to older segments of the composite record, with means to validate the results. Laser particle sizing of the coarser tail of the grain-size distribution in flood beds is the most accurate approach to differentiate between flood magnitudes in pre-historical times. The methodology can be expanded by including other proxies than grain-size parameters alone, such as geochemical XRF-scans (e.g., deployed by Jones et al., 2012).

Sedimentary sequences that have overlap with the observational discharge series or case-based reconstructions of palaeofloods (Chapter 6) have good potential to provide quantitative palaeodischarge estimates, though relative large variability in discharge estimates can occur. For example, changes in local floodplain and plug bar morphologies, flow velocities, and hysteresis effects in sediment loads (Chapter 5) may introduce considerable uncertainty. These factors are challenging to reconstruct in prehistoric times. For pre-historical sedimentary sequences, grain-size derived flood magnitudes at this stage can only be expressed in a relative sense: as coarse-tail descriptor Z-score in individual cores and as the statistical recurrence time in the compiled record.

Adding more temporally overlapping sites in a regional network of flood records will increase the quality of ensemble flood estimates considerably, and could produce palaeodischarge estimates further back in time through indirect overlap via other cored sites with discharge reconstructions or measurements. This is an important asset of the developed methodology: the network is expandable while the compilation iterates.

8.2.2 Non-stationarity

The gained experience and methodological development with a first network of sites provides important clues and opportunities on how to quantify non-stationarity and how to proceed in assessing it (from river safety management to Holocene palaeoclimatology). Many more opportunities for case study and reconstructing palaeodischarges for specific events are possible in the Rhine Delta and valley, especially for millennial floods. When such are carried out, it provides further tie-points for translating relative flood magnitudes into discharges. This can also constrain discharge estimates of individual floods and produce more detailed insight in the issue of non-stationarity. Simultaneously, if individually reconstructed flood discharges can be tied to Z-scored flood deposits in continuous channel fills, a site-specific relation can be established between absolute discharge and Z-score (similar to the approach for historical floods; Chapter 5). This relation can be used to convert entire flood chronologies, including smaller events, from oxbow fills into discharges, and unlock this information for assessment of non-stationarity.

Environmental information should be exploited in hydrological modeling; input from a set of slackwater deposits can be used to set stage-discharge relations in a specific period and region. Updating such relations with estimates from smaller floods will fine-tune the model's sensitivity and accuracy. To model the effects of linear non-stationarity by deforestation or river management, upstream proxy records on flooding, geomorphological changes, sediment budgets, and vegetation can probably be used to as input to refine models. Modelling of such mixed upstream signals may produce important reference for non-stationarity assessments in downstream flood records.

Once sufficiently understood, quantification of the effects of non-stationarity (and its causes), produces valuable information for assessing a river's response to permanent and (semi-)cyclic perturbations. This allows quantification of possible future responses of the fluvial system and flooding regime to climatic and anthropogenic induced changes, and would allow engineers to design sustainable flood defenses, which are not only valid for the current situation but remain equally robust in slightly changed conditions that are native to natural systems.

8.2.3 Exploring upstream-downstream relations

This study was carried out in the apex area of the Rhine Delta, specifically focusing on the river stretch downstream of the last major tributary and upstream of deltaic distributaries to represent the flooding regime of the full river Rhine. Although by-proxy records for flooding are available from both upstream and downstream regions, direct comparison with the current record is difficult due to important regional differences and record types.

Major limiting factors for using upstream records are the entrance points of main tributaries, which may add vast amounts of discharge. For the Rhine, large discharges of the Moselle, Neckar, and Main (besides the Upper Rhine) are required to generated downstream flooding. Major flooding in an individual tributary of a large river basin as the Rhine, however, may not produce a major

downstream peak flow. Indeed, large discharges recorded for the Upper Rhine (Wetter et al., 2011) are fairly poorly related to major flooding of the Lower Rhine.

To add to the complexity of flood pulse propagation, the configuration of a river network is important in probabilities of generating large discharge volumes. In the Rhine catchment, the Moselle and Main are positioned very closely to each other. Hence, largest discharges are generated by simultaneous arrival of the discharge waves from these catchments, rather than just large discharge volumes from individual catchments or asynchronous flood wave arrival (Disse & Engel, 2001). Changes to the general direction of cyclonic pathways or travel time of flood peaks in the catchments (by deforestation or river management; Vorogushyn & Merz, 2012) may alter probabilities of discharge peaks of multiple catchments to assemble in a catastrophic flood. On a more abstract level, the geological-geographical configuration of the Main and Moselle (following the same west-east alignment, similar to cyclone pathways, and discharging into the main Rhine in the same region) is unfortunate for downstream regions; if spaced further apart discharge volumes would likely smoothen, and reduce the likeliness of simultaneous flooding caused by the same cyclonic depression and subsequently the magnitudes of largest events. Otherwise, the large pro-Alpine lakes buffer large flood pulses from the Alps. Such basins exist in the upstream regions of many larger rivers. Consequently, devastating (flash) floods in the areas upstream of these lakes are not necessarily reflected in downstream peak flows (Schulte et al., 2009; Wetter et al., 2011).

The configuration, complexity of the river network, and the existence of large flood-buffering lakes makes it very difficult to compare flood records from sub-catchments, tributaries, and upper reaches already for a moderately-sized river such as the Rhine, but is probably even more challenging in large rivers; such as the Mississippi, Nile, Yangtze, Huang He, and Mekong, all having densely populated flood-prone downstream regions. To assess flood pulse generation, propagation, and periodicities in flood intensity, investigating a single downstream region of such large systems would probably not give all answers needed to understand dynamics (and dominant forcings) of the flooding regime – although it will assess regional flood risk. Therefore, also many upstream catchment areas and intermediate positions in the main trunk valley need to be studied of complex systems, and combined in more synthesising studies which focus on understanding the entire system, and mechanisms behind the occurrence of flood intense periods and single extreme events.

Records describing river avulsion intensity in the delta downstream (Stouthamer & Berendsen, 2001), and records of phases of geomorphological stability and change in the catchment upstream (Hoffmann et al., 2008) each contain information on flooding variability. With the results of this study as an independent third record, it has now become possible to compare records, and to identify imprints of largest floods on upstream-downstream geomorphological record. This may also allow to integrate the results of different studies. Moreover, further flood records exist describing geomorphological changes over multiple catchments areas (Macklin et al., 2006), and even on an intercontinental scale (Macklin et al., 2012). Unlocking, gathering, and combining different types of flood records, focusing on periodicities in flood intensity and the timing and spatial distribution of extreme events, may produce valuable insights in responsible large-scale forcing, and allow separation of variability induced by local settings.

8.2.4 Flood forcing factors

Although many different periodicities in flood layer deposition are encountered (Chapter 7), these are difficult to relate directly to responsible specific large controls. This is in the first place due to the many site-specific factors and inaccuracies in age-depth models that may obscure straightforward recognition. Moreover, understanding of mechanisms translating periodicities in the climate system into flood layer deposition is still lacking, which does not allow stretching conclusions of our periodicity analysis further than 'it independently detects similar cycles in several cores'. Depending on the configuration and altitude of individual catchments, flood records from upstream regions will reflect imprints of cyclonic depressions or thawing snow more directly (for the Rhine). Downstream, the discharge of heterogeneous catchments and flooding regimes will blend in a bulk – in which specific climate signals may not be preserved as well in more upstream locations, where specific forcings will have a more direct connection with local flooding. Therefore, to identify specific variable forcings behind the observed flood records (e.g., NAO patterns, solar cycles), continuous records from upstream regions are probably most successful (e.g., pro-Alpine lakes; Czymzik et al., 2013).

Besides collection of flood records along different stretches of the river, coupled climate-hydrological modeling, comparison with other terrestrial proxy records for climate change, and understanding of lagged responses in fluvial systems are necessary to understand perturbations that cause non-stationarity in flooding regimes. As demonstrated in this dissertation, the downstream flood record provides a starting point for tying together different records. Especially specific anomalous periods of flooding and the precise timing of extremes are worth further investigation, and may prove key in targeting, identifying, and resolving important forcings. In this scope it is important to have a close look at alternative proxy records for climate change in the same catchment area, but not directly reflecting flood dynamics. Such records (e.g., vegetation dynamics), may produce similar patterns as observed in flood records, and can such be used to isolate responsible forcings.

Appendix A: Supplementary Material Chapter 4

S1. Rheinberg meanders and the millennial flood marker downstream

The main text equates the cut-off event creating Rheinberg Meander A (the main site) to an event marker bed for a rare magnitude flood identified and dated at a locality ~25 km downstream in the Lower Rhine Valley (Fig. 1 and Tab. 1 in main text Chapter 4).

The claim that the flood downstream is of 'millennial' magnitude comes from:
The setting in which the markers were encountered: it is one of two such beds in ~2500 to ~5000 years of organic channel fill, in an Younger-Dryas/Early Holocene terrace adjacent to regularly inundated floodplain at the time ('high floodplain terrace'). It roughly implies this magnitude events to have occurred once in 1250 to 2500 years (Chapter 6).

Stage-discharge calculations for a cross-section at most-suitable location in the direct vicinity of the site, resulting in a 13,250 m^3s^{-1} Best Guess Estimates(12,000 – 15,000 m^3s^{-1}: most probable range), which is larger than any flood in the 20th-21th century record, and under modern circumstances approximates the current design flood discharge (15-16,000 m^3s^{-1}). See Chapter 6.

The overlap of the radiocarbon dates UtC-15064 and SUERC-37131 is mentioned in the main text and also date UtC-15065 falls within that time period. In isolation, this would make a couple more scenarios for combining dates and calibrating ages possible. These scenarios are formulated in Table S1 and S2 below, and evaluated incorporating the oxbow fill sedimentological observations and explanation. The scenarios combine the millennial flood marker date to 1) Meander A cut-off; 2) Meander B cut-off, 3) the 699-cm event layer, and tie the Meander B cut-off event to a) the Phase II/III transition and b) the 699-cm event layer. LOI-tuned age-modelling and consecutive event count results (section 5.2) are used to estimate the amount of time separating base oxbow from Phase II/III boundary and the 699 level. Only Scenario 1 turns out to be internally consistent. Scenario 2 and 3 fail to comply with the sedimentological constraints (Table S1 top row). Scenario 4 might be regarded sedimentologically consistent, but worsens the initial problem (main text and Erkens et al., 2011) of explaining the formation and preservation of two meanders in very little time. Also, from the comparison of F.I. and CPDFs (main text), Scenario 1 gains support and 4 does not.

Table S1: Evaluation of correlation scenarios.

Table S1: Evaluation of correlation scenarios

	Meander A abandonment (Phase I)	**Meander A fully disconnected / begin oxbow lake filling (Phase II/ III transition)**	**Meander B abandonment**	**699-cm event in Meander A's oxbow-fill (within Phase III)**
Constraints from oxbow fill sedimentology and geomorphology				
All scenarios must comply:	Plug bar and topping levee result from sedimentation delivered by Meander B, and morphology is preserved. Meander B cannot have migrated towards the site much, it must have existed more or less in its preserved position, at the moment that Meander A began plugging.		Is either registered as the 'change point' bounding Phase II/III, or as some LOI-spike of modest Z-score within Phase II.	Background facies below and above the spike is the same: No proximity change, and therefore the 699-cm spike does not equate to Meander B abandonment.
Order of events scenarios, with calibrated ages for these scenarios				
Scenario 1 consistent, preferred	Was caused by a millennial flood, known from a downstream site: ~4720 ±70 cal BP *	Took about ~80 years. Coincided with Meander B abandonment at ~4640 ±100 cal BP ***	Occurred before the event registered at 699-cm, at ~4640 ±100 cal BP ***	Marks a centennial flood. Post-dates the millennial flood, by some 180-200 years, at ~4525 ±70 cal BP †.
Scenario 2 ***Sedimentology inconsitent***	Occurred before the millennial flood; ~4810 ±75 cal BP ******	Took about ~100 years. Coincided with Meander B abandonment *and* the downstream millennial flood marker at ~4730 ±30 cal BP *****	Was caused by a millennial flood known from a downstream site; ~4730 ±30 cal BP *****	Marks a centennial flood. Post-dates the millennial flood, by some 80-100 years, at ~4620 ±75 cal BP †.
	No particular large or coarse bed is recognised amongst the consecutive flood beds in Phase II, making it unlikely that a very large event affected Meander B within 100 yrs after Meander A was cut-off.			
Scenario 3 ***Sedimentology inconsistent***	Occurred before the millennial flood; ~4865 ±120 cal BP **	Took about ~100 years. The Phase II/III transition is controlled by plug-bar and levee formation only: Meander B abandoned ~100 yr after.	Simultaneous to a millennial flood; 4670 ±80 cal BP ****	Marks the millennial flood. Post-dates Meander A abandonment about 200-300 years: 4670 ±80 cal BP ****
	Fails to comply with sedimentary-infill constraints of the background facies below and above the 699-cm spike.			
Scenario 4 ***(too) little millennial event impact, further complicates Meander A+B dating/interpretation mismatch***	Occurred before the millennial flood; 4825 ±100 cal BP ******	Took about ~100 years. The Phase II/III transition coincided with Meander B abandonment, at 4730 ±70 cal BP ******	Occurred before the event registered at 699-cm, at 4730 ±70 cal BP ******	Marks the millennial flood. Post-dates abandonment of both Meander A and B: 4670 ±75 cal BP ******
	The scenario attributes the millennial event only modest sedimentary trace, and no preserved geomorphological trace at Rheinberg, and implies the co-existence of Meanders B and A to be the outcome of regular events. To explain double meander existence in very little time was already problematic before this study (Erkens et al,. 2011). The time to explain the pair of meanders in this scenario is even shorter – new collected data is not used to narrow down but to complicate.			

Ages *, **, ***, ****, *****, ******: calibration details as keyed in Table S2; †: Table 3 main text.

Table S2: Age calibration results for all evaluated correlation scenarios.

Table S2: Age calibration results for all evaluated correlation scenarios

Lab nr	Lab age ± error [14C yr BP]	Depth [m below surface]	Calibrated age mean ± 1σ [cal yr BP]	Original reference
Rheinberg Meander A, deep oxbow lake fill, central in oxbow lake.				
UtC-15064	4290 ± 70	8.5	**4720 ± 70** *	Erkens et al., 2011
			(4865 ± 120) **	
			4720 ± 60 ***	
			4810 ± 75 *****	
			(4825 ± 100) ******	
25-km downstream Rheinberg, rare-magnitude flood marker in residual channel of high floodplain terrace.				
SUERC-37131	4135 ± 30	1.6	**4720 ± 70** *	Toonen et al., 2013,
			(4680 ± 80) **	*their Fig. 4*
			4720 ± 60 ***	
			4730 ± 75 *****	
			(4670 ± 75) ******	
Rheinberg Meander B, next-younger palaeochannel fill, date not positioned central in the oxbow lake.				
UtC-15065	4100 ± 50	6.22	**4590 ± 60** ***	Erkens et al., 2011
			(4640 ± 100) **	
			(4670 ± 80) ****	
			4730 ± 75 *****	
			(4730 ± 70) ******	

Remarks

Table S2 complements data presented in Table 2 in the main text

Calibrated ages calculated with OxCal 4.1 (Bronk-Ramsey, 2010) and the IntCal09 reference dataset (Reimer et al., 2009).

* Linear model 2 result, U-Sequence() calibration, pooling dates UtC-15064 and SUERC-37131

** Individually calibrated results

*** Result of a Sequence() calibration pooling UtC-15064 and SUERC-37131, and enforcing a 80±7 years younger age for UtC-15065

**** Result of a calibration pooling UtC-15065 and SUERC-37131.

***** Result of a Sequence() calibration pooling UtC-15065 and SUERC-37131, and enforcing a 80±7 years older age for UtC-15064

****** Result of a Sequence() calibration, with UtC-15064, UtC-15065 and SUERC-37131 in this order.

S2 Digital supplement: Age-depth modelling spread sheet (MS Excel 2010)

available from Dr. K.M. Cohen, Utrecht University (k.m.cohen@uu.nl)

Appendix B: Supplementary Material Chapter 7

Bienener Altrhein
Abbrevation: BAR
Town: Bienen
Country: Germany
Coordinates: 220080; 425380 (RD)
Elevation: 10.0m +mean sea level

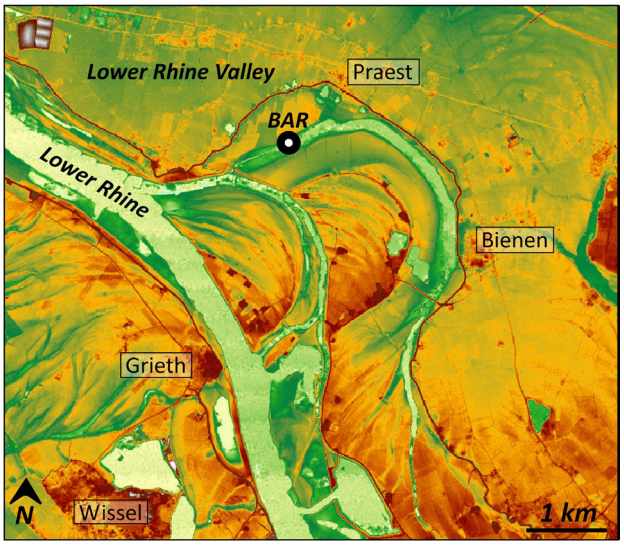

Elevation map of the BAR research area (red = high, green = low) (Landvermessungsamt Nordrhein-Westfalen, Germany; as used in Cohen et al., 2009)

Age information & Age-depth model (see Fig. 5.5 and main text in Chapter 5).
(BAR) Sedimentary data (see Fig. 5.3 and main text in Chapter 5).

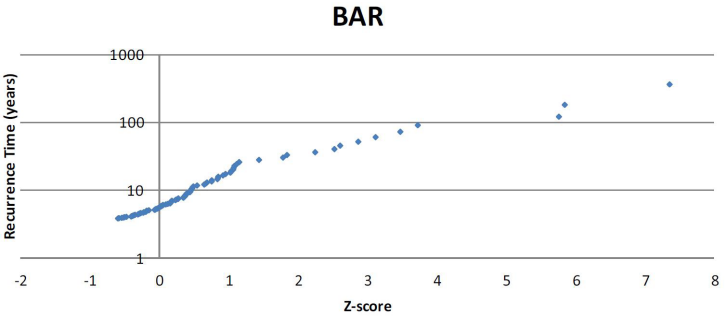

Regression plot of recurrence times versus Z-scored flood data.

Amerongen
Abbrevation: Am
Town: Amerongen
Country: The Netherlands
Coordinates: 160950; 445260 (RD)
Elevation: 5.4m +mean sea level

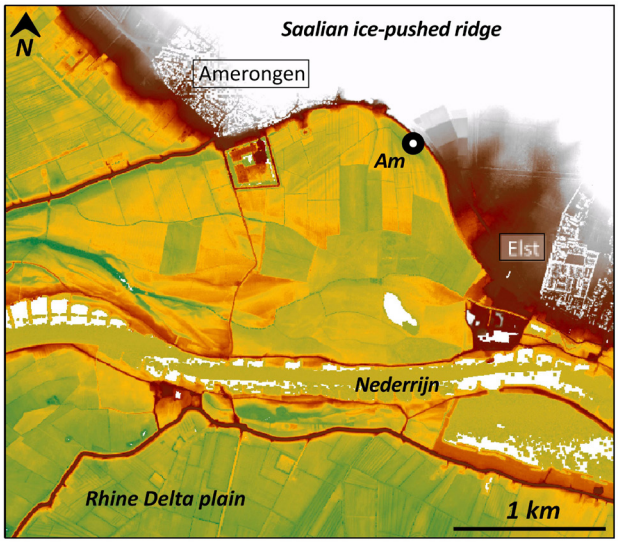

Elevation map of the Am research area (white = high, green = low) (Rijkswaterstaat-AGI, 2005).

Age Information

Age Information

Name	*Code*	*Type*	*Depth (cm)*	*Age (^{14}C yrs BP)*	*Range (yrs)*
Am2	GrA-54356	AMS-radiocarbon	117	900	35
	Salix (twigs + budscales), leaf fragments				
Am3	GrA-54357	AMS-radiocarbon	187	1190	35
	Salix (twigs, budscales), leaf fragments				
Am4	GrA-54915	AMS-radiocarbon	397	1150	50
	Leaf fragments.				
Am5	SUERC-40329	AMS-radiocarbon	649	1410	30
	Alnus (bud + budscales), *Carex* (membrane), leaf fragments.				
Am6	SUERC-40330	AMS-radiocarbon	1111	1415	30
	Fagus (leaves)				

(Am) Oxcal U-sequence age-depth model.

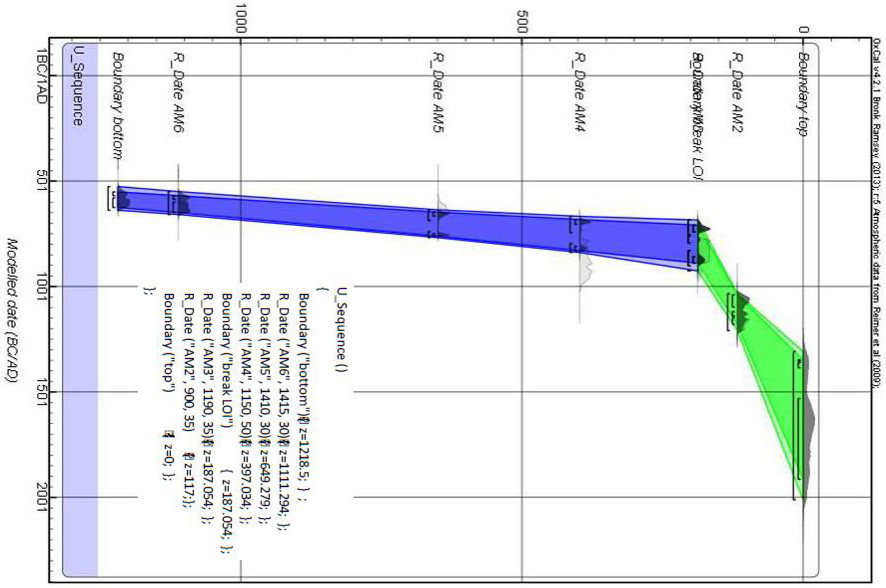

(Am) Sedimentary data

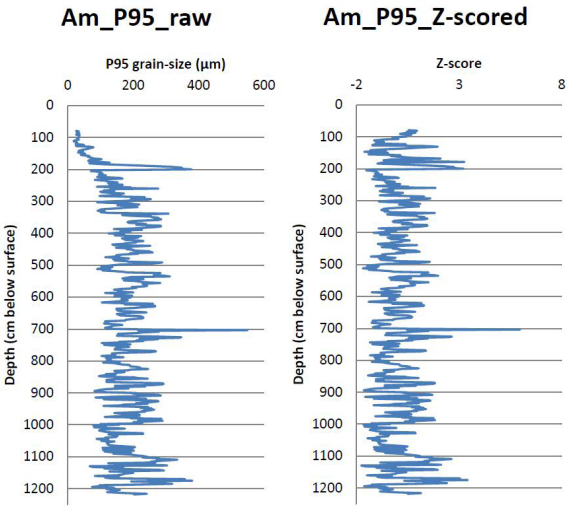

CPA trend breaks: 194/346 cm below surface (Taylor, 2000)
Confidence level: 95%
Grouping of rows: n=2

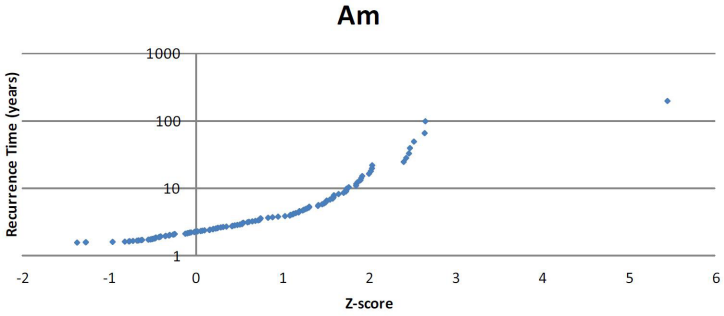

Regression plot of recurrence times versus Z-scored flood data.

Meinerswijk
Abbrevation: Mw
Town: Arnhem
Country: The Netherlands
Coordinates: 188360; 442390 (RD)
Elevation: 8.6m +mean sea level

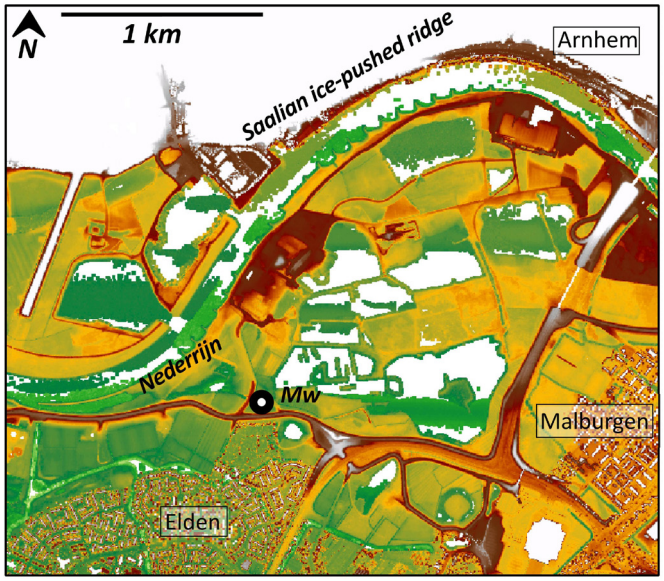

Elevation map of the Mw research area (white = high, green = low) (Rijkswaterstaat-AGI, 2005).

Age Information

Age Information

Name	Code	Type	Depth (cm)	Age (^{14}C yrs BP)	Range (yrs)
Mw2	SUERC-37136	AMS-radiocarbon	186	410	30
	Seeds: Schoenoplectus lacustris, Prunella vulgaris, Polygonum aviculare, Alisma plantago-aquatica.				
Mw3	GrA-54917	AMS-radiocarbon	357	795	55
	Salix (bark), Seeds: Scirpus sylvaticus, Juncus sp., Veronica sp., Alisma plantago-aquatica, Poa annua, Cerastrium sp.				
Mw4	GrA-54920	AMS-radiocarbon	451	820	45
	Seeds: Juncus, Urtica dioca, Veronica sp., Scirpus sylvatica, Cyperaceae sp.				
Mw5	GrA-54338	AMS-radiocarbon	801	880	35
	Seeds: Bidens cf. Tripartita, Rumex maritimus, Carex cf. Vesicaria, Ranunculus acris/repens, Alisma plantago-aquatica, Mentha aquatica/arvensis, Rorippa palustris, leaf fragments.				

(Mw) Oxcal U-sequence age-depth model.

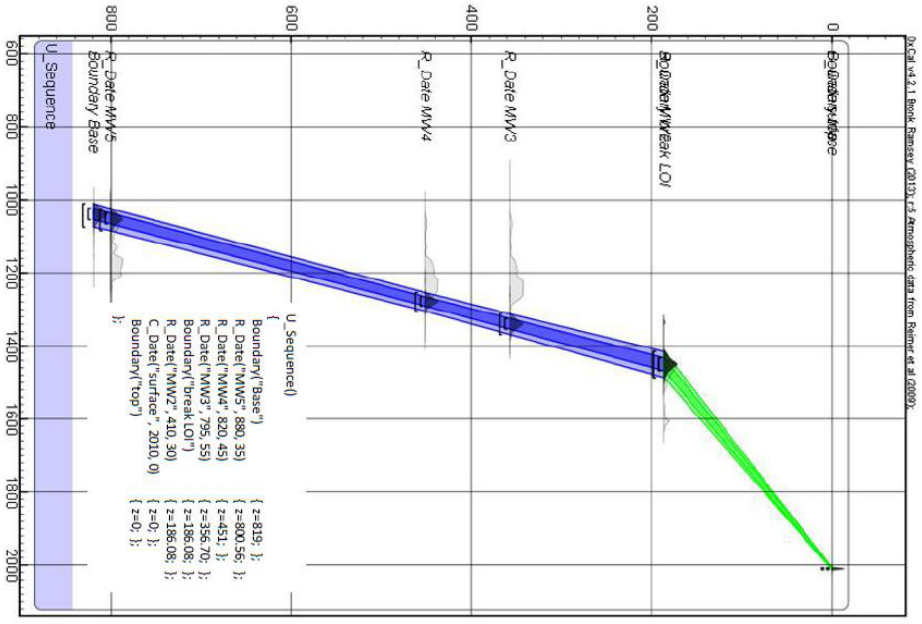

(Mw) Sedimentary data

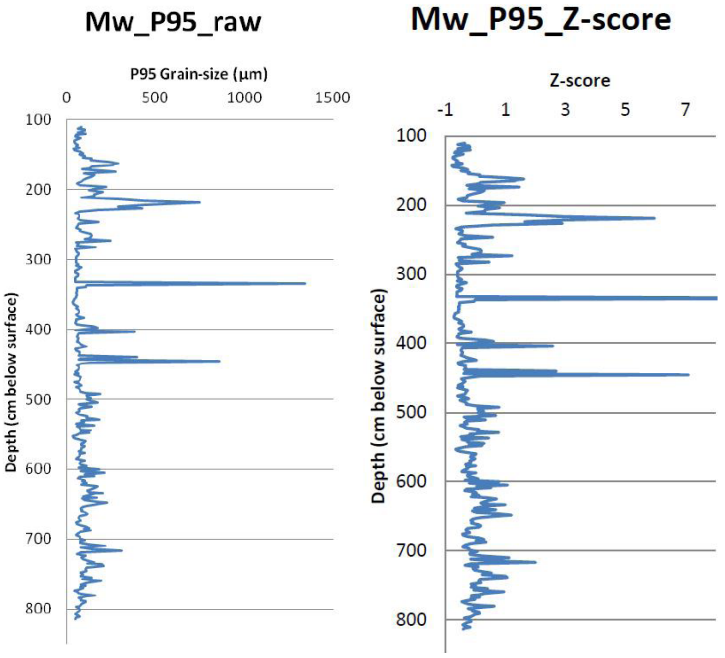

CPA trend breaks: 231/602 cm below surface (Taylor, 2000)
Confidence level: 95%
Grouping of rows: n=2

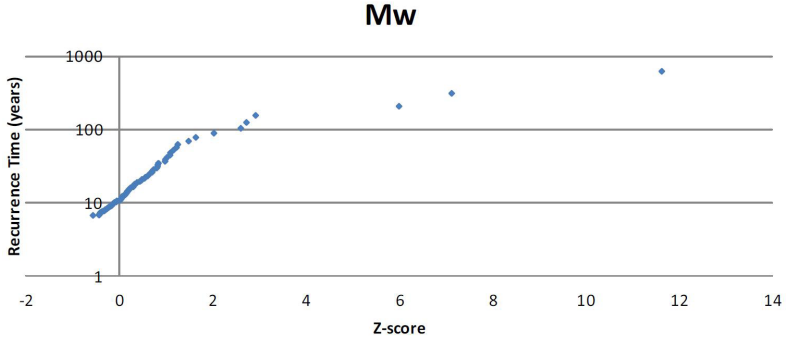

Regression plot of recurrence times versus Z-scored flood data.

Visveld
Abbrevation: Vv
Town: Lent (Nijmegen)
Country: The Netherlands
Coordinates: 187670; 431750 (RD)
Elevation: 9.0m +mean sea level

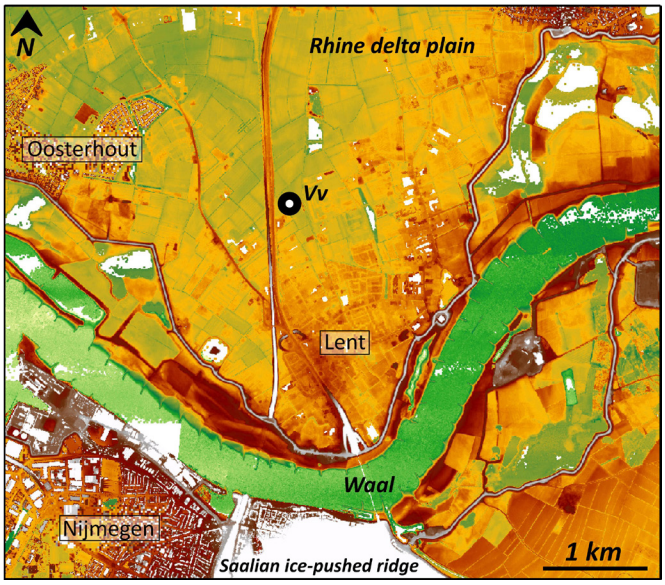

Elevation map of the Vv research area (white = high, green = low) (Rijkswaterstaat-AGI, 2005).

Age Information

Age Information

Name	Code	Type	Depth (cm)	Age (^{14}C yrs BP)	Range (yrs)
Vv2	GrA-50884	AMS-radiocarbon	375	1610	105
	Seeds: Rorippa palustris, Poaceae indet., Alisma plantago-aquatica, Ranunculus acris/repens.				
Vv3	GrA-54918	AMS-radiocarbon	450	2865	50
	Seeds: Eleocharis palustris, Rorippa palustris, Rumex sp., Leaf fragments, charcoal.				
Vv4	GrA-54921	AMS-radiocarbon	551	2910	45
	Seeds: Alnus (male catskin), Rorippa palustris, Juncus sp., Lysimacha sp., Polygonum sp. Poaceae sp., leaf fragments.				
Vv5	GrA-50885	AMS-radiocarbon	756	3000	350
	Leaf fragments.				

(Vv) Oxcal U-sequence age-depth model.

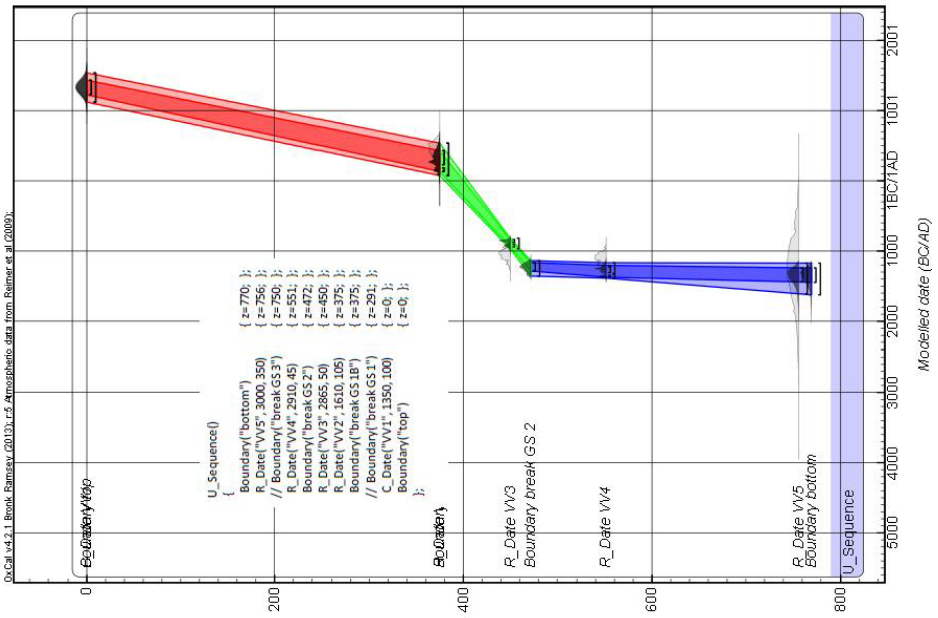

(Vv) Sedimentary data

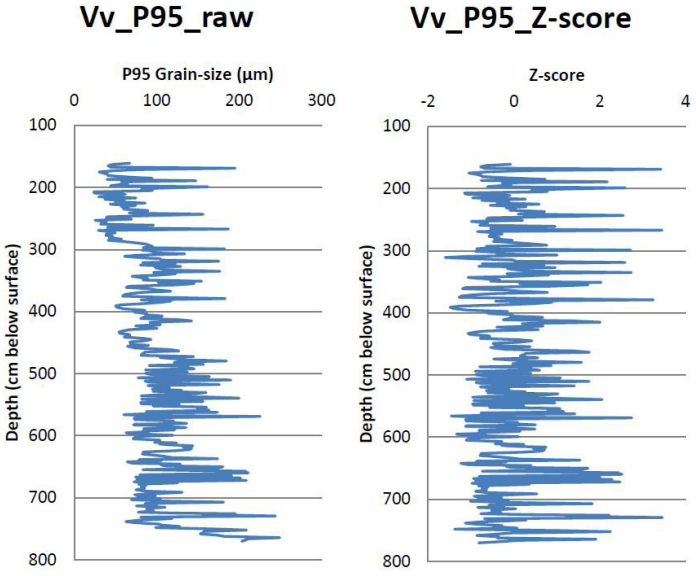

CPA trend breaks: 291/470/740 cm below surface (Taylor, 2000)
Confidence level: 95%
Grouping of rows: n=1

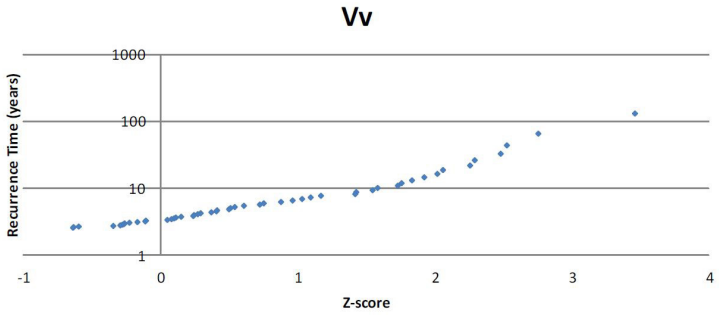

Regression plot of recurrence times versus Z-scored flood data.

Rheinberg
Abbrevation: Rb
Town: Rheinberg
Country: Germany
Coordinates: 240207; 395352 (RD)
Elevation: 20.8m +mean sea level

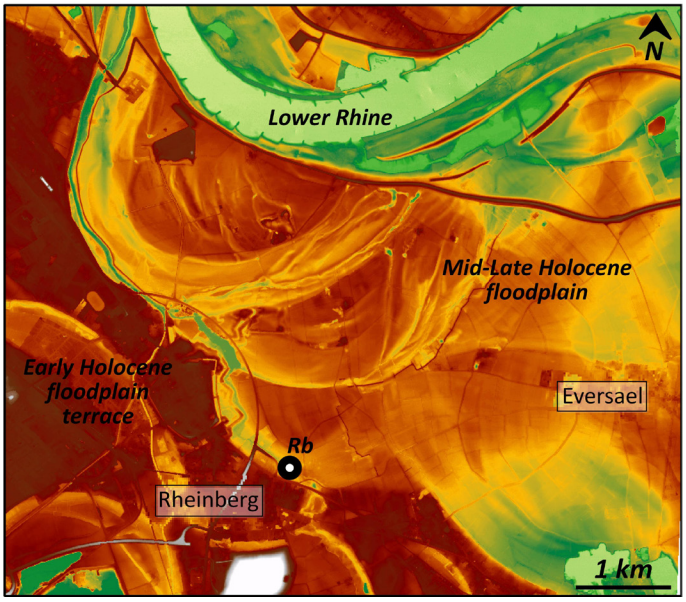

Elevation map of the Rb research area (red = high, green = low) (Landvermessungsamt Nordrhein-Westfalen, Germany; as used in Cohen et al., 2009)

Age information & Age-depth model (see Fig. 4.3 and main text in Chapter 4).

(Rb) Sedimentary data

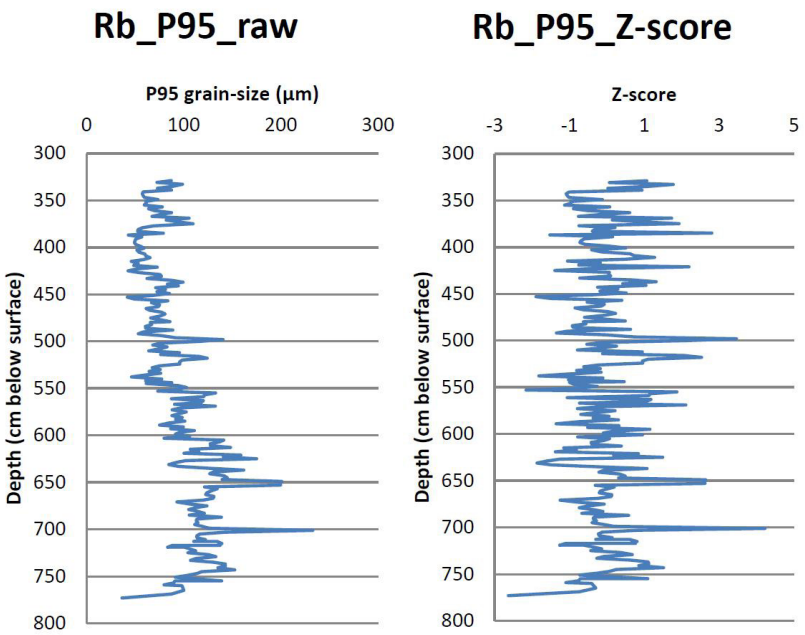

CPA trend breaks: 377/427/545/603 cm below surface (Taylor, 2000)
Confidence level: 95%
Grouping of rows: n=2

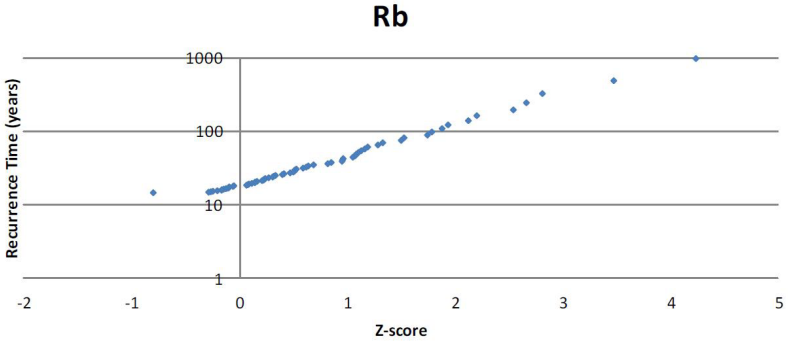

Regression plot of recurrence times versus Z-scored flood data.

Schloss Bellinghoven
Abbrevation: SB
Town: Mehr
Country: Germany
Coordinates: 231080; 417810 (RD)
Elevation: 10.0m +mean sea level

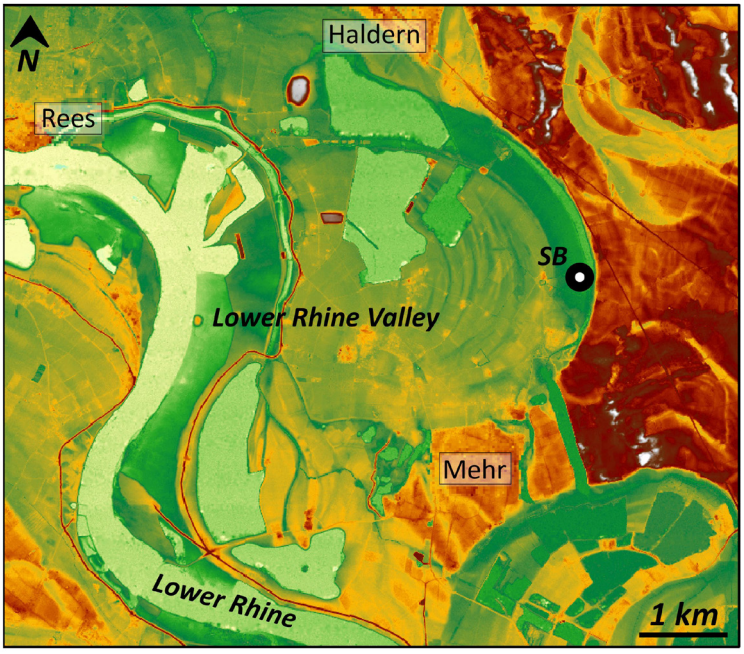

Elevation map of the SB research area (red = high, green = low) (Landvermessungsamt Nordrhein-Westfalen, Germany; as used in Cohen et al., 2009)

Age Information

Name	Code	Type	Depth (cm)	Age (^{14}C yrs BP)	Range (yrs)
SB2	SUERC-40328	AMS-radiocarbon	87	995	30
	Seeds: Cicuta virosa, Rorippa amphibia, Epilobium palustre, Ranunculus sceleratus, Carex cf. rostrata (leaf fragments and budscales), Spongilla lacustris, Menyanthes trifoliata.				
SB3	GrA-54340	AMS-radiocarbon	194	1425	35
	Alnus (female catskin).				
SB4	GrA-54923	AMS-radiocarbon	232	2835	45
	Alnus (male catskin), leaf fragments, seeds: Stellaria media, Oenanthe aquatica, Alisma plantago, Alnus glutinosa, Scirpus lacustris, Sagittaria sagittifolia, Rorippa palustris.				
SB5	SUERC-37139	AMS-radiocarbon	329	3250	30
	Seeds: Alnus glutinosa, Alisma plantago-aquatica, Schoenoplectus lacustris.				
SB6	GrA-54919	AMS-radiocarbon	526	4915	80
	Carex sect. Acute (seed), leaf fragments.				

(SB) Oxcal U-sequence age-depth model.

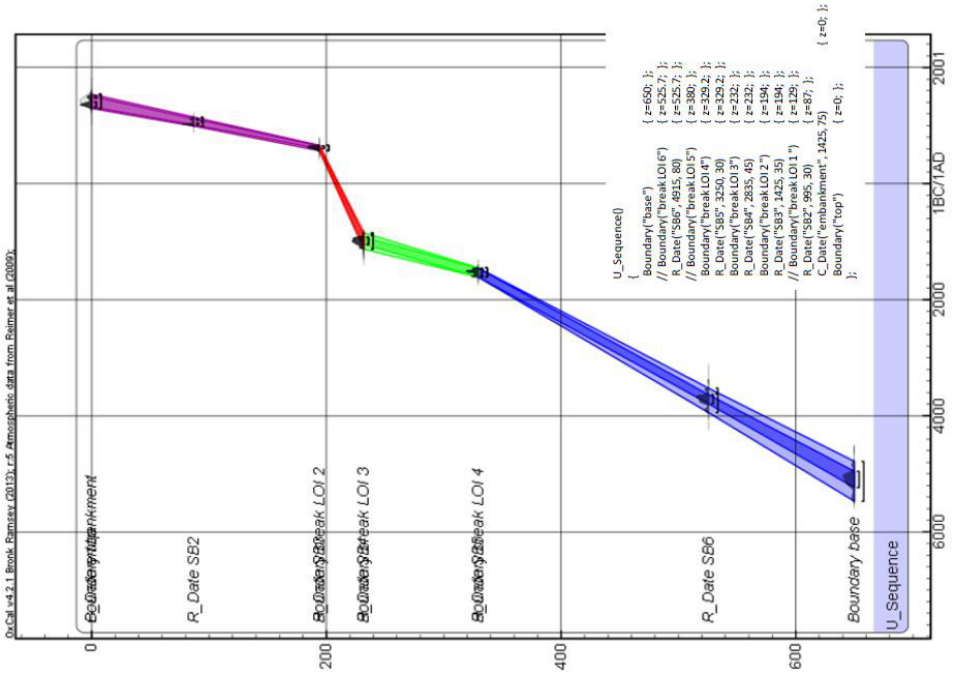

(SB) Sedimentary data

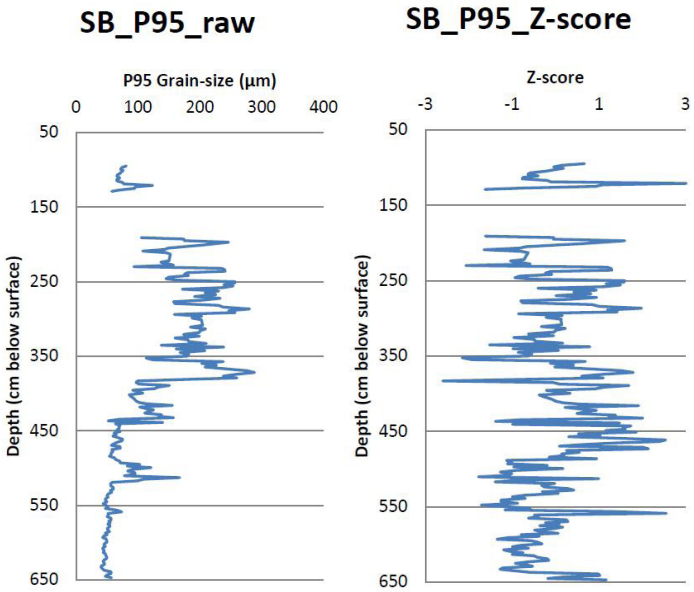

CPA trend breaks: 129/383/441/486/517 cm below surface (Taylor, 2000)
Confidence level: 95%
Grouping of rows: n=2

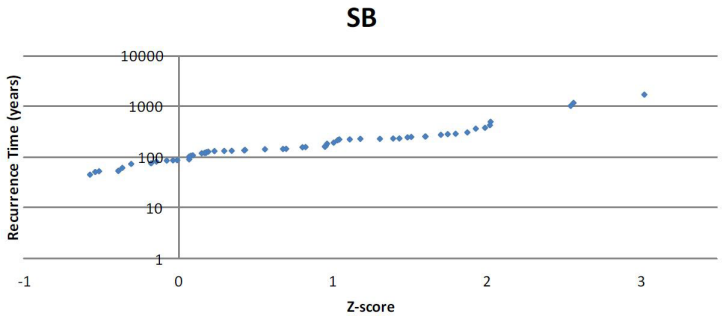

Regression plot of recurrence times versus Z-scored flood data.

Schriek
Abbrevation: Sc
Town: Netterden
Country: The Netherlands
Coordinates: 220870; 429610 (RD)
Elevation: 13.3m +mean sea level

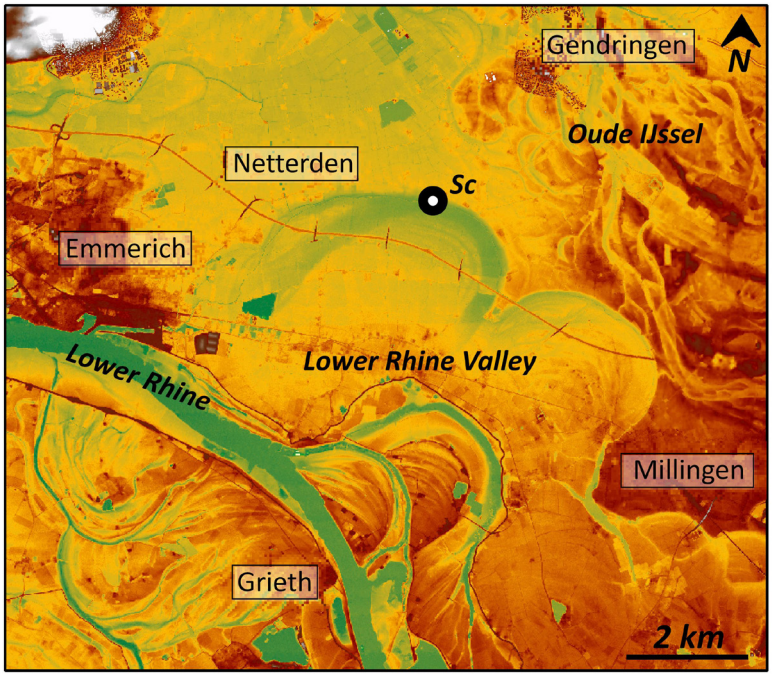

Elevation map of the Sc research area (white = high, green = low) (Rijkswaterstaat-AGI, 2005; Landvermessungsamt Nordrhein-Westfalen, Germany; as used in Cohen et al., 2009).

Age Information

Name	Code	Type	Depth (cm)	Age (^{14}C yrs BP)	Range (yrs)
Sc1	GrA-50905	AMS-radiocarbon	216	3920	80
	Alnus (fruits and male catskins), leaf fragments.				
Sc2	GrA-50005	AMS-radiocarbon	257	4355	40
	Alnus (fruits, male catskins, twig), Alisma plantago-aquatica (seed).				
Sc3	GrA-50006	AMS-radiocarbon	302	4980	40
	Alnus (fruits, male catskins).				
Sc4	Poz-49901	AMS-radiocarbon	341	5140	35
	Charcoal.				
Sc5	Poz-49902	AMS-radiocarbon	357	5490	40
	Charcoal.				
Sc6	SacA-27632	AMS-radiocarbon	390	5700	35
	Charcoal.				
Sc7	SacA-27633	AMS-radiocarbon	449	6020	35
	Charcoal.				
Sc8	GrA-50008	AMS-radiocarbon	503	6230	40
	Fruit (indet.), Seeds: Schoenoplectus lacustris, Alisma plantago-aquatica, Lythrum salixcaria, Alnus (catskin).				
Sc9	Poz-46835	AMS-radiocarbon	514	6550	40
	Charcoal.				
Sc10	Poz-46836	AMS-radiocarbon	620	6490	90
	Charcoal.				
Sc12	SacA-26156	AMS-radiocarbon	700	6840	40
	Charcoal, wood, leaves (indet.).				
Sc13	SacA-26157	AMS-radiocarbon	778	7065	45
	Wood and leaves (indet.).				
Sc17	Poz-46837	AMS-radiocarbon	906	7390	100
	Charcoal.				
Sc18	GrA-50897	AMS-radiocarbon	1056	7345	80
	Alnus (catskin), leaf fragments.				

Samples Sc4-7/9-17; courtesy of J.F. Berger (Obresoc-project, Lyon2 University, Lyon, France).

(Sc) Oxcal U-sequence age-depth model.

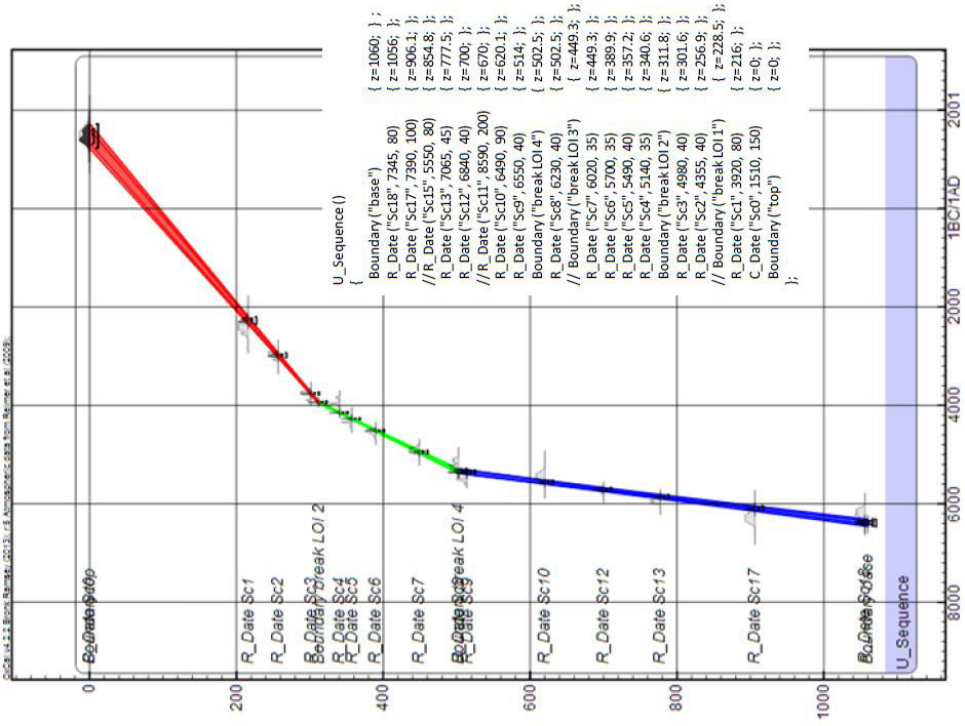

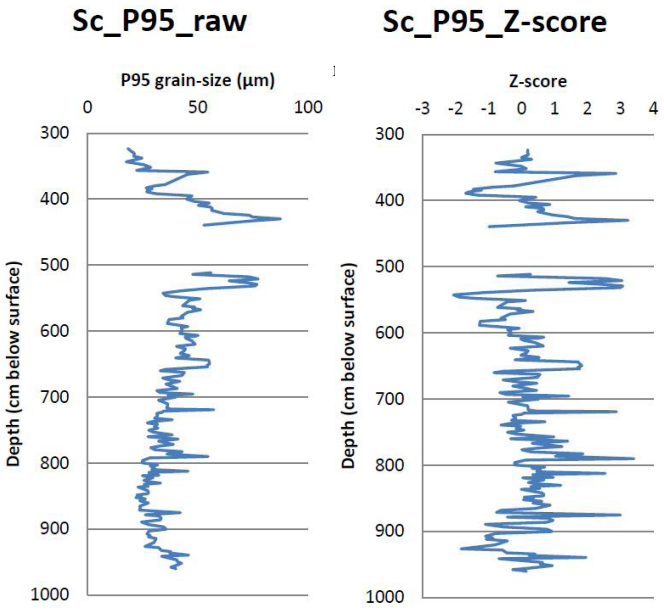

CPA trend breaks: 422/865 cm below surface (Taylor, 2000)
Confidence level: 95%
Grouping of rows: n=2

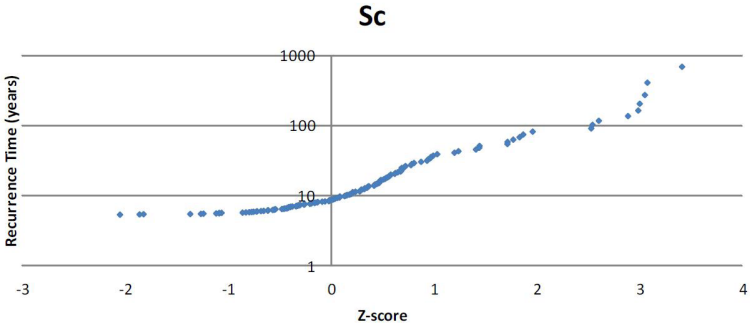

Regression plot of recurrence times versus Z-scored flood data.

Band-pass filtered stacks of dominant periodicities

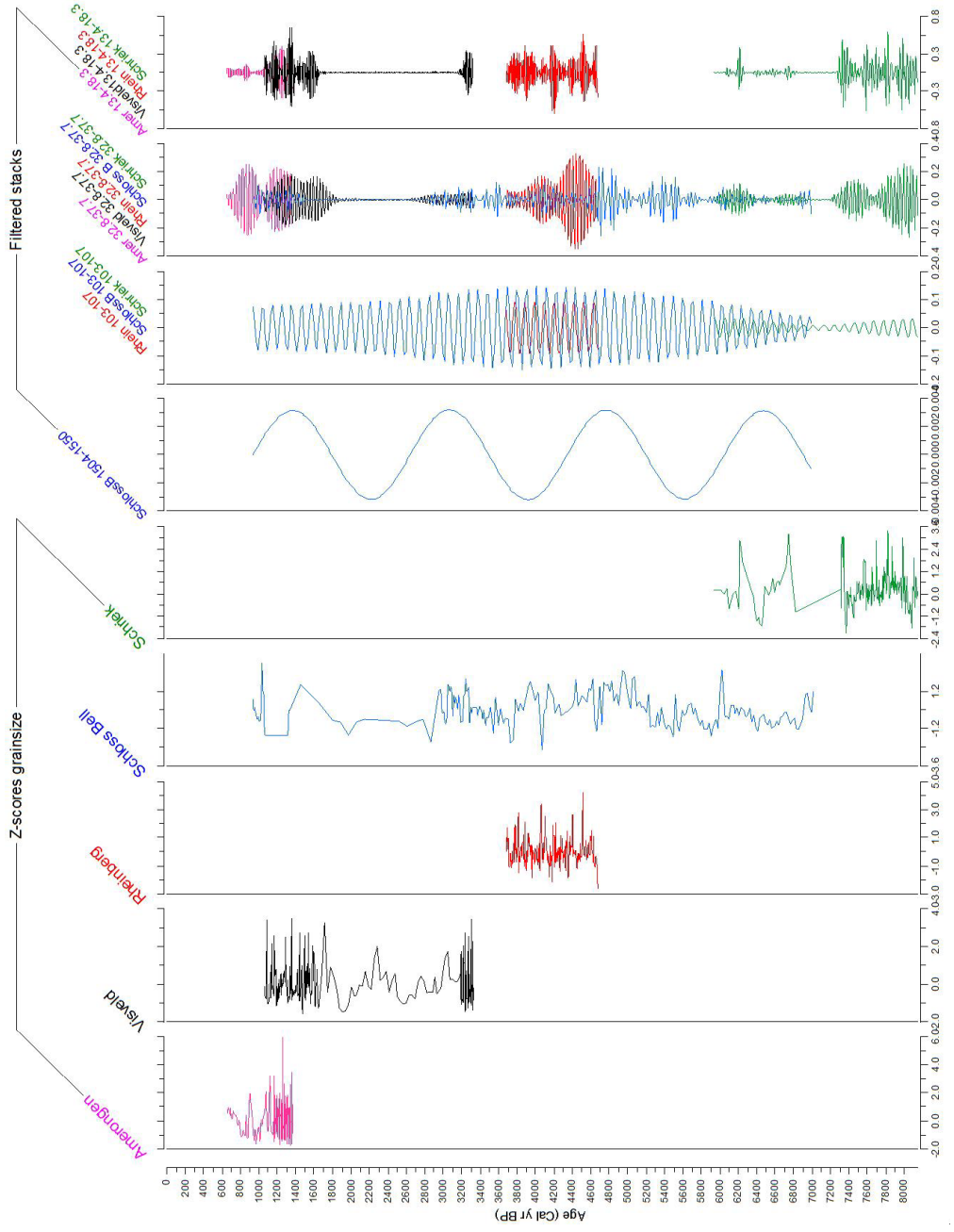

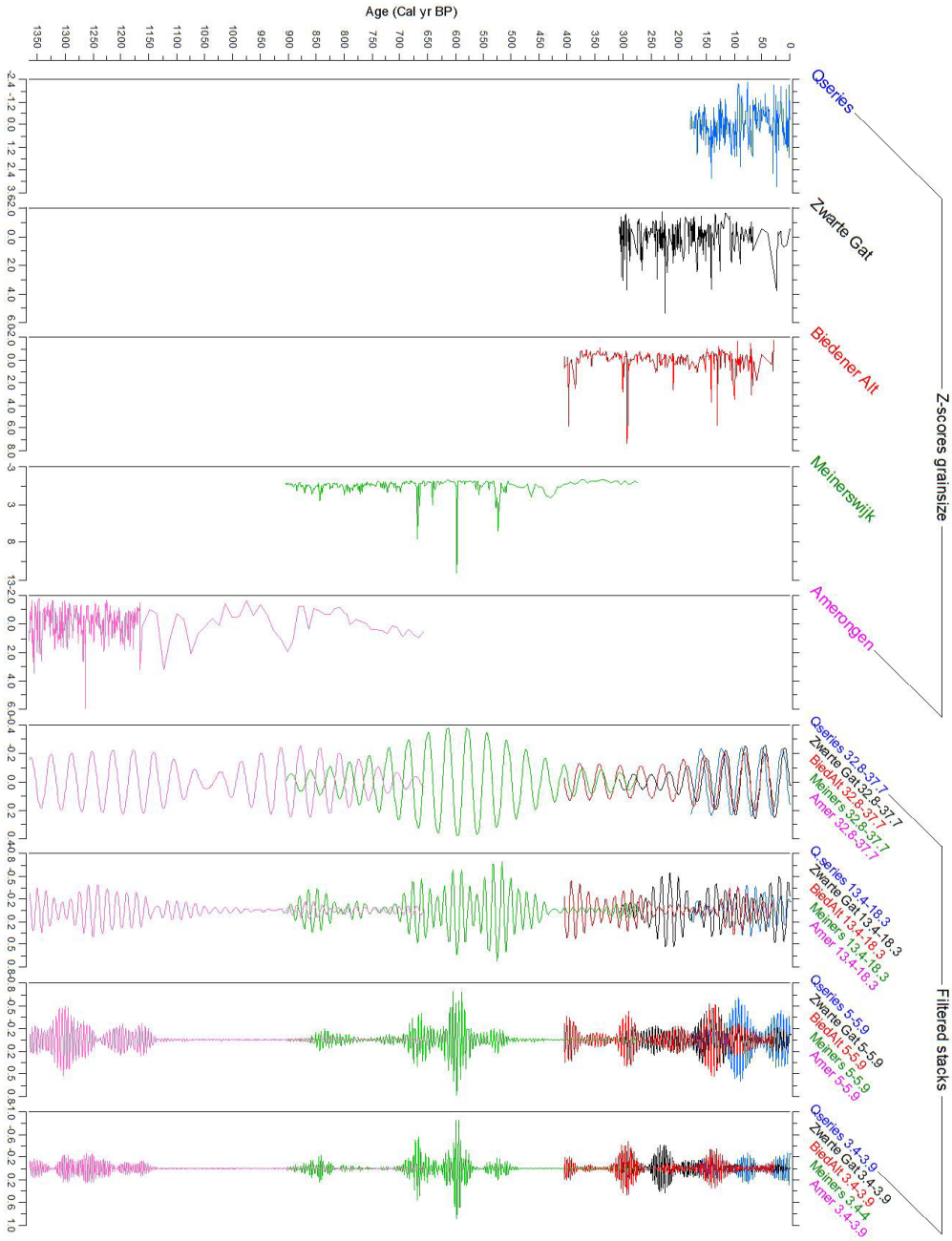
Age (Cal yr BP)
Qseries
Zwarte Gat
Biedener Alt
Meinerswijk
Amerongen
Z-scores grainsize
Qseries 32.8-37.7
Zwarte Gat 32.8-37.7
BiedAlt 32.8-37.7
Meiners 32.8-37.7
Amer 32.8-37.7
Qseries 13.4-18.3
Zwarte Gat 13.4-18.3
BiedAlt 13.4-18.3
Meiners 13.4-18.3
Amer 13.4-18.3
Qseries 5-5.9
Zwarte Gat 5-5.9
BiedAlt 5-5.9
Meiners 5-5.9
Amer 5-5.9
Qseries 3.4-3.9
Zwarte Gat 3.4-3.9
BiedAlt 3.4-3.9
Meiners 3.4-4
Amer 3.4-3.9
Filtered stacks

Summary

Problem Definition

In the last decade of the 20th century, severe floods caused extensive damage and life-loss throughout Europe (Benito et al., 2004). The magnitude of these floods, and especially the short interval over which these reoccurred, raised questions about the actual safety standards for protection against flooding. In 1993 and 1995, the Lower Rhine (Germany) and Rhine Delta (the Netherlands) suffered from discharges that were previously associated with centennial events (Chbab, 1996). Inclusion of these events in flood frequency analysis in the periodic reassessment of the design discharge, considerably increased the estimated magnitude of the design discharge for flood protection. This was reason to raise the 1,250-yr design flood for river dikes in the Netherlands (Waterwet, 2009) from 15,000 to 16,000 m^3s^{-1} (Chbab, 1999). Under projected climate change with an increase in precipitation amount and intensity (Milly et al., 2002; Pinter et al., 2006; IPCC, 2007; Veerman, 2008), it is anticipated that the design standard for dikes in the Netherlands should be further raised. A major problem in calculating the magnitude of the design flood is uncertainty, which mainly originates from limited data availability back in time, and non-stationarity of the flooding regime. Established practice has been to use an observational discharge series that goes back to 1901. This is a limited length for predicting the recurrence time of extreme events (Klemeš, 2000), as a 110-year interval probably poorly represents the distribution of extremes through time. Non-stationarity of the flooding regime further complicates the use of short discharge records for flood frequency analysis. It is not expected that the distribution and magnitudes of floods is fixed in time. During the Holocene, climate variability and growing human influence have exerted perturbations to the fluvial system, which translates to gradual changes in flood probabilities.

Unlocking sedimentary records for flood magnitude reconstructions

In this dissertation, the approach is to increase available data by lengthening data series of large flooding events back in time. This is done by harvesting information from sedimentary records from oxbow lake fills of the Lower Rhine, and cross-validating results with the instrumental record, historical records of the last six centuries, and between overlapping sedimentary records. This resulted in a flood magnitude record that stretches back to 8,200 years BP. To arrive at such a record and to make it of use for flood risk assessments, methodological advances were necessary.

First, it was shown how alternative observational information (discharge and water levels), from multiple stations along the Lower Rhine, and historical records can be used to extend the discharge record at Lobith. Although pre-processing and conversion of data types into discharge estimates introduces extra uncertainty, the added value of this data in flood frequency analysis is considerable, because extending record length by including slightly less-precise data results in much better constrained estimates for the discharges and recurrence interval of extreme floods. Based on results obtained with the generalized extreme value (GEV) distribution, it was concluded that large flooding events of the last century are of more rare occurrence than previously considered. Moreover, climatic and anthropogenic-induced non-stationarity of the flooding regime is recognisable in extended observational records, but has a limited effect on magnitude-recurrence relations for extreme floods (millennial recurrence), as most variability is of sub-centennial nature,

not leading to permanent change of the system. Another outcome of the analysis of the extended Lower Rhine observational record, is that current protection levels are presumably meeting the currently required safety standards.

Next, abandoned channel fills were studied. These sedimentary environments were considered the primary candidate sites to retrieve sedimentary palaeoflood records from. Although channel fills are common elements of alluvial river systems, surprisingly little was known about systematics of their rates of infill and sedimentary architecture. With this dissertation, it is intended to 'unlock' channel-fill sequences as records of channel abandonment processes and palaeofloods, for which improved understanding was needed of the internal build-up of channel fills. Oxbow lake infilling along meandering rivers was reviewed, in comparison to avulsion-abandoned residual channels, supplemented with descriptions of two field examples from the apex-region of the Rhine Delta. The examples show that regional setting and type of abandonment result in different channel-fill architectures. Where oxbow cutoffs generally produce thick laminated clayey fills (because the channel entrance is plugged rapidly), avulsion-abandoned channels are over considerable length filled with relative coarse deposits (because of a relative long maintained open connection with the river, during which bed load material is received and trapped). From this a sedimentary-architecture descriptive scheme is proposed that distinguishes elements from two stages of channel-fill development; (i) the abandonment stage with initial proximal fill, and (ii) the subsequent fully abandoned palaeochannel that collects distal fill.

In a next step, new methods for age-modelling were prototyped on an oxbow fill of a palaeomeander at the distal floodplain edge of the river Rhine near Rheinberg (Germany). This study aimed to make maximum use of the sedimentological properties and archiving potential of oxbow lake fills for palaeohydrological studies, for palaeogeographical reconstruction, and as containers of palaeoenvironmental records. Sedimentological information was used to adjust sedimentation rates and subsequent age-depth models. This allowed in combined with flood layer registration and flood magnitude analysis, to assess meander cut-off recurrence, the pacing of oxbow-disconnection, bankfull discharge recurrence times, and variation in flooding intensity. Major meander reorganisation was timed at 4.72 (±0.07) ka and associated to a very large flood event. At a finer scale, flooding event beds were indexed and regarded as the complete inventory of large events for a 1000-year period. By utilising suitable oxbow-fill archives, it was concluded that one can (i) resolve a valley's geomorphological evolution at unmatched temporal resolution, (ii) create independent flood-event inventories that allow for comparative validation of catchment-derived palaeohydrological reconstructions, and (iii) unlock event-stratigraphic means for dating control on overbank sedimentary archives throughout the river system.

To establish relations between relative coarseness of flood beds and measured discharges, and to explore the potential of coarse-tail grain size parameters as proxy for flood event peak magnitude, the sedimentary archive of two sub-recent sites in the floodplain of the modern Lower Rhine was studied. An abandoned channel fill and a dike breach scour hole, both with historically-known age of formation, were selected for this purpose, of which the upper half of the fill overlaps with the post-1772 measurement-based discharge series. Coarse-tail grain-size descriptors such as the 95th percentile and end-member modelling turned out as precise tools for inferring flood magnitudes, as they correlate to measured discharge peaks of the last ~240 years reasonably well (R^2 of ~0.8). The established relation can be directly used to estimate discharges back to AD ~1550. Minor

differences in the duplicate discharge estimates from the two sites were attributed to morphological changes in the vicinity of either site, which influenced the relation between discharge in the river channel and flood bed coarseness.

Another approach to estimate discharges, applicable to very-rare, extreme palaeofloods in the Middle Holocene ('millennial recurrence') makes use of slackwater deposits encountered at high floodplain terraces, combined with cross-section hydraulic modelling. A Chézy-based model was established to estimate the excess magnitude of floods producing such markers (in the vicinity of Xanten, Germany). Geometrical input parameters were reconstructed from field surveys, and supplemented with further parameters derived from palaeoenvironmental reconstruction and literature, and used in ten scenarios to calculate a best guess estimate for the minimum size of extreme floods. The modelled minimum discharge is 13,250 m^3s^{-1} for a Middle Holocene flood with an estimated recurrence interval between 1,250 and 2,500 years. Such discharges are comparable to current design flood estimates, if the effects of anthropogenic changes (e.g., deforestation and river management) are considered.

Finally, integrating the above methods and generated records, a composite flood record is presented for the Lower Rhine, spanning the last 8,200 years. The record is based on a total of eight cored sites and the discharge series for Lobith since AD 1772. Each recognized flood had its recurrence time quantified, based on the frequencies of recurrence of their linear-detrended and Z-scored P95 value. Largest floods, with 'millennial' recurrence times, occurred in AD 1374, 784, and 4.5, 4.7, and 6.2 ka BP. From each of these floods, fluvial geomorphological changes of regional importance can be pointed out in existing studies in the Rhine Delta and Lower Rhine Valley, as further confirmation of the validity of the results. Strong variability in recorded flood intensities, significant periodicities in flood deposition, and changing shapes of flood frequency curves indicate imprints of non-stationary flooding regime, which are especially strong pronounced during the Little Ice Age.

The new data provides clear results on rare flood recurrence and relative flood magnitudes over large part of the Holocene of hitherto unseen resolution and completeness. Regarding absolute discharge estimates for individual palaeofloods, questions remain. These comprise (i) the translation of sedimentary data and relative flood magnitudes into absolute discharges, and (ii) the causes, effects, and magnitude of non-stationarity. This dissertation demonstrates that within the past centuries non-stationarity is mainly associated with decadal to centennial floods. Extreme floods of millennial recurrence show no clear relation to fluctuations in flood intensities, despite their tendency to cluster with other large events. Nonetheless, it remains unclear from this study whether intensified flooding of the last decades (e.g., the 1993 and 1995 floods) fits the natural variability of the past centuries or signals anthropogenic changes to river system and climate system combined. The gained experience and methodological development with a first network of sites provides important clues and opportunities on how to proceed and how to quantify the effects of non-stationarity in flooding regimes. In the scope of this study, application and combination of absolute discharge reconstructions on a larger scale (temporally, spatially, but also aiming at resolving events of lower magnitude) can provide many more tie-points for translating currently available relative flood magnitudes into discharge estimates.

Samenvatting

Probleemstelling
In de jaren 90 van de vorige eeuw werd een groot gedeelte van Europa geteisterd door overstromingen van rivieren met aanzienlijke schade en slachtoffers tot gevolg (Benito et al., 2004). De omvang van deze overstromingen, en met name de snelle opeenvolging van dergelijke zeldzaam hoge piekafvoeren, leidde tot discussies over de huidige veiligheidsnormen voor overstromingsrisico's. De Rijn in Duitsland en de Rijn-Maas Delta in Nederland kenden in 1993 en 1995 piekafvoeren die voorheen werden bestempeld als 'overstroming van de eeuw' (Chbab, 1996). Het meenemen van deze piekafvoeren in de periodieke herberekening van de maatgevende afvoer voor dijkveiligheid - de afvoer die hoort bij een overstroming die statistisch eens in de 1250 jaar voorkomt (Waterwet, 2009) - resulteerde in een verhoging van de veiligheidsstandaard voor dijken van 15,000 naar 16,000 m^3s^{-1} (Chbab, 1999).

Klimaatsverandering zal waarschijnlijk in de toekomst leiden tot een toename in neerslag en de intensiteit daarvan (Milly et al., 2002; Pinter et al., 2006; IPCC, 2007; Veerman, 2008), waardoor de maatgevende afvoer verder verhoogd zal moeten worden. Een belangrijke complicatie in het bepalen van de huidige maatgevende afvoer is onzekerheid, voortkomend uit de beperkte hoeveelheid beschikbare data en de variabiliteit van het overstromingsregiem. Het is gebruikelijk om afvoermetingen sinds 1901 AD te gebruiken voor het bepalen van de maatgevende afvoer. Dit is echter een datareeks van beperkte lengte, indien men de herhalingstijd van uiterst zeldzame gebeurtenissen wil berekenen (Klemeš, 2000), omdat (de distributie van) zulke extremen vaak slecht vertegenwoordigd zijn in korte datareeksen. Daarnaast zorgt de variabiliteit van het overstromingsregiem, door subtiele veranderingen in het klimaat en een toenemende menselijk invloed op rivieren en het achterland, ervoor dat de kans op grote afvoeren door de tijd verandert.

Het gebruik van sedimentaire informatie voor de reconstructie van overstromingsmagnitudes
In dit proefschrift is getracht om de beschikbare datareeks voor het bepalen van de maatgevende afvoer zover mogelijk terug in de tijd op te rekken. Dit is gedaan op basis van de sedimentaire eigenschappen van overstromingsafzettingen in verlaten rivierarmen, en vergelijking van die informatie met gemeten afvoeren, informatie uit zes eeuwen aan historische bronnen, en verificatie door in de tijd overlappende reeksen uit afzonderlijke onderzoekslocaties met overstromingsafzettingen. Dit heeft geresulteerd in een overstromingsmagnitudereeks die de afgelopen 8,200 jaar bestrijkt. Om een dergelijke reeks op te bouwen en om die bruikbaar te maken voor het inschatten van overstromingsrisico's, zijn verscheidene methodologische stappen nodig geweest, welke hieronder zijn toegelicht.

Ten eerste is gepoogd om metingen (waterhoogte en afvoeren) van andere meetstations dan Lobith en historisch bronnen uit het Rijngebied te gebruiken om de huidige afvoermeetreeks te verlengen. Alhoewel het voorbereiden en omzetten van de data in afvoeren te Lobith extra onzekerheid introduceert op individuele datapunten, is de toegevoegde waarde van deze data aanzienlijk, omdat daarmee veel nauwkeurigere schattingen gemaakt kunnen worden van de maatgevende afvoer. Op basis van de resultaten van 'extreme-waarden statistiek' (GEV) en de verlengde datareeks wordt er geconcludeerd dat hoge piekafvoeren uit de jaren 90 van de vorige eeuw veel zeldzamer

zijn dan voorheen gedacht werd. Bovendien laat de verlengde datareeks duidelijk zien dat het overstromingsregiem in de afgelopen eeuwen variabel is geweest, waarschijnlijk onder invloed van klimatologische veranderingen en menselijk ingrijpen in het natuurlijke systeem. Het uiteindelijke effect van dergelijke variaties op de uitkomsten van de berekening van de maatgevende afvoer is beperkt, omdat de meeste variabiliteit zich afspeelt in cycli van enkele tientallen jaren en er geen permanente veranderingen waarneembaar zijn. Een andere uitkomst van deze studie is dat de huidige veiligheidsstandaard van de Rijndijken toereikend is om de berekende afvoer die hoort bij een herhalingstijd van 1250 jaar te weerstaan.

Vervolgens zijn met overstromingssedimenten ingevulde rivierarmen in detail bestudeerd. Alhoewel verlaten rivierarmen vrij standaard elementen zijn in gebieden met meanderende rivieren is er verrassend weinig bekend over de wijze van opvulling en processen die resulteren in de waargenomen sedimentaire opbouw. Een van de hoofddoelen van dit proefschrift was om de invulling van verlaten rivierarmen zodanig te begrijpen, dat ze gebruikt kunnen worden voor interpretatie van sedimentaire processen in de fase van verlating en voor de reconstructie van overstromingen in de prehistorie. Op basis van voorbeelden uit de ondergrond van de Rijn-Maas Delta zijn geulinvullingen van typische hoefijzermeren (gevormd door lokale bochtafsnijdingen) vergeleken met de invulling van restgeulen, ontstaan door avulsie (complete rivierverlegging). De bestudeerde voorbeelden tonen aan dat door verschillende lokale omstandigheden en het type van verlaten (bochtafsnijding versus avulsie) zeer verschillende geulinvullingen kunnen ontstaan. Invullingen ontstaan door bochtafsnijding worden getypeerd door een dik pakket van sterk gelaagde klei-afzettingen, mogelijk gemaakt door de snelle vorming van zandbanken in de geulmonding, die de achterliggende voormalige geul afschermen voor snelle sedimentatie van beddingzand. Geulen verlaten door avulsie bevatten relatief veel grofkorrelige afzettingen, ver in de verlaten geul en gedurende lange tijd afgezet doordat er geen zandbanken ontstaan in de monding zoals in het geval van bochtafsnijdingen. Aan de hand van deze informatie is een conceptueel model voor de invulling van verlaten geulen opgesteld waarin, op basis van type verlating en daaraan gekoppelde processen, twee belangrijke fasen worden onderscheiden in de opbouw van geulinvullingen, namelijk (i) de fase van verlating, waarin in hoog tempo beddingzand wordt afgezet in de verlatende geul, en (ii) de compleet verlaten fase, waarin er alleen tijdens hoogwaters (fijnkorrelig) sediment kan worden afgezet.

In een vervolgstap zijn nieuwe methoden verkend voor het reconstrueren van de ouderdommen in geulafzettingen door middel van ouderdom-diepte modellering op de geulinvulling van een oude rivierarm van de Rijn in de buurt van Rheinberg (Duitsland). Doel was om zoveel mogelijk sedimentologische informatie en registratiepotentieel van overstromingen uit te buiten voor hydrologische en palaeogeografische studies. Sedimentologische informatie is gebruikt om sedimentatiesnelheden te reconstrueren en aan de hand daarvan standaard ouderdom-diepte modellen (op basis van enkele koolstofdateringen) te verfijnen. In combinatie met het voorkomen van overstromingsafzettingen en een analyse van overstromingsmagnitude, is hieruit herleid (i) wanneer en hoe snel bochtafsnijdingen in het gebied hebben plaatsgevonden, (ii) hoe vaak het gebied gemiddeld overstroomt raakte, en (iii) of er variabiliteit waarneembaar was in de overstromingsfrequentie en het overstromingsregiem. De belangrijkste rivierverlegging vond plaats rond 4,720 jaar geleden en is zeer waarschijnlijk direct te koppelen aan een zeer grote overstroming. Op een hoger detailniveau zijn overstromingslaagjes geïndexeerd op magnitude. Door het in detail bestuderen van geulvullingen, in combinatie met verfijnde ouderdom-diepte modellering is het

mogelijk geworden om, (i) de geomorfologische ontwikkeling van het rivierdal in een ongekend hoge temporele resolutie te reconstrueren, (ii) een onafhankelijk archief van overstromingen (en overstromingsmagnitudes) te creëren, bruikbaar voor vergelijkingen met hydrologische reconstructies op basis van het stroomgebied, en (iii) het beschikbaar maken van grote overstromingen als stratigrafische 'markers', die door het een groot gedeelte van het stroomgebied herkenbaar zijn en gebruikt kunnen worden als onafhankelijke datering van rivierafzettingen.

Om het verband vast te stellen tussen de grofheid van overstromingsafzettingen en gemeten piekafvoeren, en om daarnaast het potentieel van de grofste korrels in een korrelgrootteverdeling voor het voorspellen van de overstromingsmagnitude te verkennen, zijn in de buurt van Lobith twee boorkernen verzameld van locaties waarvan de sedimentaire invulling gedeeltelijk overlapt met gemeten en gereconstrueerde piekafvoeren sinds 1772 AD. Een ingevulde meanderbocht en een wiel (dijkdoorbraakgat), waarvan bij beiden uit historische documenten bekend is wanneer ze gevormd zijn, zijn geselecteerd om de relatie tussen korrelgrootte in afzettingen en gemeten afvoeren te testen. Uit correlaties blijkt dat vooral de methodes om de grove staart van korrelgrootteverdelingen te beschrijven (zoals het 95e percentiel en de resultaten van 'End-member'-modelering) een goede weerspiegeling zijn van overstromingsmagnitude. Deze relatie is bruikbaar voor het schatten van afvoeren voor 1772, en gaat op de onderzochte locaties terug tot ~1550 AD. Kleine verschillen in uitkomsten tussen de resultaten van de verschillende locaties zijn toe te schrijven aan geomorfologische veranderingen in de directe omgeving, welke de relatie tussen overstromingsmagnitude en de grofheid van het afgezette materiaal kunnen beïnvloeden.

Een andere aanpak om afvoeren van prehistorische overstromingen te reconstrueren is door gebruik te maken van sedimentaire hoogwater markeringen ('slackwater deposits'). Deze kleilaagjes markeren de hoogstgelegen niveaus waar het water heeft kunnen komen tijdens zeer hoge piekafvoeren. Door zulke markeringen op hogere delen in de overstromingsvlakte te koppelen aan hydraulische berekeningen (gebruikmakend van Chézy-formulering) is in de omgeving van Xanten (Duitsland) de afvoer berekend van een extreem hoogwater van ongeveer 4700 jaar geleden. Invoer en de spreiding van waarden voor parameters zijn verzameld gedurende veldonderzoek, en aangevuld met gegevens uit de literatuur en reconstructies van het prehistorische landschap. In tien scenarios met verschillende randvoorwaarden is berekend dat de afvoer horend bij de hoogwatermarkeringen minstens 13250 m^3s^{-1} moet zijn geweest, en dat deze afvoer hoort bij een herhalingstijd tussen de 1250 en 2500 jaar. Een dergelijke afvoer is vergelijkbaar met de huidige maatgevende afvoer, indien de afvoerverhogende invloed van menselijk ingrijpen door ontbossing en rivieraanpassingen in beschouwing wordt genomen.

Ten slotte zijn de bovengenoemde methoden en locale overstromingsreeksen geïntegreerd, zodat een 8200-jarig overstromingsarchief voor de Rijn is ontstaan. Deze reeks is gebaseerd op acht aparte onderzoekslocaties en de reeds bestaande afvoerreeks van Lobith sinds 1772. Voor iedere te onderscheiden overstroming is een statistische herhalingstijd bepaald, op basis van de frequentie van vergelijkbare piekafvoeren. De zeldzaamste overstromingen, met een herhalingstijd van meer dan duizend jaar, vonden plaats omstreeks 784 en 1374 AD, en 4500, 4700 en 6200 jaar geleden. Voor al deze extreme overstromingen zijn parallellen te vinden in de regionale geomorfologische ontwikkeling, wat het bestaan en de impact van deze gebeurtenissen aantoont. Verder kan op basis van de overstromingsreeks geconcludeerd worden dat het overstromingsregiem sterkt varieert door de tijd, met als duidelijkste anomalie de Kleine IJstijd.

Deze nieuwe informatie geeft een duidelijk beeld van het voorkomen van extreme overstromingen en de algemene overstromingsfrequentie gedurende een groot gedeelte van het Holocene in een hiervoor nooit vertoonde resolutie en compleetheid. Op het gebied van absolute afvoeren die horen bij de gereconstrueerde herhalingstijden zijn echter nog enkele fundamentele vragen, omdat de variabiliteit van het overstromingsregiem en de mate van verandering (vooral door menselijke invloed) door de tijd moeilijk in voldoende detail te kwantificeren zijn. Dit proefschrift toont wel duidelijk aan dat de variabiliteit van overstromingen in de meest recente eeuwen vooral effect had op hoogwaters met een herhalingstijd van decades tot eeuwen, en in mindere mate te correleren is aan extremen – ondanks een vermeende clustering. Het is echter uit de huidige studie niet eenduidig op te maken of de snelle opeenvolging van overstromingen aan het eind van de 20ste eeuw past in de natuurlijke variabiliteit van het overstromingsregiem, zoals altijd aanwezig is geweest, of dat mens en klimaat voor veranderingen hebben gezorgd die niet in bij het natuurlijke systeem horen. Dit onderzoek, en de daarmee opgedane ervaring, methodologische vooruitgang en een eerste netwerk aan onderzoekslocaties, bieden echter voldoende mogelijkheden voor verder onderzoek naar kwantificering van de (natuurlijke) variabiliteit van het overstromingsregiem van de Rijn. Daarbij is van groot belang dat er in de nabije toekomst op grotere schaal onderzoek wordt gedaan naar het voorkomen en de reconstructie van extreme overstromingen, en in het verlengde daarvan ook wordt gekeken naar de conversie herhalingstijd-afvoer van minder zeldzame overstromingen.

References

Allen, J.R.L., 1965. A Review of the origin and character of recent alluvial sediments. Sedimentology 5, p 89-191.

Arnaud, F., 2005. Discriminating bio-induced and detrital sedimentary processes from particle size distribution of carbonates and non-carbonates in hard water lake sediments. Journal of Paleolimnology 34, p 519-526.

Asselman, N.E.M., Middelkoop, H., 1998. Temporal variability of contemporary floodplain sedimentation in the Rhine-Meuse delta, The Netherlands. Earth Surface Processes and Landforms 23, p 595-609.

Asselman, N.E.M., Middelkoop, H., Van Dijk, P.M., 2003. The impact of changes in climate and land use on soil erosion, transport and deposition of suspended sediment in the River Rhine. Hydrological Processes 17, p 3225-3244.

Baker, V.R., 1987. Paleoflood hydrology and extraordinary flood events. Journal of Hydrology 96, p 79-99.

Baker, V.R., Webb, R.H., House, P.K., 2002. The Scientific and Societal Value of Paleoflood Hydrology. In: House, P.K., Webb, R.H., Baker, V.R., Levish, D. (Eds.), Ancient Floods, Modern Hazards: Principles and Applications of Palaeoflood Hydrology. Water Science and Application 5, American Geophysical Union, p 1-19.

Baker, V.R., 2008. Paleoflood hydrology: Origin, progress, prospects. Geomorphology 101, p 1-13.

Baptist, M.J., Babovic, V., Uthurburu, J.R., Keijzer, M., Uittenbogaard, R.E., Mynett, A., Verwey, A., 2007. On inducing equations for vegetation resistance. Journal of Hydraulic Research 45, p 435-450.

Bárdossy, A., Filiz, F., 2005. Identification of flood producing atmospheric circulation patterns. Journal of Hydrology 313, p 48-57.

Barriendos, M., Martin-Vide, J., 1998. Secular climatic oscillations as indicated by catastrophic floods in the Spanish Mediterranean coastal area (14th-19th centuries). Climatic Change 38, p 473-491.

Baur, T., Jagers, H.R.A., 2002. Grensproject Bovenrijn/Grenzprojekt Niederrhein, Model construction, calibration and verification. Report Q2496.00, WL-Delft Hydraulics, Delft.

Beierle, B.D., Lamoureux, S.F., Cockburn, J.M.H., Spooner, I., 2002. A new method for visualizing particle size distributions. Journal of Paleolimnology 27, p 279-283.

Beijerink, F., 1809. Kaart van de doorbraak onder Loenen in het Ambt van Overbetuwe voorgevallen op den 10 januari 1809. Rijksarchief van Gelderland, Algemene Kaarten Verzameling 385.

Benito, G., Sánchez-Moya, Y., Sopena, A., 2003. Sedimentology of high-stage flood deposits of the Tagus River, Central Spain. Sedimentary Geology 157, p 107-132.

Benito, G., Lang, M., Barriendos, M., Llasat, M.C., Frances, F., Ouarda, T., Thorndycraft, V.R., Enzel, Y., Bardossy, A., Coeur, D., Bobee, B., 2004. Use of Systematic, Palaeoflood and Historical Data for the Improvement of Flood Risk Estimation. Review of Scientific Methods. Natural Hazards 31, p 623-643.

Berendsen, H.J.A., Hoek, W.Z., Schorn, E., 1995. Late Weichselian and Holocene river channel changes of the rivers Rhine and Meuse in the Netherlands (Land van Maas en Waal). Paläoklimaforschung- Paleoclimate Research 14, p 151-172.

Berendsen, H.J.A., Stouthamer, E., 2000. Late Weichselian and Holocene palaeogeography of the Rhine-Meuse delta, The Netherlands. Palaeogeography, Palaeoclimatology, Palaeoecology 161, p 311-335.

Berendsen, H.J.A., Stouthamer, E., 2001. Palaeogeographic development of the Rhine-Meuse delta, The Netherlands. Van Gorcum: Assen.

Berendsen, H.J.A., Hoek, W.Z., 2005. Eindrapport van het fysisch-geografisch onderzoek in het kader van de verbreding van de A2. Centre of Geo-ecological Research, ICG-rapport 05-1.

Berendsen, H.J.A., Cohen, K.M., Stouthamer, E., 2007. The use of GIS in reconstructing the Holocene palaeogeography of the Rhine-Meuse delta, The Netherlands. International Journal of Geographical Information Science 21, p 589-602.

Berendsen, H.J.A., Volleberg, K.P., 2007. New prospects in geomorphological and geological mapping of the Rhine-Meuse delta – Application of detailed digital elevation maps based on laser altimetry. Netherlands Journal of Geosciences 86, p 15-22.

Berner, Z.A., Bleeck-Schmidt, S., Stüben, D., Neumann, T., Fuchs, M., Lehmann, M., 2012. Floodplain deposits: A geochemical archive of flood history – A case study on the River Rhine, Germany. Applied Geochemistry 27, p 543-561.

Bøe, A.G., Dahl, S.O., Lie, Ø., Nesje, A., 2006. Holocene river floods in the upper Glomma catchment, southern Norway: a high-resolution multiproxy record from lacustrine sediments. The Holocene 16, p 445-455.

Bond, G., Showers, W., Cheseby, M., Lotti, R., Almasi, P., deMenocal, P., Priore, P., Cullen, H., Hajdas, I., Bonani, G., 1997. A pervasive millennial-scale cycle in the North Atlantic Holocene and glacial climates. Science 294, p 2130-2136.

Bonneblad 532, 1890. Chromotopografische Kaart des Rijks 532; accessed on www.watwaswaar.nl.

Bos, J.A.A., Dambeck, R., Kalis, A.J., Schweizer, A., Theimeyer, H., 2008. Palaeoenvironmental changes and vegetation history of the Upper Rhine Graben (southwestern Germany) since the Lateglacial). Netherlands Journal of Geosciences 87, p 67-90.

Braun, F.J., Thiermann, A., 1981. Erläuterungen zu Blatt 4103 Emmerich, Geologische Karte von Nordrhein-Westfalen 1:25000. Geologisches Landesamt Nordrhein-Westfalen, Krefeld, 104 pp.

Brázdil, R., Glaser, R., Pfister, C., Dobrovolny, P., Antoine, J.M., Barriendos, M., Camuffo, D., Deutsch, M., Enzi, S., Guidoboni, E., Kotyza, O., Rodrigo, F.S., 1999. Flood events of selected European rivers in the sixteenth century. Climatic Change 43, p 239-285.

Brázdil, R., Kundzewicz, Z.W., Benito, G., 2006. Historical hydrology for studying flood risk in Europe. Hydrological Sciences Journal 51, p 739-764.

Brázdil, R., Demarée, G.R., Deutsch, M., Garnier, E., Kiss, A., Luterbacher, J., Macdonald, N., Rohr, C., Dobrovolný, P., Kolář, Chromá, K., 2010. European floods during the winter 1783/1784: scenarios of an extreme event during the 'Little Ice Age'. Theoretical and Applied Climatology 100, p 163-189.

Bridge, J., 2003. Rivers and Floodplains – Forms, Processes and Sedimentary Record. Blackwell Science Ltd.: Oxford.

Bronk Ramsey, C., 2009. Bayesian analysis of radiocarbon dates. Radiocarbon 51, p 337-360.

Bronstert, A., Bárdossy, A., Bismuth, C., Buiteveld, H., Disse, M., Engel, H., Fritsch, U., Hundecha, Y., Lammersen, R., Niehoff, D., Ritter, N., 2007. Multi-scale modelling of land-use change and river training effects on floods in the Rhine basin. River Research and Applications 23, p 1102-1125.

Buishand, T.A., Brandsma, T., 2001. Multisite simulation of daily precipitation and temperature in the Rhine basin by nearest-neighbor resampling. Water Resources Research 37, p 2761-2776.

Buisman, J., 1996/1998/2000/2006. Duizend jaar weer, wind en water in de Lage Landen, Deel 2-5. Van Wijnen, Franeker.

Bulle, H., 1926. Untersuchungen uber die Geschiebeableitung bei der Spaltung von Wasserlaufen. VDI Verlag, Berlin.

Bunnik, F.P.M., 2010. Pollenscans van Waalgeulopvullingen in the kader van KIP-overstroom. TNO Geological Survey of the Netherlands. Report TNO-034-UT-2010-00992/B.

Büntgen, U., Trouet, V., Frank, D., Leuschner, H.H., Friedrichs, D., Luterbacher, J., Esper, J., 2010. Quaternary Science Reviews 29, p 1005-1016.

Busschers, F.S., Kasse, C., van Balen, R.T., Vandenberghe, J., Cohen, K.M., Weerts, H.J.T., Wallinga, J., Johns, C., Cleveringa, P., Bunnik, F.P.M., 2007. Late Pleistocene evolution of the Rhine-Meuse system in the southern North Sea basin: imprints of climate change, sea-level oscillation and glacio-isostacy. Quaternary Science Reviews 26, p 3216-3248.

Chbab, E.H., 1996. How Extreme were the 1995 Flood Waves on the Rivers Rhine and Meuse? Physics and Chemistry of the Earth 20, 455-458.

Chbab, E.H., 1999. Onderzoek 1/1250 jaar afvoer bij Borgharen en Lobith: Bayesiaanse analyse. RIZA werkdocument 2001.183x, Lelystad.

Chbab, E.H., Buitenveld, H., Diermanse, F., 2006. Estimating exceedance frequencies of extreme river discharge using statistical methods and physically based approach. Osterreichische Wasser- und Abfallwirtschaft 58, p 35-43.

Citterio, A., Piégay, H., 2009. Overbank sedimentation rates in former channel lakes: characteristization and control factors. Sedimentology 56, p 461-482.

Cohen, K.M., 2003. Differential subsidence within a coastal prism: Late-Glacial – Holocene tectonics in the Rhine-Meuse delta, the Netherlands. Netherlands Geographical Studies 316.

Cohen, K.M.; Gouw, M.J.P. Holten, J.P., 2005. Fluvio-deltaic floodbasin deposits recording differential subsidence within a coastal prism (central Rhine – Meuse delta, The Netherlands). In: Blum, M.D., S.B. Marriott Leclair, S.F. (Eds.), Fluvial sedimentology VII, IAS Special Publication 35, p 295-320.

Cohen, K.M., Stouthamer, E., Hoek, W.Z., Berendsen, H.J.A., Kempen, H.F.J., 2009. Zand in banen: zanddieptekaarten van het rivierengebied en het IJsseldal in de provincies Gelderland en Overijssel. Utrecht University and Provincie Gelderland. 130 pp.

Cohen, K.M., Stouthamer, E., Pierik, H.J., Geurts, A.H., 2012. Rhine-Meuse Delta Studies' Digital Basemap for Delta Evolution and Palaeogeography. Dept. Physical Geography. Utrecht University. Digital Dataset. http://persistent-identifier.nl/?identifier=urn:nbn:nl:ui:13-nqjn-zl

Constantine, J.A., Dunne, T., Piégay, H., Kondolf, G.M., 2010. Controls on the alluviation of oxbow lakes by bed-material load along the Sacramento River, California. Sedimentology 57, p 389-407.

Couwater, J., 1722. Caarte van den Ewijksen en Loenense rijswaarde van de freulens van Wijckraat. Rijksarchief van Gelderland, Algemene Kaarten Verzameling 51.

Czymzik, M., Dulski, P., Plessen, B., von Grafenstein, U., Naumann, R., Brauer, A., 2010. A 450 year record of spring-summer flood layers in annually laminated sediments from Lake Ammersee (southern Germany). Water Resources Research 46, W11528, doi:10.1029/2009WR008360.

Czymzik, M., Brauer, A., Dulski, P., Plessen, B., Naumann, R., von Grafenstein, U., Scheffler, R., 2013. Orbital and solar forcing of shifts in Mid-to Late Holocene flood intensity from varved sediments of pre-alpine Lake Ammersee (southern Germany). Quaternary Science Reviews 61, p 96-110.

Dalrymple, T., Benson, M.A., 1968. Measurement of peak discharge by the slope-area method. U.S. Geological Survey Techniques in Water Resources Investigations 3:A2, 12.

Davies, B.A.S., Brewer, S., Stevenson, A.C., Guiot, J., Data Contributors, 2003. The temperature of Europe during the Holocene reconstructed from pollen data. Quaternary Science Reviews 22, p 1701-1716.

Dean, W.E. Jr., 1974. Determination of carbonate and organic matter in calcareous sediments and sedimentary rocks by loss on ignition: Comparison with other methods. Journal of Sedimentary Petrology 44, 242-248.

Delft Hydraulics and Dutch Ministry of Transport, Public Works and Water Management, 1997. SOBEK, Technical Reference Manual.

Demarée, G.R., 2006. The catastrophic floods of February 1784 in and around Belgium – a Little Ice Age event of frost, snow, river ice…and floods. Hydrological Sciences Journal 51, p 878-898.

Denlinger, R.P., O'Connell, D.R.H., House, P.K., 2002. Robust determination of stage and discharge: an example from an extreme flood on the Verde River, Arizona. In: House, P.K., Webb, R.H., Baker, V.R., Levish, D.R. (Eds.), Ancient floods, modern hazards: Principles and applications of paleoflood hydrology. Water Science and Application 5, American Geophysical Union, Washington D.C., p 127-146.

De Wit, M., Buishand, A., 2007. Generator of rainfall and discharge extremes (GRADE) for the Rhine and Meuse basins. RWS RIZA report 2007.027, Lelystad. KNMI-publication 218, de Bilt.

Dieras, P.L., Constantine, J.A., Hales, T.C., Piégay, H., Riquier, J., 2013. The role of oxbow lakes in the off-channel storage of bed material along the Ain River, France. Geomorphology 188, p 110-119.

Disse, M., Engel, H., 2001. Flood Events is the Rhine Basin: Genesis, Influences and Mitigation. Natural Hazards 23, p 271-290.

Driessen, A.M.A.J., 1994. Watersnood tussen Maas en Waal. Walburg Pers, Zutphen.

Dury, G.H., 1973. Magnitude-frequency analysis and channel morphology. In: Morisawa, M. (Ed.) Fluvial Geomorphology. State University of New York at Binghamton, p 91-121.

Engel, H., 1997. The flood events of 1993/1994 and 1995 in the Rhine river basin. Destructive water: Water-caused Natural Disasters, their Abatement and Control (Proceedings of the Conference held at Anaheim, California, June 1996). IAHS Publuication 239.

Erkens, G., Cohen, K.M., Gouw, M.J.P., Middelkoop, H., Hoek, W.Z., 2006. Holocene sediment budgets of the Rhine Delta (The Netherlands): a record of changing sediment delivery. In: Rowan, J.S., Duck, R.W., Werritty, A. (Eds.), Sediment Dynamics and the Hydromorphology of Fluvial Systems, IAHS Publication 306, p 406-415.

Erkens, G., 2009. Sediment dynamics in the Rhine catchment: Quantification of fluvial response to climate change and human impact. Netherlands Geographical Studies 388, 278 pp.

Erkens, G., Cohen, K.M., 2009. Quantification of intra-Holocene sedimentation in the Rhine-Meuse delta: A record of variable sediment delivery. Netherlands Geographical Studies 388: p 117-171.

Erkens, G., Dambeck, R. Volleberg, K.P., Bouman, M.T.I.J., Bos, J.A.A., Cohen, K.M., Wallinga, J., Hoek, W.Z., 2009. Fluvial terrace formation in the Northern Upper Rhine Graben during the last 20,000 years as a result of allogenic controls and autogenic evolution. Geomorphology 103, p 476 – 495.

Erkens, G., Hoffmann, T., Gerlach, R., Klostermann, J., 2011. Complex fluvial response to Lateglacial and Holocene allogenic forcing in the Lower Rhine Valley (Germany). Quaternary Science Reviews 30, p 611-627.

Erkens, G., Toonen, W.H.J., Prins, M.A., 2012. Human impact on the Middle and Late Holocene floodplain sediment characteristics along the River Rhine. EGU General Assembly Conferece Abstracts 14, EGU2012-5971.

Erskine, W., McFadden, C., Bishop, P., 1992. Alluvial cutoffs as indicators of former channel conditions. Earth Surface Processes and Landforms 17, p 23-37.

Fisher, R.A., Tippett, L.H.C., 1928. Limiting forms of the frequency distribution of the largest or smallest member of a sample. Proceedings of the Cambridge Philosophical Society 24, p 180-190.

Fisk, H.N., 1947. Fine grained alluvial deposits and their effect on Mississippi River activity, Vols 1 & 2. Mississippi River Commission, Vicksburg, MS.

Frings, R.M., 2007. From gravel to sand. Downstream fining of bed sediments in the lower river Rhine. PhD thesis Utrecht University. Netherlands Geographical Studies 368.

Frings, R.M., Kleinhans, M.G., 2008. Complex variations in sediment transport at three large river bifurcations during discharge waves in the river Rhine. Sedimentology 55, p 1145-1171.

Fuller, I.C., Large, A.R.G., Milan, D.J., 2003. Quantifying channel development and sediment transfer following chute cutoff in a wandering gravel-bed river. Geomorphology 54, p 307-323.

Gagliano, S.M., Howard, P.G., 1984. The neck cutoff oxbow lake cycle along the Lower Mississippi River. In River Meandering, Elliot, CM (Ed). American Society of Civil Engineers: New York; p 147-158.

Gaigalas, A., Dvareckas, V., 2002. The evolution of river valleys in Lithuania from deglaciation to recent changes and data from the sediment fill of oxbow lakes. Netherlands Journal of Geosciences 81, p 407-416.

Gay, G.R., Gay, H.H., Gay, W.H., Martinson, H.A., Meade, R.H., Moody, J.A., 1998. Evolution of cutoffs across meander necks in Powder River, Montana, USA. Earth Surface Processes and Landforms 23, p 651-662.

Geurts, A., 2011. Weichselian to Early Holocene vegetation development and fluvial adjustment in the Lower Rhine Valley, Germany. Unpublished MSc thesis, Dept. of Physical Geography, Utrecht University.

Glaser, R., 2001. Klimageschichte Mitteleuropas. 1000 Jahre Wetter, Klima, Katastrophen. Darmstadt.

Glaser, R., Stangl, H., 2003. Historical floods in the Dutch Rhine Delta. Natural Hazards and Earth System Sciences 3, p 605-613.

Glaser, R., Stangl, H., 2004. Climate and floods in central Europe since AD 1000: Data, methods, results and consequences. Surveys in Geophysics 25, p 485-510.

Glaser, R., Riemann, D., 2009. A thousand-year record of temperature variations for Germany and Central Europe based on documentary data. Journal of Quaternary Science 24, p 437-449.

Glaser, R., Riemann, D., Schönbein, J., Barriendos, M., Brázdil, R., Bertolin, C., Camuffo, D., Deutsch, M., Dobrovolny, P., van Engelen, A., Enzi, S., Halíčková, M., Koenig, S.J., Kotyza, O., Limanowka, D., Macková, J., Sghedoni, M., Martin, B., Himmelsbach, I., 2010. The variability of European floods since AD 1500. Climatic Change 101, p 235-256.

Goudriaan, B.H., 1830. Kaart van de rivieren de Boven Rijn, de Waal, de Merwede en Oude en een gedeelte van de Nieuwe Maas van Lobith tot Brielle. Rijksarchief Gelderland, Algemene Kaarten Verzameling 285.

Gouw, M.J.P., Erkens, G., 2007. Architecture of the Holocene Rhine-Meuse delta (the Netherlands) – A result of changing external controls. Netherlands Journal of Geosciences 86, p 23-54.

Heiri, O., Lotter, A.F., Lemcke, G., 2001. Loss on ignition as a method for estimating organic and carbonate content in sediments: reproducibility and comparability of results. Journal of Palaeolimnology 25, p 101-110.

Heller, P.L., Paola, C., 1996. Downstream changes in alluvial architecture: an exploration of controls on channel-stacking patterns. Journal of Sedimentary Research 66, p 297-306.

Herget, J., Euler, T., 2010. Hoch- und Niedrigwasser in historischer und prähistorischer Zeit. Geographische Rundschau 62, p 4-10.

Herget, J., Meurs, H., 2010. Reconstructing peak discharge for historic flood levels in the city of Cologne, Germany. Global and Planetary Change 70, p 108-116.

Herget, J., Euler, T., Roggenkamp, T. Zemke, J., 2013. Obstacle marks as palaeohydraulic indicators of Pleistocene megafloods. Hydrology Research 44, p 300-317.

Heslop, D., von Dobeneck, T., Höcker, M., 2007. Using non-negative matrix factorization in the unmixing of diffuse reflectance spectra. Marine Geology 241, p 63-78.

Hesselink, A.W., 2002. History makes a river; morphological changes and human interference in the river Rhine, The Netherlands. Netherlands Geographical Studies 292.

Hesselink. A.W., Kleinhans, M.G., 2002. Channel pattern and flow characteristics of the Rhine distributaries in historic time, The Netherlands. In: Hesselink, A.W., 2002. History makes a river, PhD dissertation, Utrecht University.

Hoek, W.Z., Minderhoud, P.S.J., Cohen, K.M., Erkens, G., Toonen, W.H.J., 2011. Towards a decadal flood record of the river Rhine over the last 7000 years. Abstract volume: Quaternary Research Association, Annual Discussion Meeting 2011.

Hoffmann, T., Erkens, G., Cohen, K.M., Houben, P., Seidel, J., Dikau, R., 2007. Holocene floodplain sediment storage and hillslope erosion within the Rhine catchment. The Holocene 17, p 105-118.

Hoffmann, T., Lang, A., Dikau, R., 2008. Holocene river activity: analysing ^{14}C-dated fluvial and colluvial sediments from Germany. Quaternary Science Reviews 21-22, p 2031-2040.

Hoffmann, T., Erkens, G., Gerlach, R., Klostermann, J., Lang, A., 2009. Trends and controls of Holocene floodplain sedimentation in the Rhine catchment. Catena 77, p 96-106.

Hooke, J.M., 1995. River channel adjustment to meander cutoffs on the River Bollin and River Dane, northwest England. Geomorphology 14, p 235-253.

Hosking, J.R.M., Wallis, J.R., Wood, E.F., 1985. Estimation of the generalized extreme-value distribution by the method of probability-weighted moments. Technometrics 27, p 251-261.

Hundecha, Y., Bárdossy, A., 2004. Modeling of the effect of land use changes on the runoff generation of a river basin through parameter regionalization of a watershed model. Journal of Hydrology 292, p 281-295.

IJnsen, F., 1981. Onderzoek naar het optreden van winterweer in Nederland. KNMI, Wetenschappelijk Rapport W.R. 74-2.

Janssens, M.M., Kasse C., Bohncke S.J.P., Greaves H., Cohen K.M., Wallinga J., Hoek, W.Z., 2012. Climate-driven fluvial development and valley abandonment at the last glacial-interglacial transition (Oude IJssel-Rhine, Germany). Netherlands Journal of Geosciences 91, p 37-62.

Intergovernmental Panel on Climate Change (2007), Climate Change 2007: The Physical Science Basis, Contribution of Working Group I to the Fourth Assessment Report of the Intergovernmental Panel on Climate Change, edited by S. Solomon et al., Cambridge Univ. Press, Cambridge, U. K.

Jacobeit, J., Glaser, R., Luterbacher, J., Wanner, H., 2003. Links between flood events in central Europe since AD 1500 and large-scale atmospheric circulation modes. Geophysical Research Letters 30, 1172.

Jones, A.F., Macklin, M.G., Brewer, P.A., 2012. A geochemical record of flooding on the upper River Severn, UK, during the last 3750 years. Geomorphology 179, p 89-105.

Kale, V.S., 2007. Geomorphic effectiveness of extraordinary floods on three large rivers of the Indian Peninsula. Geomorphology 85, p 306-316.

Kalis, A.J., Merkt, J., Wunderlich, J., 2003. Environmental changes during the Holocene climatic optimum in central Europe – human impact and natural causes. Quaternary Science Reviews 22, p 33-79.

Kasse, C., Hoek, W.Z., Boncke, S.J.P., Konert, M., Weijers, J.W.H., Cassee, M.L., van der Zee, R.M., 2005. Late Glacial fluvial response of the Niers-Rhine (western Germany) to climate and vegetation change. Journal of Quaternary Science 20, p 377-394.

Keijzer, M., Babovic, V., Bastist, M., Uthurburu, J.R., 2005. Determining equations for vegetation induced resistance using genetic programming. Conference Proceeding GECCO 2005 – Genetic and Evolutionary Computation Conference, Washington, D.C., June 2005.

Keulegan, G.H., 1938. Laws of turbulent flow in open channels. Journal of Research of the National Bureau of Standards 21, p 707-741.

Kidson, R., Richards, K.S., 2005. Flood frequency analysis: assumptions and alternatives. Progress in Physical Geography 29, p 392-410.

Kleinhans, M.G., Jagers, H.R.A., Mosselman, E., Sloff, C.J., 2008. Bifurcation dynamics and avulsion duration in meandering rivers by one-dimensional and three-dimensional models. Water Resources Research 44: W08454.

Kleinhans, M.G., Cohen, K.M., Hoekstra, J., IJmker, J.M., 2011. Evolution of a bifurcation in a meandering river with adjustable channel widths, Rhine delta apex, The Netherlands. Earth Surface Processes and Landforms 36, p 2011-2027.

Kleinhans, M.G., Ferguson, R.I., Lane, S.N., Hardy, R.J., 2013. Splitting rivers at their seams: bifurcations and avulsion. Earth Surface Processes and Landforms 38, p 47-61.

Klemeš, V., 2000. Tall tales about tails of hydrological distributions. I. Journal of Hydrologic Engineering 5, p 227-231.

Klostermann, J., 1992. Das Quartär der Niederrheinischen Bucht. Geologisches Landesamt Nordrhein-Westfalen. Krefeld, pp. 1-200.

Knox, J.C., 1993. Large increases in flood magnitude in response to modest changes in climate. Nature 361, p 430-432.

Konert, M., Vandenberghe, J., 1997. Comparison of laser grain size analysis with pipette and sieve analysis: a solution for the under-estimation of the clay fraction. Sedimentology 44, p 523-535.

Konijnendijk, T., 2010 Reconstruction of extreme discharge events. MSc-Thesis, Dept. of Physical Geography, Utrecht University. pp. 1-74.

Kwadijk, J.C.J., Middelkoop, H., 1994. Estimation of impact of climate change on the peak discharge probability of the River Rhine. Climatic Change 27, p 199-224.

Lammersen, R., Engel., H., van de Langemheen, W., Buiteveld, H., 2002. Impact of river training and retention measures on flood peaks along the Rhine. Journal of Hydrology 267, p 115-124.

Lammersen, R., 2004. Grensoverschrijdende effecten van extreem hoogwater op de Niederrhein. Eindrapport Duits-Nederlandse Werkgroep Hoogwater, 106 pp.

Lang, A., Bork, H.R., Mäckel, R., Preston, N., Wunderlich, J., Dikau, R., 2003. Changes in sediment flux and storage within a fluvial system: some examples from the Rhine catchment. Hydrological Processes 17, p 3321-3334.

Lauer, T., Frechen, M., Klostermann, J., Krbetschek, M., Schollmayer, G., Tsukamoto, S., 2011. Luminescence dating of Last Glacial and Early Holocene fluvial deposits from the Lower Rhine – methodological aspects and chronological framework. Zeitschrift der Deutschen Gesellschaft für Geowissenschaften 162, p 47-61.

Lechner, A., 2009. Palaeohydrologic conditions and geomorphic processes during the Postglacial in the Palatine Upper Rhine river floodplain. Zeitschrift fur Geomorphologie 53, p 217-245.

Leeder M. 1999. Sedimentology and Sedimentary Basins: From Turbulence to Tectonics. Blackwell: Oxford, UK.

Levish, D.R., 2002. Paleohydrologic bounds: non-exceedance information for flood hazard assessment. In: House, P.K., Webb, R.H., Baker, V.R., Levish, D.R. (Eds.), Ancient floods, modern hazards: Principles and applications of paleoflood hydrology. Water Science and Application 5, American Geophysical Union, Washington D.C., p 175-190.

Lewin, J., Macklin, M.G., Johnstone, E.C. 2005. Interpreting alluvial archives: sedimentological factors in the British Holocene fluvial record. Quaternary Science Reviews 24, p 1873 – 1889.

Lewin, J., Macklin, M.G., 2003. Preservation potential for Late Quaternary river alluvium. Journal of Quaternary Science 18, p 107-120.

Lewis, G.W., Lewin, J., 1983. Alluvial cutoffs in Wales and the Borderlands. In Modern and Ancient Fluvial Systems, Collinson JD, Lewin J (Eds.). International Association of Sedimentologists, Special Publications 6, p 145-154.

Macdonald, N., Black, A.R., 2010. Reassessment of flood frequency using historical information for the River Ouse at York, UK (1200-2000). Hydrological Sciences Journal 55, p 1152-1162.

Macklin, M.G., Lewin, J., 2003. River sediments, great floods and centennial-scale Holocene climate change. Journal of Quaternary Science 18, p 101-105.

Macklin, M.G., Benito, G., Gregory, K.J., Johnstone, E., Lewin, J., Michczynska, D.J., Soja, R., Starkel, L., Thorndycraft, V.R., 2006. Past hydrological events reflected in the Holocene fluvial record of Europe. Catena 66, p 145-154.

Macklin, M.G., Lewin, J., 2008. Alluvial responses to the changing Earth system. Earth Surface Processes and Landforms 33, p 1374-1395.

Macklin, M.G., Fuller, I.C., Jones, A.F., Bebbington, M., 2012. New Zealand and UK Holocene flooding demonstrates interhemispheric climate asynchrony. Geology 40, p 775-778.

Makaske, B., 1998. Anastomosing rivers: Forms, processes and sediments. Netherlands Geographical Studies 249.

Makaske, B., Smith, D.G., Berendsen, H.J.A., 2002. Avulsions, channel evolution and floodplain sedimentation rates of the anastomosing upper Columbia River, British Columbia, Canada. Sedimentology 49, p 1049-1071.

Makaske, B., Maas, G.J., van Smeerdijk, D.G., 2008. The age and origin of the Gelderse IJssel. Netherlands Journal of Geosciences 87, p 323-337.

Mann, M.E., Zhang, Z., Rutherford, S., Bradley, R.S., Hughes, M.K., Shindell, D., Ammann, C., Faluvegi, F., Ni, F., 2009. Global signatures and dynamical origins of the little ice age and medieval climate anomaly. Science 326, p 1256-1260.

Micheli, E.R., Larsen, E.W., 2011. River channel cutoff dynamics, Sacramento River, California, USA. River Research and Applications 27, p 328-344.

Middelkoop, H., 1997. Embanked floodplains in the Netherlands. Geomorphological evolution over various time scales. Netherlands Geographical Studies 224, 341 pp.

Middelkoop, H., Asselman, N.E.M., 1998. Spatial variability of floodplain sedimentation at the event scale in the Rhine-Meuse Delta, the Netherlands. Earth Surface Processes and Landforms 23, p 561-573.

Milly, P.C.D., Wetherald, R.T., Dunne, K.A., Delworth, T.L., 2002. Increasing risk of great floods in a changing climate. Nature 415, p 514-517.

Milly, P.C.D., Betancourt, J., Falkenmark, M., Robert, M., Hirsch, R.M., Kundzewicz, Z.W., Lettenmaier, D.P., Stouffer, R.J., 2008. Stationarity is dead: Whither water management? Science 319, p 573-574.

Moreno, A., Valero-Garcés, B.L., González-Sampériz, P., Rico, M., 2008. Flood response to rainfall variability during the last 2000 years inferred from the Taravilla Lake record (Central Iberian Range, Spain). Journal of Paleolimnology 40, p 943-961.

Morozova, G.S., Smith, N.D., 2000. Holocene avulsion styles and sedimentation patterns of the Saskatchewan River, Cumberland Marshes, Canada. Sedimentary Geology 130, p 81-105.

Moy, C.M., Seltzer, G.O., Rodbell, D.T., Anderson, D.M., 2002. Variability of El Nino/Southern Oscillation activity at millennial timescales during the Holocene epoch. Nature 420, p 162-165.

Mudelsee, M., Börngen, M., Tetzlaff, G., Grünewald, U., 2003. No upward trends in the occurence of extreme floods in central Europe. Nature 425, p 166-169.

Mudelsee, M., Börngen, M., Tetzlaff, G., Grünewald, U., 2004. Extreme floods in central Europe over the past 500 years: Role of cyclone pathway "Zugstrasse Vb". Journal of Geophysical Research 109, p 1-21.

Nanson, G.C., Croke, J.C., 1992. A genetic classification of floodplains. In Floodplain Evolution, Brakenridge GR, Hagedorn J (Eds). Geomorphology 4, p 459-486.

Nesje, A., Dahl, S.O., Matthews, J.A., Berrisford, M.S., 2001. A ~4500 yr record of river floods obtained from a sediment core in Lake Atnsjøen, eastern Norway. Journal of Paleolimnology 25, p 329-342.

Nichols, G., 1999. Sedimentology and Stratigaphy. Blackwell Science, Malden, MA.

O'Connell, D.R.H., Ostenaa, D.A., Levish, D.R., Klinger, R.E., 2002. Bayesian flood frequency analysis with paleohydrologic bound data. Water Resources Research 38.

Oele, E., Apon, W., Fischer, M.M., Hoogendoorn, R., Mesdag, C.S., De Mulder, E.F.J., Overzee, B., Sesören, A., Westerhoff, W.E., 1983. Surveying The Netherlands: sampling techniques, maps and their applications. In Special Issue in the honour of J.D. de Jong, van den Berg MW, Felix R (Eds). Geologie en Mijnbouw 62, p 355-372.

Ojala, A.E.K., Saarinen, T., 2002. Palaeosecular variation of the Earth's magnetic field during the last 10000 years based on the annually laminated sediment of Lake Nautajärvi, central Finland. The Holocene 12, p 391-400.

Paas, W., Teunissen, D., 1975. Die geologische Geschichte der Duffel, eine linksniederrheinische Flussaue zwischen Kleve und Nimwegen. Mededelingen van de Afdeling Biogeologie van de Sectie Biologie van de K.U.Nijmegen 7.

Page, K.J., Nanson, G.C., 1996. Stratigraphic architecture resulting from Late Quaternary evolution of the Riverine Plain, south-eastern Australia. Sedimentology 43, p 927-945.

Parker, A.G., Lucas, A.S., Walden, J., Goudie, A.S., Robinson, M.A., Allen, T.G., 2008. Late Holocene geoarchaeological investigation of the Middle Thames floodplain at Dorney, Buckinghamshire, UK: An evaluation of the Bronze Age, Iron Age, Roman and Saxon landscapes. Geomorphology 101, p 471-483.

Parmet, B.W.A.H., van de Langemheen, W., Chbab, E.H., Kwadijk, J.C.J., Diermanse, F.L.M., Klopstra, D., 2001. Analyse van de maatgevende afvoer van de Rijn te Lobith. Rijkswaterstaat, Arhnem, RIZA rapport 2002.012.

Parris, A.S., Bierman, P.R., Noren, A.J., Prins, M.A., Lini, A., 2010. Holocene paleostorms identified by particle size signatures in lake sediments from the northeastern United States. Journal of Paleolimnology 43, p 29-49.

Peakall, J., Ashworth, P.J., Best, J.L., 2007. Meander-bend evolution, alluvial architecture, and the role of cohesion in sinuous river channels: a flume study. Journal of Sedimentary Research 77, p 197-212.

Piégay, H., Hupp, C.R., Citterio, A., Dufour, S., Moulin, B., Walling, D.E., 2008. Spatial and temporal variability in sedimentation rates associated with cutoff channel infill deposits: Ain River, France. Water Resources Research 44: W05420, DOI:10.1029/2006WR005260.

Pinter, N., van der Ploeg, R.R., Schweigert, P., Hoefer, G., 2006. Flood magnification on the river Rhine. Hydrological Processes 20, p 147-164.

Pons, L.J., 1957. De geologie, de bodemvorming en de waterstaatkundige ontwikkeling van het Land van Maas en Waal en een gedeelte van het Rijk van Nijmegen. 's-Gravenhage, Verslagen van Landbouwkundige Onderzoekingen 63.11, Dissertatie Wageningen: Bodemkundige studies 3.

Prins, M.A., Postma, G., Weltje, G.J., 2000. Controls on terrigenous sediment supply to the Arabian Sea during the late quaternary: the makran continental slope. Marine Geology 169, p 351-371.

Reading, H.G., 1996. Sedimentary environments: Processes, facies and stratigraphy. Elsevier: New York.

Redmond, K.T., Enzel, Y., House, P.K., Biondi, F., 2002. Climate impact on flood frequency at the decadal to millennial time scales. In: House, P.K., Webb, R.H., Baker, V.R., Levish, D. (Eds.), Ancient Floods, Modern Hazards: Principles and Applications of Palaeoflood Hydrology. Water Science and Application 5, American Geophysical Union, p 21-45.

Reimer, P.J., Baillie, M.G.L., Bard, E., Bayliss, A., Beck, J. W., Blackwell, P.G., Bronk Ramsey, C., Buck, C.E., Burr, G.S., Edwards, R.L., Friedrich, M., Grootes, P.M., Guilderson, T.P., Hajdas, I., Heaton, T.J., Hogg, A.G., Hughen, K.A., Kaiser, K.F., Kromer, B., McCormac, F.G., Manning, S.W., Reimer, R.W., Richards, D.A., Southon, J.R., Talamo, S., Turney, C.S.M., van der Plicht, J., Weyhenmeyer, C.E., 2009. IntCal09 and Marine09 radiocarbon age calibration curves, 0-50,000 years cal BP. Radiocarbon 51, p 1111-1150.

Redmond, K.T., Enzel, Y., House, P.K., Biondi, F., 2002. Climate impact on flood frequency at the decadal to millennial time scales. In: Ancient Floods, Modern Hazards: Principles and Applications of Palaeoflood Hydrology (P.K. House, R.H. Webb, V.R. Baker & D. Levish, Eds). Water Science and Application 5, American Geophysical Union, p 21 – 45.

Rijkswaterstaat, 1942. Ijsverslag winter 1939-1940. RIZA, Dienst Binnenwateren. Algemeene Landsdrukkerij, 's-Gravenhage.

Rijkswaterstaat-AGI, 2005. Actueel Hoogtebestand Nederland. Revised version. Rijkwaterstaat, Adviesdienst Geo-informatie en ICT, Delft.

Rowland, J.C., Lepper, K., Dietrich, W.E., Wilson, C.J., Sheldon, R., 2005. Tie channel sedimentation rates, oxbow formation age and channel migration rate from optically stimulated luminescence (OSL) analysis of floodplain deposits. Earth Surface Processes and Landforms 30, p 1161-1179.

Saint-Laurent, D., 2004. Palaeoflood hydrology: an emerging science. Progress in Physical Geography 28, p 531-543.

Salvador, P.G., Berger, J.F., Fontugne, M., Gauthier, E., 2005. Etude des enregistrements sédimentaires Holocènes des paleomeandres du Rhône dans le secteur des Basses Terres (Ain, Isère, France). Quaternaire 16, p 315-328.

Saucier, R.T., 1994. Geomorphology and quaternary geologic history of the Lower Mississippi Valley. Waterways Experiment Station, U.S. Army Corps of Engineers: Vicksburg, Mississippi.

Schirmer, W., 1995. Valley bottoms in the late Quaternary. Zeitschrift für Geomorphologie N.F. Supl. 100, p 27-51.

Schulte, L., Veit, H., Burjachs, F., Julia, R., 2009. Lütshine fan delta response to climate variability and land use in the Bernese Alps during the last 2400 years. Geomorphology 108, p 107-121.

Schulz, M., Mudelsee, M., 2002. REDFIT: Estimating red-noise spectra directly from unevenly spaced paleoclimatic time series. Computers and Geosciences 28, p 421-426.

Schumm, S.A., 1977. The fluvial system. The Blackburn Press, Caldwell, NJ, USA.

Shabalova, M.V., van Deursen, W.P.A., Buishand, T.A., 2003. Assessing future discharge of the river Rhine using regional climate model integrations and a hydrological model. Climate Research 23, p 233-246.

Shala, B., 2001. Jungquartäre Talgeschichte des Rheins zwischen Krefeld und Dinslaken. Doktors-thesis Universität Düsseldorf, 231 pp.

Shields, F.D. Jr., Abt, S.R., 1989. Sediment deposition in cutoff meander bends and implications for effective management. Regulated Rivers Research and Management 4, p 381-396.

Silva, W., Klijn, F., Dijkman, J., 2001. Room for the Rhine Branches in The Netherlands; what research has taught us. Technical Report 2001.031, WL Delft Hydraulics, Ministry of Transport, Public Works and Water Management, Delft, Lelystad, the Netherlands, 162 pp.

Slingerland, R., Smith, N.D., 2004. River avulsions and their deposits. Annual Review of Earth and Planetary Science 32, p 257-285.

Smith, N.D., Cross, T.A., Dufficy, J.P., Clough, S.R., 1989. Anatomy of an avulsion. Sedimentology 36, p 1-23.

Smith, N.D., Slingerland, R.L., Perez-Arlucea, M., Morozova, G.S., 1998. The 1870s avulsion of the Saskatchewan River. Canadian Journal of Earth Sciences 35, p 453-466.

Stedinger, J.R., Cohn, T.A., 1986. Flood Frequency Analysis with Historical and Paleoflood Information. Water Resources Research 22, p 785-793.

Stedinger, J.R., Surani, R., Therivel, R., 1988. Max users guide, a program for flood frequency analysis using systematic-record, historical, botanical, physical paleohydrologic and regional hydrologic information using maximum-likelihood techniques. Cornell University, Dept. Environmental Engineering, Ithaca, New York, 51 pp.

STIBOKA, 1975. Bodemkaart van Nederland schaal 1:50000. Toelichting bij de kaartbladen 40 West Arnhem en 40 Oost Arnhem. Stichting voor Bodemkartering, Wageningen.

Steiger, J., Gurnell, A.M., Petts, G.E., 2001. Sediment deposition along the channel margins of a reach of the middle river Severn, UK. Regulated Rivers: Research & Management 17, p 443-460.

Støren, E., Dahl, S.O., Nesje, A., Paasche, Ø., 2010. Identifying the sedimentary imprint of high-frequency Holocene river floods in lake sediments: development and application of a new method. Quaternary Science Reviews 29, p 3021-3033.

Stouthamer, E., Berendsen, H.J.A., 2000. Factors controlling the Holocene avulsion history of the Rhine-Meuse delta (The Netherlands). Journal of Sedimentary Research 70, p 1051-1064.

Stouthamer, E., Berendsen, H.J.A., 2001. Avulsion frequency, avulsion duration, and interavulsion period of Holocene channel belts in the Rhine-Meuse Delta, The Netherlands. Journal of Sedimentary Research 71, p 589-598.

Stouthamer, E., 2005. Reoccupation of channel belts and its influence on alluvial architecture in the Holocene Rhine-Meuse delta, The Netherlands. In River Deltas: Concepts, Models, and Examples, Giosan L, Bhattacharya JP (Eds). SEPM, special publication 83, p 319-339.

Stouthamer, E., Cohen, K.M., Gouw, M.J.P., 2011. Avulsion and its implications for fluvial-deltaic architecture: Insights from the Holocene Rhine-Meuse delta. SEPM Special Publication 97, p 215-231.

Straatsma, M., Huthoff, F., 2011. Uncertainty in 2D hydrodynamic models from errors in roughness parameterization based on aerial images. Physics and Chemistry of the Earth 36, p 324-334.

Sturm, K., Glaser, R., Jacobeit, J., Deutsch, M., Brázdil, R., Pfister, C., 2001. Floods in Central Europe since AD 1500 and their relation to the atmospheric circulation. Petermanns Geographische Mitteilungen 148, p 18-27.

Swierczynski, T., Brauer, A., Lauterbach, S., Martin-Puertas, C., Dulski, P., von Grafenstein, U., Rohr, C., 2012. A 1600 yr seasonally resolved record of decadal-scale flood variability from the Austrian Pre-Alps. Geology 40, p 1047-1050.

Taylor, W.A., 2000. Change-point analysis: a powerful new tool for detecting changes. preprint, available as http://www.variation.com/cpa/tech/changepoint.html.

Te Linde, A.H., Aerts, J.C.J.H., Bakker, A.M.R., Kwadijk, J.C.J., 2010. Simulating low-probability peak discharges for the Rhine basin using resampled climate modeling data. Water Resources Research 46, W03512.

Ten Brinke, W., 2005. The Dutch Rhine: a restrained river. Veen Magazines, Diemen.

Teunissen, D., 1986. Palynological investigation of some residual gullies in the Upper Betuwe (the Netherlands). Berichten van de Rijksdienst voor het Oudheidkundig Bodemonderzoek 36A, p 7-24.

Timmermann, A., Latif, M., Voss, R., Grotzner, R.A., 1998. Northern hemispheric interdecadal variability: a coupled air-sea mode. Journal of Climate 11, p 1906-1931.

TNO-DINO, 2009. Built Environment and Geosciences – Geological survey of the Netherlands. DINOloket (Internet portal for Geo-Information). Available at: http://www.dinoloket.nl/en/DINOLoket.html.

Toniazzo, T., Scaife, A.A., 2006. The influence of ENSO on winter North Atlantic climate. Geophysical Research Letters 33, L24704.

Törnqvist, T.E., de Jong, A.F.M., Oosterbaan, W.A., van der Borg, K., 1992. Accurate dating of organic deposits by AMS ^{14}C measurement of macrofossils. Radiocarbon 34, p 566-577.

Törnqvist TE. 1993. Fluvial sedimentary geology and chronology of the Holocene Rhine-Meuse delta, The Netherlands. Netherlands Geographical Studies 166.

Törnqvist, T.E., Kidder, T.R., Autin, W.J., van der Borg, K., de Jong, A.F.M., Klerks, C.J.W., Snijders, E.M.A., Storms, J.E.A., van Dam, R.L., Wiemann, M.C., 1996. A revised chronology for Mississippi River Subdeltas. Science 273, p 1693-1696.

Toonen, W.H.J., Kleinhans, M.G., Cohen, K.M., 2012. Sedimentary architecture of abandoned channel fills. Earth Surface Processes and Landforms 37, p 459-472.

Toonen, W.H.J., de Molenaar, M.M., Bunnik, F.P.M., Middelkoop, H., 2013. Middle Holocene palaeoflood extremes of the Lower Rhine. Hydrology Research 44, p 248-263.

Vandenberghe, J., 1995. Timescales, climate and river development. Quaternary Science Reviews 14, p 631-638.

Van de Lageweg, W.I., Van Dijk, W., Kleinhans, M.G., 2013. Channel belt architecture formed by a meandering river. Sedimentology 60, p 840-859.

Van de Ven G., 1976. Aan de wieg van Rijkswaterstaat – wordingsgeschiedenis van het Pannerdens Kanaal. De Walburg Pers, Zutphen.

Van den Berg, J.H., 1995. Prediction of alluvial channel pattern of perennial rivers, Geomorphology 12, p 259-279.

Vandenberghe, J., An, Z., Nugteren, G., Lu, H., Van Huissteden, J., 1997. New absolute time scale for the Quaternary climate in the Chinese loess region by grain-size analysis. Geology 25, p 35-38.

Van den Broeke, P., 2002. Vindplaatsen in vogelvlucht – Beknopt overzicht van het archeologische onderzoek in de Waalsprong, 1996-2001. Archeologische Berichten Nijmegen, Rapport 1.

Van den Meene, E.A., Van der Staay, J., Teoh Lay Hock, 1979. The Van der Staay suction corer – a simple apparatus for drilling in sand below groundwater table. Rijks Geologische Dienst, Haarlem.

Van Dijk, W.M., Van de Lageweg, W.I., Kleinhans, M.G., 2012. Experimental meandering river with chute cut offs. Journal of Geophysical Research 117, F03023.

Van Geelkercken, N., 1639. Kaart van de Waalstroom tegen de heerlijkheid Loenen. Rijksarchief van Gelderland, archief Rekenkamer 62.

Van Heiningen, H., 1978. Dijken en Dijkdoorbraken in het Nederlandse rivierengebied. Triangelreeks, 's-Gravenhage.

Van Munster, B., 2011. Early and Middle Holocene fluvial development near the present-day Rhine Delta apex, Germany. Unpublished MSc thesis, Dept. Physical Geography, Utrecht University.

Van Rijn, L.C., 1984. Sediment transport, part III: bed forms and alluvial roughness. Journal of Hydraulic Engineering 110, p 1733-1754.

Van Velzen, E.H., Jesse, P., Cornelissen, P., Coops, H., 2002a. Stromingsweerstand vegetatie in uiterwaarden, Deel 1 handboek versie 1.0. Rijkswaterstaat, Directie Oost Nederland, RIZA werkdocument 2002.140x.

Van Velzen, E.H., Jesse, P., Cornelissen, P., Coops. H., 2002b. Stromingsweerstand vegetatie in uiterwaarden, Deel 2 achtergronddocument versie 1.0. Rijkswaterstaat, Directie Oost Nederland, RIZA werkdocument 2002.141x.

Van Vuuren, W., 2005. Met balen vol sigma's de Rijn en Maas afzakken. Werkdocument RIZA 2005.145X, 73 pp.

Veerman, C.P., 2008. Samenwerken met water. Bevindingen van de Deltacommissie 2008, 134 pp.

Verbraeck, A., 1984. Toelichtingen bij de Geologische Kaart van Nederland, schaal 1:50.000, blad Gorinchem Oost (38O). Rijks Geologische Dienst, Haarlem.

Von Wiebeking, K.F., 1800. Karte von der Waal, von dem unteren Rhein, dem Leck von der Merwede und der Maas, und von den Gegenden welche an diesen Flüssen liegen. Rijksarchief van Gelderland, Algemene Kaarten Verzameling 281.

Vorogushyn, S., Merz, B., 2012. What drives flood trends along the Rhine River: climate or river training? Hydrology and Earth Science System Sciences Discussions 9, p 13537-13567.

Walker, M.J.C., Berkelhammer, M., Björck, S., Cwynar, L.C., Fisher, D.A., Long, A.J., Lowe, J.J., Newnhamn, R.M., Rasmussen, S.O. Weiss, H., 2012. Formal subdivision of the Holocene Series/Epoch: a Discussion Paper by a Working Group of INTIMATE (Integration of ice-core, marine and terrestrial records) and the Subcommission on Quaternary Stratigraphy (International Commission on Stratigraphy). Journal of Quaternary Science 27, p 649-659.

Walling, D.E., Hu, Q., 1998. The spatial variability of overbank sedimentation on river floodplains. Geomorphology 24, p 209-223.

Wanner, H., Beer, J., Bütikofer, J., Crowley, T., Cabasch, U., Flückiger, J., Goosse, H., Grosjean, M., Joos, F., Kaplan, J.O., Küttel, M., Müller, S.A., Prentice, I.C., Solomina, O., Stocker, T.F., Tarasov, P., Wagner, M., Widmann, M., 2008. Mid- to Late Holocene climate change: an overview. Quaternary Science Reviews 27, p 1791-1828.

Ward, P.J., Renssen, H., Aerts, J.C.J.H., van Balen, R.T., Vandenberghe, J., 2008. Strong increases in flood frequency and discharge of the River Meuse over the Holocene: Impacts of long-term anthropogenic land use change and climate variability. Hydrology and Earth Science System Sciences 12, p 159-175.

Ward, P.J., Renssen, H., Aerts, J.C.J.H., Verburg, P.H., 2011. Sensitivity of discharge and flood frequency to twenty-first century and late Holocene changes in climate and land use (River Meuse, northwest Europe). Climatic Change 106, p 179-202.

Waterbase, 2012. Ministry of Infrastructure and the Environment, live.waterbase.nl. Accessed in January, 2013.

Waterwet, 2009. Ministry of Infrastructure and the Environment, www.helpdeskwater.nl/onderwerpen/wetgeving-beleid/waterwet. Accessed in January, 2013.

Webb, R.H., Jarrett, R.D., 2002. One-dimensional estimation techniques for discharges of paleofloods and historical floods. In: House, P.K., Webb, R.H., Baker, V.R., Levish, D. (Eds.), Ancient Floods, Modern Hazards: Principles and Applications of Palaeoflood Hydrology. Water Science and Application 5, American Geophysical Union, p 111-125.

Weerts, H., 1996. Complex confining layers. Architecture and hydraulic properties of Holocene and Late Weichselian deposits in the fluvial Rhine-Meuse delta, The Netherlands. Ph.D. Thesis, Utrecht University.

Weltje, G.J., 1997. End-member modeling of compositional data: numerical-statistical algorithms for solving the explicit mixing problem. Journal of Mathematical Geology 29, p 503-549.

Weltje, G.J., Prins, M.A., 2007. Genetically meaningful decomposition of grain-size distributions. Sedimentary Geology 202, p 409-424.

Werritty, A., Paine, J.L., Macdonald, N., Rowan, J.S., McEwen, L.J., 2006. Use of Multi-proxy flood records to improve estimates of flood risk: Lower River Tay, Scotland. Catena 66, p 107-119.

Wetter, O., Pfister, C., Weingarter, R., Luterbacher, J., Reist, T., Trösch, J., 2011. The largest floods in the High Rhine basin since 1268 assessed from documentary and instrumental evidence. Hydrological Sciences Journal 56, p 733-758.

Wilbers, A.W.E., ten Brinke, W.B.M., 2003. The response of subaqueous dunes to floods in sand and gravel bed reaches of the Dutch Rhine. Sedimentology 50, p 1013-1034.

Wilhelm., B., Arnaud, F., Sabatier, P., Magand, O., Chapron, E., Courp, T., Tachikawa, K., Fanget, B., Malet, E., Pignol, C., Bard, E., Delannoy, J.J., 2013. Palaeoflood activity and climate change over the last 1400 years recorded by lake sediments in the north-west European Alps. Journal of Quaternary Science 28, p 189-199.

Wolf, R.J.A.M., Stortelder, A.H.F., de Waal, R.W., 2001. Ooibossen. Bosecosystemen van Nederland. KNNV Uitgeverij, Utrecht.

Wolfe, B.B., Hall, R.I., Last, W.M., Edwards, T.W., English, M.C., Karst-Riddoch, T.L., Paterson, A., Palmini, R., 2006. Reconstruction of multi-century flood histories from oxbow lake sediments, Peace-Athabasca Delta, Canada. Hydrological Processes 20, p 4131-4153.

Woodyer, K.D., 1968. Bankfull frequency in Rivers. Journal of Hydrology 6, p 114-142.

About the author

Born on the 9th of March 1984 in Oss (province of Noord-Brabant), I grew-up in the rural area in between the towns of Wilbertoord and Mill. Retrospective, this area has probably awakened the interest in nature, which started immediately at my doorstep. After attending secondary school in the town of Uden, I started to study Earth Sciences at Utrecht University in 2002. After a short intermezzo as a postman, I was given the opportunity to join the fieldwork of Sanneke van Asselen to the Saskatchewan River Delta in Canada. To finalise my MSc, I was offered the opportunity to join two traineeship projects. Early 2008, I joined an archaeological mission to the Western Nile Delta in Egypt under supervision of Joshua Trampier. I was involved as a quaternary geologist and responsible for a palaeo-environmental reconstruction of the deltaic landscape, aimed at creating a context for archaeological site configuration and temporal dynamics in settlement patterns. After return, I worked three months at the Royal Dutch Meteorological Institute (KNMI) as a modeller of methane emissions from natural wetlands under supervision of Nanne Weber.

Although I had excellent experiences with research projects during my Masters, I started to work at Vestigia after graduation in 2008. At Vestigia I was mainly involved in several minor projects as a quaternary geologist in prospective fieldwork, targeted to identify archaeological remains prior to construction projects. Working at Vestigia was fun and gave me some useful experiences about working in 'the real world' – a nice perk was carrying out projects at many different locations, also outside the fluvial part of the Netherlands. Early 2009, I left Vestigia when I was offered a PhD-position at Utrecht University concerned with palaeofloods of the river Rhine.

Now, four years later and on the brink of finishing my dissertation, I am still happy that I got into research. During my PhD project I had ample opportunities to meet interesting people and I was offered sufficient time to get involved in other projects.

Utrecht, early 2013.

List of publications

Peer-reviewed publications

Toonen, W.H.J., Kleinhans, M.G., Cohen, K.M., 2012. Sedimentary architecture of abandoned channel fills. Earth Surface Processes and Landforms 37:4, p 459-472. DOI:10.1002/esp.3189.

Toonen, W.H.J., de Molenaar, M.M., Bunnik, F.P.M., Middelkoop, H., 2013. Middle Holocene palaeoflood extremes of the Lower Rhine. Hydrology Research 44, p 248-263.

Trampier, J., Starbird, J., Toonen, W.H.J., Simony, A., accepted. Missing Koms and Abandoned Channels: The potential of regional survey in the Western Nile Delta landscape. Accepted for publication in the Journal of Egyptian Archaeology.

Weber, S.L., Drury, A.J., Toonen, W.H.J., Van Weele, M., 2010. Wetland methane emissions during the Last Glacial Maximum estimated from PMIP2 simulations: Climate, vegetation and geometric controls. Journal of Geophysical Research (Atmospheres) 115, DOI:10.1029/2009JD012110, 2010.

Non-refereed publications

Toonen, W.H.J., 2010. Paleogeografie en veiligheid tegen overstromingen. Reconstructie van extreme afvoeren van de Rijn in de laatste 5000 jaar. Geobrief 35:4, p 8-9.

Weber, S.L., Drury, A.J., Toonen, W.H.J., van Weele, M., 2010. Glacial wetland distribution and methane emissions estimated from PMIP2 climate simulations. Journal of Integrative Environmental Sciences 7, Issue SUPPL. 1, p 119-124.

Selected conference proceedings

Berger, J.F., Salvador, P.G., Erkens, G., Toonen, W.H.J., Purdue, L., Barra, A., Houben, P., 2012. Hydroclimatic signal and LBK cultural activity in the Upper and Lower Rhine, inferred from abandoned channel fill deposits. EGU General Assembly Conference Abstracts 14, 6076.

Cohen, K.M., Toonen, W.H.J., Hijma, M.P., Kleinhans, M.G., Minderhoud, P.S.J., Hoek, W.Z., Stouthamer, E., Middelkoop, H., Prins, M.A., Erkens, G., 2012. Holocene Rhine delta evolution: resolving larger flooding events amidst gradual trends. 4th International Geologica Belgica Meeting 2012.

Erkens, G., Prins, M.A, Toonen, W.H.J., 2012. Human impact on the Middle and Late Holocene floodplain sediment characteristics along the River Rhine. EGU General Assembly Conference Abstracts 14, 5971.

Toonen, W.H.J., Trampier, J., 2010. The holocene Nile settlement dynamics in the western Nile delta. In Y. Tristan, M. Ghilardi (Eds.), Landscape Archaeology. Egypt and the Mediterranean World, International Colloquium on Geoarchaeology, Programme and Abstracts Volume, Cairo, 19–20 September (2010), p. 116.

Toonen, W.H.J., 2011. Advances and prospects in deltaic palaeoflood hydrology. Quaternary International, vol. 279-280, p 496. INQUA conference 2011, Bern.

Toonen, W.H.J., Winkels, T.G., Prins, M.A., de Groot, L.V., Bunnik, F.P.M., Middelkoop, H., Cohen, K.M., 2013. A 400-year discharge record of Lower Rhine floods, based on the sedimentary characteristics of flood deposits. In D.R. Parsons, P.J. Ashworth, J.L. Best and C.J. Simpson (Eds.), Conference Programme & Abstract Volume, 10th International Conference on Fluvial Sedimentology (pp. 237). Leeds, 10th International Conference on Fluvial Sedimentology.